

**DEVELOPMENT OF A UNIFORM-DROPLET SPRAY APPARATUS FOR HIGH  
MELTING TEMPERATURE METALS**

by

**HADY K. JOUMAA**

B.E. in Mechanical Engineering, American University of Beirut (AUB), 2003

Submitted to the Department of Mechanical Engineering  
in Partial Fulfillment of the Requirements  
for the Degree of

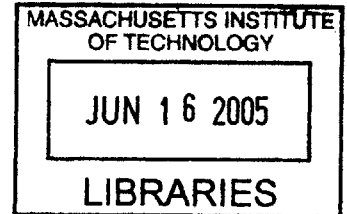
Master of Science  
In Mechanical Engineering

at the

**MASSACHUSETTS INSTITUTE OF TECHNOLOGY**

June 2005

©2005 Massachusetts Institute of Technology  
All rights reserved



Signature of Author \_\_\_\_\_  
Department of Mechanical Engineering

Certified by \_\_\_\_\_  
Jung-Hoon Chun  
Professor, Mechanical Engineering  
Thesis Supervisor

Accepted by \_\_\_\_\_  
Lallit Anand  
Chairman, Departmental Committee on Graduate Studies  
Department of Mechanical Engineering

**BARKER**

# DEVELOPMENT OF A UNIFORM-DROPLET SPRAY APPARATUS FOR HIGH MELTING TEMPERATURE METALS

by

HADY K. JOUMAA

Submitted to the Department of Mechanical Engineering  
on May 6, 2005 in partial fulfillment  
of the requirements for the degree of  
Master of Science in Mechanical Engineering

## ABSTRACT

The building and operation of a high-temperature *uniform droplet spraying* (UDS) apparatus extend the performance and capabilities of powder based manufacturing processes. Although the main concepts of operation of the high-temperature apparatus are typical to the ones currently existing in the Droplet Based Manufacturing (DBM) laboratory, they are implemented with some different systems whose capabilities satisfy the process needs for solder alloys. The motivation of this research is to design, test, optimize, and assemble the new UDS apparatus systems aiming to produce the powder of high melting temperature metal, mainly copper.

At first, the limited capabilities of the current apparatuses are revealed and the characteristics of the high-temperature apparatus are presented. A new design concept is set according to these characteristics. The UDS apparatus is then described in detail with emphasis on the newly installed systems that give the apparatus its desirable features. After that, the assembly processes of all the systems are explained. The next step is the testing process of the systems that analyzes and optimizes their performance. At the end, the experimental outcome of this research is presented. In conclusion, partial success in spraying 300 to 700 $\mu$ m copper droplets is achieved. These results are evaluated and their influencing factors are discussed. Further improvements in orifice mounting and prevention of degassing from the crucible and insulation need to be considered for consistent success.

Thesis Supervisor: Dr. Jung-Hoon Chun

Title: Professor of Mechanical Engineering

## ACKNOWLEDGEMENTS

I would like to express my sincere gratitude to my advisor Prof. Jung Hoon Chun for his outstanding guidance and insightful remarks. This work wouldn't become possible without his understanding, support, encouragement, and patience.

I must also thank Dr. Wayne Hsiao, my predecessor in the DBM lab. He is the one who introduced me to the UDS technique, explained to me all the process tricks and helped me in taking the right steps in building the new apparatus. I owe him the most part of my knowledge in this research area.

Special thanks to Profs. Pierre Azouri, Nesreen Ghaddar, and Alan Shihadeh, of the ME Department of the American University of Beirut (AUB). I had a wonderful time attending their classes and seminars at AUB. They were the most to encourage me to consider a graduate program at MIT, and supported me with their letters of recommendations on top of that.

I will never forget the wonderful dinners and events that I had with my host family (a program arranged by the International Student Office, *ISO* at MIT). Dr. Amin and Dr. Amal Arnaout were my extended parents and provided me with all love and care. I appreciate their generous hosting that made me forget that I am away of my home. Also, I enjoyed the time I spent with Dr. Rima and especially Dr. Rami at the athletics center and basketball courts.

In this occasion, I express my deep recognition to my mother Mrs. Fadwa Bouji who was watching me since my early childhood. Her sincere love and concern about my education and future were the main incentive behind all my achievements and success...

I also express my merits to my father, Mr. Khaled Joumaa whose wood shop was my first place to get in touch with some basic manufacturing processes and gain tendency toward mechanical engineering.

I wish the best of luck for Dr. Kyung Yoon Noh and Mr. Kristof Kopanski, my sincerest friends and wonderful officemates. I will always remember the fun and joy we used to share.

My sincere thanks go to all the generous technical representatives of the companies I have dealt with. I appreciably mention Mr. Paul Oranges of the US Huttinger, Mr. Micheal Krupitzer of Kurt Lesker and Mr. Greg Golowski of IR Chino. They all helped me in selecting and testing the crucial equipment of my system.

Mr. Mark Belanger and Gerald Wentworth (senior technicians of the LMP machine shop) helped me in machining some necessary parts. Their aid was crucial for the successful operation of our system.

Special “thank you” to Ms. Leslie Regan (ME Graduate office), Ms. Catherine Nichols, and Ms. Lisa Falco (current and ex. Prof. Chun’s Office assistant) for their excellent administrative assistance.

Finally, I wish a prosperous and joyful future to my brother Ghassan, my sister Ghaida’a and her husband Mr. Samer Sadek. All three were wonderful in remembering me in the past two years with the funny tales and news they used to bring up ...

# TABLE OF CONTENTS

TITLE PAGE .....	1
ABSTRACT.....	2
ACKNOWLEDGEMENTS.....	3
TABLE OF CONTENTS.....	5
LIST OF FIGURES .....	9
LIST OF TABLES.....	14
1. INTRODUCTION .....	15
1.1 Background and Problem Identification .....	15
1.1.1 UDS application.....	16
1.1.2 Rayleigh instability theory.....	17
1.1.3 Typical UDS practice and apparatus.....	18
1.2 Research Objective and Motivation.....	22
1.2.1 UDS system improved characteristics .....	22
1.2.2 New apparatus implementations.....	23
2. THE UDS APPARATUS DESIGN.....	25
2.1 Heating Supply.....	26
2.1.1 The generator .....	28
2.1.2 The oscillator .....	29
2.1.3 The coil .....	30
2.2 Temperature Measurement .....	32
2.2.1 Radiation review .....	32
2.2.2 Pyrometer description .....	34
2.3 The Closed Loop Temperature Control .....	35
2.3.1 The controller.....	36
2.3.2 The input/output connections.....	37
2.4 The Crucible Set .....	40
2.4.1 The melt container .....	40
2.4.2 The insulation.....	44

2.4.3	The sealing .....	48
2.5	The Vibration System .....	49
2.5.1	The function generator .....	50
2.5.2	The amplifier.....	51
2.5.3	The vibrator and oscilloscope .....	52
2.5.4	The vibration rod.....	53
2.6	The Charging System.....	54
2.6.1	The voltage supply .....	55
2.6.2	The charging plate.....	56
2.7	The Imaging System .....	56
2.7.1	The stroboscope .....	58
2.7.2	The camera assembly .....	60
2.8	The Gas Management System .....	61
2.8.1	The source part.....	62
2.8.2	The control panel .....	64
2.8.3	The chambers part.....	69
2.8.4	The evacuation part.....	73
2.9	Vacuum Parts .....	75
2.9.1	Vacuum sealing techniques.....	76
2.9.2	Heating chamber .....	79
2.9.3	Top plate .....	80
2.9.4	Powder collection chamber.....	81
2.9.5	Bottom plate and collection cup .....	83
2.10	The water Cooling System.....	85
2.10.1	The recirculator unit.....	85
2.10.2	The water channels .....	88
2.11	The Frame and Hoisting System.....	90
2.11.1	The main frame .....	90
2.11.2	The powder collection chamber and secondary frames.....	91
2.11.3	The hoist.....	92

3.	THE UDS SYSTEMS ASSEMBLY .....	94
3.1	The UDS General Layout .....	95
3.2	The Crucible Assembly.....	96
3.2.1	The crucible machining.....	97
3.2.2	The crucible preparation .....	99
3.3	The Top Plate Assembly .....	101
3.4	Bottom Plate Assembly.....	106
3.5	The Coil Assembly .....	108
3.6	The Vacuum Chambers Assembly.....	110
3.7	The Gas Management System Assembly .....	113
3.8	The Imaging System Assembly .....	116
4.	THE UDS SYSTEMS TESTING .....	120
4.1	The Water cooling Test.....	121
4.1.1	Operation.....	122
4.1.2	Examination .....	122
4.2	The Induction Heater Test .....	124
4.3	The Crucible Test.....	132
4.4	The Pyrometer Test.....	138
4.5	The Oxygenmeter Calibration.....	141
4.6	The Gas Management System General Test.....	144
4.6.1	The evacuation test .....	145
4.6.2	The filling and control test.....	145
4.7	The Focus Range Test.....	146
5.	CONCLUSION.....	149
5.1	Results.....	149
5.2	The Spraying Problems.....	150
5.3	Recommendations.....	151
	NOMENCLATURE .....	155
	REFERENCES .....	157

APPENDICES ..... 159

- A Materials Data Sheet ..... 159
- B Parts Drawings ..... 180
- C Induction Heating Calculations ..... 223
- D Recirculator Flow Channels ..... 229



## LIST OF FIGURES

Figure 1.1: Several atomization methods for producing random size metallic powder [1]. .....	16
Figure 1.2: The jet breakup behavior [4]. .....	17
Figure 1.3: The current UDS system. ....	18
Figure 1.4: Schematic diagram of the current UDS apparatus [5]......	19
Figure 1.5: The UDS generator of the current apparatus [6]......	20
Figure 1.6: Principle of the new powder chamber configuration. ....	23
Figure 2.1: Schematic diagram of the high-temperature UDS apparatus. ....	26
Figure 2.2: A copper billet is being heated by induction.....	27
Figure 2.3: Schematic diagram of the induction heater. ....	28
Figure 2.4: The induction heater generator.....	28
Figure 2.5: The equivalent oscillator circuit. ....	29
Figure 2.6: The oscilloscope sitting on the main frame.....	30
Figure 2.7: The induction coil fixed inside the heating chamber. ....	31
Figure 2.8: The connection from oscillator to the RF feedthrough. ....	31
Figure 2.9: The functional layout of a ratio pyrometer [15]......	34
Figure 2.10: The pyrometer set: probe, fiber-optic cable, display, and DC adaptor. ....	35
Figure 2.11: Closed loop temperature control block diagram. ....	36
Figure 2.12: The controller displaying the actual and set temperatures. ....	37
Figure 2.13: The controller electrical connections. ....	38
Figure 2.14: Heater input connection.....	38
Figure 2.15: Controller input connection.....	40
Figure 2.16: The crucible setup of the current equipment. ....	41
Figure 2.17: Exploded section view of the multiple-piece crucible design. ....	42
Figure 2.18: residual billet removal from the crucible. (a) straight, (b) tapered.....	43
Figure 2.19: The graphite crucible.....	44
Figure 2.20: The insulation block. ....	46
Figure 2.21: The insulation blanket. ....	48

Figure 2.22: The graphite gasket supposed to seal between the top plate and insulation block..... 48

Figure 2.23: The graphite gasket is being cut from a graphite sheet. .... 49

Figure 2.24: The vibration system functional layout. .... 50

Figure 2.25: The function generator. .... 51

Figure 2.26: The amplifier. .... 51

Figure 2.27: The vibrator attached to the top plate..... 52

Figure 2.28: The oscilloscope displaying the vibrator signal. .... 53

Figure 2.29: The vibration rod before and after being assembled. .... 54

Figure 2.30: Layout illustrating the droplet charging [5]. .... 55

Figure 2.31: The voltage supply set at 3kV. .... 56

Figure 2.32: The imaging system functional layout. .... 57

Figure 2.33: The frequency divider. .... 59

Figure 2.34: The stroboscope lighting through the viewprot..... 59

Figure 2.35: The camera focusing through the viewport..... 61

Figure 2.36: Schematic diagram of the gas management system. .... 62

Figure 2.37: One of the inert gas tanks with its gages and valves. .... 63

Figure 2.38: The flow line of the filling process. .... 65

Figure 2.39: The controlling processes flow paths. .... 66

Figure 2.40: The gas control panel. .... 69

Figure 2.41: The chamber inert gas supply..... 70

Figure 2.42: The dual purpose port assembly..... 71

Figure 2.43: The crucible inert gas supply connected to the top plate. .... 72

Figure 2.44: The oxygenmeter..... 72

Figure 2.45: The pump attached to the evacuation hose..... 74

Figure 2.46: The vacuum gage displays the vacuum pressure with a timer next to indicating the time required to evacuate the system. .... 75

Figure 2.47: A CF blank port with knife edge shown..... 77

Figure 2.48: CF port with indented copper gasket on top..... 77

Figure 2.49: A QF viewport with corresponding O-ring and clamp..... 78

Figure 2.50: The ISO K seal shown with double hooking clamps pressing on the flanges. .....	79
Figure 2.51: The heating chamber. ....	79
Figure 2.52: The top plate clamped to the heating chamber by ISO F seal. ....	81
Figure 2.53: The top plate inner surface. ....	81
Figure 2.54: The powder chamber sitting on its frame. ....	82
Figure 2.55: The upper flange of the chamber with waste cup support and linear motion feedthrough. ....	83
Figure 2.56: The waste cup is placed inside or removed from the powder chamber via the ISO port. ....	83
Figure 2.57: The bottom plate clamped to the powder chamber. ....	84
Figure 2.58: The collection cup clamped to the bottom plate. ....	84
Figure 2.59: The recirculator unit. ....	86
Figure 2.60: The cooling processes inside the heat exchanger. ....	87
Figure 2.61: One of the manifolds (inlet or outlet). ....	88
Figure 2.62: The cooling water supply channels. ....	89
Figure 2.63: The filter. ....	90
Figure 2.64: The lock nut assembly on the frame bars. ....	91
Figure 2.65: The hoist on top of the main frame, carried by the sliding beam. ....	93
Figure 2.66: The auxiliary cable rolling on the pulley fastened to the slot. ....	93
Figure 3.1: The UDS assemblies' classification. ....	95
Figure 3.2: The major UDS components arrangement. ....	96
Figure 3.3: The crucible machining processes. ....	98
Figure 3.4: The crucible preparation steps. ....	100
Figure 3.5: The top plate assembly. ....	102
Figure 3.6: The top plate assembly exploded view. ....	103
Figure 3.7: The steps taken in the top plate assembly. ....	105
Figure 3.8: The top plate assembly section view. ....	106
Figure 3.9: The bottom plate section view. ....	107
Figure 3.10: The bottom plate assembly steps. ....	108
Figure 3.11: The coil assembly elements configuration. ....	109

Figure 3.12: The coil assembly steps.....	109
Figure 3.13: The powder chamber fixed on the frame.....	111
Figure 3.14: The vacuum chambers assembly steps.....	112
Figure 3.15: Powder chamber is lifted and attached to the heating chamber. ....	113
Figure 3.16: The gas panel front plate. ....	114
Figure 3.17: The assembled control panel. ....	115
Figure 3.18: The control panel nomenclature.....	116
Figure 3.19: The camera assembly. ....	117
Figure 3.20: The stroboscope assembly.....	118
Figure 3.21: The stroboscope lighting into its viewport. ....	119
Figure 4.1: The UDS systems testing roadmap. ....	121
Figure 4.2: Checking the flowmeter indicator.....	123
Figure 4.3: Checking water leakage from supply and return manifolds.....	123
Figure 4.4: A typical DC resistive heating circuit. ....	124
Figure 4.5: Power flow line of the induction heater machine.....	125
Figure 4.6: The modeling circuit of the induction heating elements in case of a conductor crucible.....	126
Figure 4.7: The current flowing in the billet is opposite in direction to the one flowing in the coil as to satisfy Lenz's law [12]. ....	127
Figure 4.8: The equivalent circuit of the heater.....	128
Figure 4.9: The transfer efficiency plot as function of frequency for two different crucible material; case (a): graphite; case (b): quartz or other electrically insulator material. .....	129
Figure 4.10: A capacitor is being removed to enhance matching.....	130
Figure 4.11: The precoil is adjusted to have matching. ....	131
Figure 4.12: The induction heater display. ....	132
Figure 4.13: Heated bar: (a) unconstrained bar extends and no stresses are generated; (b) bar is constrained and compressive stresses take place. ....	134
Figure 4.14: Alumina crucible failing to contain molten copper.....	137
Figure 4.15: Actual and theoretical radiations.....	138
Figure 4.16: The process flowchart of the pyrometer test in the measurement mode. ...	140

Figure 4.17: The oxygenmeter test setup..... 142

Figure 4.18: The oxygenmeter calibration process..... 144

Figure 4.19: The inlet valve closure. .... 144

Figure 4.20: The vacuum gage displaying the vacuum pressure with timer showing the  
time to reach that pressure. .... 146

Figure 4.21: The focus range test setup. .... 147

Figure 5.1: Copper droplets collected from the UDS apparatus..... 150

Figure 5.2: Recommendation of implementing different orifice mounting setup. .... 151

Figure 5.3: The plan of crucible guarding. .... 153

## LIST OF TABLES

Table 1.1: UDS based processes and their advantages.....	16
Table 1.2: The typical operating range of the UDS components.....	21
Table 2.1: The crucible geometrical design criteria.....	42
Table 2.2: The heat loss results.....	45
Table 2.3: Heating chamber ports' characteristics.....	80
Table 4.1: Effects due to changes in the oscillator circuit. ....	132
Table 4.2: The plate stress analysis.....	135
Table 4.3: The cylindrical stress analysis for boron nitride.....	135
Table 4.4: The cylindrical stress analysis for graphite. ....	136
Table 4.5: The cylindrical stress analysis for quartz.....	136
Table 4.6: The experimental results of the pyrometer test.....	141
Table 4.7: The evacuation-filling test results.....	146

# Chapter 1

## INTRODUCTION

### 1.1 Background and Problem Identification

Numerous metal powder production processes were developed and used in industry [1]. These processes are mainly categorized according to the mechanisms for the droplets' generation. Among these processes, the "atomization" is a well known droplet generation process that has been implemented as shown in Figure 1.1 producing droplets in a wide range of size, velocity, and temperature, the issue that makes it unsatisfactory for some manufacturing necessities [2]. Another powder production process is the "uniform droplet spraying" (UDS) process which could also be implemented by several means. One of these means is the "continuous jet" breakup, a process driven by the Rayleigh jet instability theory, producing droplets of uniform size. The object of this thesis is to build a UDS apparatus for metals with melting points exceeding 1000°C, such as copper.

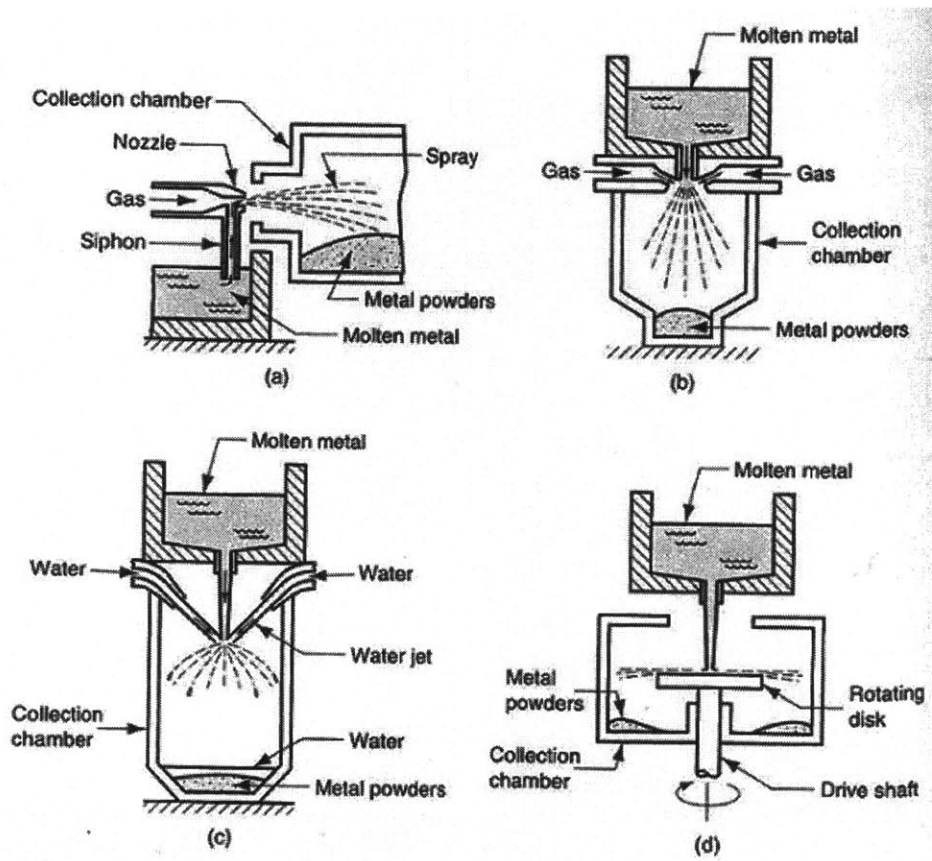


Figure 1.1: Several atomization methods for producing random size metallic powder [1].

### 1.1.1 UDS application

The major applications that employ the UDS along with their advantages are summarized in Table 1.1.

Table 1.1: UDS based processes and their advantages.

Applications	Advantage
The production of solder balls 300-750 $\mu$ m in diameter which are used in the ball grid-array (BGA) electronics packaging technology [3].	The BGA packing technology has reduced the size of electronic components without altering their performance [3].
The spray forming process which produces near-net-shape prototypes by spraying and then accurately depositing micron-sized droplets onto a well guided target [2].	Rapid prototyping of the model to generate parts of high strength with no need of post-treatment if they were sprayed by the same material of their fully functional parts [2].



### 1.1.2 Rayleigh instability theory

The phenomenon of “capillary instability” occurs when a liquid jet fails to maintain itself and breaks into droplets after being exited from an orifice. Lord Rayleigh analyzed this phenomenon and pointed out that a liquid jet could be broken into uniform droplets if it were subjected to a periodic oscillation of wavelength sufficiently greater than the jet diameter [4]. The perturbation initiated at the nozzle exit (orifice) will propagate sinusoidally in space and grow exponentially with time until breakup resulting in the droplet generation. Figure 1.2 shows how the molten jet breaks into droplets.

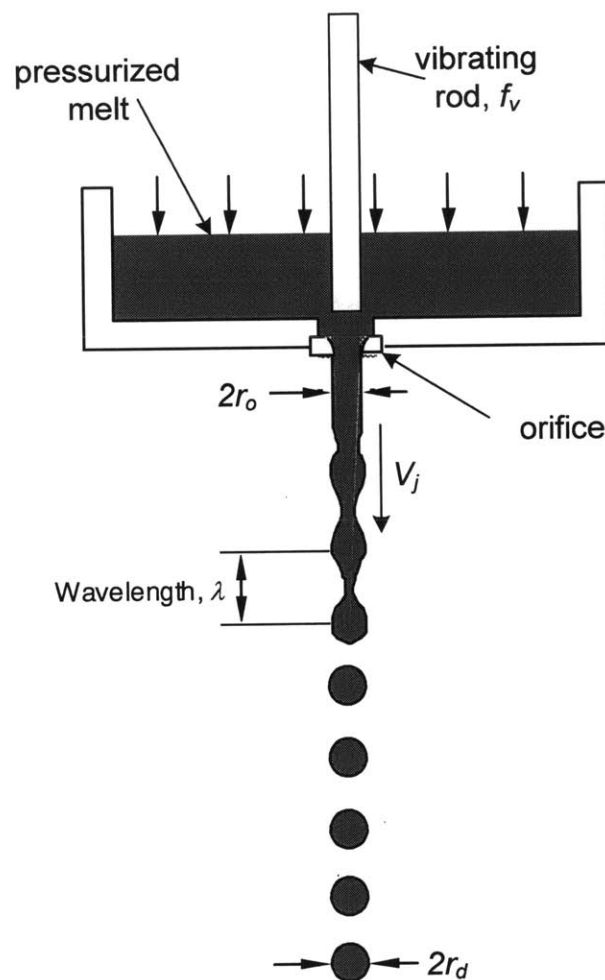


Figure 1.2: The jet breakup behavior [4].

The droplet diameter  $d_d$  is obtained by:

$$d_d = 2r_d = \left( \frac{6r_o^2 V_j}{f_v} \right)^{1/3} \quad (1.1)$$

where  $f_v$  is the frequency of the vibrating rod,  $2r_o$  is the orifice diameter,  $V_j$  is the jet exit velocity. The typical droplet size generated by the UDS process ranges from 100 to 800 $\mu$ m. Also the breakup wavelength  $\lambda$ , which defines the distance between two successive droplets directly after breakup is obtained by

$$\lambda = \frac{V_j}{f_v} \quad (1.2)$$

The wavelength typically varies between 0.5 and 1.5mm.

### 1.1.3 Typical UDS practice and apparatus

Chun and Passow (1992) have developed the first UDS apparatus [2]. Figure 1.3 shows a UDS apparatus. The following part describes the apparatus major components and explains its operating procedure.

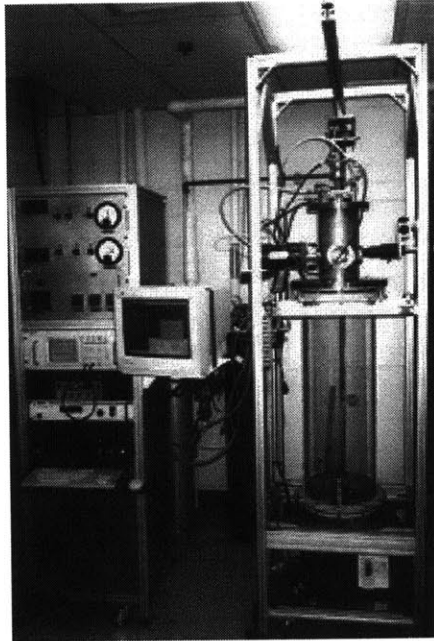


**Figure 1.3: The current UDS system.**

A schematic diagram of the entire UDS apparatus is shown in Figure 1.4. It basically consists of two main parts: the generator, shown in Figure 1.5 and the vacuum

chamber. The generator is named so because it is where the droplets are generated. Its major components are the crucible and the vibrator. The crucible is wrapped by band heaters. A thermocouple probe is immersed in the crucible for temperature measurement. A closed loop heating control for the heater maintains constant melt temperature. Spraying a high melting point material requires a different method of heating and melting. A gas inlet supplies the crucible with inert gas.

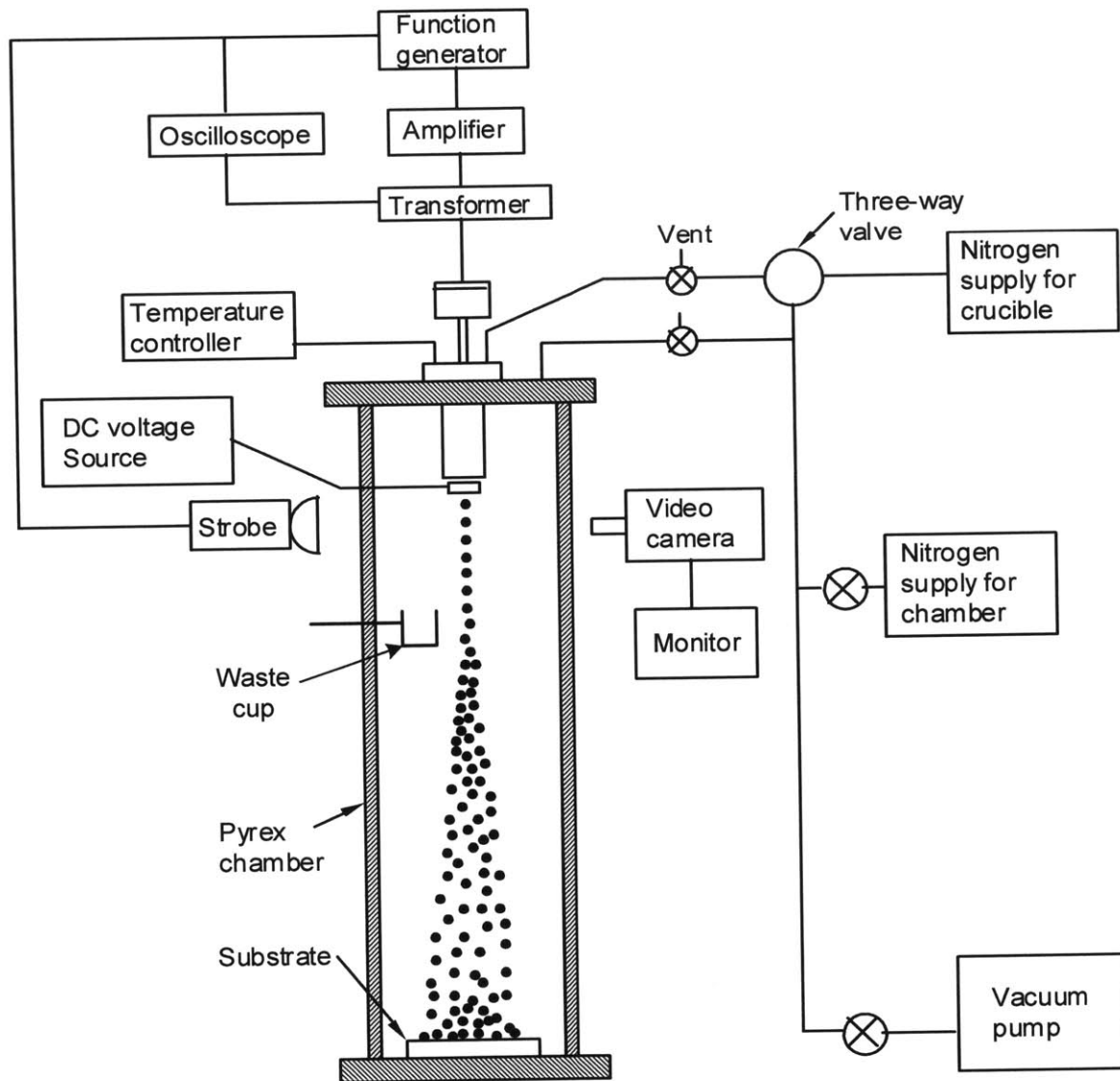
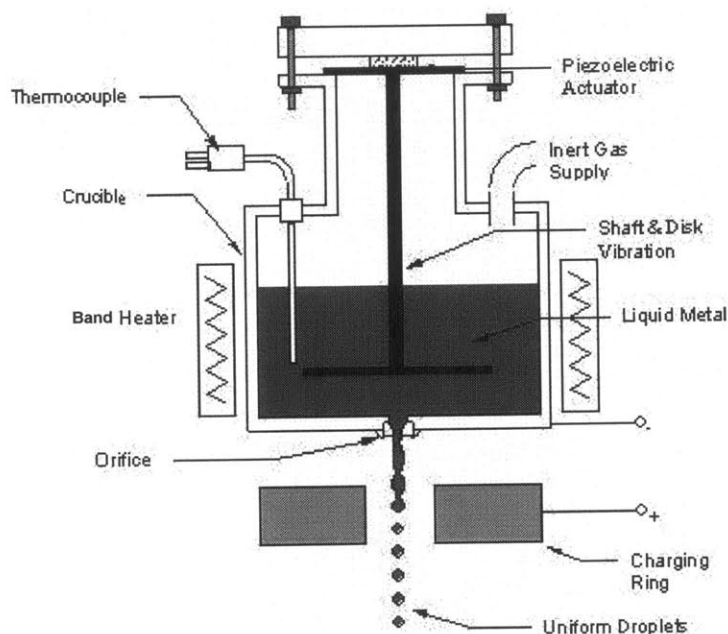


Figure 1.4: Schematic diagram of the current UDS apparatus [5].

A vibrator containing a piezoelectric actuator composed of stack of disks generates the necessary periodic oscillation that is transmitted to the liquid metal via a solid rod. Once the metal becomes fully molten, the crucible is pressurized and a stream flows out through a micron-size sapphire orifice glued to the bottom part of the crucible. Since periodically disturbed by the vibration shaft, the stream obeys the Rayleigh's jet instability theory and breaks into uniform-size droplets. In order to prevent droplet merging afterwards, a high voltage charging plate is fixed to the bottom of the crucible and charges the droplets instantly at their formation forcing them to repel each other by electrostatic interaction. The vacuum chamber used in the current apparatus is a Pyrex glass hollow cylinder. The chamber, as part of the apparatus, needs to be filled with inert gas ( $N_2$ , Ar, or forming gas) to prevent metal oxidation that itself prevents breakup. For example, spraying a very reactive material like aluminum requires a much cleaner (oxygen content < 40ppm) environment than that the solder alloy (Sn 63% wt, Pb 37%wt) requires (oxygen content < 200ppm) [5]. This chamber contains a waste cup in the upper part; this is where molten metal accumulates during unstable breakup or in case of undesirable spraying.



**Figure 1.5: The UDS generator of the current apparatus [6].**

**Table 1.2: The typical operating range of the UDS components.**

Current UDS apparatus parameters	
crucible capacity, mL	100
thermocouple type	K
heaters power, kW	1.5
vibrating frequency, kHz	0.5-5
time to melt, min.	5-10
driving pressure, kPa	10-60
orifice diameter, $\mu\text{m}$	50-400
jet velocity, m/sec	3-6
charging voltage, kV	3
chamber diameter, cm	30
chamber length, cm	100
forming gas constituents	95%N <sub>2</sub> + 5%H <sub>2</sub>
piezoelectric material	lead zirconate titanate

Generated powder is collected in a collection cup at the bottom of the chamber. This collection medium is set according to the droplet thermal state, liquid or solid. A monitoring system is provided to better observe the breakup. This system comprises a stroboscope and a CCD camera facing each other and placed each at one side of the chamber. Finally, as a supporting feature, the addition of a droplet size control system maintains the droplets' size variation to less than 3% [3]. The typical values of some operational parameters for the several UDS parts mentioned above are listed in Table 1.2.

Several UDS systems were later built but were much similar to this original one. However, high-temperature processes (above 1000°C) and experiments can't be performed on this apparatus mainly due to the limitations of the heater and crucible. The need to build a new system that performs high temperature processes is the aim of this research. New systems must be installed to achieve this goal. The following section interprets the UDS innovations and the role they play in the practical implementation of the research which is the production of uniform size copper powder.

## **1.2 Research Objective and Motivation**

This section explains the major points behind the fabrication of the new UDS apparatus. The design concept of this system will not be simple because its requirement is much higher in temperature handling capability. The appropriate applications, that need to be included in the new system in order to reach the set goals, are then described. The basic research objective is not only to build the new system but to try to provide an easy to operate feature for various research tasks.

### **1.2.1 UDS system improved characteristics**

This high temperature UDS apparatus whose design layout is shown in Figure 1.6 should have the ability to handle many experiments while minimizing the number of the required components for the apparatus. Therefore, a modular system approach is adopted. Several experiments involving droplet deflection and high speed (50m/sec) impact experiments are possible to perform with the current setup. The main objective of this research is to be able to spray high melting point metals such as Cu in the cleanest possible environment. The copper melting requires a new crucible of material that withstands this high temperature, resists the generated thermal stresses, along with maintaining the chemical inertness and corrosion resistance that are substantial for preserving the melt's purity. Second, the heating method should be changed in order to reduce melting time and minimize heat losses. Induction heating is used for this purpose. Third, the temperature measurement process implemented in the high-temperature UDS is indirect; it extends the range of measurement without affecting its accuracy and maintains the melt's purity with its remote probe. Moreover, an independent closed loop temperature control is designed and built to maintain constant melt temperature at spraying. Finally, the environment inertness is characterized by a better chamber evacuation ( $P_{\text{vacuum}} < 30\text{millitorr}$ ) resulting in a lower oxygen content ( $\text{O}_2 \text{ conc.} < 30\text{ppm}$ ). These conditions are to guarantee the successful spraying of reactive metals and a stable breakup.

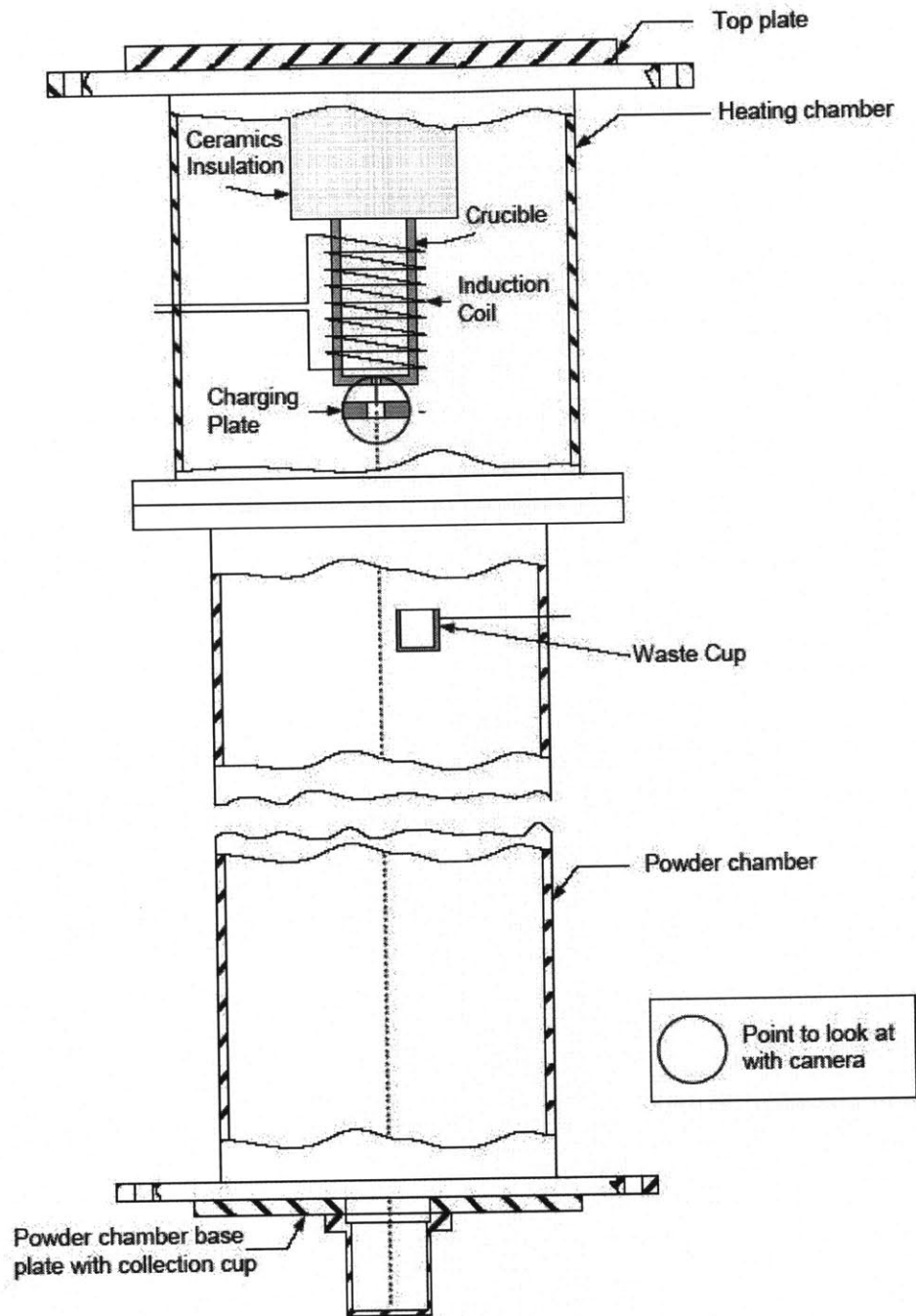


Figure 1.6: Principle of the new powder chamber configuration.

### 1.2.2 New apparatus implementations

As noticed, the improvements specified in Section 1.2.1 did not alter the basic principles that trigger the process in the current apparatus. All what is sought is to

implement more difficult-to-use materials and devices that could achieve the desired functions. To ease the process of understanding of all these materials and devices, the new system is divided into many subsystems, each discussed on its own. For example, the heating method, temperature measurement method and gas management are all subsystems of the new UDS apparatus. The plan followed in this thesis first describes and explains the design steps of all the subsystems involved, then it emphasizes their concepts and the advantages they bring to the UDS apparatus. The systems assembly is the second step. Separate testing and optimization of each system is then carried out before the final operation of the apparatus.



## **Chapter 2**

### **THE UDS APPARATUS DESIGN**

As mentioned in Chapter 1, the apparatus is composed of many subsystems that will be simply called “systems”. This chapter goes through all the systems, describes their components, explains the way they work, and shows interactions among each other. This method of analysis eases the understanding of the systems assembly and testing processes that are discussed in the coming chapters. The UDS apparatus has eleven systems; their components were built or purchased separately. The design concept offers the opportunity to work on a system independently from another, while taking into consideration some constraints. The systems are listed below:

- 1 – Heating supply
- 2 – Temperature measurement
- 3 – Temperature control
- 4 – Crucible
- 5 – Vibration source
- 6 – Charging
- 7 – Imaging
- 8 – Gas management
- 9 – Vacuum parts
- 10 – Water cooling
- 11 – Frame and hoisting

A schematic diagram of the high temperature UDS apparatus with all systems labeled with their corresponding numbers as shown in the above list, is shown in Figure 2.1.

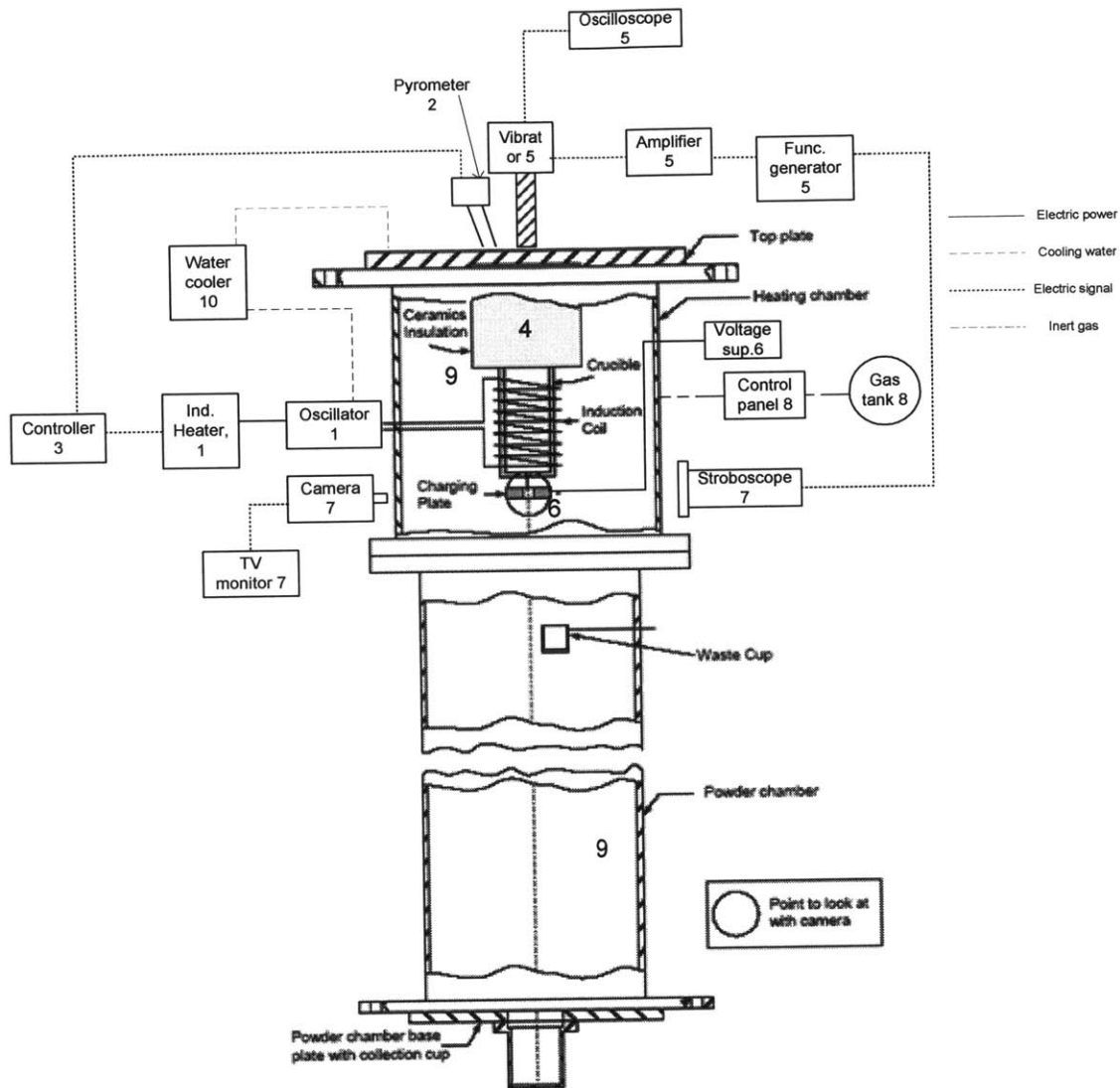
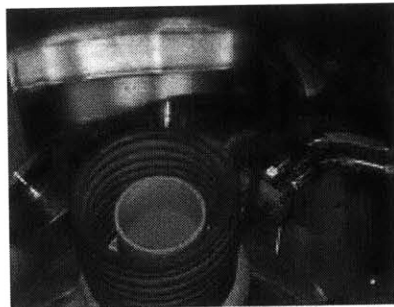


Figure 2.1: Schematic diagram of the high-temperature UDS apparatus.

## 2.1 Heating Supply

The main change brought to the new UDS system is the use of an induction heating supply. Resistive band heating cannot be used to melt copper. Band heaters in the current system function in the following way: electric current passing through the bands wrapped around the crucible, heat them up by Joule Effect. Part of this heat is conducted through the crucible walls and then transferred to the billet required to be melt. But since the conduction rate is slow, the heating elements will burn off if the input power is increased

to melt copper. Induction heating however implements the concept of electromagnetic induction to heat matter. A conductive coil of many turns is passed by an alternating current, thus an alternating (sinusoidally time variant) magnetic field is generated mainly inside the coil (Ampere's law). The magnetic flux of that field varies with time and thus *induces* a voltage across any object subject to it (Faraday's law). If a conductive billet is placed inside the coil, the induced voltage will generate electric current passing through it that heats it up by simple Joule effect. Induction heating is then able to transfer power from source (coil) to sink (billet) without the intervention of a secondary medium (crucible) as is the case with band heating. Figure 2.2 shows a typical induction heating setup. The heating becomes more concentrated on the billet as long as it is the only electrically conductive element influenced by the magnetic flux variation.



**Figure 2.2: A copper billet is being heated by induction.**

If the billet container (crucible) were electrically conductive, it would be heated too by induction, thus making all the advantages thought to be gained by induction heating vanish. For this reason, only ceramics (electrically insulator) were considered as possible materials to make the crucible.

An important point to mention is that metals with high magnetic susceptibility such as steel are very well heated not to say dangerously, by induction heating. This is because their own magnetic field will align itself with that of the coil and build up higher values of flux and induced voltage that intensifies the heat generated [14]. Because of that, the heating chamber is purposely made of 304 stainless steel which is susceptible to electromagnetic induction to a very low extent. In conclusion, no part placed inside the heating chamber is made out of steel or any high magnetic susceptibility material.

The induction heater installed in the UDS apparatus has a maximum output power 10 kW. The induction heater unit is composed of three main parts: the generator, the oscillator and the coil. Their function and description are the topic of the following subsections. A schematic diagram of the induction heater is shown in Figure 2.3.

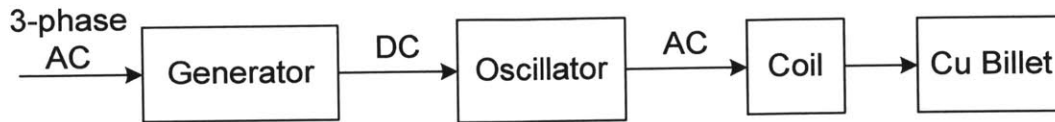


**Figure 2.3: Schematic diagram of the induction heater.**

### 2.1.1 The generator

The generator is the bulkiest and heaviest part of all equipment installed in the new UDS system. It is placed next to the main frame as shown in Figure 2.4 but raised from ground by wooden stand-up bars to a sufficient distance (10cm) to avoid electric shock problems in case of water flooding or wire fusion.



**Figure 2.4: The induction heater generator.**

This unit has the user interface, display screen, mains power input, and controller connections. The generator takes electric power from the mains supply (3-phase, AC power), converts it to DC power with user able to control voltage, current, or power values. These parameter values could also be set by built-in functions in case a closed loop control process is taking place. The analogue interfaces are used in connecting the

control circuits for melt temperature stabilization. Generated DC power is transmitted to the oscillator, with efficiency approaching 96%. Heat dissipated from the generator's inner circuits is removed by four cooling fans mounted on rear side.

### 2.1.2 The oscillator

The oscillator, as its name suggests, receives the DC power from the generator and produces the required oscillating (sinusoidally alternating) current that passes through the coil. A single generator like this one could at most feed four separate oscillators in four different heating processes. Obviously, not more than one oscillator is required for this application. For the sake of simplicity, the entire oscillator can be modeled by a simple circuit containing a DC voltage source  $V_{in}$ , an inductance  $L$ , and a capacitance  $C$  all in series as shown in Figure 2.5 [5].

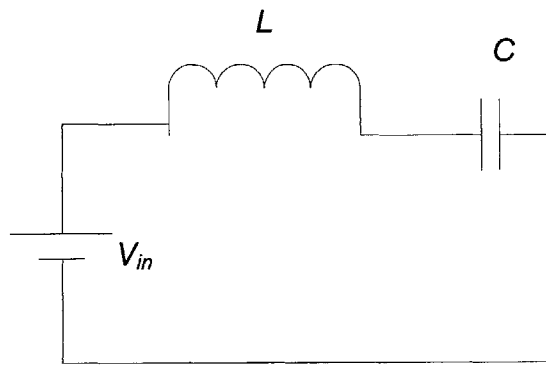
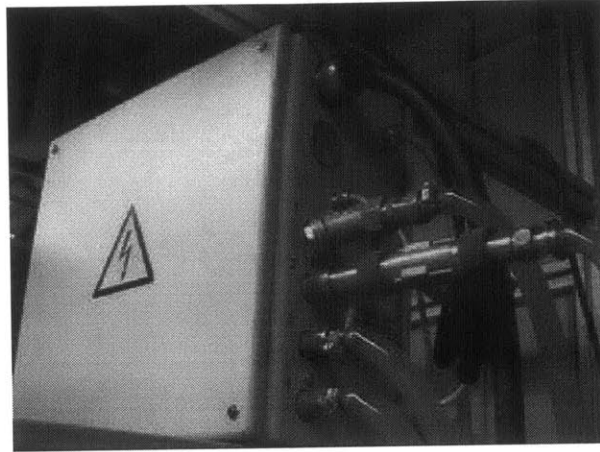


Figure 2.5: The equivalent oscillator circuit.

The DC source is supplied by the generator; the capacitance  $C$  is obtained from a stack of adjustable capacitors embedded to the oscillator; and the inductance  $L$  comes from an adjustable inductor “precoil” mounted in the oscillator and placed in series with the non-adjustable inductance: the coil. All inductances and capacitances are made of copper (very low resistivity) to minimize their Joule effect losses.  $L$  and  $C$  are made adjustable because the alternating current flowing in the circuit has frequency  $f$  that depends on their values as

$$f = \frac{1}{2\pi\sqrt{LC}} \quad (2.1)$$

This frequency is the same as that of the magnetic flux variation and the induced voltage. Its value plays a major role in optimizing the power transfer to the billet. This problem is known as “matching” and its key parameters are not just  $L$  and  $C$ , but many other geometrical, physical and electrical parameters involved in the induction heating process. This problem is discussed in details in Section 4.2. The oscillator has its own stand on the main frame where it sits close to the heating chamber as shown in Figure 2.6.



**Figure 2.6: The oscilloscope sitting on the main frame.**

### **2.1.3 The coil**

The coil is the last part where electric power circulates before being transferred to the billet. It is placed in the middle of the heating chamber as shown in Figure 2.7. The coil is circulated by a large current, and like any other conductor, it will be subject to severe Joule heating. In addition, the coil is placed completely around the hot crucible, and thus surface radiation heats it up and dangerously raise its temperature. Water cooling is therefore a must to remove all that heat. The coil has a helical shape hollow tube (6.3mm) so that water could flow inside. The coil material is intentionally chosen to be copper (low electrical resistivity) in order to reduce the Joule heating loss.

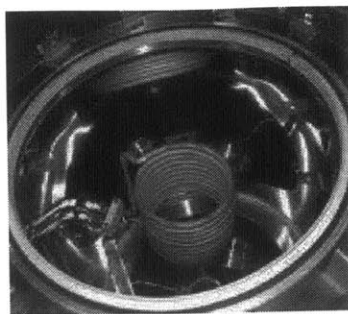


**Figure 2.7: The induction coil fixed inside the heating chamber.**

The oscillator is also subject to heating because of its inner electric circuits. The oscillator has its own water cooling loop. The coil cooling water, although flowing in an independent loop, is first supplied to the oscillator which then bypasses it to the coil along with transferring the electric power. This dual transfer takes place through the radio frequency (RF) feedthrough which connects the oscillator to the coil. The RF feedthrough has a CF 7 flange connection it is fastened to one of the chamber CF ports (see Table 2.3). This feedthrough has two copper tubes that are concentrically adhered to two alumina cylindrical shields. The shields insulate between the tubes and the remaining part of the feedthrough. The tubes' vacuum ends are connected to the coil ends with swagelok connectors; the same applies to the air-side ends which are connected to the oscillator outer ports as shown in Figure 2.8. The entire RF feedthrough-oscillator connection is covered with acrylic (polymer) half tubes wrapped around the CF flange as a safety precaution.

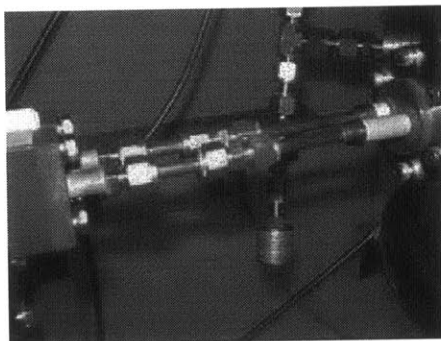


**Figure 2.8: The connection from oscillator to the RF feedthrough.**

Concerning the coil fixture inside the chamber, alumina twin holders (two identical portions) were especially made for this task. Once assembled, the two portions hold the coil via its tube ends that are inserted into the holders' cavities. The holders are fastened by two screws to a stainless steel link fixed to one of the heating chamber bracket. The coil assembly is discussed in details in Section 3.5.

## 2.2 Temperature Measurement

The temperature measurement technique is one of the innovations employed in this UDS apparatus. As previously explained, thermocouple immersion in the melt is not applicable in this situation. The electromagnetic induction in the thermocouple conductive material is a potential problem that justified the use of another technique to measure temperature. Optical pyrometry is the right solution to all these problems. Optical pyrometry is an indirect method for temperature measurement: it relies on the surface radiated energy to predict the temperature. This remote sensing method does not require a physical contact between the melt and the probe as it is the case with other thermometers (thermocouple, resistance thermometers...). However an optical contact (straight transparent path) must be preserved to ensure that radiated heat from the surface reaches the probe (pyrometer) without any interference. The mechanism of predicting the surface temperature from radiated heat requires a brief review of some radiation basics. This review eases the understanding of the probe mode of operation that will be discussed later.

### 2.2.1 Radiation review

All surfaces at all temperatures emit radiation. The radiant power density  $L(\lambda, T)$ , and total emitted heat  $Q(T)$  are expressed as follows [14].

$$L(\lambda, T) = \varepsilon(\lambda, T) \times \frac{C_1}{\lambda^5 (e^{C_2/\lambda T} - 1)} \quad (2.2)$$

$$Q(T) = \int_0^{\infty} L(\lambda, T) d\lambda = \varepsilon_{av} \sigma T^4 \quad (2.3)$$



where  $\lambda$  is the wavelength,  $T$  is the temperature,  $C_1$  is the first Planck's constant,  $C_2$  is the second Planck's constant,  $\sigma$  is Stefan-Boltzmann constant,  $\varepsilon(\lambda, T)$  is the emissivity at the given temperature and wavelength, and  $\varepsilon_{av}$  is the wavelength average emissivity.

“Single-color” pyrometers rely solely on the value of the power density  $L(\lambda, T)$  to determine the temperature. The main issue that makes pyrometry subject to measurement uncertainties is the lack of knowledge of the exact value of the emissivity. Pyrometers are blind to surface emissivities; it is up to the users to predict them correctly if they wish to obtain exact measurements. In this UDS process, the measured temperatures range from 25°C to 1100°C; knowledge of the surface emissivity over this wide range is practically impossible. Even if found, the emissivity-temperature curve can't be input to the pyrometer since pyrometers only accept one value of emissivity (it will be the average one in this case), and the billet temperatures will be measured according to this value.

The pyrometer installed in this UDS apparatus is however not a single-color one. A better pyrometer than single-color pyrometer is called two-color pyrometer. A color in this context means a wavelength (in the visible range, every color emits radiation at a specific wavelength). The remaining part of this section discusses how a two-color pyrometer is better than single-color one.

A grey body is a special type of non-black-body with emissivity independent of wavelength. Therefore  $\varepsilon(\lambda, T) = \varepsilon(T)$ . The radiation calculation of grey bodies becomes simpler because of that. The total emitted power for grey bodies is rewritten as

$$P(T) = \int_0^{\infty} L(\lambda, T) d\lambda = \varepsilon(T) Q(T) = \varepsilon(T) \sigma T^4 \quad (2.4)$$

A two color pyrometer which is better used with grey bodies, detects power density at two different wavelengths  $\lambda_1$  and  $\lambda_2$ , thus,

$$L_1(\lambda_1, T) = \varepsilon(T) \times H_1(\lambda_1, T) \quad (2.5)$$

$$L_2(\lambda_2, T) = \varepsilon(T) \times H_2(\lambda_2, T) \quad (2.6)$$

where  $H(\lambda, T)$  is the black body radiant power density. The emissivity is still present but when taking the ratio of  $L_1$  to  $L_2$ , the emissivity vanishes as noticed below

$$R_T = \frac{L_1}{L_2} = \frac{\varepsilon(T) H_1(\lambda_1, T)}{\varepsilon(T) H_2(\lambda_2, T)} = \frac{H_1(\lambda_1, T)}{H_2(\lambda_2, T)} \quad (2.7)$$

and the temperature is determined as follows

$$T = \frac{C_2 \left( \frac{\lambda_1 - \lambda_2}{\lambda_1 \lambda_2} \right)}{\ln \left( R_T \left( \frac{\lambda_1}{\lambda_2} \right)^5 \right)} \quad (2.8)$$

The ratio equation (Eq. 2.7) best describes the main concept behind the two-color pyrometer which is also called “ratio” pyrometer. It is because the body is assumed grey that the emissivity was simplified. The emissivity dependence on temperature does not affect the above technique. But how accurate can a copper billet be assumed to be a grey body? Results from literature included in Appendix A.11 show that it is very accurate to consider solid copper as a grey body [15]. Molten copper however is not very grey. Nevertheless, the temperature measurement is more focused in the solid range where the control process is active. Errors in molten stage are less harmful to the overall process.

### 2.2.2 Pyrometer description

The ratio pyrometer functional layout is shown in Figure 2.9. The radiating metal is exposed to the pyrometer. A lens is mounted at the front where total radiation (of all wavelengths) is converged and collected. The radiation is transmitted via a light pipe (fiber-optic cable) as optic waves. In the thermometer, the entire radiation is filtered by a band pass filter where only radiation of wavelengths very close to a set value of  $\lambda_1$  (0.9 $\mu\text{m}$ ) and another value  $\lambda_2$  (1.5 $\mu\text{m}$ ) are allowed to pass. The two detectors measure the intensities and output their values to a divider to later find the temperature.

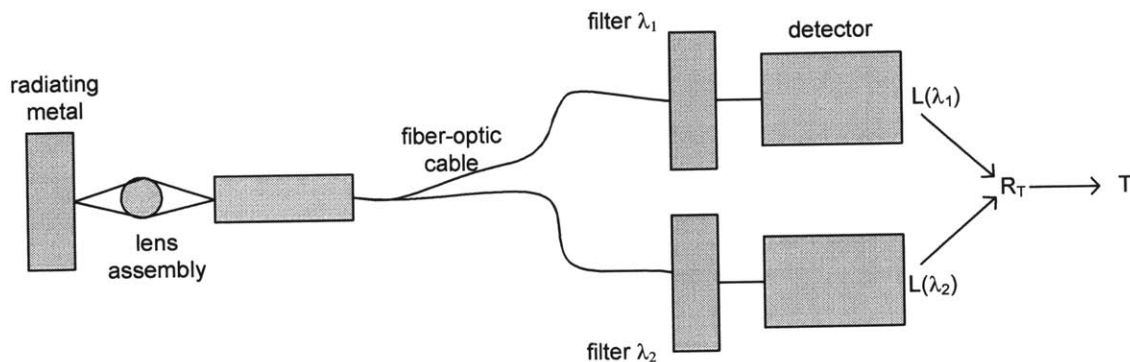
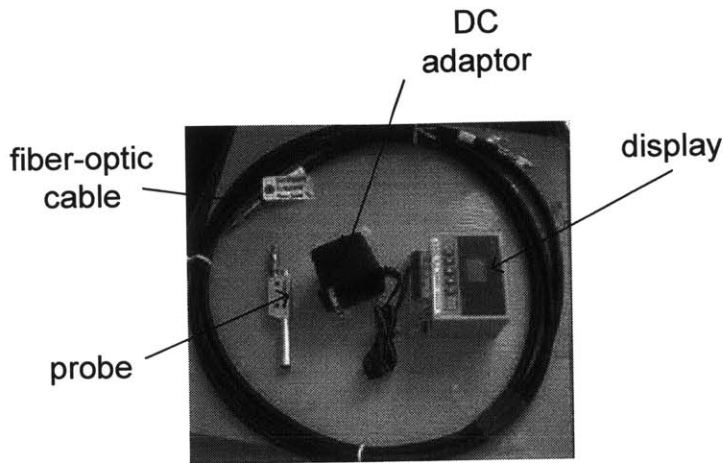


Figure 2.9: The functional layout of a ratio pyrometer [15].



**Figure 2.10: The pyrometer set: probe, fiber-optic cable, display, and DC adaptor.**

Physically, the pyrometer is made of three parts, all shown in Figure 2.10:

- 1 – The probe contains the converging lens. It is mounted by a special holder on the optical viewport. The viewport is made of transparent quartz passing most wavelengths.
- 2 – The fiber optic cable that transmits the generated electromagnetic waves to the thermometer.
- 3 – The thermometer which contains the user interface, display screen, and control connections.

The temperature range of the pyrometer is between 700 and 2000°C. It runs on 24V DC power supply. In order to be integrated in the control loop, the pyrometer outputs an electric signal (current) ranging from 4 to 20mA; this current varies linearly with the measured temperature. Section 2.3 elaborates how the pyrometer and heater are integrated in the temperature control loop.

### **2.3 The Closed Loop Temperature Control**

The process of heating, melting, and maintaining the melt at stable temperature requires the correlation between the induction heater (heat source) and pyrometer (temperature measurement). The DC power reaching the oscillator, which affects the heat supplied to the copper billet, could be manually adjusted from the induction heater user interface.

This straightforward control method is useful in testing the heater and other systems of the UDS. However, during spraying, the user is more concerned about the jet stabilization and uniform breakup; temperature adjustment becomes a secondary task at that point. The presence of a closed loop temperature control solves this problem. The induction heater has many digital and analogue input ports and it could also be operated by software programs in case special heating events are to be implemented (sequences of heating and cooling for example). The UDS temperature control closed loop is achieved by using an analogue port whose voltage difference triggers the DC power sent to the oscillator. This voltage difference varies between 0 (0% of DC power) and 10V (100% of DC power).

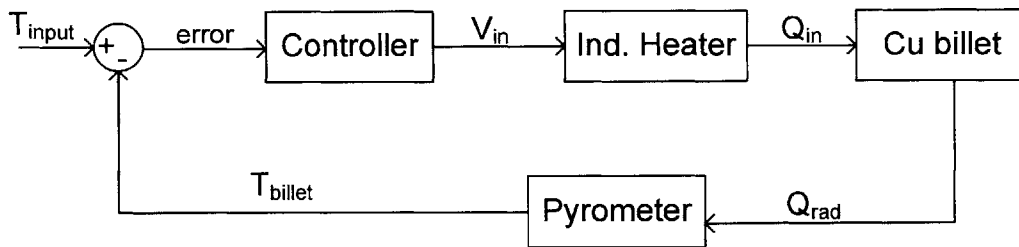


**Figure 2.11: Closed loop temperature control block diagram.**

The implemented control loop shown in Figure 2.11 is similar to any simple feedback control loop. It has four main elements or blocks (sensor, controller, comparator and plant), and four main signals: measured, desired, error and activation. All elements were previously discussed except the controller which will be described in the following section.

### 2.3.1 The controller

The controller manipulates the error signal to generate the necessary triggering signal to the heater. The important factors that determine the type of controller needed for any control application are the steady state accuracy, response time, and overshoot. The UDS process has considerable tolerances in all three criteria. As a proof, extending the heating and melting time by roughly 5% from the ideal theoretical time or going to

temperatures above the set ones by few degrees will not cause any problem to the spraying process. Unusual in control analysis, the control loop elements of Figure 2.11 were not modeled by their Laplace transforms for two reasons: first, the modeling is difficult because of the many complex non-linear operations, and second it is not helpful since the focus is on the process outcomes and not the process dynamics. A standard proportional plus integral plus derivative (PID) controller is chosen for this application. PID controllers have zero steady state error when operating with first-order systems [5]. The controller is powered by a separate voltage supply of 120V AC. Its display screen and user interface are shown in Figure 2.12.



**Figure 2.12: The controller displaying the actual and set temperatures.**

### **2.3.2 The input/output connections**

The connections made to the controller will now be discussed. As noticed from Figure 2.11, two connections are involved with the controller, the first deals with the controller output and heater input, while the second is about the controller input and the pyrometer output. These connections which are made on the controller rear side are shown in Figure 2.13.

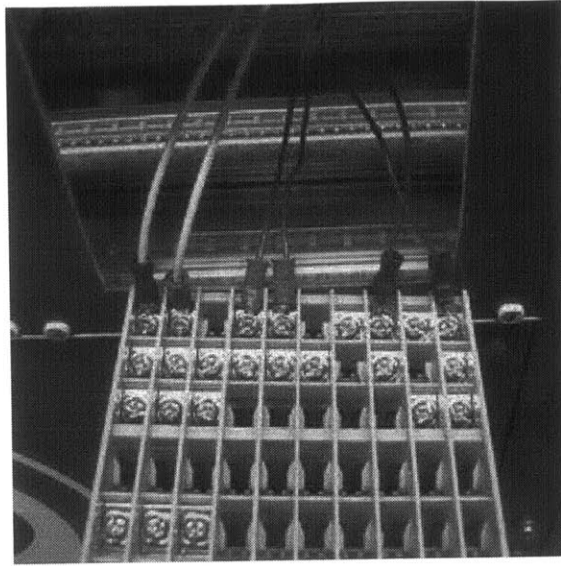


**Figure 2.13: The controller electrical connections.**

The controller is of the current output type with output ranging from 4 to 20mA DC. A large value output corresponds to a large error signal, thus a large actuation needs to take place. Physically, the controller output current  $i$  must match the equivalent heater voltage input  $V_{out}$ . The right way to achieve this match is by placing a resistance in between the heater and controller terminals. The value of this resistance is determined by working the upper values matching, i.e. 20mA should correspond to 10V (maximum heater input). The required resistance would then be  $R_{out} = 10/(20 \times 10^{-3}) = 500\Omega$ . Figure 2.14 shows how this connection is made.

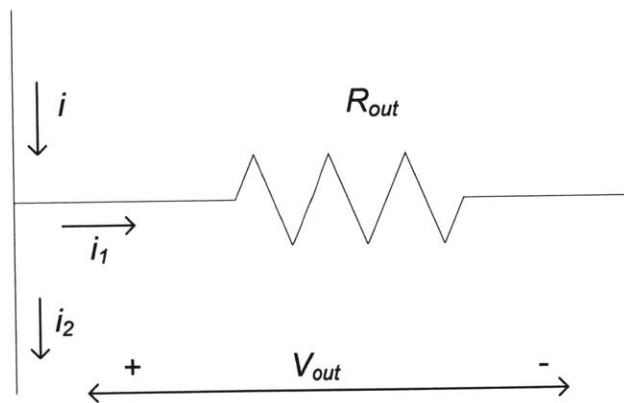


**Figure 2.14: Heater input connection.**

This method turned out to be successful as recognized from controlling practices. Nevertheless, an assumption is made in this calculation. The current  $i$  actually branches into two currents  $i_1$  and  $i_2$ . The current  $i_2$  is assumed negligible, this is only valid in case the equivalent heater input resistance, which is not listed in the heater's manual, is very large ( $R_{heater} \gg 500\text{Ohm}$ ). This turned out to be true because testing results did not contradict the assumption made.

Concerning the lower values matching, a 4mA current will equivalently generate a heater input of 2V. This triggers 20% of the maximum heater input. This amount of heat compensates for the heat losses and maintains the melt temperature constant.

For the controller input connection, a match between the pyrometer output signal and the controller input signal is achieved. But, before considering this match, let's first scale the pyrometer output current (4 to 20mA DC) according to a certain temperature range set by the user. The maximum temperature that is supposed to be reached in this application is 1100°C (20°C superheat above copper melting temperature). The maximum output current (20mA) is scaled with respect to this temperature. Equivalently, the minimum output current (4mA) is scaled to 700°C, the lowest temperature that could be detected by the pyrometer. Therefore this 16mA current range corresponds to 400°C temperature range. The desired melt temperature (1100°C) is set on the controller which has an input voltage signal  $V_{in}$  of 5V DC as maximum value.

As was done with the output connection, the controller input connection problem is solved by adding a fixed-value resistor that transfers the current signal to voltage one. The upper signal values matching is also used to determine the resistance, in other words  $R_{in} = 5\text{V}/20\text{mA} = 250\text{Ohm}$ . The error signal is found by subtracting 5V (corresponds to controller "set value" of 1100°C) from the converted voltage obtained from the thermometer signal. For example, when the melt temperature reaches 1100°C, the error signal is therefore  $5\text{V} - 20\text{mA} \times 250\text{Ohm} = 0\text{V}$ . This result is reasonable because at the time when the set value is reached, zero error signal is generated, and thus no need to trigger further heating. The electric connection of the controller input is shown in Figure 2.15.

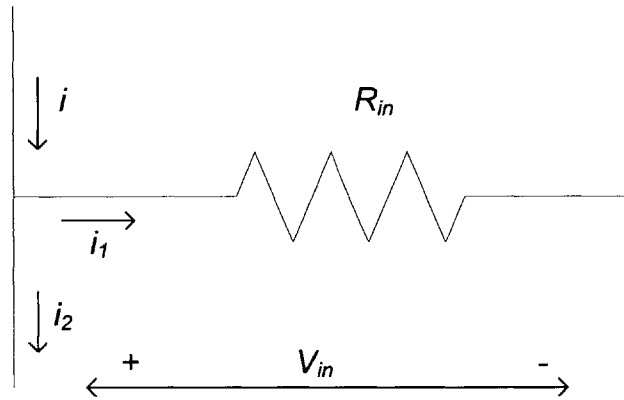


Figure 2.15: Controller input connection.

## 2.4 The Crucible Set

The need to design and build a new crucible set is the main task to process high melting temperature metals. There were many design concepts to consider when building the crucible. The crucible insulation, loading and sealing were among the design factors considered. In the current apparatus, the crucible is made of two parts, the flanged cylinder and the orifice plate, all shown in Figure 2.16. Once the crucible is loaded from the bottom, it is then attached to the bottom plate by screws. The new crucible however has a different design, as will be shown. The sealing and insulation relevant to the crucible design will be also discussed.

### 2.4.1 The melt container

The main part of the crucible is the melt container. The molten metal will flow out of this container through an orifice attached to its bottom. Candidate materials for this crucible part must show extremely good mechanical, chemical and thermal properties. Some of these properties are: high operating temperature (at least above copper melting point), strength at high temperature, chemical inertness, resistance to molten metal, low porosity, machinability if possible, and most importantly thermal shock resistance. As previously explained, the crucible material must be a ceramic. Metals even refractory ones are rejected because of their high electrical conductivity that causes crucible overheating because of induction heating. Ceramics however have two main



disadvantages: first, their raw material is expensive and second, most of them are brittle and hard, they could only be machined with the expensive diamond tooling that is not accessible in local machine shops. To have a cost-effective design, a compromise must be set in which most of the required properties could be acquired in the most cost effective material possible. The crucible design and number of parts is then considered. This feature affects the choice of material and the loading process. The multi-piece crucible has an advantage over the single piece is that the cleaning process becomes easier, and in case one part fails, this part will be only replaced and not the entire crucible. But the idea of having a multi-part crucible made out of ceramic material raised two problems: assembly and sealing. No way could the current apparatus crucible's concept of assembly and sealing be implemented in the new one.

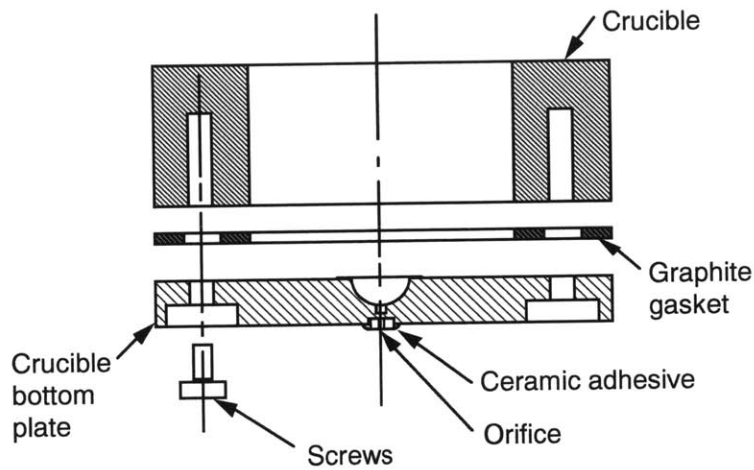


**Figure 2.16: The crucible setup of the current equipment.**

First tapping a small size thread hole in ceramics is hard because of the ceramics brittleness (threads may even break when fastening the screws). Second and for the same reason, it is impossible to have a very sharp knife edge to press against the gasket and seal the assembly. Third, even if tapping succeeds, the fastened metallic screws will heat up by induction, expand more than their tapped holes do (metals have a higher coefficient of expansion than ceramics [9]), and thus induce stresses and cracks that may lead to complete failure. The remaining alternative to implement a multi-piece crucible is to have a threaded connection on the crucible main part as shown in Figure 2.17. This requires the addition of a threaded cap that holds the orifice plate. The sealing of such an assembly would require strong cap tightening that could crack the threads.

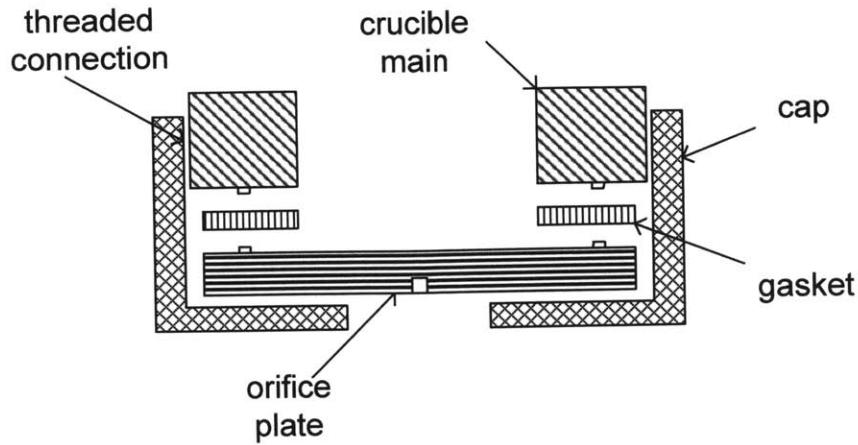


**Figure 2.17: Exploded section view of the multiple-piece crucible design.**

For all these reasons a single piece crucible is employed, and the difficulty of assembly and sealing is avoided. This choice reduced the machining cost, and thus the overall crucible price. The finally operated crucible is an assembly of standard parts. This assembly is explained in detail in Section 3.2.1. The geometrical criteria that were considered while designing the crucible are listed below.

**Table 2.1: The crucible geometrical design criteria.**

Geometrical Characteristics	Affected Design Points
The outer diameter should be smaller than the coil one by about 1.25cm.	Allowing for an insulation sleeve to be wrapped around the crucible.
The melt capacity should be around 160mL.	Contain a billet of reasonable size that takes more than 5min. to be totally sprayed.
The inner diameter larger than 5cm.	Allows for a clear optical path.
Length about 150cm.	Observe breakup in the focus range.
Flange outer diameter larger than 10cm.	Sealing the crucible with the insulation block
Flange outer diameter smaller than 14cm.	The bolts of the support ring reach the top plate.
Wall thickness not less than 4mm	Allow for #2 screw hole to be made.
Bottom thickness of 3mm	Orifice pocket could be added.

It is a good practice to have a tapered-shape crucible, at least from inside. In general, it is easier to remove the residual solidified metal part from a tapered crucible rather than to do it with straight-wall one. The advantage of tapering is illustrated in Figure 2.18.

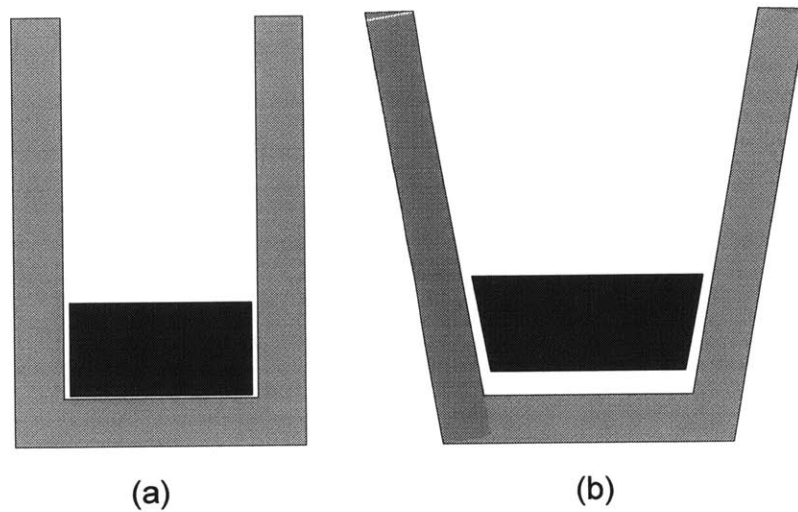


**Figure 2.18: Residual billet removal from the crucible. (a) straight, (b) tapered.**

Many refractory ceramics were considered in making the crucible, but those that passed the thermal shock test (Section 4.3) are Boron Nitride, Quartz and Graphite. The boron nitride properties perfectly match the requirements of the crucible, but it is very expensive. Unfortunately, no standard crucible (close to the dimensions set) was available to be modified and fit into the system. Therefore one choice is left: build a custom crucible, and that would be very expensive. For this reason, the boron nitride option is eliminated.

The quartz material has superb thermal shock resistance, but an operating temperature not sufficiently higher than the copper melting point (around 1120°C). It is cheaper than boron nitride but much harder therefore it could only be machined with the diamond tooling (not accessible in local machine shops). The available standard crucibles were not flanged form top and had a very thin bottom thickness prohibiting the orifice to be placed. Interestingly, quartz could be fused by a special adhesive. This fusing process could be used to build a crucible that fits into the system from standard quartz pieces. This crucible, in this case would be made from a cylinder fused at the bottom to a circular plate and fused on top to a ring (to make a flange). Regardless of the high cost of machining and fusing the plate and ring, the most important issue is that there was no guarantee from the specialized manufacturer that the adhesion especially the bottom one (between plate and cylinder) which will be in direct contact with the molten copper could

withstand the high temperature without failing or detaching. For this reason, the quartz option was dropped.

Graphite is the remaining option to consider. This material is cheap and machinable with regular (HSS or carbide) tooling. A standard crucible close to the desirable dimensions is found but without having an outer flange on the top. It was custom flanged. As a remark, graphite has a relatively higher electrical and thermal conductivity than any other ceramics. This disadvantage causes first the crucible to be heated by induction; it also eases the melt's heat dissipation to the surrounding. This problem is solved by adding an insulation system that minimizes the heat losses. The graphite crucible is shown in Figure 2.19.

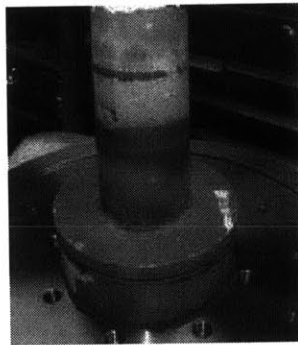


**Figure 2.19: The graphite crucible.**

### **2.4.2 The insulation**

Thermal insulation is a requirement for every well-designed thermal system. In the current UDS apparatus the addition of insulation is not permissible between heater and crucible; it could only be added around the heater's outer surface, where in this case, it shortens the melting time [4]. Insulation wasn't added to the current apparatus. In the high temperature apparatus however, the addition of insulation around the crucible is necessary to speed up the heating process. On top, the involved parts of the crucible assembly (top plate for example) are made out of materials that cannot withstand the anticipated operating temperature (1100°C) of the crucible, therefore the role of the insulation is not only to reduce heat losses but also to save the surrounding parts from overheating. From a heat transfer point of view, the absence of insulation in the system

hurdles the melting process; it could be either slowed down or even impossible. The radiation losses from the crucible's outer surface are found as follows:

1 – The Stefan Boltzmann law is implemented by the equation

$$Q_{loss} = \epsilon \sigma A_{cru} T^4 \quad (2.9)$$

where  $A_{cru}$  is the total exposed area of the crucible given as

$$A_{cru} = \pi(R_{cru}^2 + 2 \times R_{cru} \times L_{cru}) \quad (2.10)$$

2 – The results are summarized below:

**Table 2.2: The heat loss results.**

Crucible Properties	Results
$R_{cru}$ cm	3
$L_{cru}$ cm	14
$A_{cru}$ cm <sup>2</sup>	296
$\epsilon_{graphite}$	0.9
Stefen Boltzmann const.	$5.669 \times 10^{-12}$
$T_{outer\ surface}$ °K	1073
$Q_{loss}$ W	2000

This loss is obviously very large. The total power supplied by the induction heater to the crucible will not be larger than 4 kW. So the radiation loss alone accounts for at least 50% of the totally supplied heat. The insulation is therefore a must to reduce it. The two critical locations where the insulation should be placed are: the crucible lateral walls (because of radiation) and the upper part (conduction to top plate). The upper part insulation will now be discussed and then the lateral one will be explained.

The upper part insulation block saves the top plate from overheating and its both upper and lower surfaces play a role in the sealing mechanism of the crucible set. The block will thus be under severe compression loading. It must therefore be made out of a rigid material. Standard insulation boards deform significantly under compression and thus they can't seal. The material properties required for this block are:

- 1 – Low thermal conductivity.
- 2 – High operating temperature.
- 3 – Good thermal shock resistance.

4 – High compression strength.

Two commercially available materials satisfy these requirements: the magnesia stabilized zirconia and the alumina silicate (data sheet included in Appendix A.9). The zirconia is expensive and hard (diamond machined). The standard part closest in shape to the desirable block is just a square piece that requires extensive machining. The alumina silicate on the other hand is cheaper, softer (carbide tool machined) and available in standard cylinders. The latter material was therefore chosen and the insulation block was fabricated in the machine shop. The insulation block is shown in Figure 2.20.

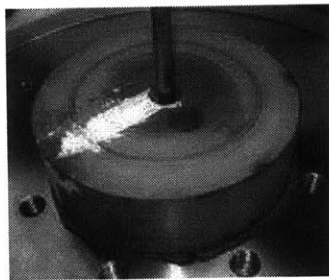


**Figure 2.20: The insulation block.**

The insulation block is cylindrical with 12.7cm diameter and 3.8cm thick. The thicker the block, the better it insulates and the more robust it becomes (withstands larger compression). It has three main features:

- 1 – A central hole in the middle to allow the vibration rod to reach the melt in the crucible.
- 2 – A second eccentric inclined hole (aligned with the pyrometer viewport) to provide optical path for the pyrometer to reach the copper billet upper surface.
- 3 – A bossed knife edge on the bottom part to seal against the crucible flange (discussed in the following subsection)

The second insulation target is the crucible lateral walls. This insulation does not interfere in the crucible sealing mechanism. It however raises the problem of how to hold it and adhere it to the crucible walls while the crucible itself is held free in space with nothing underneath it. This insulation will have the shape of hollow cylinder (sleeve) with inner diameter matches the crucible outer diameter, and outer diameter less than the coil inner diameter. The required material characteristics for this application are:

- 1 – High thermal shock resistance.
- 2 – Low thermal conductivity.
- 3 – Low emissivity.
- 4 – Strength at high temperature.

If solid materials are to be used for this insulation, quartz or magnesia stabilized zirconia are the two alternatives to consider. The crucible walls have a very odd shape: they are straight at the top then taper inward as they go down to the bottom. A standard hollow cylinder made out of either zirconia or quartz will not cover the entire crucible surface, and thus it will not reduce the losses considerably. The process of contouring the cylinder or straightening the crucible is very delicate. And even if one of the past cases takes place, the process of holding the insulation sleeve around the crucible will not be easy. There isn't an available adhesive that glues graphite to the either quartz or zirconia up to high temperature. Also the mismatch in thermal expansion between graphite and the insulation sleeve may induce thermal stresses in the sleeve and cause it to fail. For all these reasons, a flexible insulation blanket that could be wrapped and deformed easily against any surface was finally used. The blanket is made of the alumina silica fibers (data sheet included in Appendix A.8), and has an operating temperature to above 1500°C. It has very low thermal conductivity and low emissivity (<0.05) because of its white color. It is on top cheap and easily cut using regular scissors up to a thickness of 6.4mm. Concerning the holding mechanism, high temperature tape is wrapped around the sleeve pressing it against the crucible walls. The sleeve is therefore held by friction contact against the crucible outer surface, independently of the shape of this surface. The only disadvantage of using a blanket in this insulation is its high porosity that could help moistures and air stored within its pores. The insulation blanket is shown in Figure 2.21.

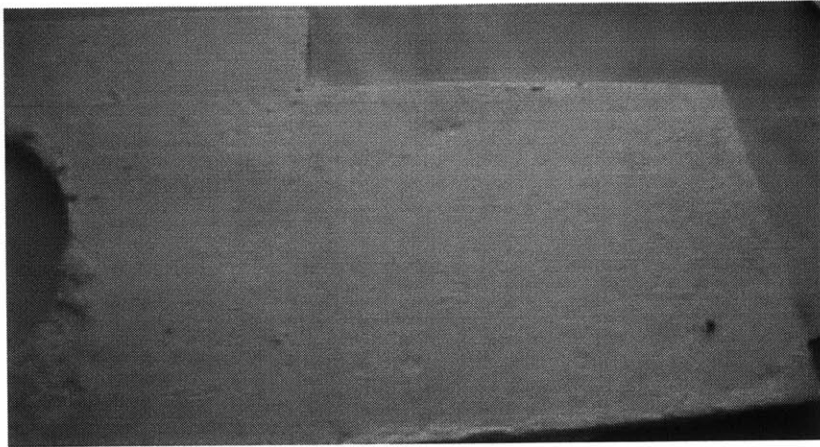


**Figure 2.21: The insulation blanket.**

### **2.4.3 The sealing**

The sealing mechanism is required for building a pressure difference between the crucible and the chamber in order to force the melt out of the orifice. Any place where two surfaces contact each other could be subject to leakage. As explained in Section 2.4.1, there was a concern to minimize the number of contacting surfaces in order to ease the sealing job. The only two inevitable sealing locations are:

- 1 – Between the top plate and the insulation block, hybrid (metal to ceramic).
- 2 – Between the crucible and the insulation block, pure ceramic.

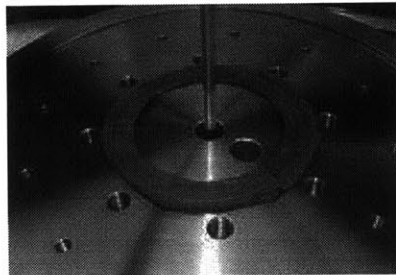


**Figure 2.22: The graphite gasket supposed to seal between the top plate and insulation block.**

The hybrid sealing between the top plate (metal) and the block (ceramics) is made as follows: a sharp knife edge is featured on the top plate surface while the insulation block mating surface is kept smooth. A soft graphite gasket, as the one shown in Figure



2.22 is inserted in between the two surfaces. The metallic knife edge is able to deform the gasket alone and achieve sealing.

The second pure ceramic sealing requires that both surfaces have knife edge. The knife edge of these parts however is more like a bossed step of width no more than 1.5mm and height no more than 0.75mm. The sharp (metal like) knife edge is difficult to machine on ceramic parts and if made, it may crack at run time because of its very small edge width around which a large stress concentration resides.

Unlike some commercially available gaskets designs, the ones used here have no metallic inserts. This enhances their compression and thus their ability to seal. The gaskets used are cut from a large graphite sheet (data sheet included in Appendix A.7). Their inner and outer diameters are first marked on the sheet via a compass as shown in Figure 2.23, and then a regular steel cutter goes gently around the marked circles to cut them away from the sheet.

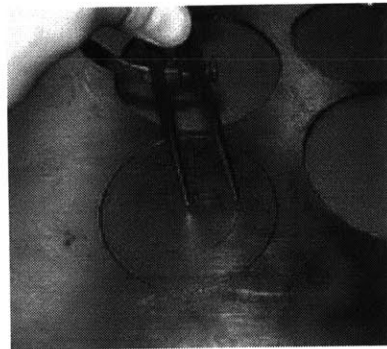


**Figure 2.23: The graphite gasket is being cut from a graphite sheet.**

## **2.5 The Vibration System**

Rayleigh's jet instability theory has specified that external vibration acting on top of the orifice exit is necessary to generate uniform-size droplets. The vibration, which has a sinusoidal variation, affects the size of the generated droplet through its frequency (refer to Eq. 1.2). The forced vibration is created by first generating an electrical voltage signal that will then be amplified before it reaches the vibrator placed on the top plate. Inside the vibrator, piezoelectric disks are triggered generating mechanical vibration of the same

frequency. This vibration is later transferred to the melt through a rod immersed into it. The vibration could be again monitored through an oscilloscope. The functional layout of this system with all elements and signals involved is shown in Figure 2.24. The mode of operation of the system elements is the topic of the following subsections.

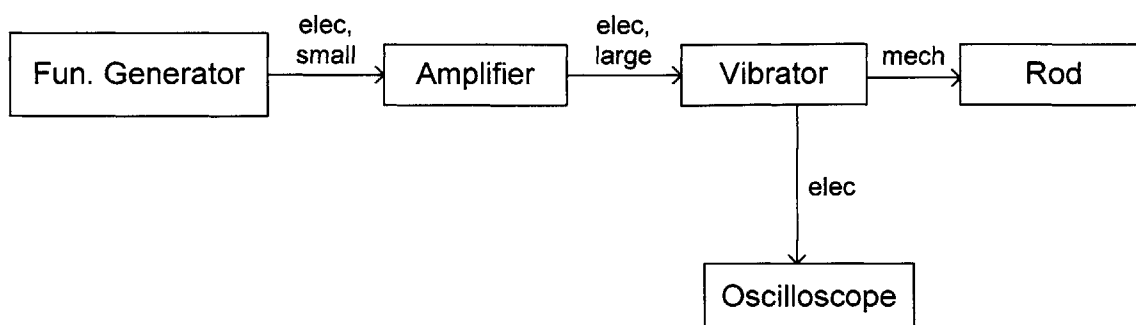


**Figure 2.24: The vibration system functional layout.**

### 2.5.1 The function generator

This equipment generates voltage signals that the user is left to specify their type and frequency. The signals generated are all periodic, they could be sinusoidal, square or even the less common triangular. The frequency range is wide; it goes from 1Hz up to 50 kHz. The amplitude of the generated signals is low (<1mV); the signals have therefore zero power and this makes them incapable of triggering any electrical process. The generator has two channels that could output at most two signals of different type but at the same frequency. The first channel emitting the sinusoidal signal is used for the vibrator. The second channel outputs a square wave signal feeding the stroboscope that will be discussed later in the imaging system. The function generator front side is shown in Figure 2.25.

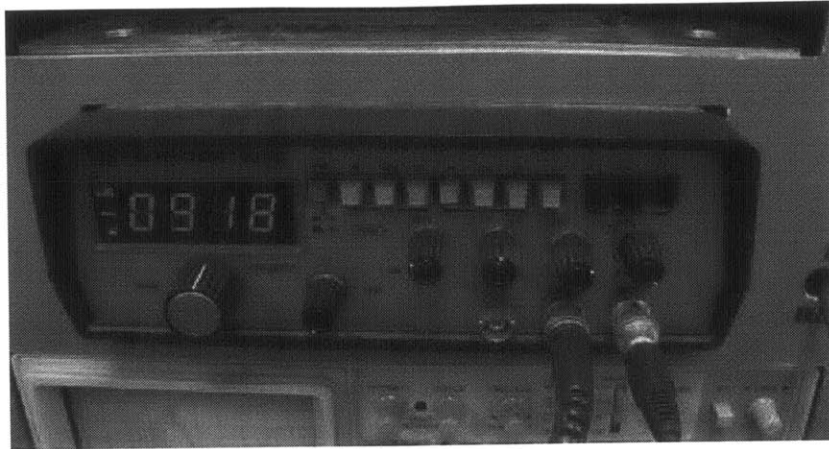


**Figure 2.25: The function generator.**

### **2.5.2 The amplifier**

The amplification of the generated electrical signal is necessary to excite the piezoelectric crystals in the vibrator. The amplifier is audio and relies on basic op-amp circuits as all other amplifiers do. The amplification factor is definitely a user selective but it is an unimportant factor for the process. Previous DBM researchers have determined the maximum amplification value that is not supposed to be exceeded as long as to keep the piezoelectric crystals behavior within the linear elastic range. The amplifier control panel is shown in Figure 2.26.



**Figure 2.26: The amplifier.**

### 2.5.3 The vibrator and oscilloscope

The vibrator is the equipment that transforms the electrical vibrating signal to uniform mechanical vibration. It has two connection ports: the first labeled “in” is where the amplifier signal cable is connected, and the second labeled “sensor” is where the oscilloscope cable is connected. The vibrator is made out of series of piezoelectric discs stacked on top of each other. The number of these actuating discs is not an influencing parameter for the process. The disks are made of lead zirconate titanate with charge constant  $37.4 \times 10^{-9} \text{cm/V}$ . The amplitude of vibration will be around  $7.5 \mu\text{m}$  if 200V is applied to the stack. According to jet instability theory, the jet breakup process is a frequency driven process, however, the amplitude should be sufficiently higher than those of white noises existing in the system [4]. The piezoelectric disks are altered by some same size copper disks to conduct the electric signal between them. In the bottom the vibrator is spring-loaded to an outer extension, which is connected to the vibration rod. One of the piezoelectric crystals acts as a sensor to detect the displacement of the entire stack; it is wired to the second electrical connection from which the oscilloscope is fed. The vibrator is attached to the upper part of the top plate central tube. It is sealed with 1.25cm swagelok connection as shown in Figure 2.27. The user could check for the frequency and the amplification on the oscilloscope shown in Figure 2.28. The displayed sinusoid becomes wider if the frequency is reduced and squeezes in if it is increased. The sinusoid stretches out if the amplification ratio is increased. In case the amplification limit (mentioned in Section 2.5.2) is exceeded, the sinusoid curve distorts and becomes irregular. This proves that above that limit, the piezoelectric crystals exhibit an odd (non-linear) behavior that could later lead to their destruction.

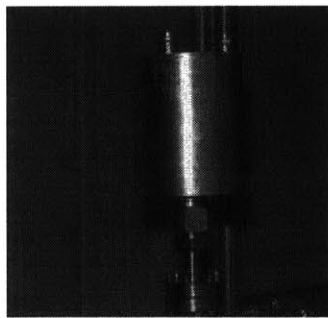
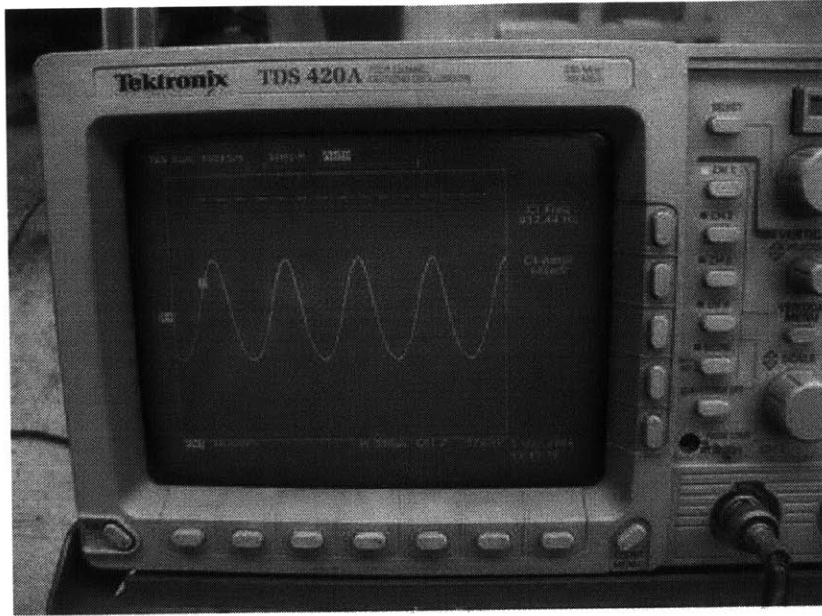


Figure 2.27: The vibrator attached to the top plate.



**Figure 2.28: The oscilloscope displaying the vibrator signal.**

#### **2.5.4 The vibration rod**

The vibration rod transmits the vibration from the vibrator to the melt. It has the shape of a long tube that is threaded on top to the vibrator's nipple, and then traverses the top plate tube and the insulation block central hole until it reaches the bottom of the melt. The closer the vibration is to the melt exit, the stronger its effect on the breakup will be. Therefore, the clearance distance between the rod bottom end and the nozzle exit is minimized. There is no specific rule that determines what the exact value of this clearance should be, but previous DBM practices have specified that a clearance value of 1mm is considered close enough for the vibration effects to take place [2]. There shouldn't be any consideration in the clearance calculation about the rod extension or contraction due to its vibration because the clearance value is at least 100 times larger than the rod vibration amplitude.

The rod is made of two parts: an upper metallic portion and a lower ceramic one. Both are shown in Figure 2.29. The ceramic part will be immersed in the melt, therefore its material requirements are the same as those set for the crucible (refer to Section 2.4.1). But for this application, the electrically insulator boron nitride is chosen rather than

graphite. If an electric conductor rod is used, the melt eddie currents effects could reach the piezoelectric crystal, induce electric noise, and affect the vibration. The rod is a standard solid tube (6.5mm diameter) so its price will slightly differ between graphite and boron nitride.

The metallic portion is made of stainless steel. From top, the rod is threaded so that it could be fastened to the vibrator nipple. From bottom, it is pocketed to fix the ceramic portion in place. The two parts are glued to each other by a ceramic adhesive, and become a single part afterwards. The straightness of the entire rod is a critical requirement for a stable breakup. There is no need to worry about the straightness of the ceramic part. But concerning the metallic one, care must be taken when turning it on the lathe; extra alignment elements may be necessary when doing this job. In addition, the pocket clearance must not be larger than 0.05mm so that the ceramic part won't be tilted when glued to its metallic mate.

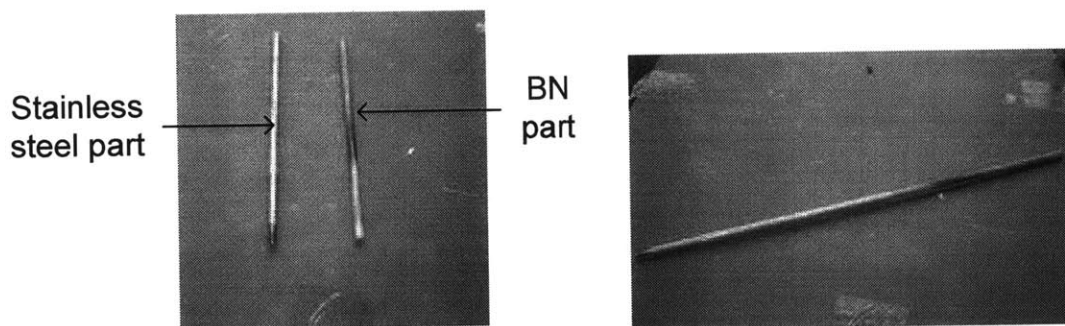


**Figure 2.29: The vibration rod before and after being assembled.**

## **2.6 The Charging System**

The charging system involves the last steps encountered in the UDS process, it is only after a stable breakup is achieved and uniform droplets are produced that charging is applied to electrostatically charge the droplets to prohibit them from merging. Charged droplets repel each other and scatter away from the molten stream. In this case, not only their shape and uniform volume are conserved but also their convective heat transfer with the inert gas and cooling rate is enhanced [10]. Previous DBM researches generated a

software code simulating the cooling process of the droplets taking into consideration the charging effect. The components of this system are the voltage supply and the charging plate. Their required design characteristics and mode of operation will now be explained. A schematic diagram of this system is shown in Figure 2.30.

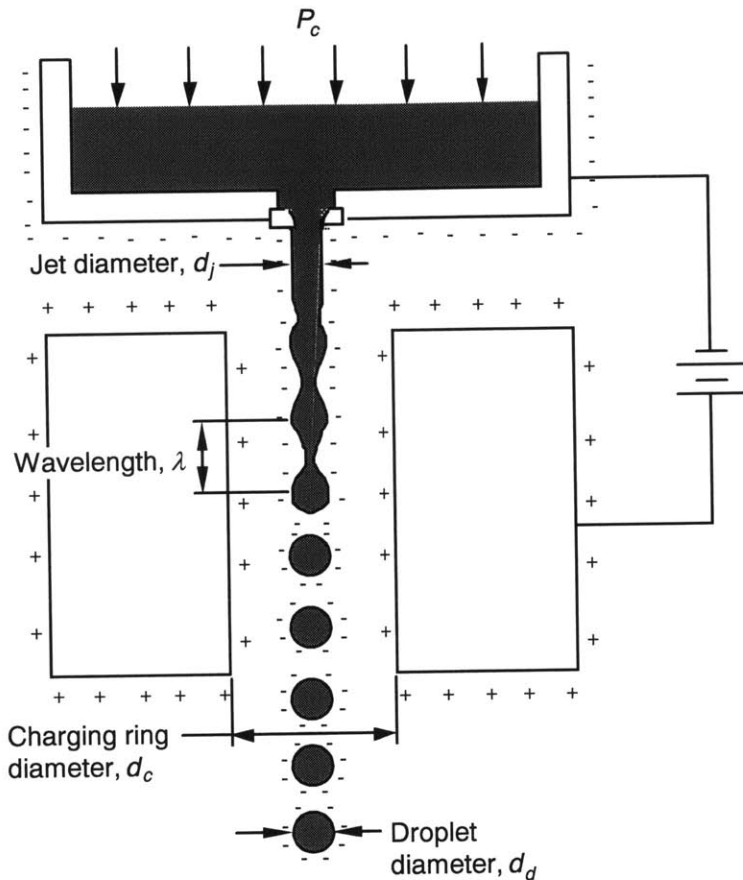
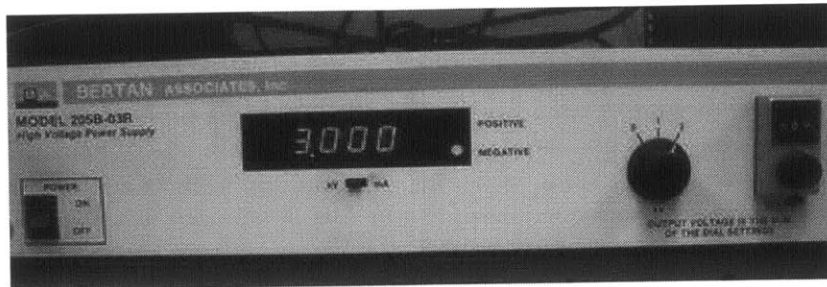


Figure 2.30: Layout illustrating the droplet charging [5].

### 2.6.1 The voltage supply

The charging process of the droplets requires a constant electric field within the breakup scheme. The simplest way to generate this electric field is by having a sufficient DC voltage supply acting across a conductor. The higher is the voltage, the larger is the intensity of the electric field and the stronger is the repulsion. The voltage supply could provide up to 4kV signal. But the common DBM practice recommends only 3kV regardless of the droplet size. This high voltage signal is transferred to the inside of the

chamber through the power feedthrough (refer to Table 2.3). The voltage supply set at 3kV is shown in Figure 2.31.



**Figure 2.31: The voltage supply set at 3kV.**

### **2.6.2 The charging plate**

The charging plate is obviously located inside the heating chamber, below the crucible's orifice. The electric field is generated inside this plate. The best location to charge the droplets is at breakup; in this case the melt and the crucible bottom are grounded and the formed droplets will all be negatively charged. Figure 2.30 illustrates this charging methodology. The location of the charging ring must coincide with the breakup point which should also be monitored by the imaging system. The focus range test results (Section 4.7) determine the plate's location. The charging plate is made out of stainless steel; it has a middle hole and has two vertical edges standing in between the hole. The edges are made to increase the coverage distance around the stream for better charging. Breakup is supposed to occur in between these plates. The voltage signal coming through the feedthrough reaches the plate via a heat-sheathed wire. The plate is fixed to one of the heating chamber's internal brackets with an alumina (electrical insulation) bead separating between the plate edge and the bracket. The engineering drawing of the charging plate is included in Appendix B.8.

## **2.7 The Imaging System**

The imaging system implemented in the high temperature UDS apparatus is 100% similar to the one used in the current UDS apparatus. The imaging system is a necessity that is



independent of the process material or temperature. The importance of the imaging system in the UDS process is explained as follows: The stability of the jet breakup is crucial for successful spraying and droplet uniformity. The operator usually stabilizes this breakup by altering its regulating variables (crucible pressure and vibration frequency). The good jet observation is obviously essential for a precise regulation. Nevertheless, it is by far very difficult to scrutinize in a molten metal jet of approximately 100 to 400 $\mu\text{m}$  diameter by the naked eye through a two inch wide viewport. This physical limitation justifies the use of an imaging system to watch not only the breakup but all other jet actions (beginning and end of spray, jet deflection...). On top, the imaging system played a major role in determining the size of the droplet in a control process designed to reduce the droplets size variation by altering the vibration frequency during runtime [3].

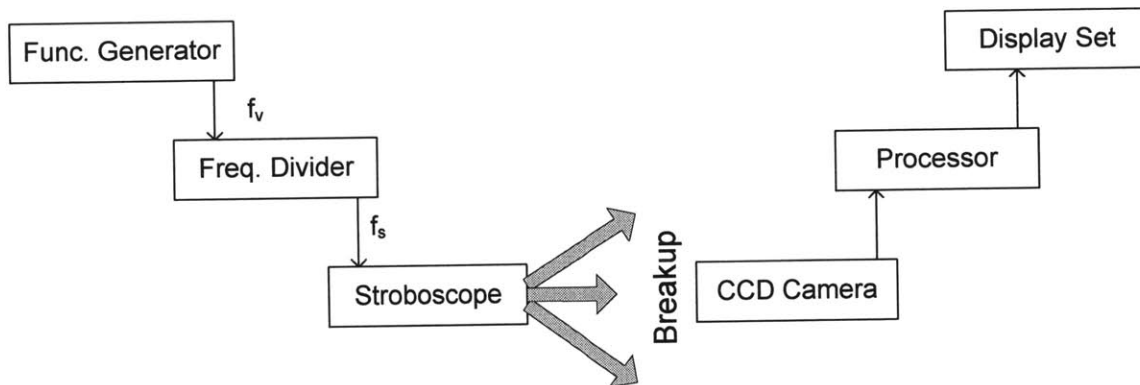


**Figure 2.32: The imaging system functional layout.**

The imaging system works as follows: A stroboscope lights the inside of the chamber on the flowing jet, a CCD camera monitors the jet breakup and a magnified image of the jet is shown on a display set. The strobe and the camera have their own viewports in the heating chamber. These viewports are designed to face each other. A functional layout of the imaging system is shown in Figure 2.32. In the following parts, the system components mode of operation will be explained.

### 2.7.1 The stroboscope

The stroboscope used is similar to any simple laboratory stroboscope. Its frequency's upper limit  $f_{s,max}$  is 400 Hz. The input frequency to the strobe  $f_s$  could be either specified by its own regulator or synchronized with the frequency of an external signal after the regulator being disabled. The second case is the one that matches the process requirements. The synchronization of the jet breakup phenomenon with the imaging collection process shows the breakup as a frozen image on the display set. The jet vibration frequency and that of the droplet generation have the same value as the frequency imposed in the function generator  $f_v$ . Since  $f_v$  is supposed to be modified during run time (to stabilize breakup or even move its initiation point), the imaging frequency must be modified accordingly to account for this variation. This requires the strobe and the vibrator to be fed from the same function generator. Making  $f_s$  equal to  $f_v$  is acceptable and the most obvious solution. But  $f_s$  could also be any integer divider of  $f_v$ . In such a case, if the proportionality constant between the two frequencies is a given integer  $k$  ( $f_s = f_v/k$ ), this means that out of  $k$  droplets generated or breakups taking place, only one of them is monitored. A frequency division is implemented because  $f_v$  lies typically outside the strobe frequency range ( $f_v \gg f_{s,max}$ ). As a commercially available product, a frequency divider of 1/10 is used for this task. This makes the frequency input to the strobe within its range (200 - 300Hz if 2 to 3kHz is applied on the vibration signal), and gives a frozen image (snap shot) of one droplet out of ten generated. The stroboscope accepts a square wave signal and never a sinusoidal one; the function generator square wave port is therefore synchronized with the generated sinusoidal one. The square signal is then sent to the frequency divider shown in Figure 2.33 where only its frequency is modified and the amplitude remains intact. The divided signal finally reaches the stroboscope to trigger it. It is unnecessary to amplify any of the strobe related signals because the strobe is only concerned about the frequency contained in these signals that could be identified regardless of the amplitude.

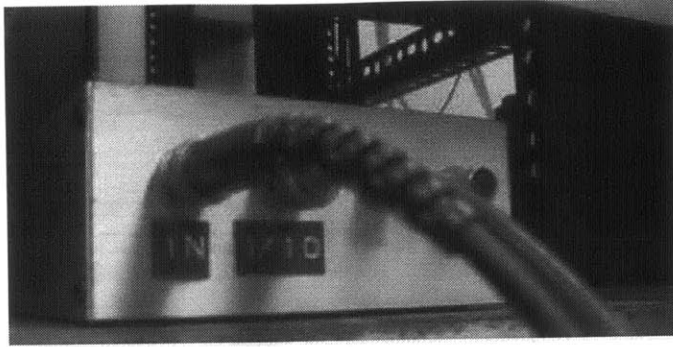


**Figure 2.33: The frequency divider.**

The CF port on which the strobe operates has a transparent part as wide as the strobe bulb, thus allowing maximum amount of light to go through. Shading will not occur if the camera and strobe are properly aligned. The strobe is fixed to the main frame through a fixture. This fixture is explained in Section 3.8. Once the appropriate positioning of the strobe is set as shown in Figure 2.34, it is then clamped so that it doesn't lose focus on the breakup. The strobe's plastic outer cover raises a concern of overheating, so as a safety precaution, the strobe is always kept a small distance away from the hot viewport flange.

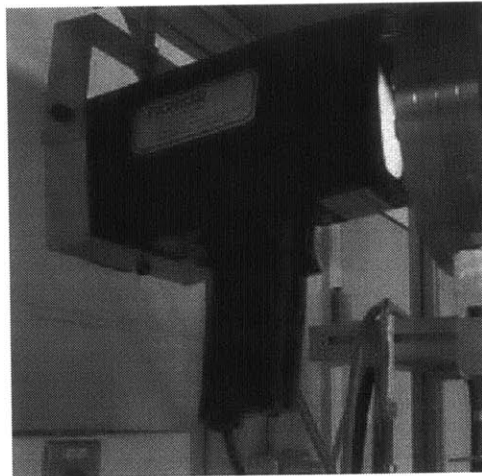


**Figure 2.34: The stroboscope lighting through the viewprot.**

### **2.7.2 The camera assembly**

The remaining part of the imaging system is the camera assembly which consists of the camera itself, and the display panel. The camera is of CCD type that grabs the image in a certain frame into which it is focusing. Obviously, the camera is focused on the point where the jet is supposed to break. The camera viewport is of the ISO type (refer to Table 2.3). Its transparent area is small so the camera could only observe a determined location inside the heating chamber. The vertical range of this location must be determined so as to force the jet breakup to occur within it. If breakup occurs outside this range, it will not be observed by the imaging system that becomes useless in this situation. The determination of this range is the topic of the focus range test, discussed in Section 4.7. The camera, similar to the strobe, is fixed to main frame frontal horizontal bar. Its fixture consists of a hollow tube on which the camera could slide, the tube is welded to the bar holder. The camera has its built-in motion sliders that ease its positioning in the desired target. The camera needs to be placed on the frontal side of the frame and the rear viewport is left to the stroboscope. This choice is made as such because the user needs to adjust its location and focus it while being able to see its targeted image on the display. The camera is powered by a 12V DC power supply. The overheating problem is also taken into consideration with the camera which is kept a little farther away from the viewport flange. The camera is viewed in Figure 2.35 focusing through the viewport.

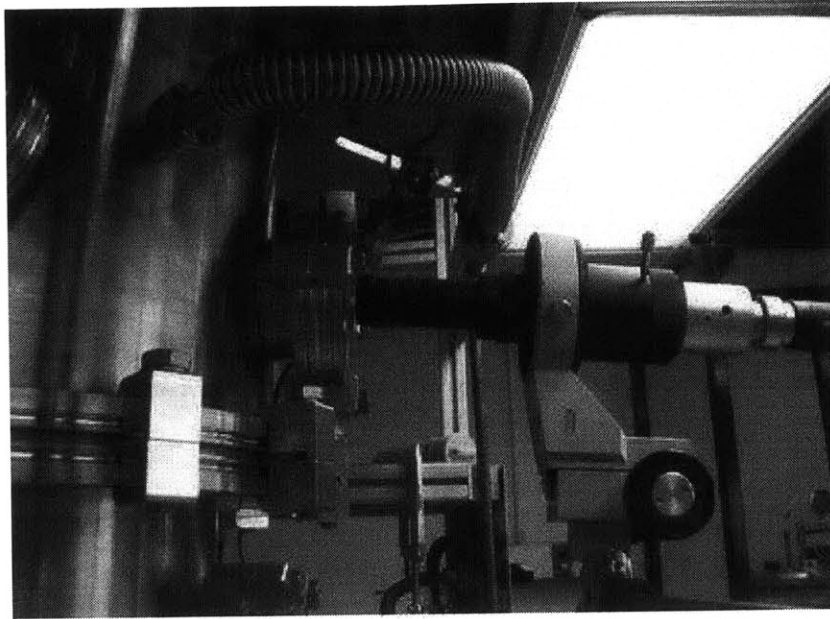


**Figure 2.35: The camera focusing through the viewport.**

The camera transfers the image as a data series to the display. It appears on the screen around 25 times larger in size. Both the display and camera power supply are placed on the secondary frame next to the main one.

## **2.8 The Gas Management System**

The presence of oxygen in the chamber environment creates oxides that block the small orifice preventing the stable jet breakup. This trouble is solved if oxygen is pumped out of the system and replaced by inert gas. The latter process is the main reason behind the installation of the gas management system in the UDS apparatus. Another reason for employing this system is the need to have a pressure difference between the crucible and the heating chamber as a driving force for the melt stream to flow out of the orifice. As design requirements, the tasks supposed to be fulfilled by this system are: the chamber evacuation, inert gas filling, leakage prevention, pressure regulating, and oxygen content determination. The many gas management system components, which will be described later, run together to provide the most inert possible environment for the UDS apparatus.

Because of the many process improvements that were sought, the gas management system of the high temperature UDS apparatus included some modifications

over the current apparatus' one. The system's parts were distributed at many spots on the apparatus; nevertheless, the system could be clearly divided into four major parts. Three parts are directly related by the involvement of the gas flow, they are:

- 1 – The source part: tanks.
- 2 – The flow control part: control panel.
- 3 – The sink part: chamber and crucible.

The fourth part which is somehow not related to the previously mentioned ones is the evacuation part. Each of these parts will be discussed separately in the following subsections. A schematic diagram of this system is shown in Figure 2.36.

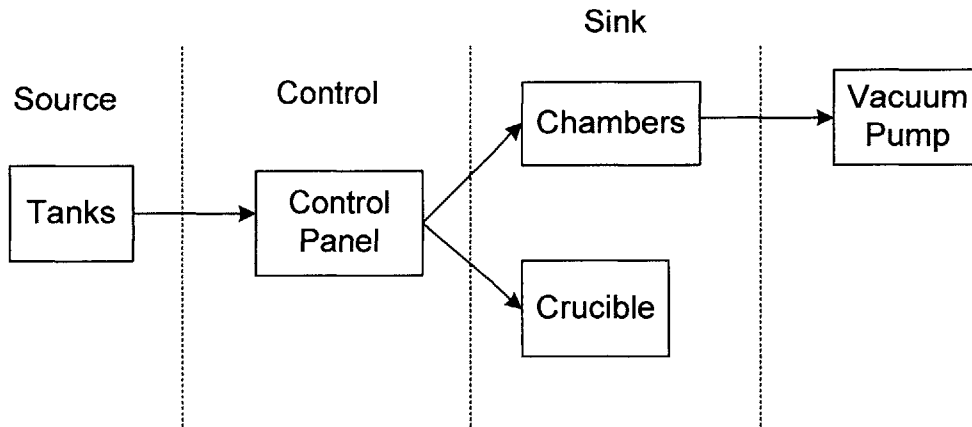
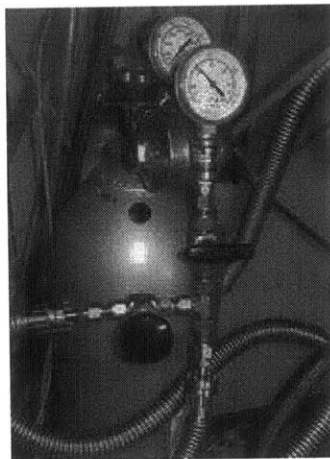


Figure 2.36: Schematic diagram of the gas management system.

### 2.8.1 The source part

As its name indicates, the source part supplies inert gas from a given source: the tanks. Several inert gases could be used in this application. Helium (He) and argon (Ar) are noble inert gases that were used in old UDS apparatuses. Pure nitrogen ( $N_2$ ) is also inert to most molten metals (Cu, Pb, Sn, and Solder alloy). Nevertheless, forming gas (95%  $N_2$ , 5%  $H_2$ ) is used. The forming gas excels over pure  $N_2$  because of the extra 5%  $H_2$  added to it. This hydrogen content, although minor, strongly reacts with the residual oxygen molecules to form water vapor. Because of this addition, the oxygen-free environment is not only physically supplied, but also chemically enhanced.

Inert gas is supplied in two steel tanks; each has a volume of 55l. The tanks could be easily assembled, disassembled and replaced when empty. When full, the typical tank pressure is around 13.7MPa. Tanks are generally discarded when their pressure drops to below 1MPa; small debris from the tank inner walls along with the contaminating residuals are better involved into the system if filled from low pressure tanks. Keeping the gas passages and the overall environment clean improves the process outcomes. On average, one of the tanks that will be later referred to as “low pressure” tank lasts for 8 runs, while the second “high pressure” tank lasts for more than 20 runs. This discrepancy will be better understood when explaining the role of each tank. Figure 2.37 shows one of the gas tanks.



**Figure 2.37: One of the inert gas tanks with its gages and valves.**

The two tanks, although identical, perform different tasks. The first tank has the following role:

- 1 – Supplies gas for the entire apparatus during the filling process.
- 2 – Supplies gas necessary for the chamber pressure control during spraying.

Since the chamber pressure is always lower than that of the crucible, this tank is referred to as “low pressure source”. On the other hand, the second tank is only used during spraying to pressurize the crucible; therefore it is called the “high pressure source”. There is no role for this tank in the filling process. Filling an entire apparatus with the inner volume of 200l requires a larger quantity of gas than that required to fill 5 to 10l of

crucible supply line. For this reason, the low pressure tank will be emptied before the high pressure one. Also, the repeated evacuation and filling of the system as will be noted, increases the consumption of gas from the low pressure source and empties it quickly.

Both tanks are fixed to the frame by the belt fixtures as a safety regulation. They are placed as close as possible to the control panel so as to reduce the length of the connection lines which are made using flexible stainless steel hoses. The hoses have CF flange ends, but CF to swagelok adaptors are placed on their both ends to accommodate for the swagelok fittings used in both control panel and gas ports. As a note, CF type hoses were chosen and not QF because the connections made are meant to be permanent; the tanks disassembly takes place from the swagelok end fittings and not the CF ones.

The tank pressure, which is on the order 10MPa, is high enough to be handled by an instrumentation-type moderate-range pressure regulator. High pressures are generally controlled by industrial (heavy duty) regulators. One such regulator is placed directly next to the tank port. The role of this regulator is specified by two points.

1 – It sets the maximum pressure that the chamber line could reach.

2 – Once this maximum pressure is set, it is impossible to decrease it or control it down. In other words it is a one way or a “control-up” controller. The excess pressure could be only dissipated from the panel controllers.

Each pressure tank has two pressure gages; one indicates the tank pressure (criterion to replace the tank) and the second determines the controlled pressure (parameter of the process).

### **2.8.2 The control panel**

The control panel is the user interface to manage the gas flowing to the UDS system. The three main elements of this panel are the valves, gages and controllers. Three different processes are handled from the control panel. They are:

1 – The entire system filling.

2 – The chamber pressure regulation and relieving.

3 – The crucible pressure regulation and relieving.



These three processes require at least three defined lines that guide the gas flow from the right source to the right destination while allowing the user to set and measure the flow pressure.

In the filling process, the crucible and the chamber are linked together (isobaric); therefore a single line is sufficient to fill the entire system. On the other hand, the two controlling processes target different pressure levels, their paths are thus kept independent. A switching valve is needed to connect and disconnect the crucible and chamber paths when necessary; this valve, because of this connection feature, is called the “bypass” valve. The filling line starts by the “filling” valve, it is then divided into two branches, one goes to the bypass valve and then to the crucible, and the second goes directly to the heating chamber. The flow line of the filling process is shown in Figure 2.38.

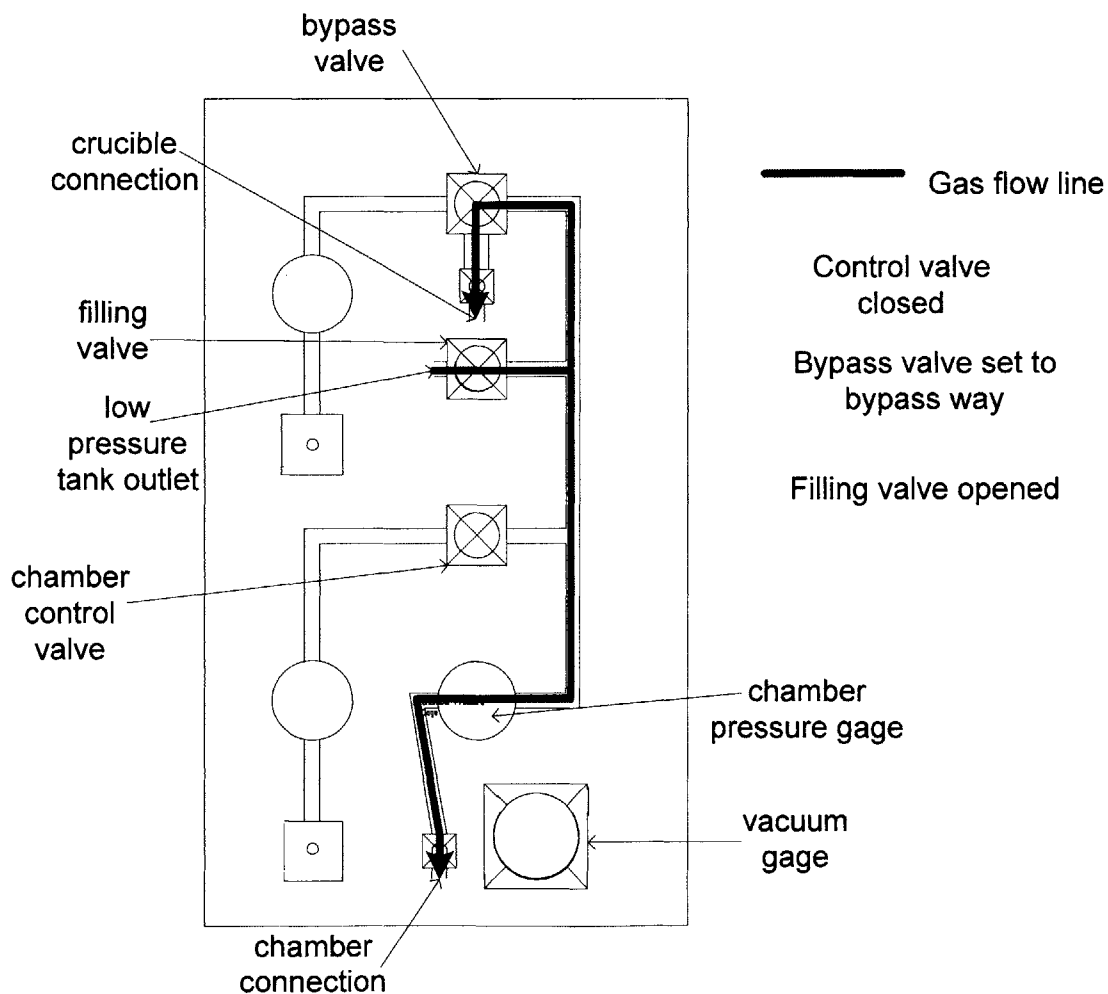


Figure 2.38: The flow line of the filling process.

The pressure controlling processes have the pressure regulators as key elements. These controllers, unlike the tank regulators, allow for up and down control. A pressure gage is placed directly after each regulator in order to measure and thus adjust the pressure accurately. For the crucible pressure regulation, the bypass valve must in this case be switched to the regulation mode rather than the bypass mode. And for the chamber pressure regulation, the chamber regulator valve is opened and the filling valve is closed. The process of controlling the chamber pressure is rarely used, however. The spraying process depends on the pressure difference between the chamber and crucible and not the value of each of the pressures, thus altering one pressure is enough to set a required pressure difference. The controlling processes flow lines are shown in Figure 2.39.

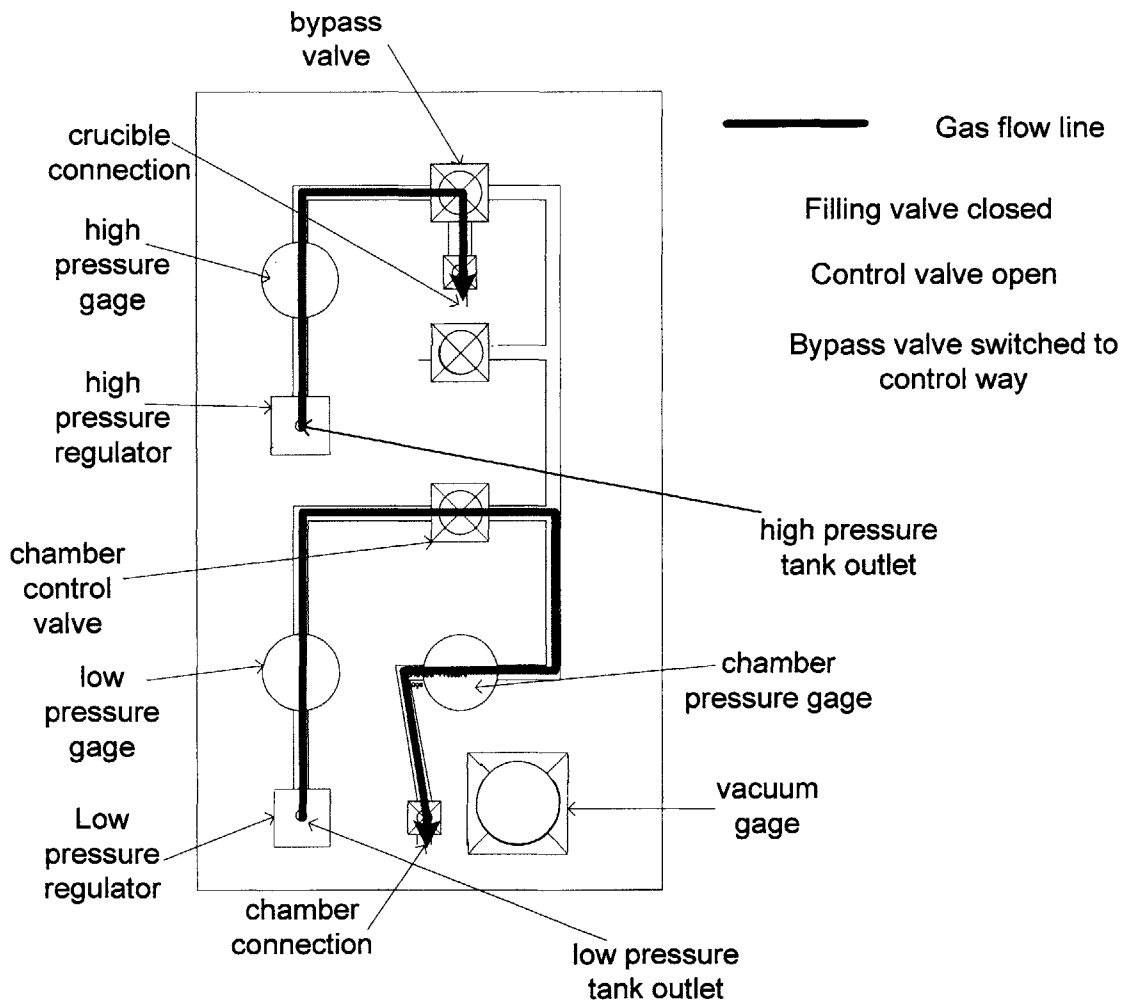


Figure 2.39: The controlling processes flow paths.

The pressure relief process is implemented to suddenly reduce the pressure of a certain environment. The advantage of using the relief valve over a pressure regulator is the very short response time. Whenever it is necessary to stop the melt spraying; relieving the crucible gas to the outside air reduces its pressure and stops the flow instantaneously. The bypass valve should be closed while relieving otherwise high pressure gas will keep flowing to repressurize the crucible. The same procedure is also implemented when relieving the chamber.

In brief, the steps taken on the control panel to realize all three processes discussed above are listed below.

#### 1 – Filling process:

- a – bypass valve set to the bypass mode.
- b – chamber control valve closed.
- c – both relief valves closed.
- d – filling valve open while filling tank valve is open too.

The process effective elements are: chamber pressure gage only (common to both crucible and chamber in this case).

#### 2 – Crucible pressure control process

- a – high pressure tank valve open and maximum pressure set on the tank regulator.
- b – crucible relief valve closed.
- c – bypass valve switched to the control mode.

The process effective elements are: high pressure regulator and high pressure gage.

#### 3 – Chamber pressure control process

- a – filling valve closed.
- b – chamber relief valve closed.
- c – low pressure tank regulation valve open.
- d – chamber regulator valve open.

The process effective elements are: low pressure regulator, low pressure gage and chamber pressure gage.

#### 4 – Crucible pressure relief

a – bypass valve switched to the closed mode.

b – crucible relief valve open.

For the sake of convenience, the vacuum gage display, although independent from all the processes lines, is fixed on the control panel. The process of building the control panel required two criteria: the first is to arrange all the necessary elements to achieve the required flow lines, and second is to align these elements straight in a compact way to ease the panel assembly. Solid tubing is used for the straight connections, and flexible or convoluted tubing is used for eccentric ones. The front panel is made out of an aluminum sheet and attached to the main frame. The control panel assembly process is explained in detail in Section 3.7. The user interface of the panel is shown in Figure 2.40. Its engineering drawing is included in Appendix B.

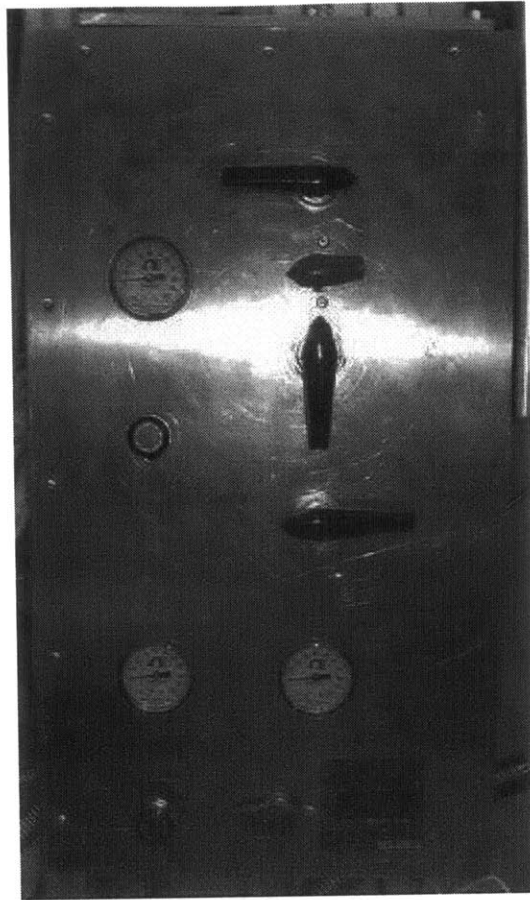


**Figure 2.40: The gas control panel.**

### **2.8.3 The chambers part**

The last destination of the gas flow is the vacuum chambers and the crucible. One port (CF 3.38) of the heating chamber is used for gas inlet to this chamber. The powder collection chamber never operates separately, therefore no filling port is added and the chamber is automatically filled from the heating chamber. The gas inlet connection line from the control panel to the chamber is made from both solid tubing and flexible hose at the end. The chamber inlet port matches perfectly with that of the hose and no adaptors were used. A CF type port and not a QF one is chosen here because this connection is meant to be permanent as long as the chamber sits in its place. Figure 2.41 shows how the hose is bended while it is clamped to the port.

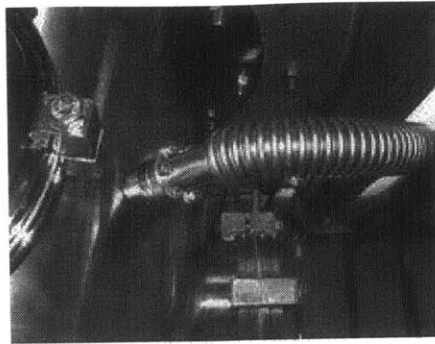


**Figure 2.41: The chamber inert gas supply.**

The second gas port on the heating chamber is the CF 7 port which is used to supply chamber gas to both the oxygenmeter and the vacuum gage. To do so, two outlets must be present to feed both equipments. This is achieved as follows:

- 1 – CF to swagelok adaptor is clamped to the port.
- 2 – A T-shape connector (1.27cm) is added as to generate two ports out of a single one.
- 3 – Reducers (1.27cm to 0.64cm) are used to accommodate size between outlets and equipment inlets.

This port is shown in Figure 2.42. An important flange design criterion which is flange tapping is considered in this assembly. The flange of this port is made very close to the chamber outer wall (focal distance close to chamber radius) as to compact the chamber volume. A very small clearance is left between the rear side of the flange and the chamber walls. This clearance does not allow for a nut to be placed or even a wrench to tighten it. The holes of the flange are therefore tapped in order to avoid an assembly problem.

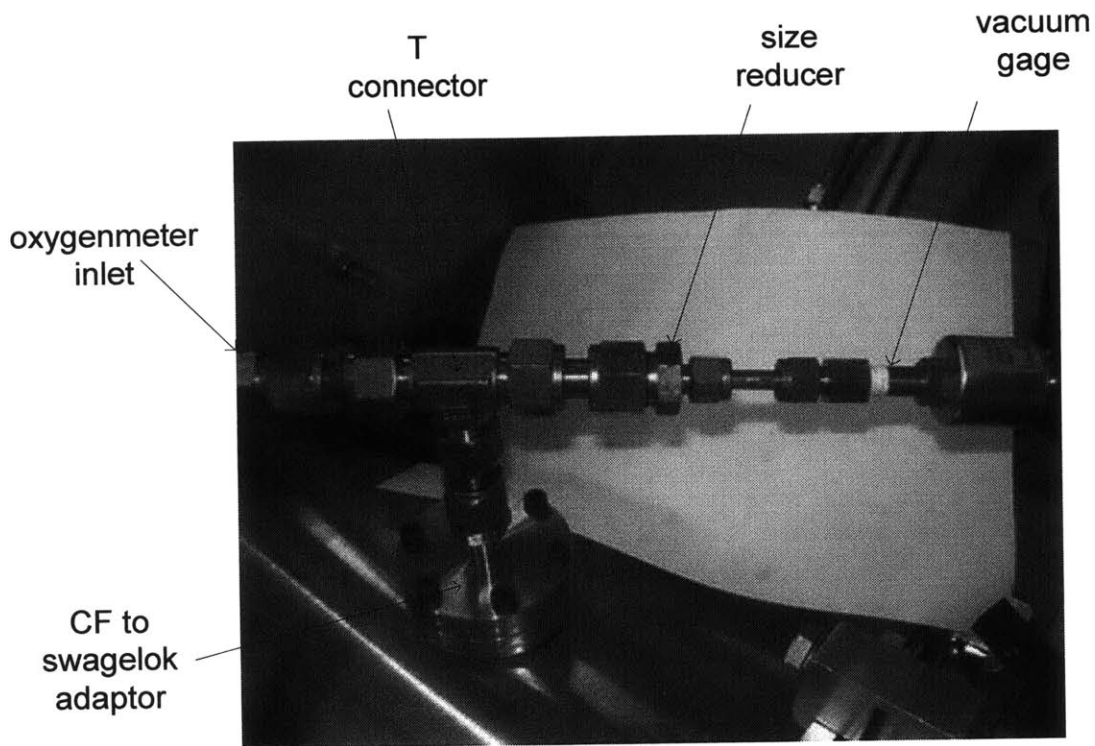


**Figure 2.42: The dual purpose port assembly.**

The vacuum pressure and oxygen content are purposely measured from this specific location because it is very close to the crucible orifice. Having a vacuum gradient inside the system is very likely because the evacuation port is at the bottom of the powder chamber (far from the crucible and top plate). The measurement of oxygen level from this location gives a true sense of this parameter. The oxygen sensor display is placed on the secondary frame therefore a long copper tube is used to connect the sensor to the gas outlet.

The same method of connection is used between the top plate and the control panel. The unique difference is that the top plate port type is made of QF connection and not CF because of the assembly and disassembly of the top plate in every run. The top plate connection leading to the crucible is shown in Figure 2.43.

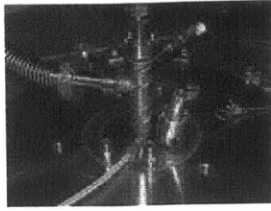


**Figure 2.43: The crucible inert gas supply connected to the top plate.**

The  $O_2$  concentration determination process taking place in the sensor is now described. The main part of the sensor, shown in Figure 2.44, is the fuel cell, which is comprised of an anode, a cathode, and an electrolyte. Inside this cell, an oxidation reduction chemical reaction takes place. The electric current flowing between the anode and the cathode is proportional to the  $O_2$  concentration of the gas stream flowing in the cell. This current, which is very small (in the order of nanoamperes), is later amplified and converted to an  $O_2$  concentration value (either in ppm or in percentage) and then displayed on the front panel screen. Since a linear relation between the circulating current and the  $O_2$  concentration exists, a calibration test is needed to set a specific fixed point and scale the entire readings. The calibration test is discussed in details in Section 4.5. Operationally, the fuel cell becomes depleted after a certain time of exposure to  $O_2$ . As a precaution, the inlet and exhaust valves of the fuel cell should always kept closed when the sensor is not in use, otherwise ambient air, rich in  $O_2$ , will flow inside and deplete the cell in a very short time. As for the output reading, it could be displayed in three different ranges varying according to concentration level. The ranges are:

- 1 – High, concentration measured in percentage.
- 2 – Medium, concentration is displayed up to 200ppm.
- 3 – Low, concentration is measured up to 20ppm.

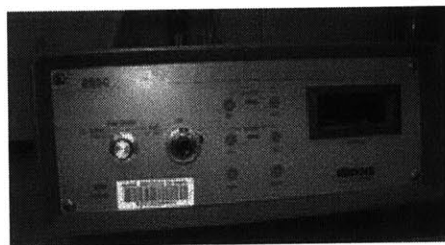


**Figure 2.44: The oxygenmeter.**



The user could switch from a range to another during run time to get a better accuracy in reading. In the UDS application, measurements are first read from the high range; once the concentration drops, the medium range is picked. The low range was not useful because concentrations below 20ppm were rarely reached. The only problem with the oxygenmeter is the long response time. This is because the O<sub>2</sub> concentration is evaluated through a chemical reaction whose speed affects the stabilized value of this concentration. The sensor never stabilizes at one value, it also overshoots. But when it starts oscillating within a small interval (less than 8ppm), the measurement ends and the concentration is approximated as the average between the upper and lower values. It takes around 10 minutes to reach this small range oscillation. During that time, inert gas must be supplied to the chamber to compensate for the lost gas flowing through the oxygenmeter.

#### **2.8.4 The evacuation part**

In this section, the process of evacuation and its relevant components, the vacuum pump and the vacuum pressure gauge are discussed. The importance of this part lies in the fact that the process of filling the chambers with inert gas generates a highly inert environment only if low vacuum level is reached. In fact, there is a strong correlation between the vacuum pressure and the oxygen concentration. Apparently, the oxygen concentration is the parameter that characterizes the inertness of the system, but technically the vacuum pressure is the key factor that affects this inertness.

The UDS system is evacuated from the powder collection chamber evacuation port. Although the heating chamber is the common part to all possible setups, the evacuation port is nevertheless placed in the powder chamber for three reasons:

- 1 – The powder chamber is open to all the vacuum system parts, thus it could be used as an evacuation port carrier.
- 2 – The heating chamber has already eight ports occupying most of its surface; it will impractical to add another large port for evacuation.
- 3 – The powder collection chamber has the bottom portion close to ground; it could be easily connected to the vacuum pump by a short flexible vacuum hose.

The vacuum pump used in the UDS is of the rotary vane type. It has two stages, and it is oil-sealed. Its motor is single phase, 110V, 60Hz with rotational speed of 1720rpm. The pump has two ports: inlet and outlet, and a gas ballast valve to help the pump preventing vapor condensation on its blades causing corrosive deterioration. The operation of the pump is triggered by a simple ON/OFF switch. The pump maintenance requires that the oil level in the oil tank be kept within the level marked on the glass sight indicator. The inlet port to the pump is made of a QF25 flange therefore a size adaptor is used to match with the QF40 flange of the evacuation port. A flexible stainless steel hose connects the pump to the system. The pump outlet port is a plastic nipple that should never be blocked. The pump exhaust is a mixture of the gas pumped out from the system with a small but malodorous oil vapor. Because of that, the outlet port should never be kept open to the surrounding. A long polymer hose tightened to the port nipple connects the pump outlet to an environmentally isolated ventilation hood where exhaust gas is sunken. The pump vibration is damped by its base supports. Next to the evacuation port, a switching valve is placed to disconnect the system from the pump. The pump with inlets and outlets connected is shown in Figure 2.45.

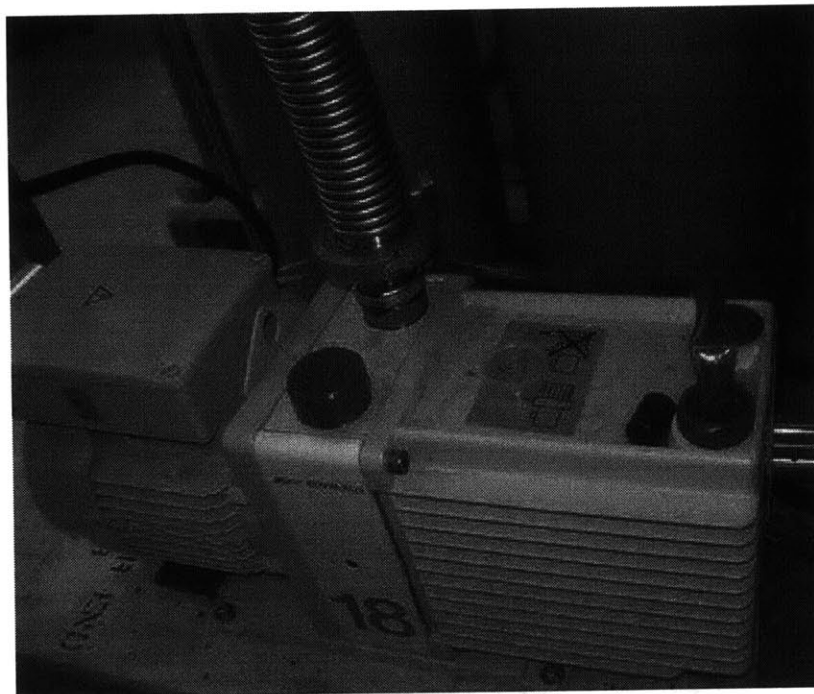


**Figure 2.45: The pump attached to the evacuation hose.**

The second part discussed in this section is the vacuum gage. The gage has two separate components, the transducer and the display. The transducer is connected to one of the chamber port as was discussed in Section 2.8.3. It detects the pressure by piezoelectric membrane deformation that generated a voltage signal proportional to the deformation. This signal is transferred from the transducer to the display by an electric wire. The reference value of the pressure/voltage scale is built in the transducer so no need for a sensor calibration. The gage range is form 0 to 2000millitorr. No pressure is displayed outside this range. The transducer is chosen to withstand a maximum pressure of 200kPa gage. This limit is above the chamber pressure that is not supposed to exceed 70kPa gage. Weren't the gage able to withstand the chamber operating pressure, a switching valve would be needed to disconnect it from the chamber at high pressures. The transducer has an immediate response since no retarding dynamics are involved to delay the measurement. The gage display is digital and it is fixed on the control panel with the other gages. The vacuum gage is shown in Figure 2.46 displaying a vacuum pressure of 17millitorr.

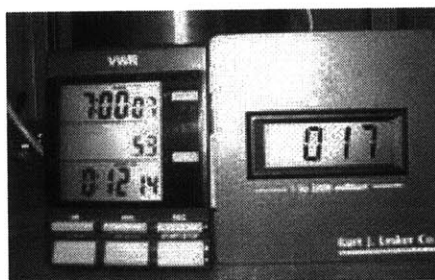


**Figure 2.46: The vacuum gage displays the vacuum pressure with a timer next to indicating the time required to evacuate the system.**

## 2.9 Vacuum Parts

The vacuum parts are among the innovations of this UDS apparatus. The research topic, “powder production process” requires the use of the top plate, heating chamber, powder collection chamber, bottom plate, and collection cup as vacuum elements. The understanding of parts’ configuration along with their functions requires first to explain

the sealing techniques implemented in these parts. The first section interprets these techniques and shows the details of their use.

### **2.9.1 Vacuum sealing techniques**

The vacuum parts are all made out of stainless steel. The following discussion is only valid for metallic-type sealing which is different from ceramic or polymer. The standard types of sealing that are implemented in the new UDS vacuum parts are: the ConFlat (CF) standard, the QF standard (which is also known as NW) and the ISO standard.

The CF sealing works as follows: two vacuum ports, as the one shown in Figure 2.47 press an annular groove in a flat ring “gasket” inserted in between the flanges; the gasket deformation is due to the “knife edge” indentation which is caused by flanges bolting to each other circumferentially by a certain number of screws depending on the flange size. The knife edge material needs to be harder than that of the gasket for indentation and sealing to occur. Stainless steel flanges best operate with annealed copper gaskets. The tightening should be strong enough to secure gasket indentation as shown in Figure 2.48. The disassembly of the sealing requires a new gasket to be installed; deformed gaskets cannot be recompressed and thus do not prevent leakage. This reason, in addition to the relatively long assembly time, make CF standard often used for permanent connections. CF has pressure range that goes down to the lowest measurable pressure and a temperature range lying between 400°C and -196°C. CF 3.38 and CF 7 are some CF sealing connections with 3.38cm and 7cm nominal flange diameter, respectively.

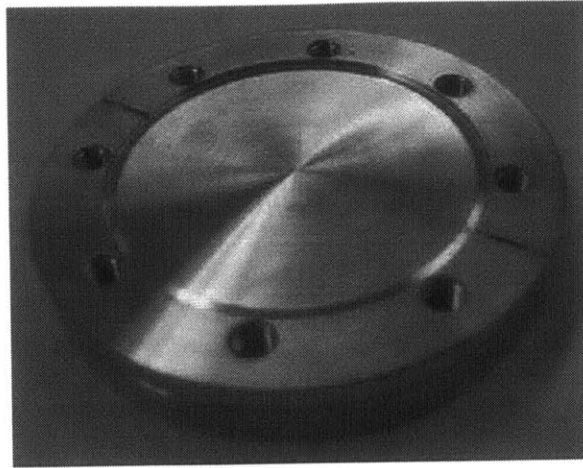


**Figure 2.47: A CF blank port with knife edge shown.**

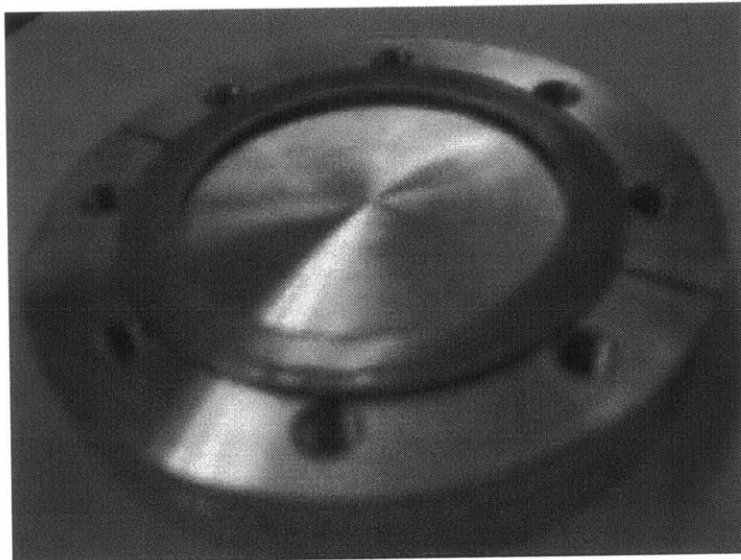


**Figure 2.48: CF port with indented copper gasket on top.**

The second type of sealing used is the QF standard. QF is schematically similar to CF, but in this case the two smooth-faced flanges have an “annular groove” where a rubber flexible “O-ring” is inserted with a centering ring to align the flanges and prevent the O-ring from collapsing. A circular clamp encloses the two flanges, and once tightened the sealing is made. The disassembly process is very simple (loosening the clamp) and the O ring could be reused without any problem. The QF is therefore a multi-assembly sealing. The QF operating pressure range is the same as that of the CF but the temperature is limited to only between  $-20^{\circ}\text{C}$  and  $200^{\circ}\text{C}$ , the point at which the rubber

melts or loses its flexibility. The QF sealing is more common in SI units; QF25 and QF40 are two QF connections of 25mm and 40mm nominal ring diameter respectively. A QF viewport with corresponding O-ring and clamp are shown in Figure 2.49.

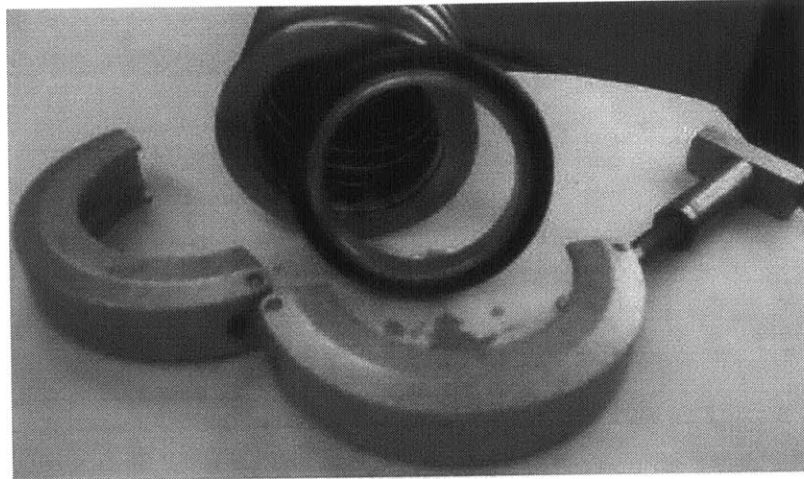


**Figure 2.49: A QF viewport with corresponding O-ring and clamp.**

The third and last sealing standard used is the ISO. This technique is generally implemented for large diameter connections (ex: connection between two chambers). The CF and QF standards are limited to 17.8cm flange diameter. The ISO however could seal up to 65cm diameter flanges. The sealing concept is similar to the QF one; however the clamping mechanism is done by either using single clamp bolts (ISO F), shown in Figure 2.52, or double hooking clamps that press on the outer rim of the two flanges (ISO K) as shown in Figure 2.50. The K type is easier to assemble. One size of the ISO K is the ISO K320, which is a 320mm flange diameter connection.

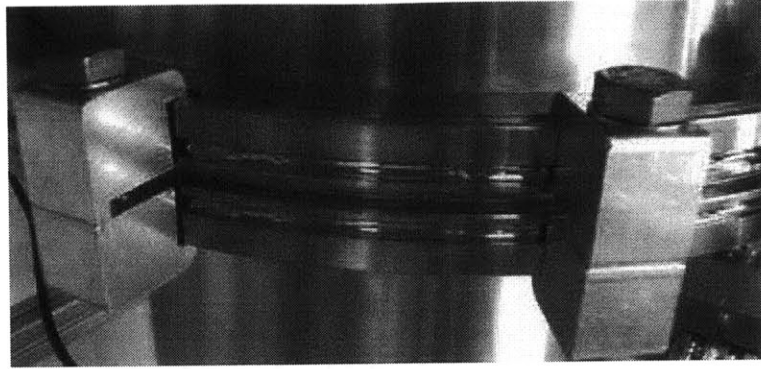


**Figure 2.50: The ISO K seal shown with double hooking clamps pressing on the flanges.**

### **2.9.2 Heating chamber**

The heating chamber shown in Figure 2.51 is by far the most important part in the new apparatus. The chamber interacts with most of the other UDS systems via its ports. It is made out of 304 stainless steel for leakage prevention (100% non-porous), excellent corrosion resistance, low magnetic susceptibility, and durability. It has a thin cylindrical shape (thickness of 3.1mm, and diameter of 35cm) with ports placed on its lateral surface. Each port has size and type chosen according to the specific function it fulfills.

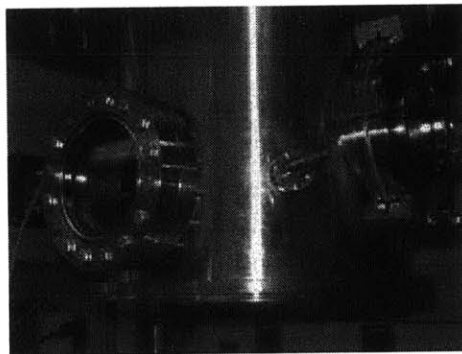


**Figure 2.51: The heating chamber.**

The upper and lower flanges are fully welded to the chamber; this is where the top plate and the powder collection chamber are respectively attached. A flanged ring welded to its upper edge, lays the chamber on an aluminum plate fixed to the main frame; the plate and chamber are fastened together. Any equipment that needs to be placed inside the chamber could be held by two mounting brackets welded to its inner wall. The heating chamber

contains the crucible set, heating coil, and the charging plate. Table 2.3 summarizes the type and function of all the chamber's ports.

**Table 2.3: Heating chamber ports' characteristics.**

Heating Chamber Ports		
Port #	Port Type	Function
1	CF 15.24	Viewport for the CCD camera
2	CF 7	Inlet to RF feedthrough
3	CF 7	Blank port
4	CF 7	Inlet to oxygenemter and vaccuam gage
5	CF 3.38	Inlet to inert gas flow
6	CF 3.38	Power feedthrough, charging
7	ISO K 80	Viewport for the strobe
8	ISO K 160	Handling port

The upper flange is an ISO F 320 (impossible to use the double clamps with this connection), but the lower is an ISO K 320.

### 2.9.3 Top plate

The top plate shown in Figure 2.52 (air side) and Figure 2.53 (vacuum side) covers the upper part of the heating chamber, thus it must have a mating ISO F 320 flange. The plate has four main functions.

- 1 – It holds the crucible assembly via its internal (vacuum) side.
- 2 – It provides an optical path for the pyrometer probe (temperature measurement apparatus) through a special viewport.
- 3 – In its center, the top plate has a slim tube with two ports:
  - a – The upper one centrally holds the vibrator.
  - b – The lateral one feeds the crucible with high pressure inert gas.

The top plate could be subject to overheating because it is in direct contact with the crucible. A cooling channel is grooved inside the plate where cooling water circulates.



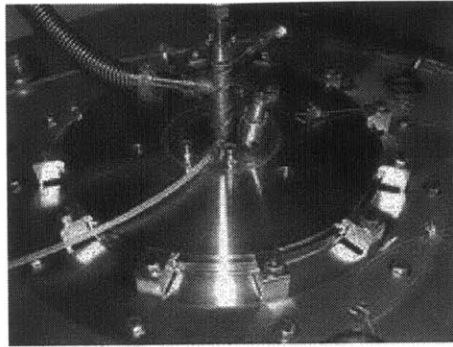


Figure 2.52: The top plate clamped to the heating chamber by ISO F seal.

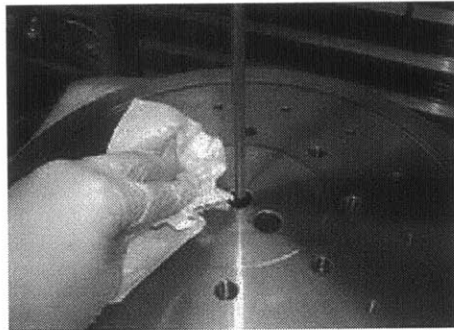


Figure 2.53: The top plate inner surface.

Also, a small-diameter (3.1mm) cooling tube is silver-soldered around the slim tube in order to prevent overheating from reaching the vibrator and to maintain the piezoelectric stacks in their normal operating temperature. The vacuum surface of the top plate has two equally spaced circular sets of threads; they could be used as alignment elements for any possible assembly inside the vacuum chambers. The top plate is relatively heavy (10 kg), it would rather be hoisted and not lifted manually; three eyehook threads are made on its outer surface for this purpose.

#### 2.9.4 Powder collection chamber

As the name indicates, the powder chamber shown in Figure 2.54 is where the droplets precipitate and cool down (by forced convection) before being collected in the collection cup. The copper droplets' cooling process was numerically simulated and the results show that the larger is the droplet, the longer should the falling distance be to achieve solidification [10]. For example 500 $\mu\text{m}$  droplets require more than 2m of

downward flight to solidify. The length of this chamber is just 1.4m therefore 350 $\mu$ m droplets or smaller size ones fully solidify. Nevertheless, the solidification could be remedied by adding a cooling liquid to the collection cup.

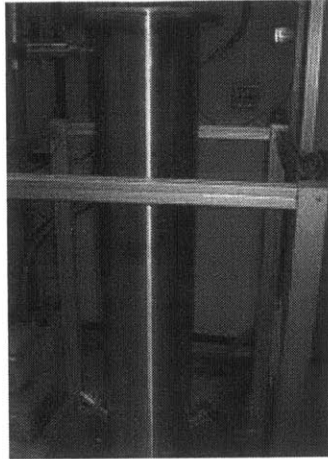


**Figure 2.54: The powder chamber sitting on its frame.**

Concerning the chamber layout, four ports were added. The ports type and function are summarized as follows:

1 – A small CF 3.38 port is used to install the linear motion feedthrough which holds the waste cup. This feedthrough could be extended and retracted by an outer adjustable screw shown in Figure 2.55. During collection, the feedthrough with the waste cup is retracted so that droplets could fall down and reach the collection cup.

2 – The second port placed in the upper part is the handling port; this port allows the user to manually access the inside of the chamber to perform some minor tasks (removing the waste cup once it is full as shown in Figure 2.56 is one possible task). The access through the handling port adds convenience to the process by avoiding the frequent disassembly of the chamber.

3 – The evacuation port (QF 40) where the pump flexible hose is connected, is placed in the bottom side of the chamber near the vacuum pump to reduce the length this hose.

4 – A CF 7 port is also placed in the bottom side with focal axis coincides with the chamber central axis. This port has no concrete use at the moment; nevertheless it could be later useful in an imaging process of a droplet deposition behavior.

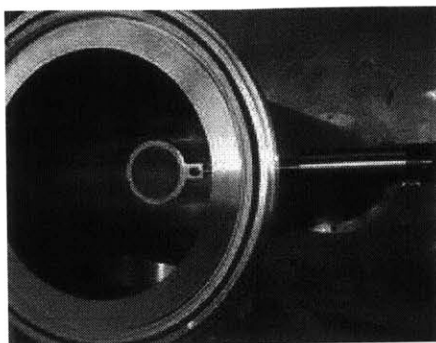


**Figure 2.55: The upper flange of the chamber with waste cup support and linear motion feedthrough.**

As shown in Figure 2.54, the powder chamber has its own frame that is displaceable; it sits on an aluminum plate similarly to the heating chamber but from the bottom. The frame could be raised or lowered when the chamber needs to be assembled or disassembled from the heating chamber.

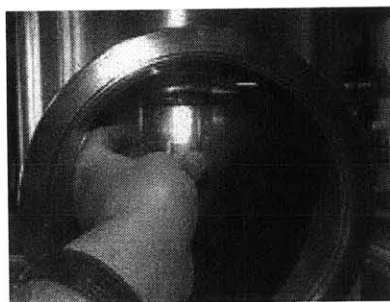


**Figure 2.56: The waste cup is placed inside or removed from the powder chamber via the ISO port.**

### **2.9.5 Bottom plate and collection cup**

The last two vacuum parts described here are the bottom plate shown in Figure 2.57 and the collection cup of Figure 2.58. The bottom plate covers the bottom part of the powder chamber with an ISO F type connection. This plate has a central hole where the collection cup is externally clamped. The collection cup is placed outside the chamber and not inside as was done in the current apparatus. If the cup were placed inside the chamber, its removal would require the disassembly of the powder chamber or the bottom plate, the two steps that are cumbersome to implement with the new vacuum system. As

designed, the collection cup has its own flange and could be independently and frequently removed from the bottom plate without any other parts being affected.

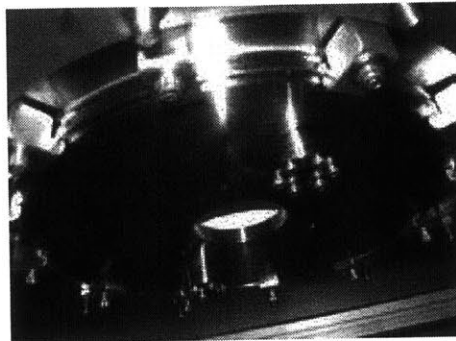


**Figure 2.57: The bottom plate clamped to the powder chamber.**

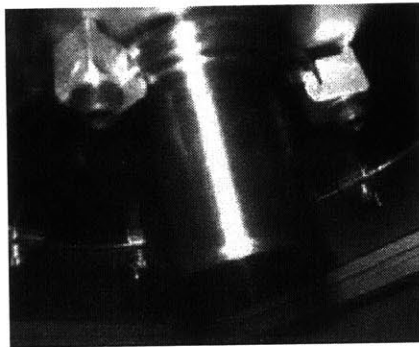


**Figure 2.58: The collection cup clamped to the bottom plate.**

The bottom plate has two CF 3.38 connection ports. Their use is summarized below. As mentioned before, medium and large size droplets (400 to 700 $\mu$ m) only attain skin solidification during their downward flight in the powder chamber. While their inner content is still liquid, they could be subject to bursting if they were directly quenched in the cooling liquid of the collection cup. To overcome this problem, an oil bath heated with band heaters, could be installed on top of the bottom plate to secure a transient temperature drop for the droplets. The two ports are used to achieve this setup. The first carries the power feedthrough that transfers electric power to the heater and the second holds the sensor feedthrough that transmits the thermocouple signal used in the bath temperature measurement. In spite of their presence, both ports are now blanked and the oil bath setup is disregarded for the moment. The collection cup is filled with silicone oil

as cooling liquid. The silicone oil used should have very low vapor pressure (preferably lower than the required vacuum pressure); otherwise it will evaporate during the chamber evacuation process and then condensates all over the bottom plate and the powder chamber walls. Silicone oil can be used for several runs without any problem. It is anyway expensive to be frequently discarded.

## **2.10 The water Cooling System**

So far, the water cooling requirement has been raised twice, first with the top plate in Section 2.9.3 and second and most importantly in the induction heating process in Section 2.1.3. The quality of water flowing in the cooled parts is an important factor to consider in designing the cooling system. Regular sink water for example has high concentration of minerals that if accumulated in the coil or in the 3mm cooling tube of the top plate, they would block the passage of water and impair the whole cooling process. For this reason, water flowing in the cooled equipment needs to be pure, commercially available distilled water is a good example of pure water. These channels are referred to as the *clean loops*. The cooling mechanism could be achieved by several means like the implementation of a refrigeration cycle (freon circulation) or the use of another cooler medium in a well applied heat removal process. The second option is implemented by using the MIT special cooling grid. The cooling system is therefore composed of the water recirculator where the cooling process occurs and two sets of water connections, one going from the cooling grid supply to the recirculator and the second, which is the clean loops, feeds the equipments from the recirculator. The properties and functions of these parts will be now described in details.

### **2.10.1 The recirculator unit**

The recirculator is the central element of the entire water cooling system. It has two main functions mentioned below:

- 1 – Make use of the chilling water supply brought from the cooling grid to cool and control the temperature of the water circulating in the clean loops.

2 – Pump up the clean water (CW) so that it could be used at higher elevation or farther distances (in case the application requires so).

The recirculator unit, shown in Figure 2.59, has three main components: the heat exchanger, the pump and the temperature control loop.

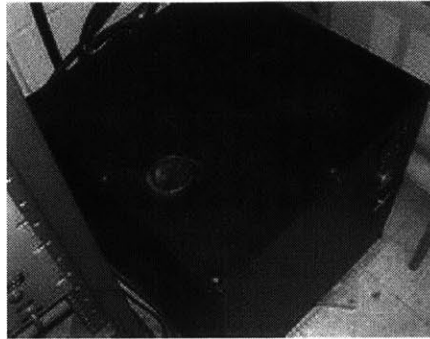


**Figure 2.59: The recirculator unit.**

The heat exchanger is a well insulated box where both flows circulate in two different copper coils interfering with each other. The CW exiting the heat exchanger is first collected in a small reservoir before being pumped to the cooled systems. This reservoir has an inlet to the outside; this is where CW is poured in. The clean flow also has a drain valve located on the extreme bottom of the recirculator. Using this valve, CW could be drained from the entire UDS system. The used water discard and new pure water addition should be done after several runs are made (typically 15 runs). This maintains cleanliness of the CW passages, and enhances the cooling process as a whole. The facilities water could also be drained from a gate valve placed on the lower side of its passage. While draining, the unit is supposed to be switched off. The recirculator internal channels layout is included in Appendix D.

The key element of the facilities water flow is the solenoid valve. This valve placed on the inlet port of the heat exchanger, opens and closes automatically (by electromagnetic interaction) according to the control action of the temperature closed loop control shown in Figure 2.60. This control actuation operates in the following way. A comparator checks the sign of the error signal ( $T_{in} - T_{act}$ ). Negative errors actuate the solenoid valve to open allowing facilities water to flow and intensify the cooling effect (heat exchanger mode) until the actual temperature matches the desired one. Positive

errors however shut down the valve preventing the facilities water from flowing in. The heat exchanger becomes in this case a heat sink where CW dumps part of its heat to a fixed mass system. In the heat sink mode, the facilities water will heat up and the CW temperature will rise over time, until it matches the set inlet temperature. Obviously, the cooling effect in the cooled parts of the UDS apparatus is much greater in the first mode of operation (solenoid switched on) than it is in the second mode.

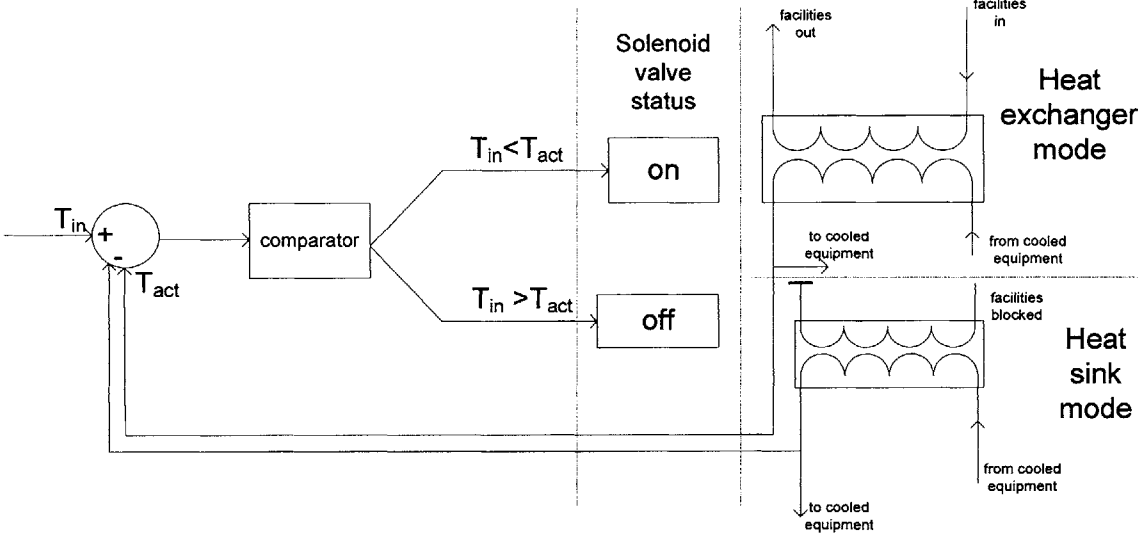


**Figure 2.60: The cooling processes inside the heat exchanger.**

The CW exit temperature is limited to between 40°C and 10°C. The facilities water temperature is rarely lower than 13°C. Therefore the CW exit temperature will always be above 13°C. But as a design criterion, the oscillator’s manufacturer settings require that the cooling water temperature to be above 20°C in order to avoid condensation problems on the capacitors. Thus desirable inlet temperatures are never set below this threshold.

In case of small thermal loading, it will be enough to just partially cool the CW. For this purpose, a bypass valve is placed before the CW coil inlet to control the amount of water flowing into the heat exchanger. Since most of the pressure loss occurs in the heat exchanger coil passages, bypassed stream does not need to be pressurized. The discharge pressure is adjusted using this valve. The discharge temperature and pressure are both displayed on two different front panel gages.

### 2.10.2 The water channels

In this section, the clean loops and then the facilities connections are discussed. The clean loops have simpler configuration than the facilities loop which contains several flow elements to visualize and manipulate the flow characteristics.

The clean loops are made of flexible polymer tubes and hoses. This choice provides the required water cleanliness over long time of use. The recirculator cold flow has only one inlet and outlet port. Two necessary manifolds as shown in Figure 2.61 (inlet and outlet) are thus made to bifurcate the recirculator flow into four channels, two serve the top plate and the other two serve the oscillator.

The oscillator channels, made out of hoses, have permanent connections. The oscillator has the end fittings already built in. The top plate is however subject to frequent disassembly, the issue that could cause water spilling while disconnecting the channels. The “quick disconnect” connections remedy this problem. During disassembly, the “quick disconnect” valve goes into two closed parts each on one side of the sliced tube, preventing water from spilling.

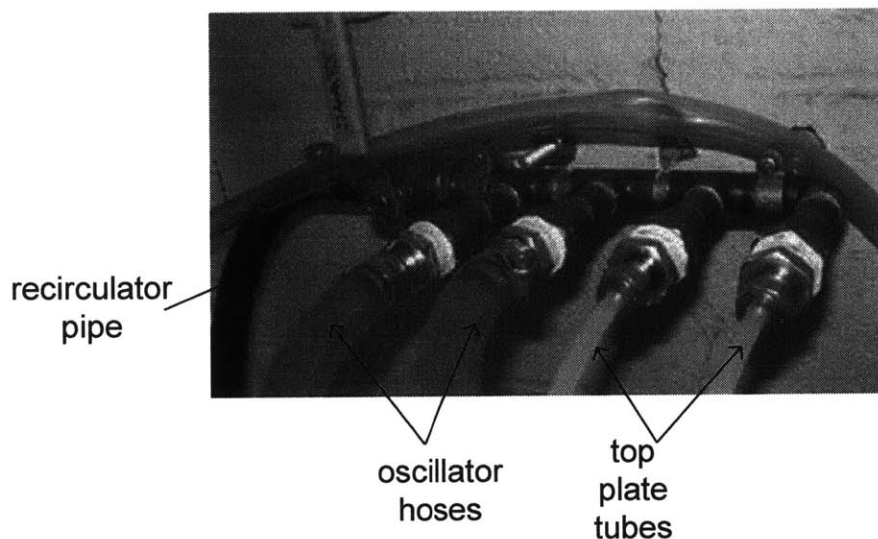
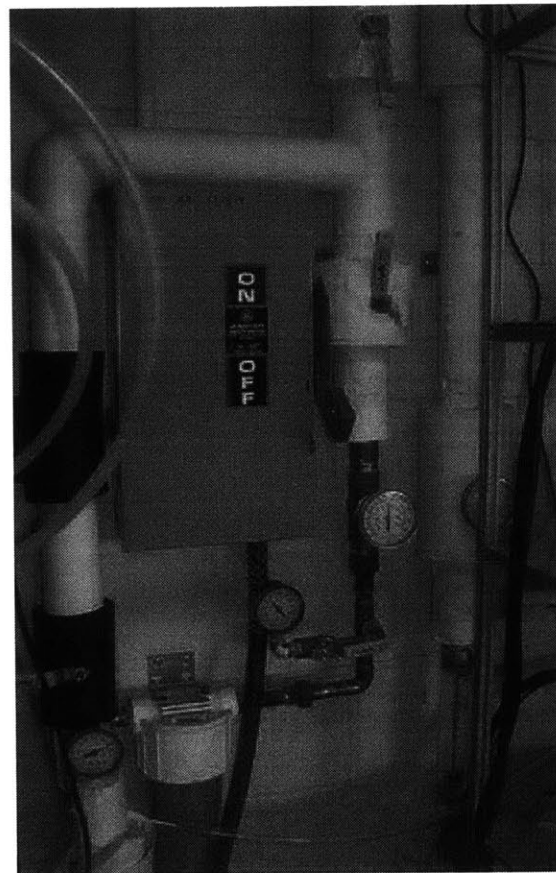


Figure 2.61: One of the manifolds (inlet or outlet).



The facilities loops shown in Figure 2.62 are fixed channels between the facilities grid and the recirculator. The water flowing inside contains large-size impurities which could block the recirculator passages. A filter, shown in Figure 2.63, is therefore installed to clean the water before entering the recirculator. Two temperature gages (spiral type) are installed on both inlet and outlet to observe the temperature drop and corroborate the cooling effect. Three pressure gauges are also placed in the facilities loops, two in the inlet before and after the filter, and one in the outlet. The filtering effect must be accompanied with a pressure loss equal to the pressure gages' readings difference. The heat exchanging process also involves a pressure drop notified with inlet and outlet gages. A flowmeter measuring the volume flow rate in liters/min is placed on the return side of the loop. Concerning the switching valves, two of them are placed on inlet and outlet to stop the flow and the third, "drain valve", is placed on the bottom of the loops to drain the water upon need.



**Figure 2.62: The cooling water supply channels.**



**Figure 2.63: The filter.**

## **2.11 The Frame and Hoisting System**

The frame was the first system to be installed in the new UDS apparatus. This system is comprised of the main frame, powder collection chamber frame, and the hoist. The frames hold the apparatus components and the hoist displaces the elements required to be moved each time the apparatus is disassembled or under preparation for a new run. The design of this system and its usefulness are discussed in the following subsections.

### **2.11.1 The main frame**

Since the new UDS apparatus is modular in design, other chambers could be later installed to the apparatus. The main frame is the part that assembles all the apparatus components that must operate in all possible experiments. These components are:

- 1 – The heating chamber, which is obviously the most common part.
- 2 – The oscillator which is placed next to the heating chamber because of power supply.
- 3 – The hoist which needs to be the highest element of all the UDS parts.

4 – The imaging system parts: camera and stroboscope.

5 – The gas control panel, close to gas tanks and heating chamber.

The main frame is fabricated from grooved aluminum bars that are joined to each other. Slotted nuts are easily inserted into the grooves thus easing the assembly of fixtures on the bars. Figure 2.64 shows how a lock nut is inserted inside the groove. In its upper part the frame is joined by horizontal bars on which the heating chamber support plate sits. This plate has a central hole where the heating chamber falls, a circular drill set via which the heating chamber is assembled, and four diagonal slots that serve in the powder chamber assembly process discussed below. The oscillator sits on a plate fixed to lower cantilevered horizontal bars. At the extreme top, the frame has two long bars across which sits a large beam that carries the hoist. These long bars have solid steel rods inserted in their grooves so that the hoist's beam could slide back and forth along the bars. The frame perpendicular connections are strengthened by short, diagonally placed, bars to reduce the frame shaking during hoisting.

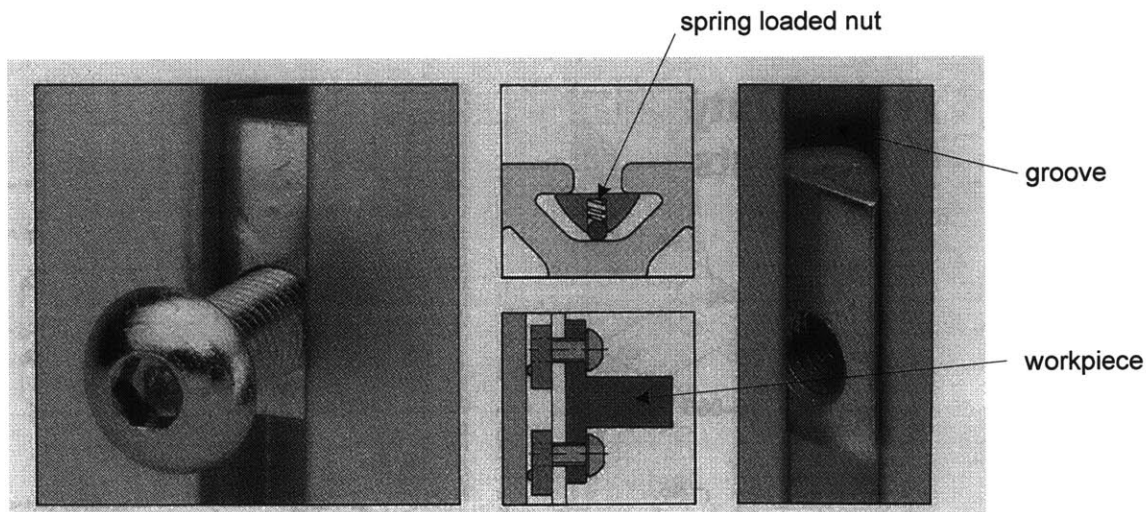


**Figure 2.64: The lock nut assembly on the frame bars.**

### **2.11.2 The powder collection chamber and secondary frames**

The powder collection chamber is an independent part of the UDS that is assembled to the heating chamber only if metal powder is the anticipated outcome of the process; it thus has its own frame. This frame, in contrary to the main one, needs to be

displaced during disassembly; so it has wheels. The frame also slides up and down to raise the powder chamber and lower it. The vertical bars are inserted in other hollow bars to realize this motion. The hollow bars are fastened to some eyehooks that connect the frame to the hoist. The frame horizontal bars are exactly similar to those used in the main one; it results that the powder chamber assembly with its frame is exactly similar to the heating chamber assembly with the main frame.

The secondary frame carries all the remaining equipment of the UDS apparatus. Its bars are similar in design to those of the other two frames but have a smaller cross section because of the lighter load supposed to be carried. The frame is made out of four shelves resulting in left free space that could be occupied if extra equipment is later installed. The UDS components placed on this frame are: the oxygenmeter, TV set, pyrometer display, function generator, amplifier, frequency divider and charging voltage supply. The function generator is the only component whose location on this frame is critical because the user needs to tune the output frequency and the crucible pressure regulator simultaneously to achieve a stable breakup.

### **2.11.3 The hoist**

The new UDS apparatus includes an electric hoist. It is useful for the following tasks:

- 1 – The top plate assembly is relatively heavy (12kg) and has the brittle graphite crucible in it, so it is safer to be lifted to the top of the main frame by an electric hoist.
- 2 – The powder chamber when assembled or disassembled from the heating chamber is lifted up and down by the electric hoist.

The hoist is located on the main frame sliding beam, as shown in Figure 2.65. The hoist needs to glide because its position from which it picks the top plate is different from that it occupies when it settles the plate. The plate is connected to the hoist cable via three eyehooks threaded to its top surface. The hoist motion is controlled by an up-down switch.

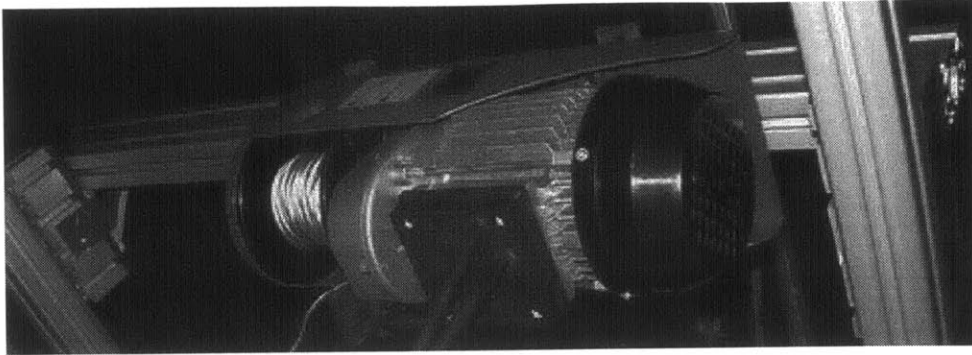


**Figure 2.65: The hoist on top of the main frame, carried by the sliding beam.**

The powder collection chamber frame is connected to the main hoist cable through four auxiliary cables, each one attached to one vertical bar. These cables traverse through the heating chamber support plate slots shown in Figure 2.66, before being connected to the hoist cable. The cables roll on pulleys fixed in the middle of the slots. During motion, the outer hollow bars of the frame slide against the inner bars. The exact positioning of the hoist on the sliding beam is adjusted by aligning the hoist cable with the heating chamber central axis which coincides with the powder collection chamber axis when both chambers are assembled. In this way, the matching surfaces will stay parallel and the cables' loading is balanced.

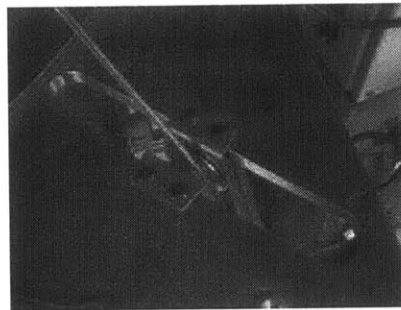


**Figure 2.66: The auxiliary cable rolling on the pulley fastened to the slot.**

## Chapter 3

# THE UDS SYSTEMS ASSEMBLY

In this chapter, the assembly processes of the UDS apparatus will be discussed. These assemblies are made to join the UDS systems together and prepare the apparatus for operation. The assemblies are listed below:

- 1 – UDS general layout.
- 2 – Crucible assembly.
  - a – machining.
  - b – preparation.
- 3 – Top plate assembly.
- 4 – Bottom plate assembly.
- 5 – Coil assembly.
- 6 – Vacuum chambers assembly.
- 7 – Gas management system assembly.
- 8 – Imaging system assembly.

The diagram of Figure 3.1 shows some of the UDS assemblies on the apparatus layout. The discussion in the following sections will follow a trend that shows the assembly importance, lists the elements involved, orders the steps taken to accomplish it and stresses on some important points that require a special consideration.

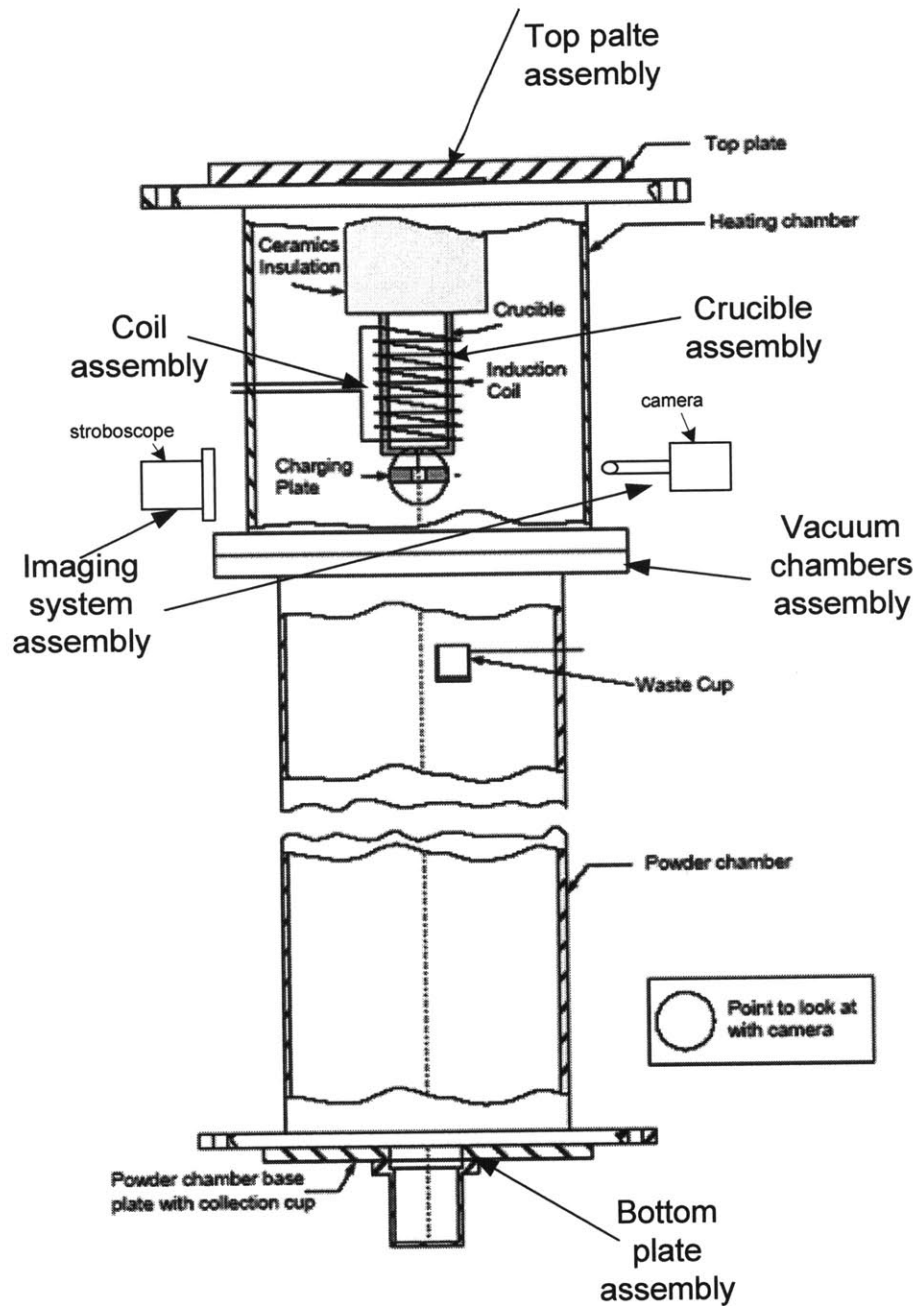


Figure 3.1: The UDS assemblies' classification.

### 3.1 The UDS General Layout

This assembly is the first to be made. It basically involves the determination of the exact location in the DBM lab (area and height) that should be left for the new UDS apparatus

to be placed so that all its systems could be accessed easily. The considered factors of this assembly are listed below in their order of importance:

- 1 – The main and secondary frame size.
- 2 – The unframed parts accessibility.
- 3 – The cooling water supply connection.
- 4 – The apparatus ease of assembly.
- 5 – The induction heater electric connection.

All the above criteria are satisfied in this assembly and the schematic diagram of the apparatus systems is shown in Figure 3.2.

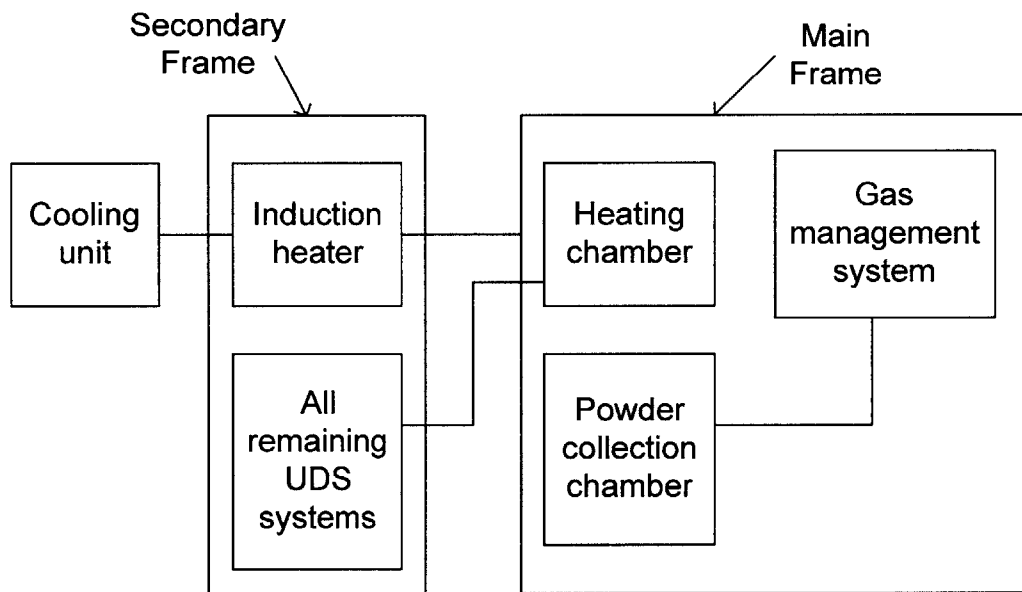


**Figure 3.2: The major UDS components arrangement.**

### **3.2 The Crucible Assembly**

This assembly has two parts. The first describes how a crucible that could fit into the system is designed from custom graphite parts. The second explains how this designed crucible could be prepared to be later used in the UDS experiments. Obviously, the first assembly is permanent but the second is necessary for every run.



### 3.2.1 The crucible machining

The crucible requires, by design, to have a knife edge machined on a flange in order to seal it against the insulation block. Unfortunately, the standard crucible with dimensions and capacity that closely match the designed one was unflanged. Therefore the crucible needed to be custom flanged. The flange has the following features:

- 1 – An inner diameter set to the inner diameter of the crucible.
- 2 – A thickness of 1.25cm.
- 3 – Has eight equally spaced holes that are counterbored to hide the screws head down form this sealing surface.
- 4 – It is attached to the crucible by two reinforcing means:
  - a - bolts were used to join it to the crucible.
  - b - graphite adhesive is added on the contact edges from inside and outside to better bonds the two parts together and fills the gaps that could be a source of leakage.

Eight tapped holes were also made on the crucible's upper thin edge. The screws used in the first joining step were made of the non magnetic stainless steel so as not to heat up by induction. The graphite adhesive has a very high operating temperature (2700°C) so the junction made is in a considerable margin of thermal safety. The adhered surfaces should be cured at 150°C for two hours in order for the adhesive to solidify and harden.

The steps of crucible production and assembly are listed below with some of the steps shown in Figure 3.3.

#### A: Crucible machining [equipment used]

- 1 – A bolt circle (8 holes, equally spaced) is drilled on the crucible upper edge (a).  
[automated milling machine]
- 2 – The holes are tapped with the #2-20 thread. [tapping tool]
- 3 – An orifice pocket and central hole are made on the crucible bottom surface (b). [lathe]

4 – A nozzle shape cone is countersunk on the inner surface of the crucible bottom (c). [lathe]

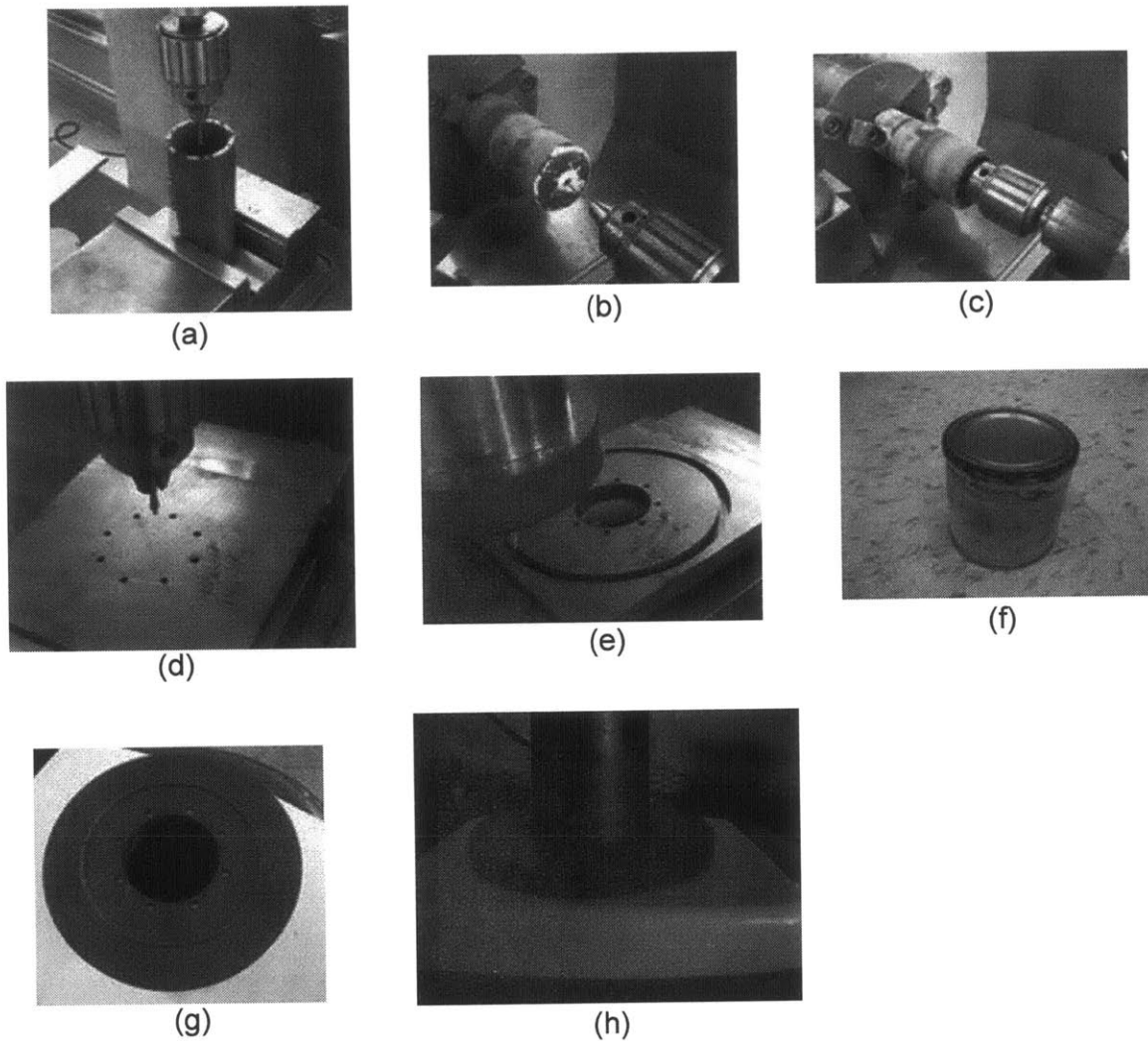


**Figure 3.3: The crucible machining processes.**

#### **B: Flange Machining**

5 – The bolt circle is drilled on the plate (d). [automated milling machine]

6 – The drilled holes are counterbored (d). [automated milling machine]

7 – The flange boundaries are milled (e). [automated milling machine]

8 – The knife edge is turned onto the surface. [lathe]

#### **C: Joining the crucible to the flange**

9 – The graphite adhesive is added on the mating surfaces (f).

10 – The bolts are fastened and tightened (g).

11 – The adhesion is cured on the heating plate (h).

The crucible by now becomes ready to be prepared and then used in the UDS process.

### **3.2.2 The crucible preparation**

This process is all about the orifice insertion into the crucible so that it could be later incorporated into the top plate assembly. This preparation lasts only for a single run. Once the crucible is disassembled, the orifice can't be cleaned or reused; it must be removed, disposed and replaced by a new one. The oxides accumulating around the orifice hole form a layer that prevents it from being used for another run. The orifice removal is achieved as follows: a metal pin is inserted into the orifice pocket from the crucible upper part, pushes against the orifice until the adhesive layer is broken or detached and the orifice is pulled out. A cleaning process of the bottom part of the crucible using an ultrasonic cleaner is recommended to remove residual oxides and adhesives. Adhesion is stronger when the surfaces it bonds are cleaner. The steps involved in this process are listed below and illustrated in Figure 3.4.

#### **A: Cleaning**

1 – The residual copper part of the billet (part that was not sprayed) is first removed. The removal process is not a problem because of the graphite non wetting copper characteristic; it is further eased with a tapered shape crucible.

2 – The used orifice is pulled out from the crucible (a).

3 – The crucible bottom part is immersed in the ultrasonic cleaner's beaker (30 minutes). The solution could be either alcoholic (acetone, 10%) or even acidic (0.1% nitric acid) (b) and (c).

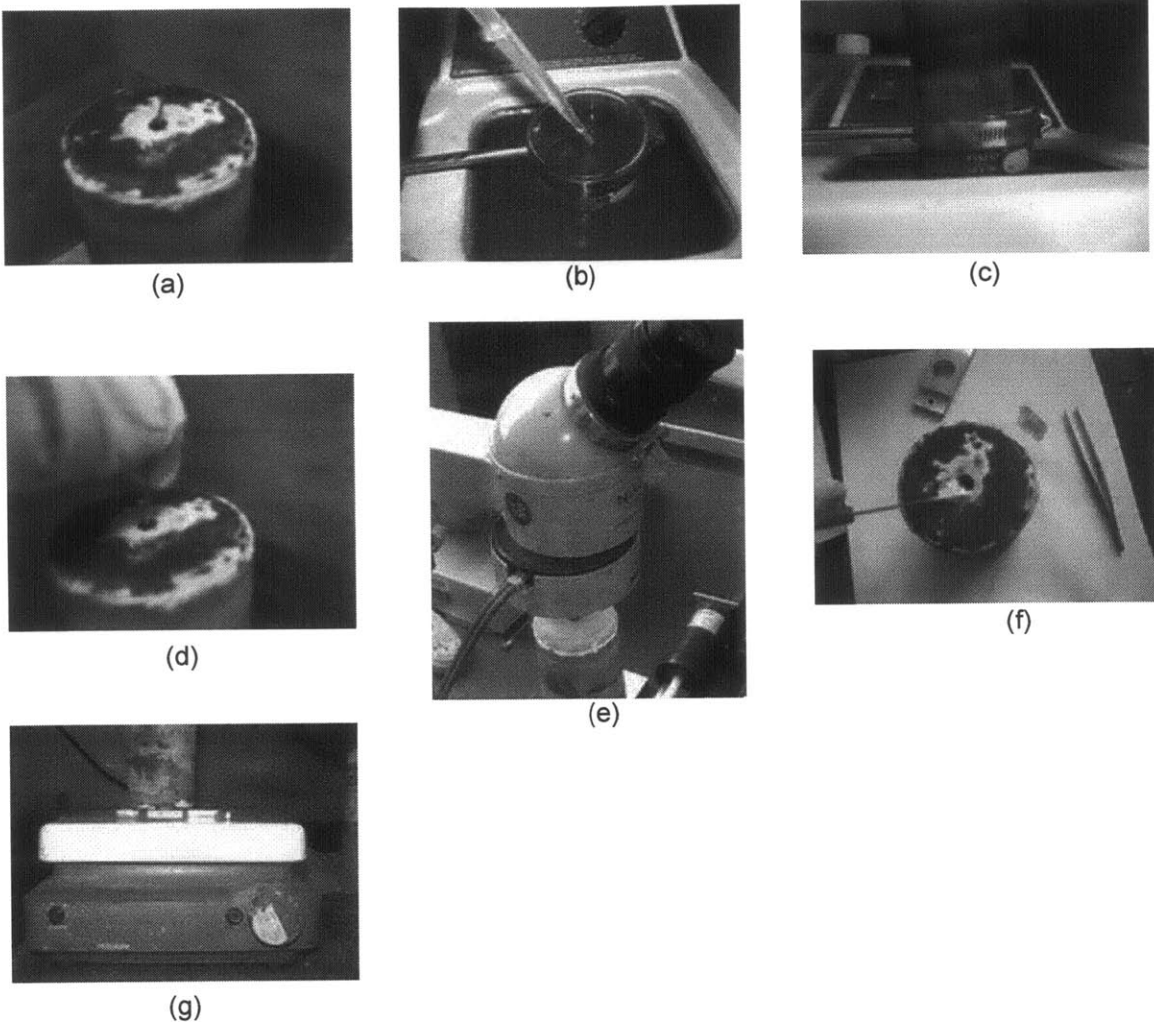


**Figure 3.4: The crucible preparation steps.**

#### B: Orifice Insertion

- 4 – A new orifice (required size) is inserted into the crucible orifice's pocket (d).
- 5 – The orifice is observed on the microscope to check for both hole size and cleanliness (e).
- 6 – The adhesive solution (thinner and adhesive) is prepared on a sheet of paper and the adhesive bottle is immediately closed so that it doesn't dry out (f).
- 7 – The orifice is glued with extreme care; all the boundaries must be covered with adhesive (f).
- 8 – The orifice is again inspected on the microscope; the adhesion and the central hole clearance must be checked (e).

9 – The adhesion is cured (100°C, 2 hours) by heating the crucible lower part on the heating plate (g).

### **3.3 The Top Plate Assembly**

This assembly which is shown in Figure 3.5 and Figure 3.6 is crucial for every UDS run. It mainly aims to insert the copper billet into the crucible. The parts involved in this assembly are the top plate, the crucible and its insulation entities, the sealing gaskets, and the vibrator. Since the crucible has a closed bottom, the only way it could be loaded is from top. The top however can't be reached unless all the interconnected parts are disassembled. The sealing parts are evidently subject to frequent disassembly, and thus their design criteria need to be thoroughly considered to satisfy this requirement. The sealing isolating the crucible environment from the chamber one is the most important of all the UDS apparatus' sealings. In the top plate connections (vibrator and gas hose), no CF flange type ports were allowed so as not to replace the gaskets for every assembly; the standard QF and swagelok sealing techniques were implemented. However, the uncommon crucible sealing problem (ceramic and hybrid) lack standard guidelines. In such a case, the physical life of the graphite gaskets in terms of number of runs is only determined by testing. These gaskets obviously deteriorate because of both thermal and compressive loadings. The upper gasket is in contact with the cold side of the insulation, thus it has a longer life than the lower gasket which has a higher deterioration rate because of its direct contact with the heated crucible. The upper gasket could be used for more than 10 runs; however the lower one must be replaced every 4 runs.

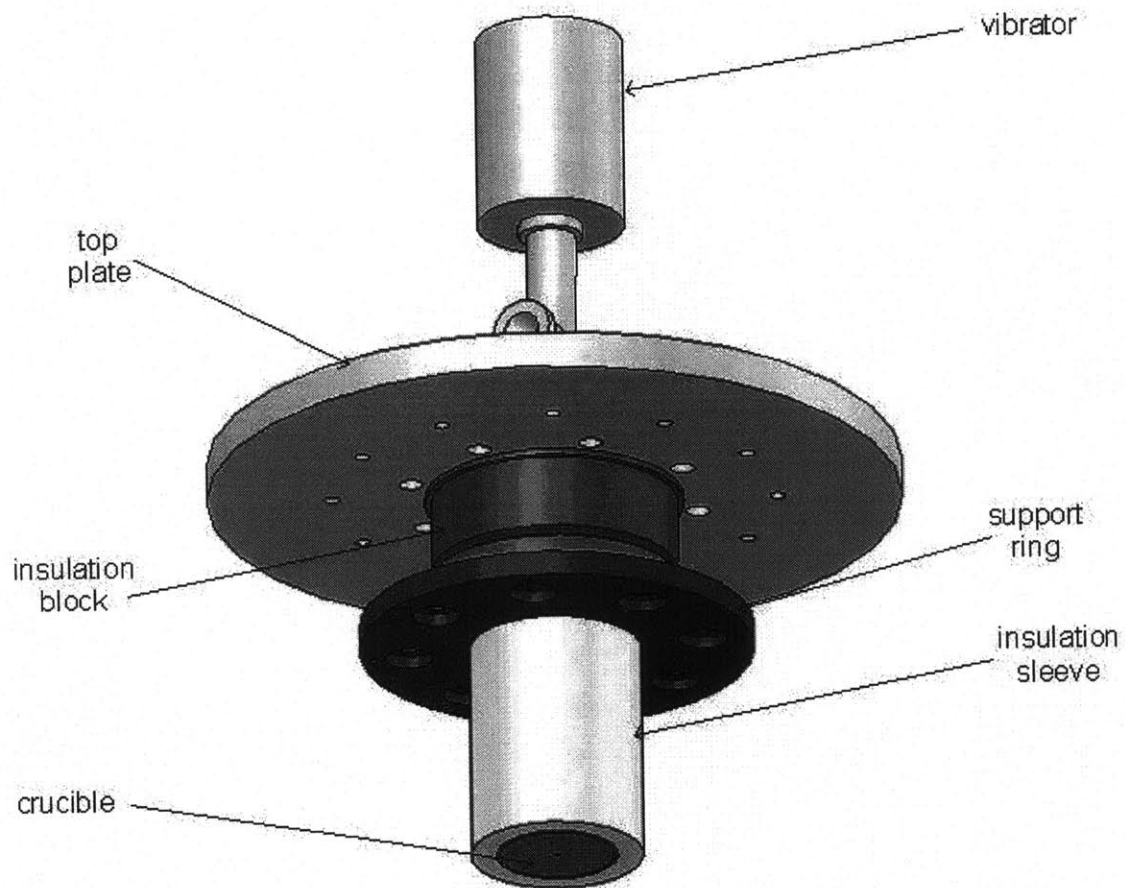


**Figure 3.5: The top plate assembly.**

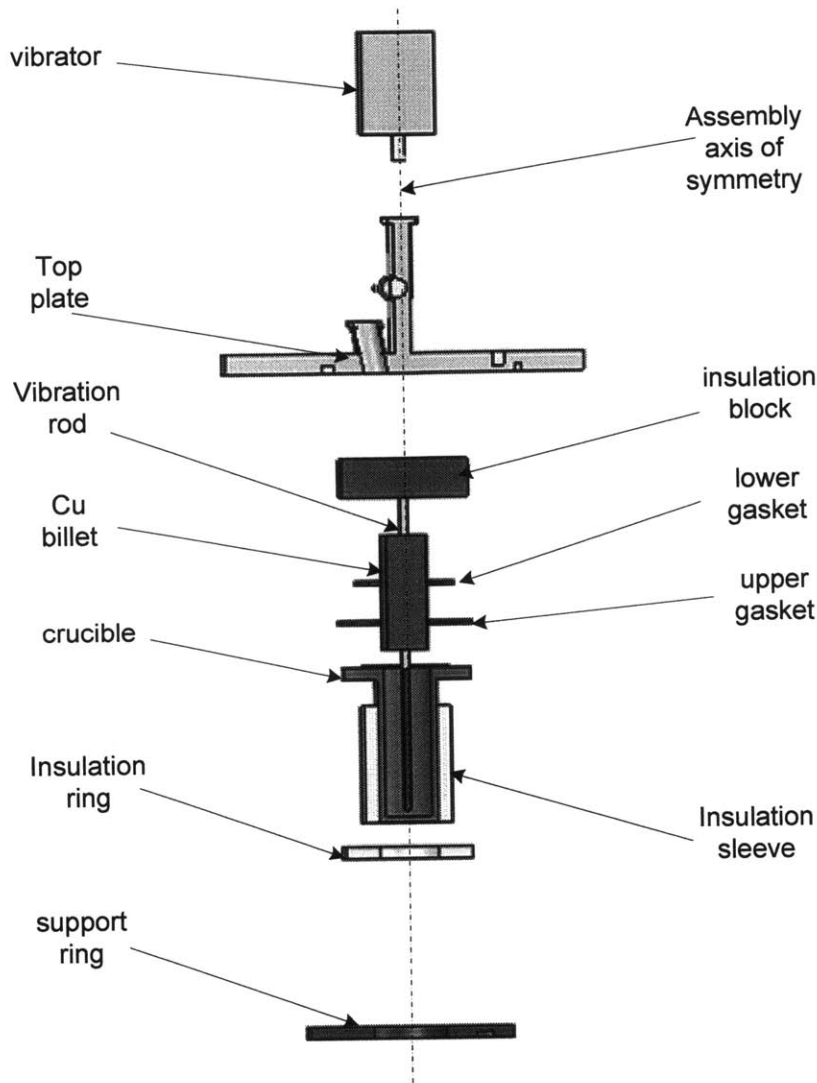


**Figure 3.6: The top plate assembly exploded view.**

The engineering drawings of all the elements are included in Appendix B. This assembly has an axial symmetry on which the alignment of all these parts is based. Because of this symmetry the vibration rod which coincides with the symmetry axis could be used as the alignment tool when arranging the parts. However, the vibration rod ceramic part (made of Boron nitride AX05) is a very brittle and soft material that will definitely break once the assembled top plate is tilted before being sent to the hoist. Therefore, an aluminum rod of the same size of the vibration rod, threaded to the vibrator fitting, is temporarily inserted into the assembly. Once the assembly is done and the top plate clamped to the heating chamber, the alignment rod is removed and the vibration rod takes its place. The

disassembly process obviously starts from the last step and ends at the first one with no need to insert the alignment rod. The detailed assembly steps are as follows. Figure 3.7 illustrates some of these steps, which are labeled from “a” to “z”.

- 1 – The top plate is tilted and placed on two support cylinders so that its vacuum surface faces upward.
- 2 – The alignment rod is positioned and fastened to the vibrator swagelok fitting (a).
- 3 – The top plate sealing contours are cleaned by acetone or any other alcohol (b).
- 4 – The upper gasket is placed with radial width covering the sealing knife edge (c).
- 5 – The insulation block is placed on top of the gasket (d).
- 6 – The insulation block is relocated (e) so that its eccentric hole is aligned with the transparent viewport insertion to secure clear optical path for the pyrometer (a special alignment tool is used to check this clearance).
- 7 – The lower gasket is placed on top of the insulation block knife edge (f).
- 8 – The copper billet is then inserted; its central hole falling in the alignment rod (g).
- 9 – The orifice loaded crucible is then placed on top of the gasket (h).
- 10 – The insulation ring is inserted on top of the crucible flange surface (i).
- 11 – The support ring is placed on top of the insulation ring (j).
- 12 – The ring is fastened to the top plate with 8 screws equally spaced on a circle (k).
- 13 – The insulation sleeve is wrapped around the crucible lateral wall (l, m).
- 14 – The sleeve is firmly taped by the high temperature taping roll (n).
- 15 – The top plate is removed from its support cylinders, tilted upward and placed inside a box (o).
- 16 – The three lifting eyehooks are clamped to the top plate upper surface (o).
- 17 – The box is dragged next to the main frame where the hoist cable is lowered and hooked to the eyehooks (p).
- 18 – The O ring for the top plate-heating chamber ISO seal is placed in the groove (s).



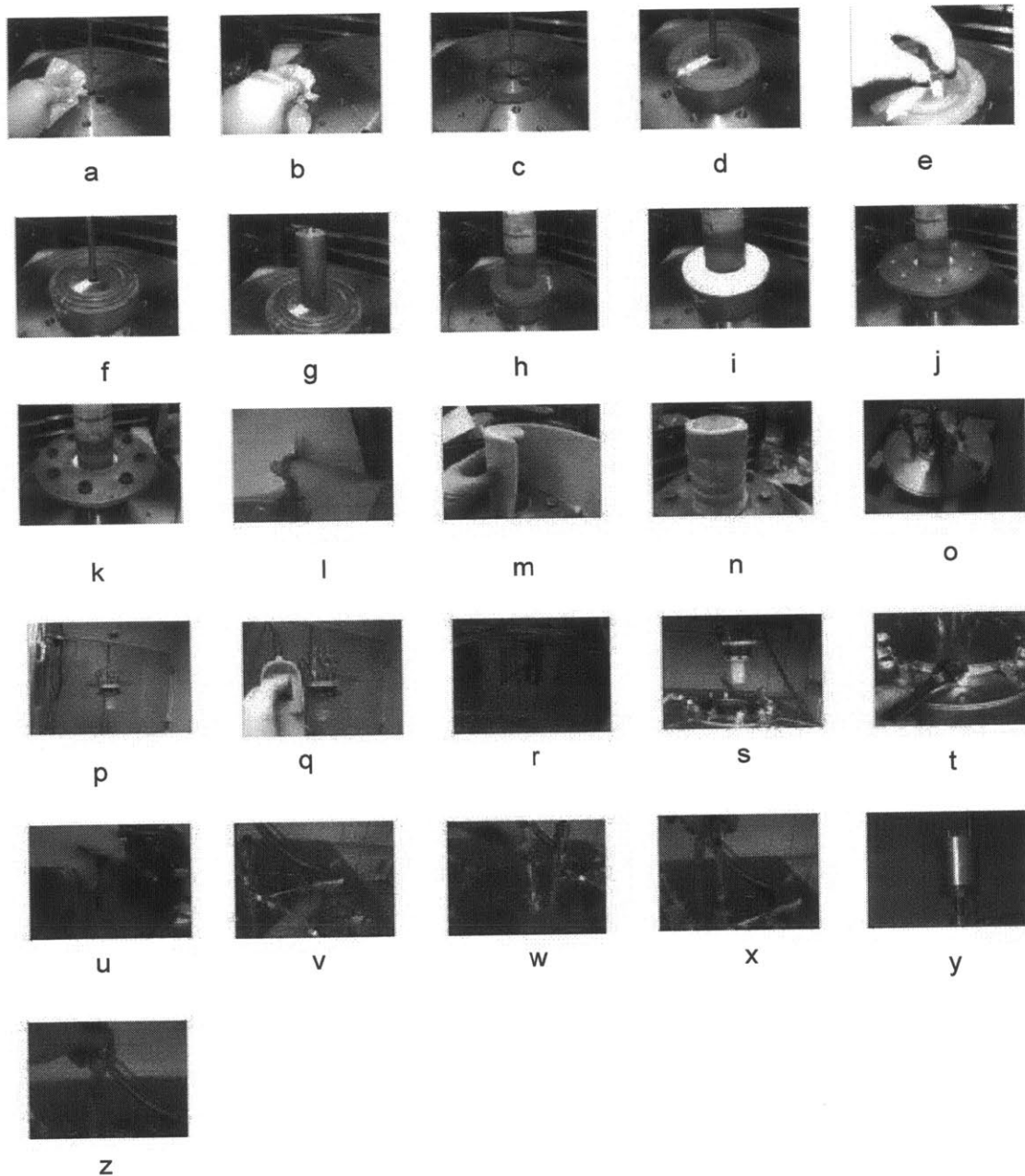


**Figure 3.7: The steps taken in the top plate assembly.**

- 19 – The top plate is lifted upward, traveled to above the heating chamber and then lowered above the O-ring (q,r,s).
- 20 – The top plate is clamped to the heating chamber (t).
- 21 – The eye hooks are removed from the top plate (u).
- 22 – The crucible gas supply hose is clamped to the top plate (v).

- 23 – The top plate water cooling quick disconnects are joined together (w).
- 24 – The alignment rod is removed and the vibration rod is placed instead (x).
- 25 – The vibrator is fastened to the rod and connected to the top plate (y).
- 26 – The pyrometer probe is inserted in the viewport nipple (z).

Figure 3.8 shows a section view where the optical path necessary for the pyrometer is arrowed.

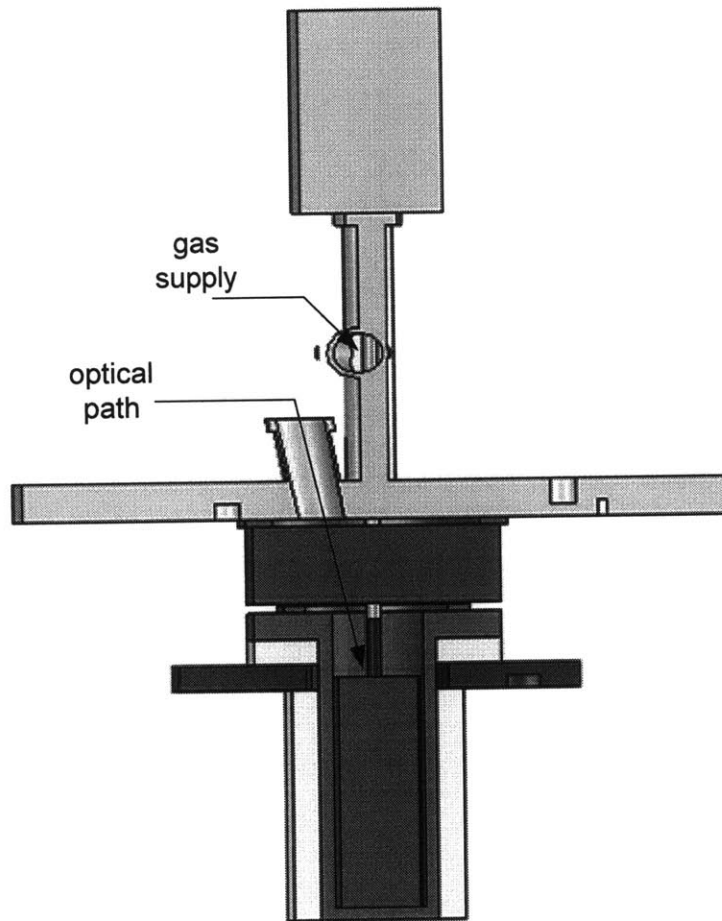
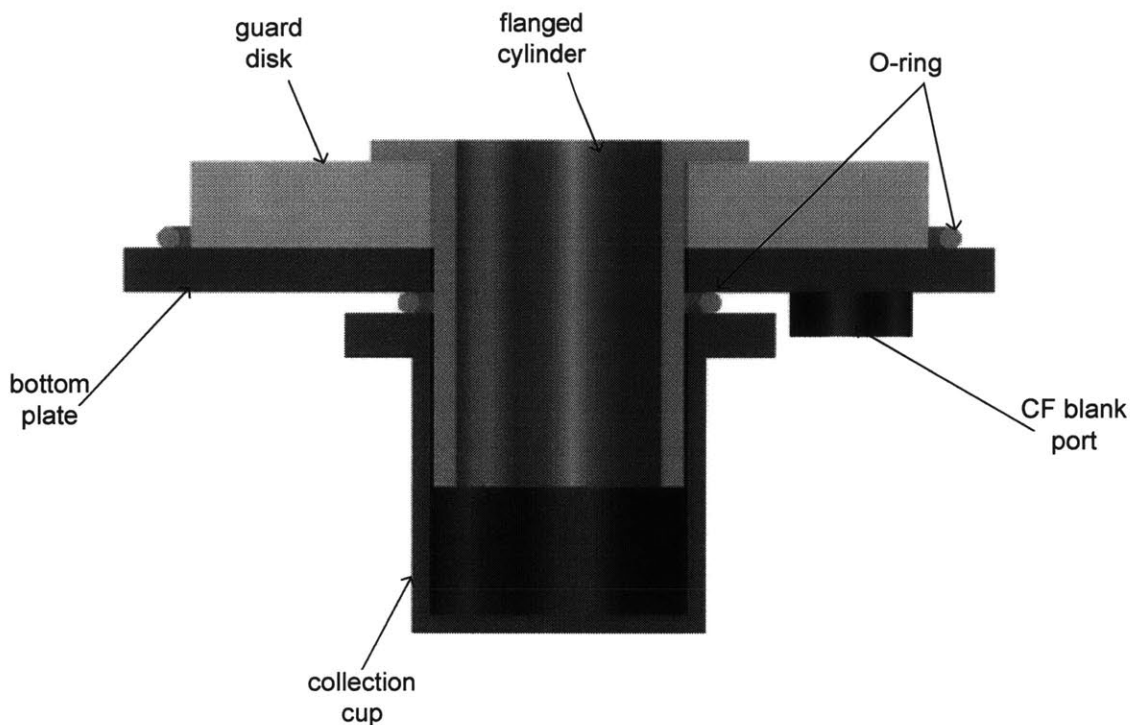


Figure 3.8: The top plate assembly section view.

### 3.4 Bottom Plate Assembly

This assembly deals with joining the bottom plate and the collection cup with the powder chamber. The collection cup is the unique part of this assembly that is supposed to be removed at the end of each run. Its removal is quick and simple, because it is made of an ISO flange type that doesn't require any gasket replacement. On top, the cup is the very last item assembled here, thus its removal doesn't require any other part dislocation. The assembly however is not just involved with vacuum parts. A safety guard disk (alumina silica insulation) is added to save the bottom plate from any possible molten copper deposition. In fact, deflected jets could end up depositing on the top plate rather than in the collection cup. The molten copper could then solidify on the stainless steel plate and harm its face. In addition, the collection cup gasket assembly is not grooved and thus molten copper could reach the uncovered rubber gasket, heat it, and melt it, causing the entire system to leak. This problem could be solved if a flanged cylinder is added to hide the O-ring and make it out of the molten copper reach. A section view of the assembly is shown in Figure 3.9. All the drawings of the parts are included in Appendix B.



**Figure 3.9: The bottom plate section view.**

The steps taken to perform the assembly are listed with the illustrative pictures shown in Figure 3.10.

#### A: Guarding the top plate

- 1 – The bottom plate vacuum side and sealing areas are cleaned (a).
- 2 – The guard disk is placed on top of vacuum side (b).
- 3 – The flanged cylinder is inserted in the central hole (c).
- 4 – The O-ring (powder chamber to top plate, sealing) is placed inside the plate's groove.

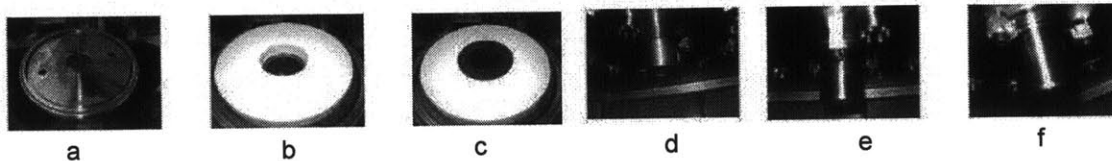


Figure 3.10: The bottom plate assembly steps.

#### B: Joining to powder chamber

- 5 – The powder chamber is lifted on the hoist so that its bottom part is accessible.
- 6 – The guarded plate is positioned and clamped to the powder chamber (d).
- 7 – The collection cup (filled with silicone oil if necessary) and its O-ring are finally placed and clamped to the bottom plate (e).
- 8 – The entire chamber is lowered and ready to be assembled to the heating chamber (f).

### 3.5 The Coil Assembly

The induction coil assembly inside the heating chamber takes into consideration the electric current and the flow of water circulating inside it. The elements involved in this assembly are: the coil, the RF feedthrough, the insulator coil holders and the metal link. The heating chamber has two brackets welded to its inner wall; one of them is used in this assembly. This assembly is permanent regardless of the number of UDS runs. The holders are chosen from alumina (high electrical resistivity  $\approx 10^{15}\Omega\cdot\text{m}$ ) to block the flow of electric current through the chamber. The very end connection between the feedthrough and the oscillator is covered with plastic half cylinders wrapped around the flange as a safety precaution from what may be an unintentional but fatal touch. The

annotated layout of the coil assembly is shown in Figure 3.11. Appendix B contains all the engineering drawings of the assembly elements. The steps taken in assembling the parts are listed with each step illustrated with its picture from Figure 3.12.

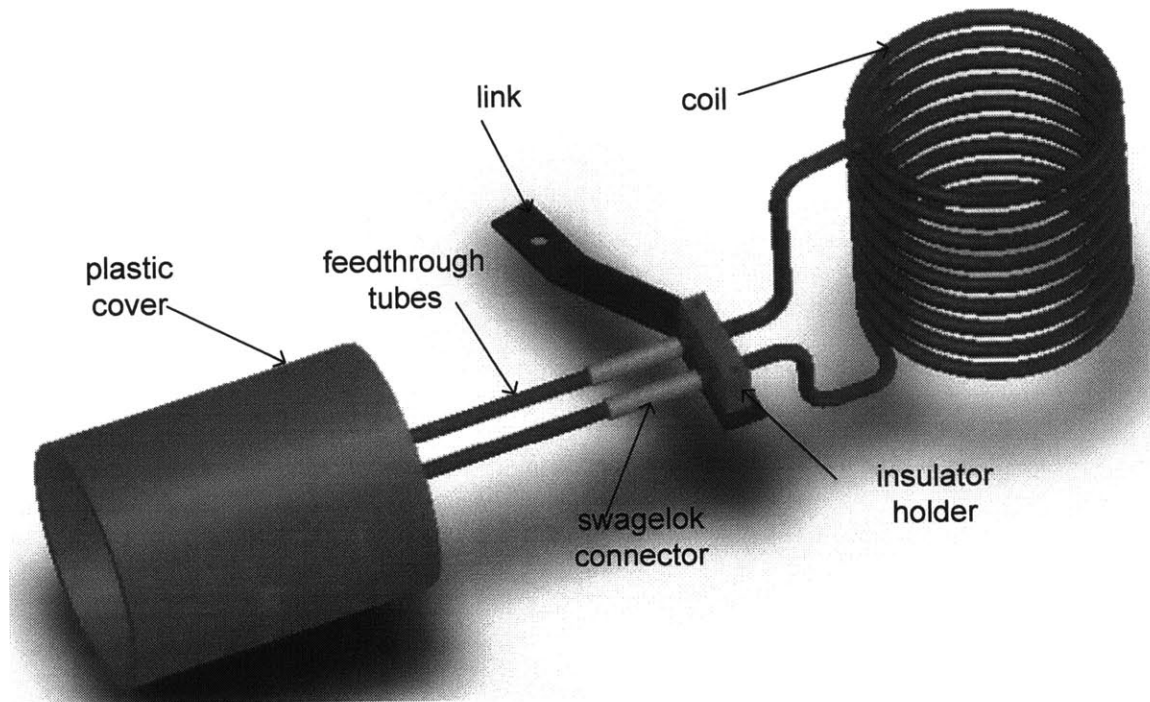


**Figure 3.11: The coil assembly elements configuration.**

1 – The RF feedthrough with swagelok connectors on both sides is fastened to its port but not tightened so that it could still rotate around the port (a).

2 – The metal link is fastened to the bracket (b).

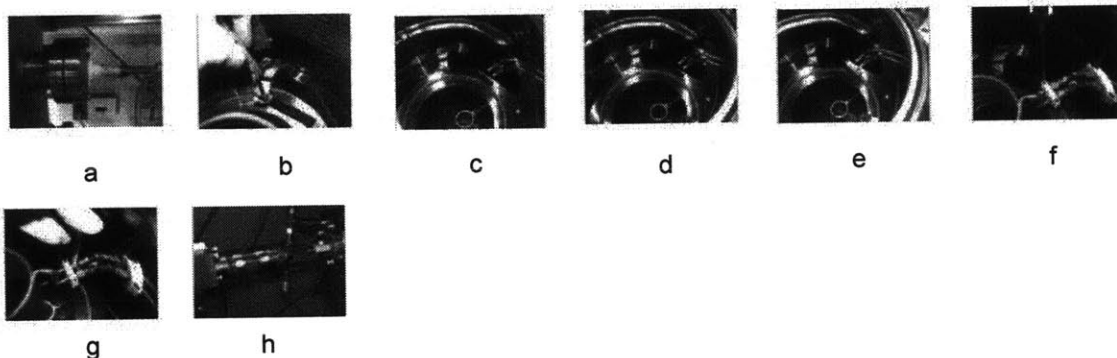


**Figure 3.12: The coil assembly steps.**

3 – The holders are positioned on the link with screws in them but not tightened to each other (c, d, and e).

- 4 – The coil is then brought with its tubes inserted to the swagelok connectors and sandwiched by the insulator holders (f).
- 5 – The two holders are then fastened with the metal link, clamping the coil tubes (g).
- 6 – The RF feedthrough is fully tightened to its port (h).
- 7 – The swagelok connectors between the coil and the feedthrough are tightened (h).
- 8 – The connectors on the air side of the feedthrough are tightened to the oscillator (h).
- 9 – The plastic half cylinders are wrapped around the feedthrough flange to cover this connection

CF port flanges could be either fixed or rotating. This port has a rotating flange because the distribution of flange holes should not enforce any alignment restrictions on the copper tubes of the RF feedthrough. These tubes must be horizontal so that they could be connected to the oscillator and coil ends.

### **3.6 The Vacuum Chambers Assembly**

This assembly involves the joining of the heating chamber to the powder collection chamber. Interestingly, the two chambers could be joined together for several runs of the UDS process. The waste cup could be removed from the handling port and the collection cup could be disassembled from the bottom plate without messing with the chambers assembly. The powder chamber is disassembled only in case the bottom plate or the chamber itself needs to be cleaned. The mating flange is an ISO 320 type. The powder chamber is shown sitting on its frame in Figure 3.13. The engineering drawings of the assembly elements are included in Appendix B.

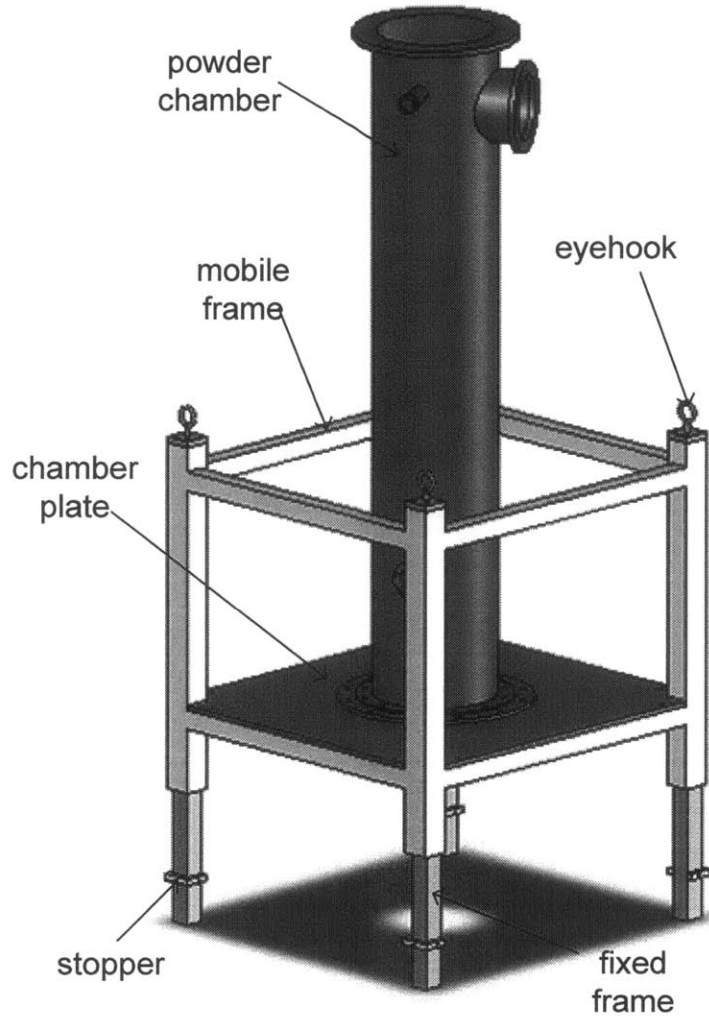


**Figure 3.13: The powder chamber fixed on the frame.**

The steps taken to fulfill this assembly are listed below. Each step is accompanied by an illustrative picture shown in Figure 3.14.

The steps are:

- 1 – The O-ring is inserted in the powder chamber flange's groove (a).
- 2 – The powder chamber frame is dragged inside the main frame until the upper part of the powder chamber sits directly below the heating chamber (b).
- 3 – The four auxiliary cables are attached from top to the hoist and from bottom to the frame cornered eyehooks (c).

- 4 – The hoist is turned on and lifting starts until the slack cables are completely taut (d, e).
- 5 – The locking handles are released so that the outer bars of the powder chamber frame could slide on the inner ones (f).
- 6 – The lifting process is continued until the two surfaces mate each other (g, h).
- 7 – The two flanges are sealed with ten clamps equally spaced along the flange circumference (i).
- 8– The locking handles are locked (j).
- 9 – The cables are lowered so they could slack and be easily removed (k).

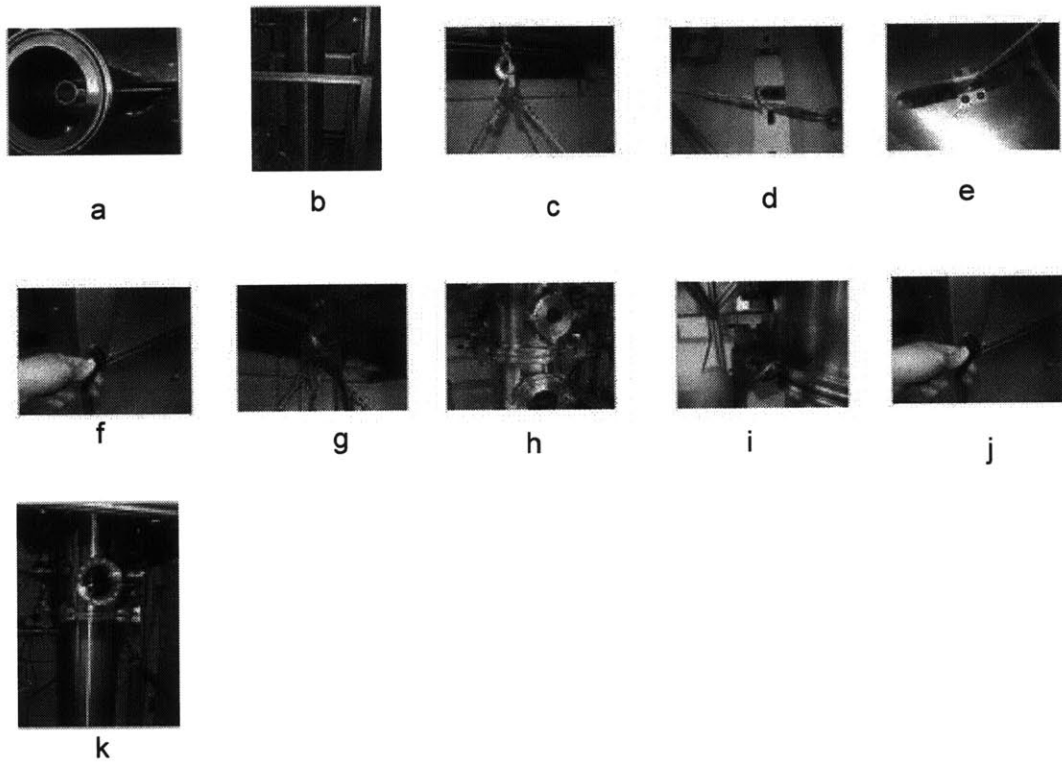


**Figure 3.14: The vacuum chambers assembly steps.**

Important to note that the locking handles should never be released unless the cables are fully taut otherwise the weight of the chamber pushes the outer bars downward. Safety stoppers are collared around the inner bars in order to prevent the mobile part of the frame from a complete slide down resulting in the collection cup hitting the ground. Figure 3.15 shows the powder collection chamber assembled to the heating chamber.



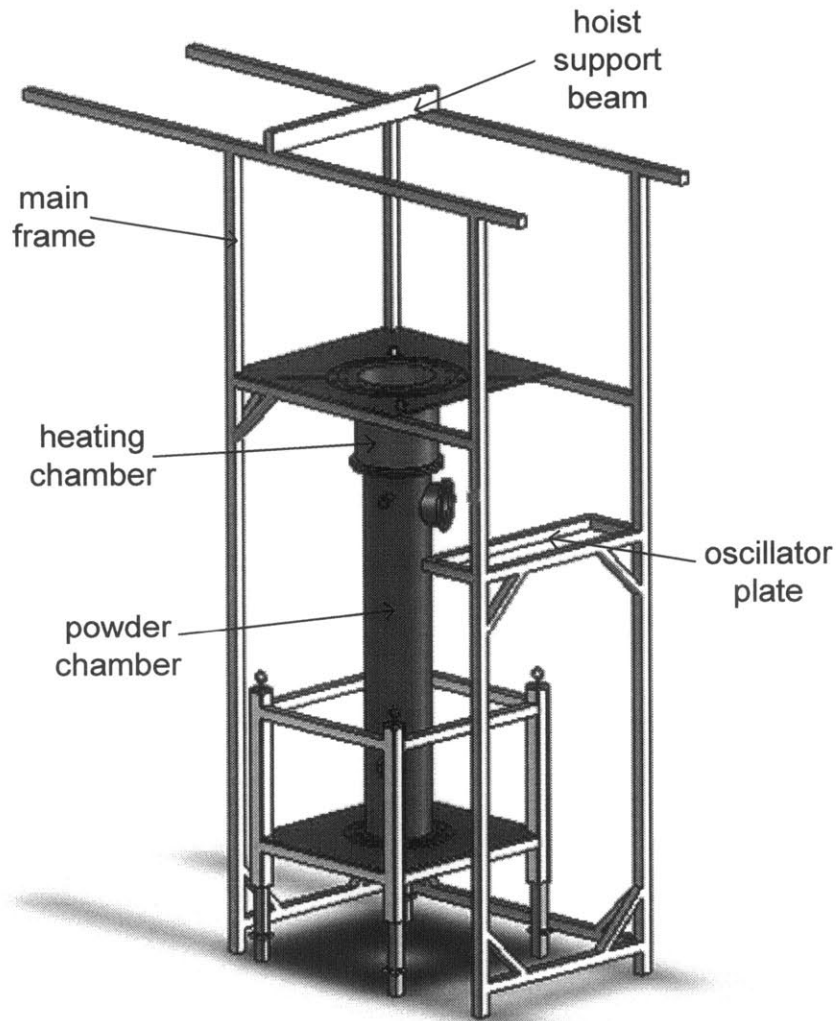


**Figure 3.15: Powder chamber is lifted and attached to the heating chamber.**

### **3.7 The Gas Management System Assembly**

The Gas management system is comprised of three parts. The source (tanks), the control panel, and the sink (chamber and crucible). The assemblies involved in the first and third are very straightforward. However, the control panel has many elements linked together that should be arranged in a proper way to realize the flow paths. The steps considered in assembling the control panel are described as follows:

- 1 – All the elements (valves, gages, regulators) were chosen of the panel mount type.
- 2 – The required hole for every element is considered in the control panel design.

3 – An aluminum rectangular sheet (3.1mm), containing all the holes is cut with a water-jet cutter (Figure 3.16).

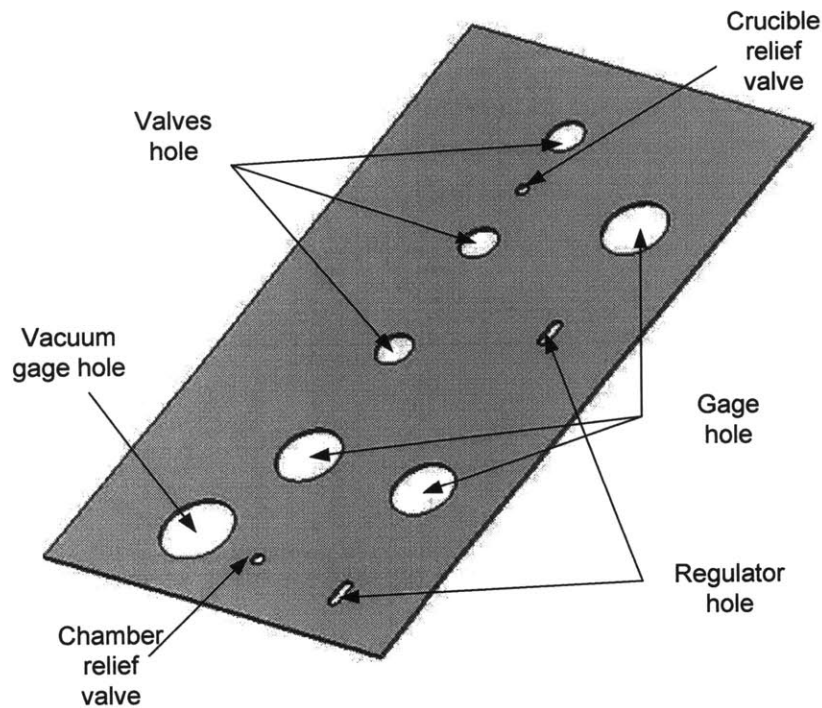


**Figure 3.16: The gas panel front plate.**

- 4 – The straight connections between regulators and gages are constrained, thus they were assembled first.
- 5 – The flexible connections between valves and gages are then made.
- 6 – The straight unconstrained connections between valves and chamber and crucible lines are made.
- 7 – The vacuum gage (independent element) is mounted.
- 8 – The control panel is connected to the main frame bars.
- 9 – The tank hoses are connected to the inlet ports of the panel.
- 10 – The chamber and top plate connection are made.

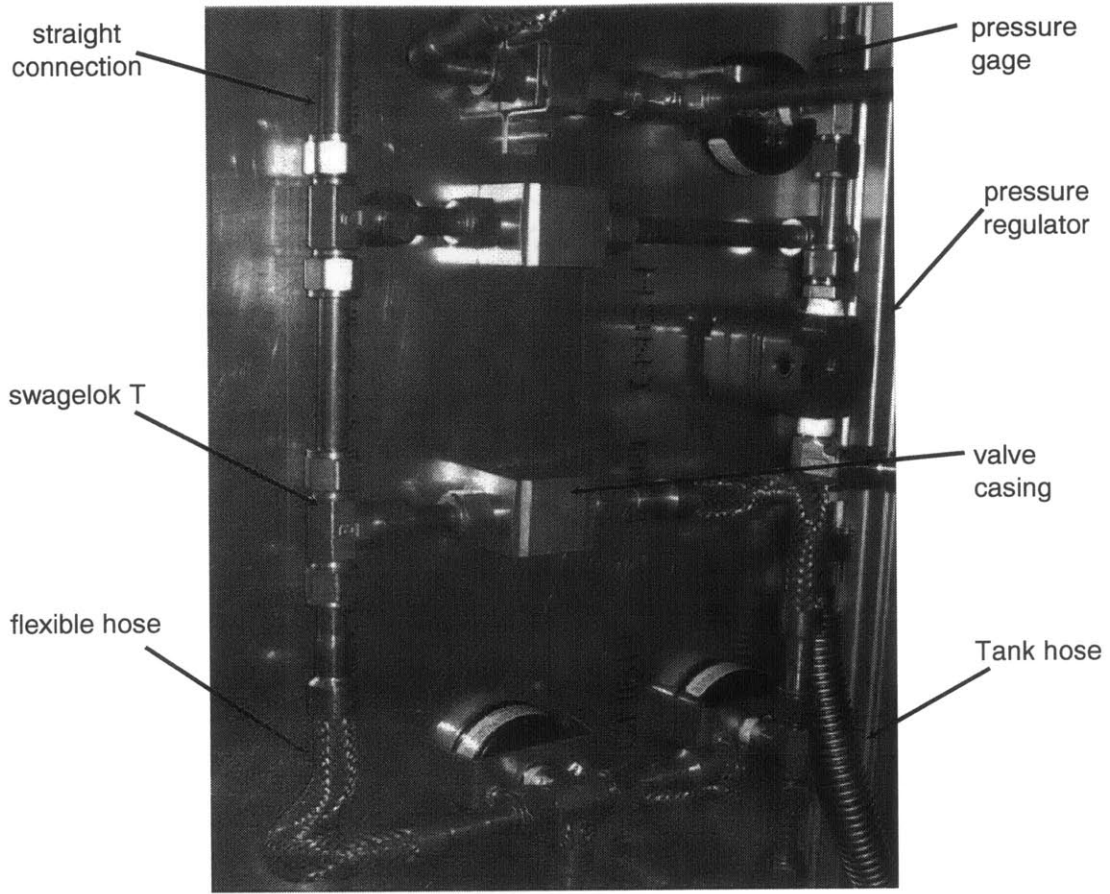


**Figure 3.17: The assembled control panel.**

All vacuum connections between the panel elements are made using the swagelok fittings. The tubing used is copper with 12.7mm diameter. Figure 3.17 shows the connections made in the rear side of the panel, while Figure 3.18 shows the user-interface mounted elements.

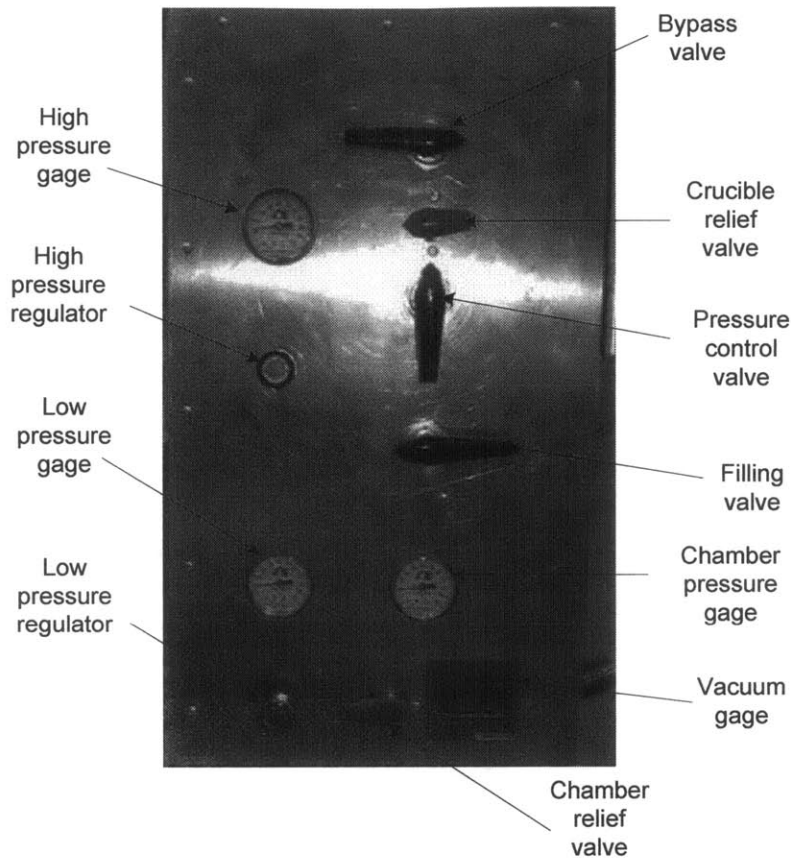


**Figure 3.18: The control panel nomenclature.**

### **3.8 The Imaging System Assembly**

The imaging system assembly is easy and simple that it could be done during the apparatus evacuation process. The camera is mounted on a multi-degree of freedom fixture in which it could slide up and down, right and left, and back and forth; all that to ease its focusing setup. The camera assembly is shown in Figure 3.19. Concerning the stroboscope, it sits on double U shape holders that are both attached to the main frame through a fixture and a connecting rod as shown in Figure 3.20. This assembly allows the strobe to move back and forth and tilt up and down. The stroboscope bulb should be aligned with the viewport as shown in Figure 3.21, with being in its contact as not to over heat. The engineering drawings of this assembly are included in Appendix B. The first part is fixed to the frame rear horizontal bar and has a slotted extension. The second part is made out of two U shapes that carry the strobe from underneath and fastened to each

other from both side. The fixture allows the strobe to slide up and down, back and forth, and even tilt with respect to the horizontal axis.

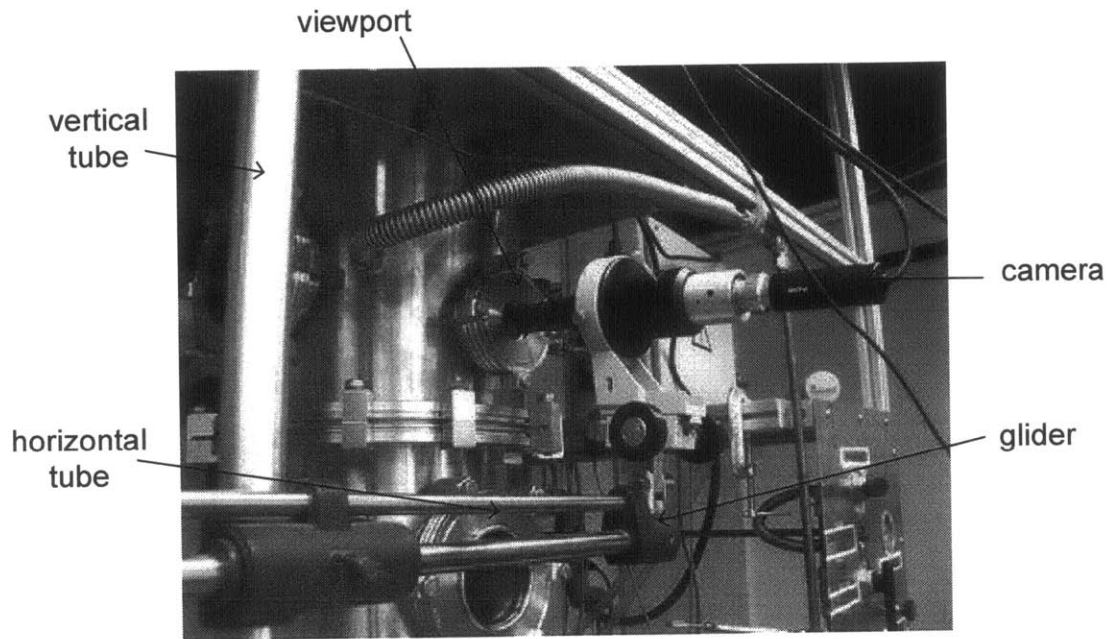


**Figure 3.19: The camera assembly.**

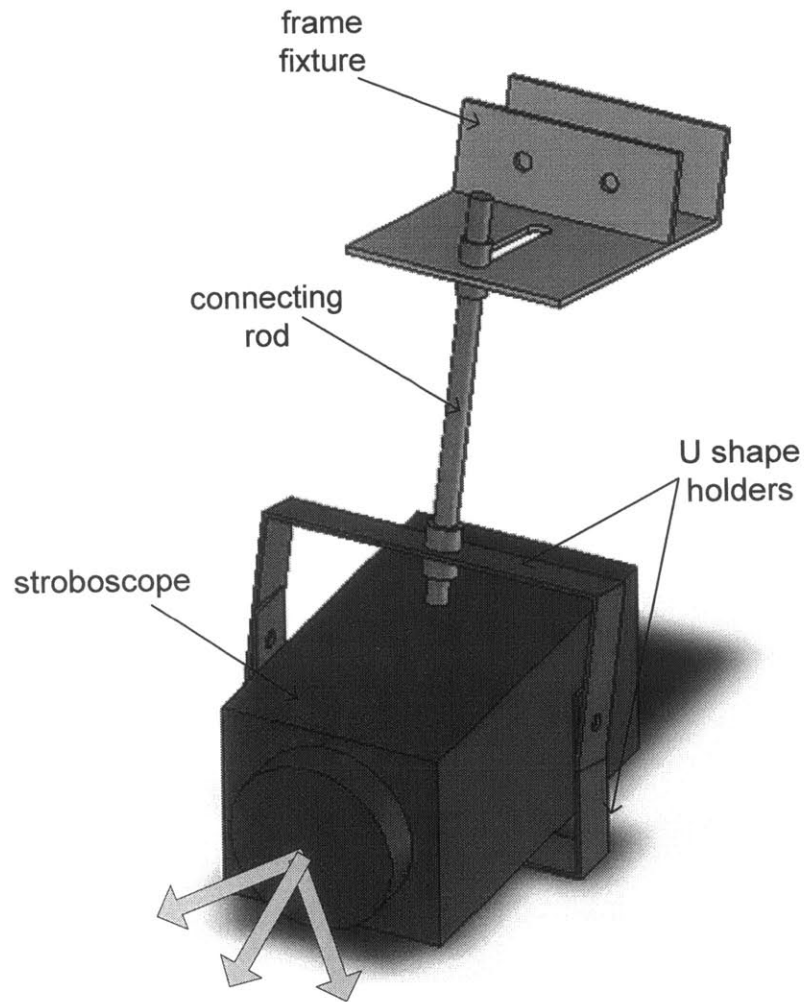


**Figure 3.20: The stroboscope assembly**

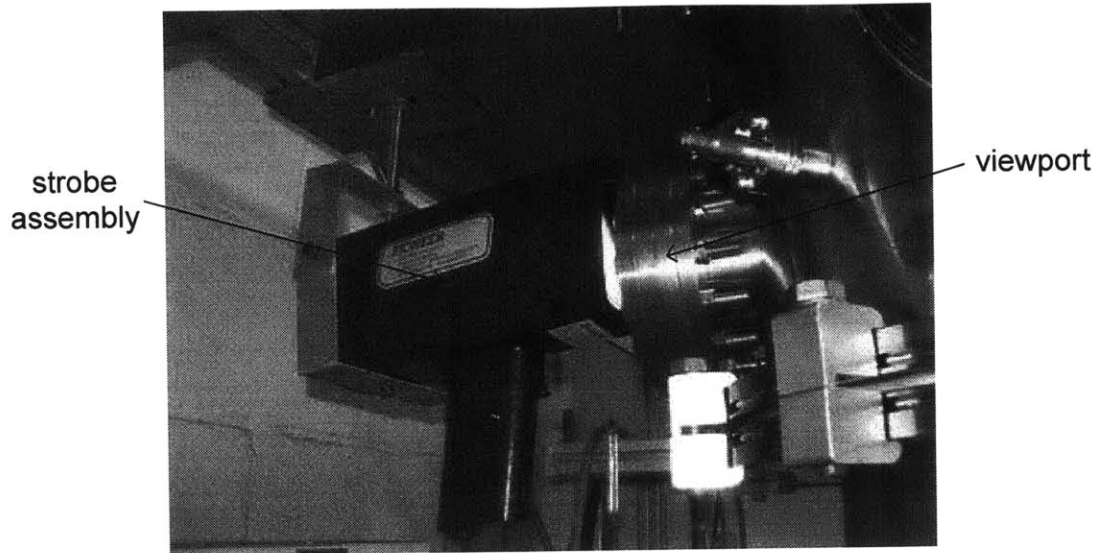


**Figure 3.21: The stroboscope lighting into its viewport.**

## **Chapter 4**

# **THE UDS SYSTEMS TESTING**

The full operation of the new UDS apparatus requires its systems to be examined separately to guarantee that each system fulfills its role satisfactorily and according to the design criteria. The testing of some systems cannot be realized unless other systems have been already tested and are insured to work properly. The stage of every test on the roadmap is set according to the reliance of its system on other already tested systems as shown in Figure 4.1. The first stage includes tests of fully independent systems and the last stage is the final run that requires all systems to be tested and guaranteed a harmonic performance. This chapter analyzes in detail each and every test performed on the UDS components.



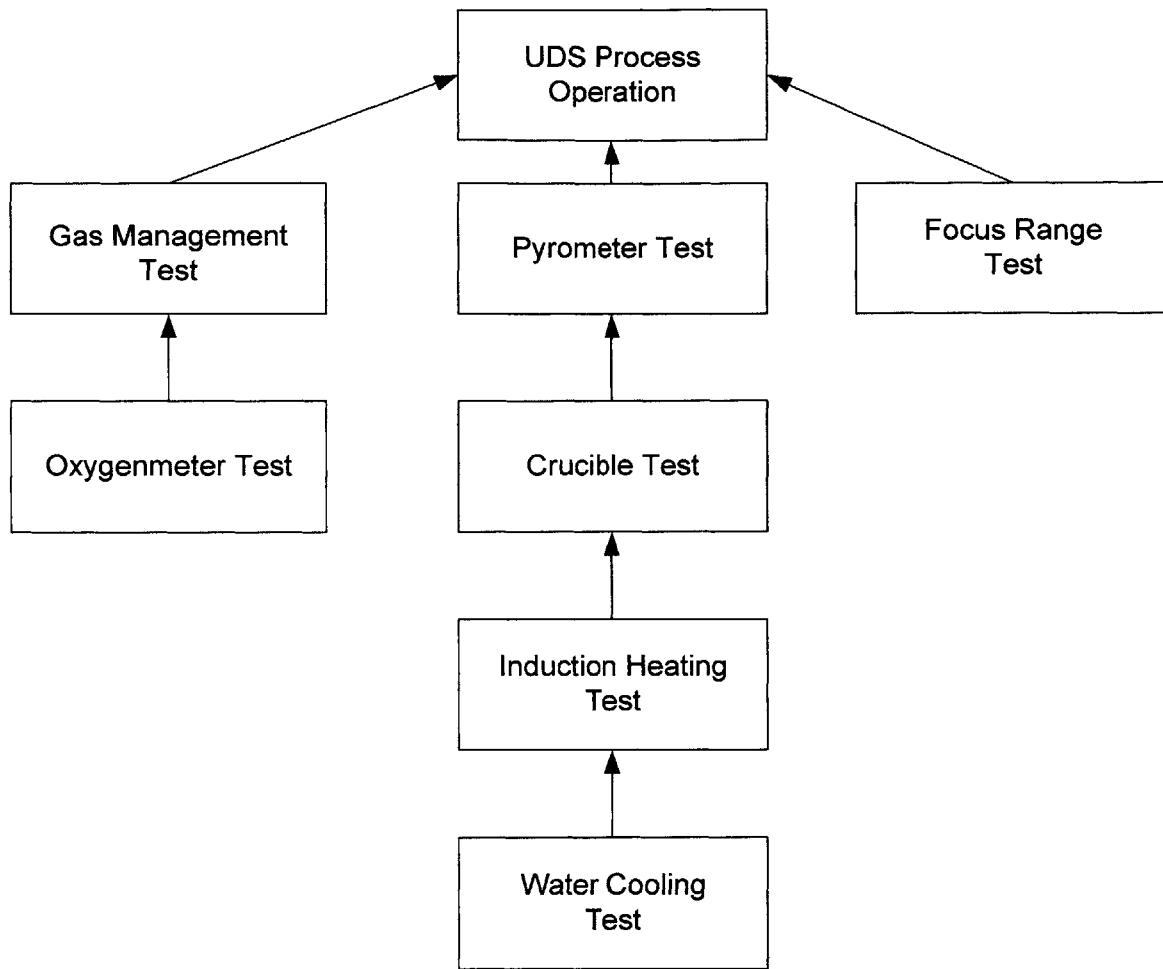


Figure 4.1: The UDS systems testing roadmap.

## 4.1 The Water cooling Test

This test is the first step in the UDS testing process. It is straightforward in a sense that it does not require any calibration procedure or past calculations. The test involves parts observation and training on the equipment operation. This test could be very well divided into two parts: the operation part and the examination part. The following sections go through these parts in detail.

### **4.1.1 Operation**

The operation of the water cooling system is easy. The recirculator unit control panel is the user interface. The operation steps are listed below:

- 1 – Turn the recirculator on.
- 2 – Open the manifold valves
- 3 – Set the desirable cooling water temperature.
- 4 – Control the pressure and the flow rate.

Running the equipment in idle operation (no heating load) is not the actual objective of this test. In such case the solenoid valve will only open for a while to cool the clean loops water and then switches off. The water temperature is not supposed to increase at no load. For this reason, this test is unsatisfactory to determine if the system exhibits a normal operation. Testing the equipment with heater on in the further steps would be a more reasonable tool to evaluate its performance.

### **4.1.2 Examination**

The examination process consists of checking all the parts that are critical in evaluating the cooling water flow characteristics. The good operation of the cooling system requires that the following parameters are checked:

- 1 – The water temperature on the return pipe is higher than that of the supply pipe so that heat removal is taking place.
- 2 – The water pressure on the return is lower than that of the supply due to pressure losses in the heat exchanger.
- 3 – The flowmeter indicator shown in Figure 4.2 moves up and down in case supply water flows through the recirculator.



**Figure 4.2: Checking the flowmeter indicator.**

4 – Leakage detection at the following points:

- a – supply connections manifold shown in Figure 4.3.
- b – clean loops pipes.
- c – quick disconnects.
- d – coil and oscillator connections.

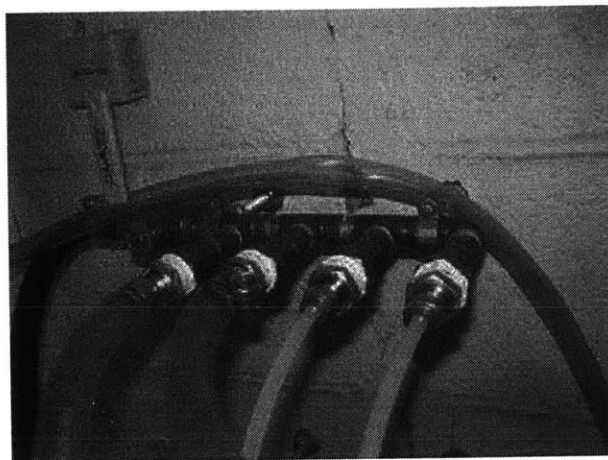


**Figure 4.3: Checking water leakage from supply and return manifolds.**

Water leakage is observed and detected without the use of special equipment. Its prevention is also easy to achieve by firmly tightening the fittings' connections.

## 4.2 The Induction Heater Test

The aim of the induction heater test is to tune the induction heater parameters in order to extract the maximum possible power and reduce heating time. This process is called matching. Matching also exists in DC type heating (simple resistive heating), but in that case it is easier to be implemented because of direct electric power transfer from source to load and absence of inductance and capacitance elements in the circuits. Let's consider the simple DC circuit shown in Figure 4.4. The voltage source is  $E_s$  (assumed constant), the source and wiring resistances is  $R_s$  (assumed constant) and the load resistance is  $R_l$  (variable).

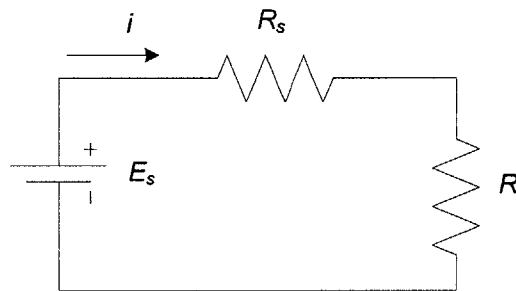


Figure 4.4: A typical DC resistive heating circuit.

The matching problem is how to tune the resistances in order to maximize the power transfer to the load resistance. Equations 4.1, 4.2 and 4.3 show the current  $i$ , load power  $P_l$ , and optimization criterion, respectively.

$$i = \frac{E_s}{R_s + R_l} \quad (4.1)$$

$$P_l = i^2 R_l = \frac{E_s^2}{(R_s + R_l)^2} R_l \quad (4.2)$$

$$\frac{dP_l}{dR_l} = 0 \Rightarrow R_l = R_s \quad (4.3)$$

As a conclusion, maximum power transfer requires that the load resistance be equal to the series equivalent of all remaining resistances in the circuit [7].

Matching resistances in induction circuit has a similar trend but a more complicated analysis. Impedances ( $R$ ,  $L$ , and  $C$ ) of both heater elements (oscillator and coil) and copper billet affect the process instead of the simple resistances as in the DC circuit. In addition, the frequency of the signal has a prime effect on the power transfer as will be shown. The analysis of the induction heater matching requires three steps:

- 1 – Showing the power transfer flow line from heater to billet.
- 2 – Modeling each part in this flow by a simple circuit reflecting its function.
- 3 – Combining the circuits and solve the matching equation.

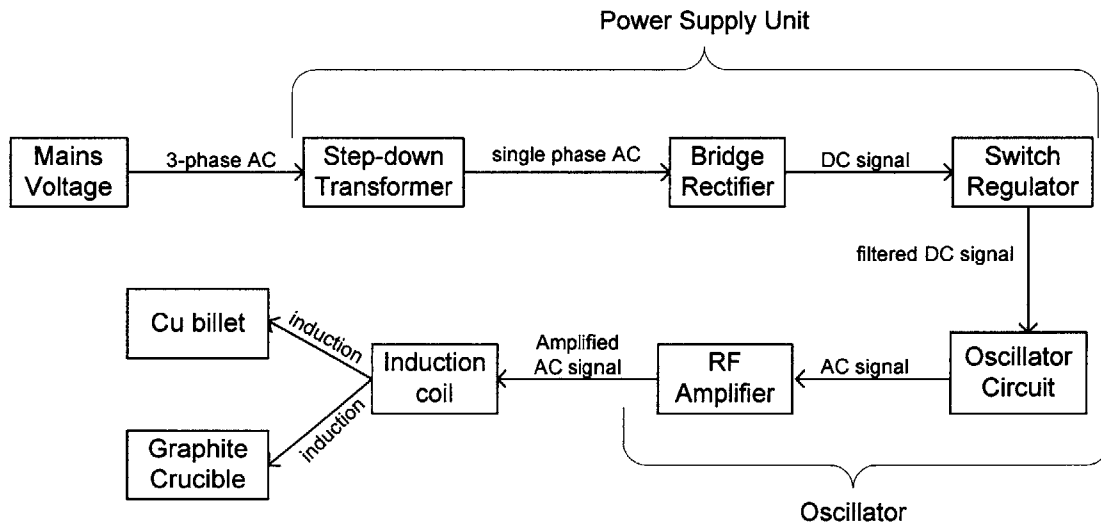


**Figure 4.5: Power flow line of the induction heater machine.**

The power flow inside the heating system is shown in Figure 4.5. The power supply unit generates a DC voltage out of the AC supply. For the sake of simplicity, the output of this unit will be modeled as a variable DC voltage supply. The oscillator generates an AC signal out of the DC voltage, thus the best model will be a resonator circuit that contains the inductance  $L_o$  and the capacitance  $C_o$ . The coil circuit is placed in

series with the oscillator one, therefore its major elements (inductor and resistance) could be directly added to the oscillator ones. The power transfer from the coil to the copper billet resembles the magnetic circuit of the transformer [4]. The primary is the coil and the secondary is the copper billet. If the crucible is made of a conductor material (ex: graphite), eddy currents will circulate in it too. Therefore, there must be two secondary circuits in this case, one for the billet and the other for the crucible. In case the crucible is insulator (ex: quartz) the crucible secondary circuit could be safely disregarded. In a transformer, when alternating current flows in the primary, voltage is induced in the secondary causing currents to flow in it, these currents tend to cancel the flux that created them according to Lenz's law. The modeling process of the heating systems is shown in Figure 4.6.

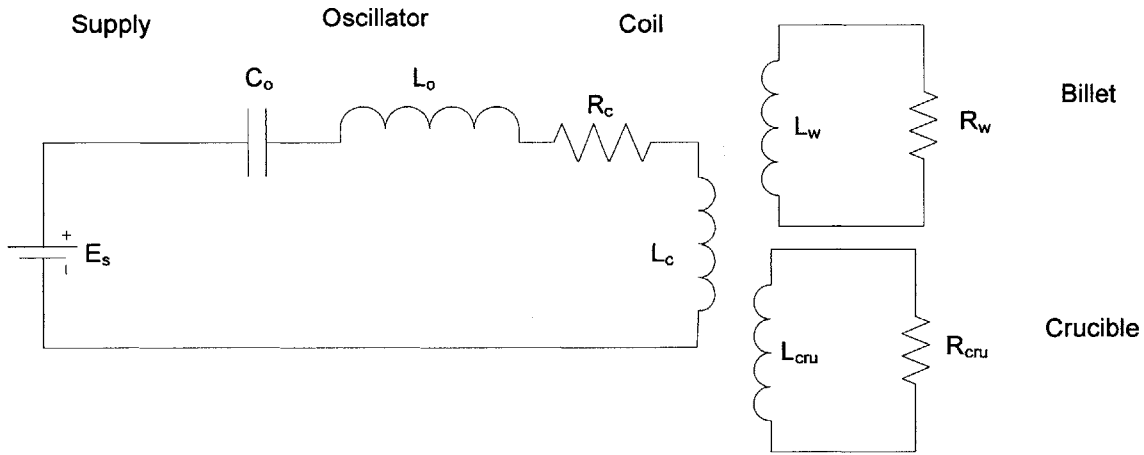


**Figure 4.6: The modeling circuit of the induction heating elements in case of a conductor crucible.**

For this transformer model, the maximum efficiency of power transfer between the coil and the billet should be determined. This efficiency depends on the coil material's electrical resistivity  $\rho_c$ , the billet's electrical resistivity  $\rho_w$  and relative permeability  $\mu_w$ . If the power available on the coil is  $P_c$  and the power reaching the billet is  $P_w$ , then the maximum transfer efficiency is expressed as [11]:

$$\eta_{\max} = \frac{P_w}{P_c} = \frac{1}{1 + \sqrt{\frac{\rho_c}{\rho_w \mu_w}}} \quad (4.4)$$

The primary circuit (coil) is always constructed of copper to minimize losses. If the billet

is made of copper too ( $\mu_w = 1$ ), the maximum efficiency is therefore 50%. Magnetic materials like steel have higher  $\mu_w$  (between 100 and 1000), thus their transfer efficiency could reach 90% and even higher values. Unfortunately, in the best case scenario, the coil will be heated as much as the Cu billet would be. The coil doesn't melt and stays at room temperature because of the cooling water circulating through it. The task of the heater test becomes to make the actual efficiency approach as much as possible its upper limit value.

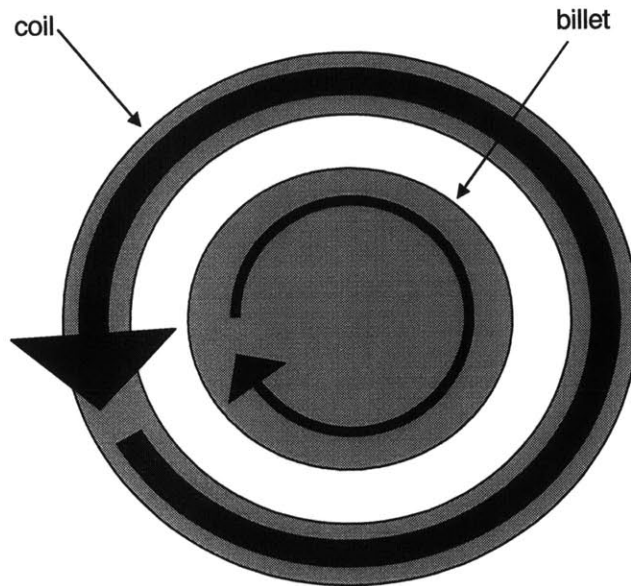


**Figure 4.7: The current flowing in the billet is opposite in direction to the one flowing in the coil as to satisfy Lenz's law [12].**

Carrying on with the transformer circuit, the billet eddy currents flow in opposite direction to that of the coil as shown in Figure 4.7. The current however is not uniform throughout the billet thickness, its density is higher at the outer surface and it gradually decreases to zero at the billet center. This results in an uneven heating where the outer surface (skin) heats up more than the inner part. The tendency of the current density and heat power to be greatest at the outer surface is called the "skin effect". The depth, at which the magnitude of the current density drops to  $1/e$  ( $= 0.368$ ) of its surface (maximum) value, is given the special name "skin depth", and denoted  $\delta$ . The smaller the skin depth, the more the skin effect is pronounced [12]. The skin depth depends on the

billet's material properties  $\mu_w$ ,  $\rho_w$ , and the frequency of the coil current,  $f$ , which is equal to the billet one. The skin depth is given as [13]:

$$\delta = 503 \sqrt{\frac{\rho_w}{\mu_w f}} \quad (4.5)$$

Obviously a more uniform heating requires a low frequency to reduce the skin depth. But internal thermal conduction throughout the billet diffuses the heat inward and balances the temperature distribution. As a result of the skin effect, the outer surface of the billet melts before the inner part does so.

The second part of the analysis constitutes of transferring the secondary circuit (billet) to the primary one (coil and oscillator). In regular transformers, the ratio of the number of coil turns between primary and secondary is the scaling factor between the circuit elements. However, in induction heating, the transfer problem is more complicated. It involves the implementation of Bessel functions and other tedious calculations that require a special software code to solve for it. The code is included in Appendix C. The equivalent circuit of the heater is shown in Figure 4.8.

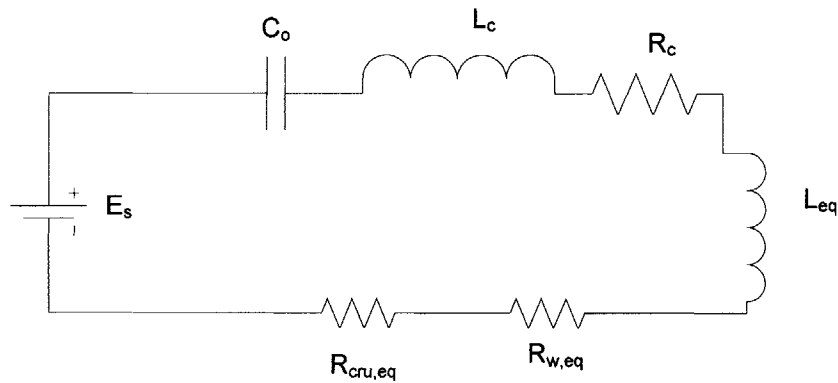


**Figure 4.8: The equivalent circuit of the heater.**

The billet and crucible equivalent resistances  $R_{w,eq}$  and  $R_{cru,eq}$  depend on the frequency flowing in the circuit. This is the only parameter that we could adjust to improve the efficiency of the heater. The heater efficiency depends only on the dissipative elements of the circuit (resistances). The reactive elements ( $L$  and  $C$ ) do not show up in the efficiency equation but they play an indirect role in its value by altering the frequency which affects



the billet equivalent resistance that itself modifies the efficiency. Two expressions for the transfer efficiency are defined here; the first describes the transfer process: *coil* → *billet* + *crucible* and the second evaluates the process: *coil* → *billet*. As shown in Eqs. 4.6 and 4.7, the two efficiencies are close when the crucible material is electrically insulator [13]. The first efficiency is always higher than the second. This explains why it is to our advantage to use an insulator material for the crucible. The aim now is to optimize the second efficiency and not the first because the billet is the part that needs to be heated and not the crucible.

$$\eta_1 = \frac{R_{w,eq} + R_{cru,eq}}{R_{w,eq} + R_{cru,eq} + R_c} \quad (4.6)$$

$$\eta_2 = \frac{R_{cru,eq}}{R_{w,eq} + R_{cru,eq} + R_c} \quad (4.7)$$

The transfer efficiency-frequency relation problem is solved using the Matlab code, and the result is plotted in Figure 4.9.

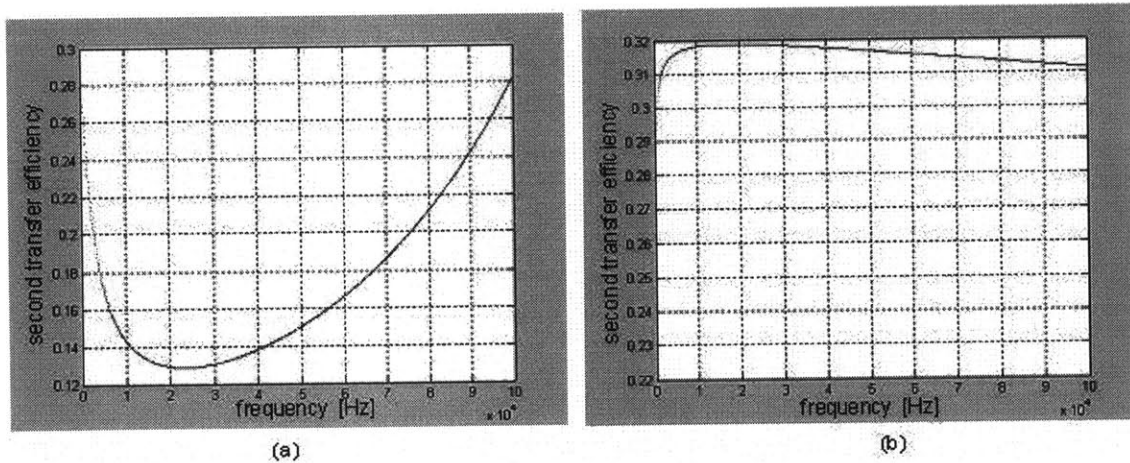


**Figure 4.9: The transfer efficiency plot as function of frequency for two different crucible material; case (a): graphite; case (b): quartz or other electrically insulator material.**

The frequency range of the induction heater varies from 10 kHz to 100 kHz, thus the efficiency was only found in this range. As noticed in Figure 4.9, the efficiency trend differs significantly from one crucible material to another. In conclusion:

- 1 – For a graphite crucible, the heater is highly efficient at high frequencies (>85kHz).

2 – For quartz or any other insulator material crucible, the heater is efficient at medium frequencies (20-30 kHz).

3 – The maximum efficiency in the quartz case is higher than in the graphite case (32% for quartz compared to 28% for graphite). This corroborates the fact that conductor crucibles get heated by induction in addition to the billet. The difference is nevertheless minor.

4 – Both efficiency curves lie below the upper limit of 50%.

The operating frequency is altered via the oscillator capacitors shown in Figure 4.10 and inductor shown in Figure 4.11. The oscillator could have at most 4 capacitors that are placed in parallel, thus their equivalent value is their sum. The available capacitances are 330nF and 660nF. The inductor is nothing but the “precoil” of the oscillator; it also varies discretely in four values starting with 0.2mH (smallest) to 0.8mH (largest) with a step of 0.2mH. Equation 2.1 is not very accurate in determining the exact value of the frequency, because it only considers the oscillator elements and disregards the billet and coil inductances.

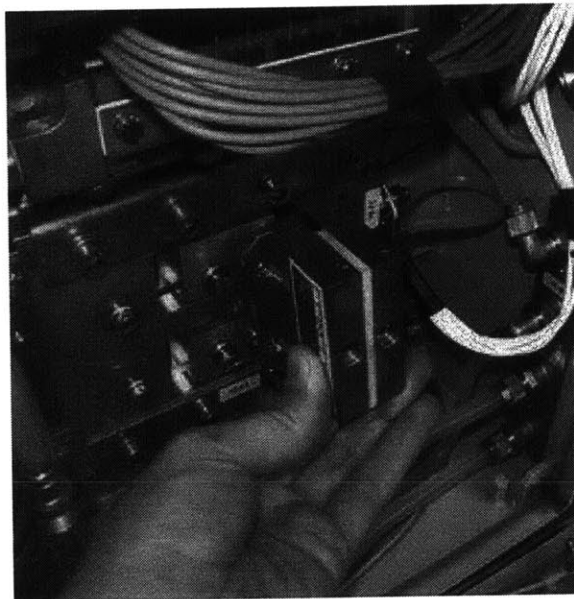


**Figure 4.10: A capacitor is being removed to enhance matching.**

The final designed crucible is made out of graphite, so the frequency must be raised to above 85kHz to reach high efficiency. However the maximum frequency

reached with the available capacitances-precoil set is just 83kHz.

The display panel of the induction heater shows the frequency value, voltage, current, and power as percentage of maximum possible values. In case the matching is realized at the exact frequency, the current and voltage tabs will be close to each other; this allows for higher power and thus higher efficiency to be reached. If on the other hand, the frequency is wrongly set, the current and the voltage tabs will be mismatched. One of them will reach its maximum value while the other is still far from its maximum. In such case, the power cannot be further increased and the overall efficiency is below its maximum value.

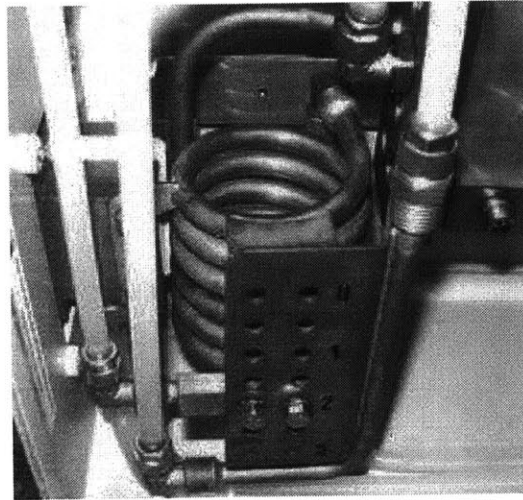


**Figure 4.11: The precoil is adjusted to have matching.**

The type of mismatch could be detected from the display as shown in Figure 4.12. If the current is high or low, something must be done in the circuit to adjust it; same thing applies to the voltage.

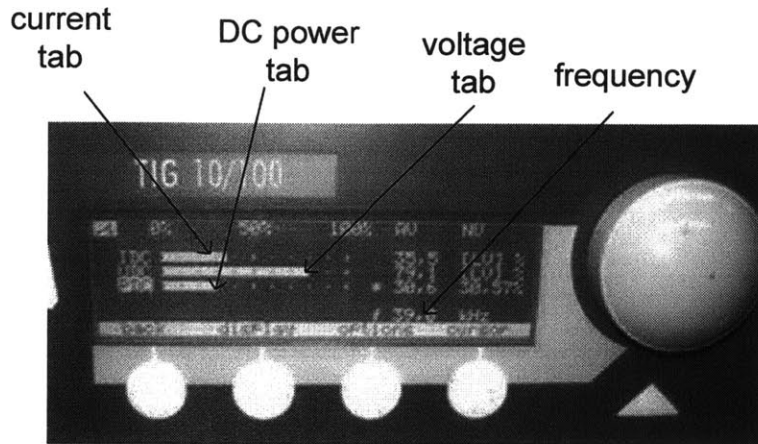


**Figure 4.12: The induction heater display.**

Table 4.1 shows the required tasks necessary to be done in the circuit element to achieve matching. The symbols +, -, and = mean to increase, decrease, and keep the same respectively. As an example, if a mismatching problem was noticed on the display panel, in which the current needs to be increased, then either task 1 (increase  $C$  keeping  $L$  the same) or task 4 (reduce  $L$  and keep  $C$  the same) must be performed. Obviously, achieving matching using this table is easier than going through all the previous calculations to determine the exact frequency and set  $L$  and  $C$  accordingly.

**Table 4.1: Effects due to changes in the oscillator circuit.**

Task	Changed Values		Effect		
	$C$	$L$	$f$	$I$	<i>Impedance</i>
1	+	=	-	+	-
2	-	=	+	-	+
3	=	+	-	-	+
4	=	-	+	+	-

### 4.3 The Crucible Test

All the possible materials whose properties were thought to match with the crucible requirements were examined to test their properties and select the most convenient

material to make the crucible. As specified in the crucible design part, the required material that should be used to make the crucible must be a ceramic. Induction heating is quick and uneven resulting in thermal gradients around the crucible walls. These gradients could be severe and cause large thermal stresses that lead to a thermal shock and failure [2]. Lots of ceramics have an operating temperature above the copper melting point, and satisfy all the required characteristics that were set for the crucible material. Their data sheets are included in Appendix A. However, the failure by thermal shock rendered them useless for this application.

Thermal stresses are generated in a solid part when the part's temperature changes while the part stays constrained and not being able to deform according to the temperature change. For example, if a bar of length  $l$  and cross section area  $A$  is made of certain material with modulus of elasticity  $E$  and coefficient of linear thermal expansion  $\alpha$ , is heated by temperature difference  $\Delta T$  while held fixed from both ends as shown in Figure 4.13(b), it will be subject to compressive stresses. The reason for this stress generation is explained as follows: the bar needs to extend due to this temperature change by an amount  $\Delta l = \alpha \Delta T l$ , but because it is constrained and not allowed to deform (extend), stresses take place and their values generate fictitious strains that balance the deformation caused by the temperature change [2]. These stresses are called thermal stresses. Mathematically the unconstrained thermal strain is

$$\varepsilon_t = \Delta l / l = \alpha \Delta T \quad (4.8)$$

The balancing strain is

$$\varepsilon_b = -\varepsilon_t = -\alpha \Delta T \quad (4.9)$$

The thermal stress is therefore

$$\sigma_t = E \varepsilon_b = -\alpha \Delta T E \quad (4.10)$$

Equivalently, cooling the bar results in tensile stress. When a material is subject to a sufficiently large thermal load that generates stresses exceeding its ultimate strength, the material is subject to failure.

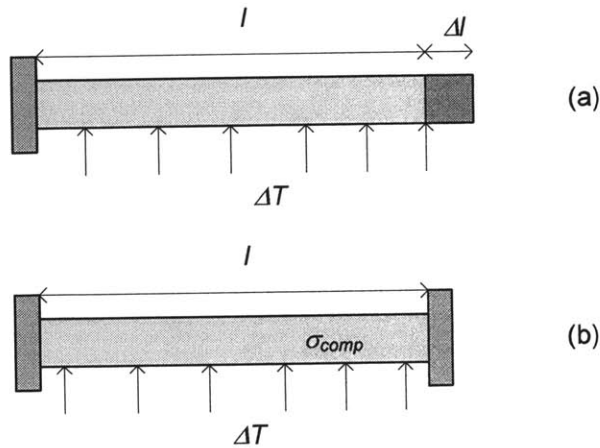


**Figure 4.13: Heated bar: (a) unconstrained bar extends and no stresses are generated; (b) bar is constrained and compressive stresses take place.**

Thermal stresses are higher for a higher Young's modulus and higher coefficient of thermal expansion. In fact, high resistance to thermal shock requires a small  $E$  and  $\alpha$  and high strength. Quartz has an excellent resistance to thermal shock because of its very low expansion coefficient (the lowest among all materials,  $4.5 \times 10^{-7} \text{ }^\circ\text{K}^{-1}$ ). The bar example is useful in illustrating the concept of thermal stresses and giving a brief idea about the effects of the material properties on it. The crucible has a more complicated shape than the straight bar; the resulting stress equations will not be derived. Equations of thermal stresses for standard shapes are available in mechanics references [2]. The overall shape of the crucible is not standard but it could be divided into standard shapes and the stresses' equations could be then implemented. The walls of the crucible were modeled as a hollow cylinder; the bottom part is nothing but a circular plate. Reference [2] gives the thermal stresses equations for these two shapes. The thermal load is set to  $\Delta T = T_{melt,Cu} - T_{amb} \approx 1100^\circ\text{K}$  applied at all points. The cylindrical coordinates are used in the stress equations. The stress distribution as expected is axisymmetric.

For a cylinder (inner radius  $r_i$ , outer radius  $r_o$ ), of material ( $E$ ,  $\alpha$ , and Poisson's ratio  $\nu$ ) the thermal stresses for a constant radial heat flux are:

$$\begin{aligned}
\text{set } \beta &= \frac{r_o}{r_i} \\
\sigma_r &= \frac{E\alpha\Delta T}{2(1-\nu)\ln\beta} \left[ -\ln\beta \frac{r_i}{r} - \frac{1}{\beta^2-1} (1-\beta^2 \frac{r_i^2}{r^2}) \ln\beta \right] \\
\sigma_\theta &= \frac{E\alpha\Delta T}{2(1-\nu)\ln\beta} \left[ 1 - \ln\beta \frac{r_i}{r} - \frac{1}{\beta^2-1} (1+\beta^2 \frac{r_i^2}{r^2}) \ln\beta \right] \\
\sigma_z = \sigma_r + \sigma_\theta &= \frac{E\alpha\Delta T}{2(1-\nu)\ln\beta} \left[ 1 - 2\ln\beta \frac{r_i}{r} - \frac{2}{\beta^2-1} \ln\beta \right]
\end{aligned} \tag{4.11}$$

For a plate of high radius to thickness ratio (thin plate,  $R/t \gg 10$ ) with clamped edges:

$$\sigma_{\max} = \frac{\alpha E \Delta T}{2(1-\nu)} \tag{4.12}$$

The stress analysis is first done for the plate because it has simpler equation to implement. The results obtained are summarized in Table 4.2. The materials failing to withstand the plate stresses (factor of safety < 1) are automatically rejected from the harder to analyze cylindrical test.

**Table 4.2: The plate stress analysis.**

$\Delta T = 1100^\circ\text{K}$	$E$ [GPa]	$\alpha \times 10^6$ [ $1/^\circ\text{K}$ ]	$\nu$	$S_{ult}$ [MPa]	Factor of safety
alumina	375	8.4	0.22	379	0.17
silicon carbide	410	4	0.14	550	0.52
mullite	151	5.4	0.2	180	0.32
zirconia	207	2.3	0.25	248	0.71
boron nitride	47	0.57	0.05	55	3.55
graphite	4.8	2.4	0.25	23	2.72
quartz	70	0.45	0.17	48	2.30

In the cylinder analysis, only the materials that made the plate test were analyzed. The three stress components were first found at several radial distances, and then the equivalent stress (Von Mises) is calculated and compared to the material strength. The factor of safety is lowest at the inner and outer walls. Luckily, all the materials tested here have passed this test (no factor of safety was found to be smaller than 1 as shown in Table 4.3, Table 4.4, and Table 4.5). The decision becomes to make a crucible using one of these materials.

**Table 4.3: The cylindrical stress analysis for boron nitride.**

Boron nitride
---------------

$r[cm]$	$\sigma_r$ [MPa]	$\sigma_\theta$ [MPa]	$\sigma_z$ [MPa]	factor of safety
2.5	0.00	-16.94	-16.94	3.25
2.58	-0.46	-12.96	-13.42	4.32
2.66	-0.78	-9.22	-10.01	6.21
2.74	-0.98	-5.72	-6.70	10.38
2.82	-1.06	-2.42	-3.48	26.22
2.9	-1.06	0.70	-0.35	35.84
2.98	-0.97	3.66	2.69	13.02
3.06	-0.81	6.46	5.65	7.97
3.14	-0.59	9.12	8.53	5.83
3.22	-0.32	11.66	11.34	4.65
3.3	0.00	14.08	14.08	3.91

**Table 4.4: The cylindrical stress analysis for graphite.**

Graphite				
$r[cm]$	$\sigma_r$ [MPa]	$\sigma_\theta$ [MPa]	$\sigma_z$ [MPa]	factor of safety
2.5	0.00	-9.23	-9.23	5.96
2.58	-0.25	-7.06	-7.31	7.93
2.66	-0.43	-5.02	-5.45	11.40
2.74	-0.53	-3.12	-3.65	19.06
2.82	-0.58	-1.32	-1.90	48.14
2.9	-0.58	0.38	-0.19	65.79
2.98	-0.53	1.99	1.46	23.90
3.06	-0.44	3.52	3.07	14.64
3.14	-0.32	4.97	4.65	10.71
3.22	-0.17	6.35	6.18	8.54
3.3	0.00	7.67	7.67	7.17

**Table 4.5: The cylindrical stress analysis for quartz.**

Quartz				
$r[cm]$	$\sigma_r$ [MPa]	$\sigma_\theta$ [MPa]	$\sigma_z$ [MPa]	factor of safety
2.5	0.00	-22.80	-22.80	2.41
2.58	-0.62	-17.44	-18.06	3.21
2.66	-1.05	-12.42	-13.47	4.61
2.74	-1.31	-7.70	-9.01	7.71
2.82	-1.43	-3.25	-4.68	19.48
2.9	-1.42	0.95	-0.48	26.63
2.98	-1.31	4.92	3.61	9.67
3.06	-1.09	8.69	7.60	5.92
3.14	-0.80	12.28	11.48	4.33
3.22	-0.43	15.69	15.26	3.46
3.3	0.00	18.95	18.95	2.90



The numerical analysis was not enough to indicate a convenient material for the crucible and some materials were physically tested with the induction heater to check the analytical analysis and have a better insight about the crucible material. The tested materials are: alumina, mullite, graphite, and quartz. The experimental results did not contradict the analytical ones. Alumina and mullite failed before the billet has reached a temperature of 300°C as shown in Figure 4.14. Graphite and quartz however were able to contain molten copper without any problem.

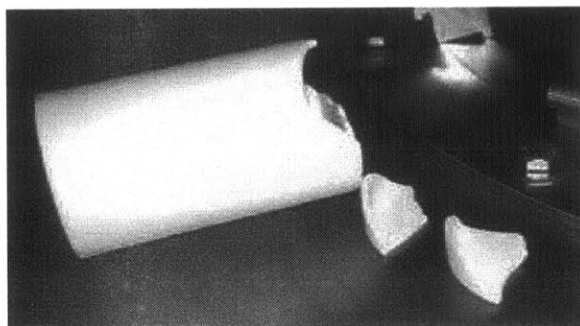


**Figure 4.14: Alumina crucible failing to contain molten copper.**

The testing procedures were as follows: standard crucibles of roughly similar shape and size to the system's required one were purchased. These crucibles were placed inside the heating chamber in a special assembly. A cylindrical copper billet was placed inside the crucible. The alumina and mullite crucibles failed very quickly while the billet is still solid. A crack that is first initiated at the bottom of the crucible, later led to its failure. Graphite and quartz crucibles didn't have any problem melting the copper billet. Another series of tests was conducted and new crucibles were brought in. The aim of having a second test is to remove the doubt that the first crucibles could have defects. The same results were obtained. A durability and corrosion resistance test was then conducted solely on graphite and quartz to test their ability to operate for several runs. Five consecutive melting and cooling processes were made and the crucibles withstood all five runs. Both materials passed but graphite has shown a deterioration that was mainly due to oxidation. All these tests were anyway done in open atmosphere and this was the reason behind the oxidation.

In conclusion, this test has shown that quartz and graphite are both excellent materials to be used for this application. Boron nitride is also a good material but it was rejected because of its high cost.

#### 4.4 The Pyrometer Test

The pyrometer methodology of operation, relevant radiation theory, and the advantage of having a two-color pyrometer over a single-color one were thoroughly explained in Section 2.2. The radiation analysis in that section was performed on a single ray basis. This means that the considered radiated heat was solely emitted from a single point (single ray) or many points (many rays) with parallel emitted rays heading toward the pyrometer surface as shown in Figure 4.15(b). The actual case however is not as such; radiation theory predicts that gray bodies will emit radiation in all directions as shown in Figure 4.15(a), with emissivity depending on the direction too. This means that part of the emitted radiation will not be entirely collected on the pyrometer lens assembly and will go toward the surrounding surfaces.

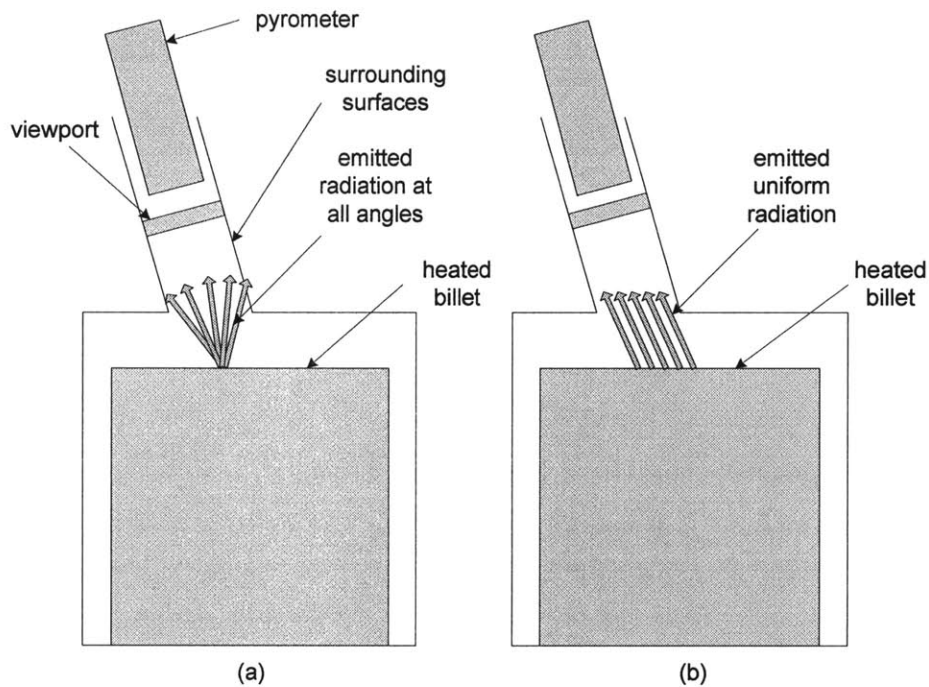
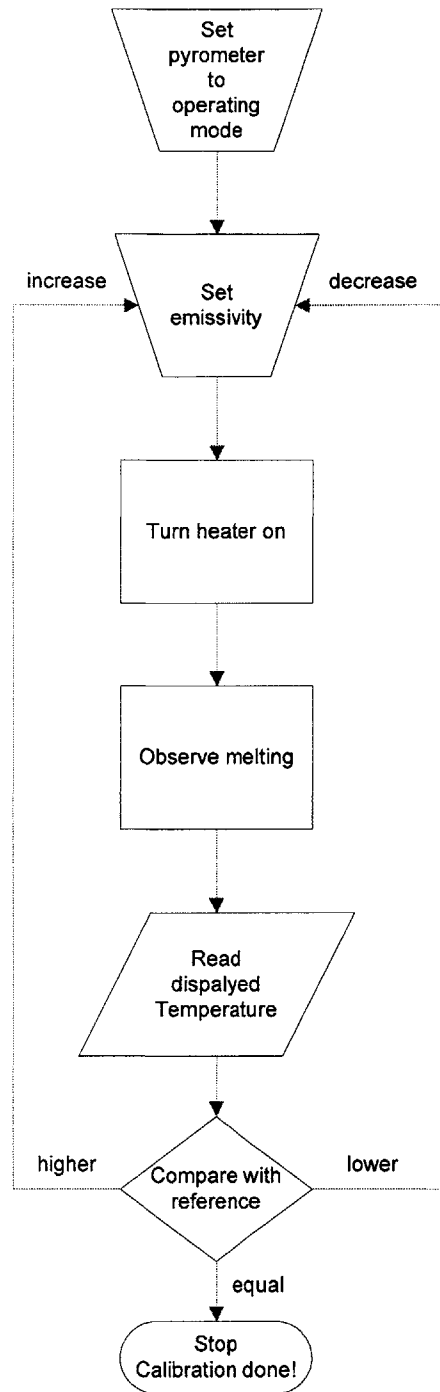


Figure 4.15: Actual and theoretical radiations.

Radiation heat transfer solves this problem by introducing a parameter representing the portion of the radiated heat from a certain surface (billet in this example) to another surface (pyrometer). This parameter is called the “view factor” and depends on the geometrical status of both surfaces. View factors could easily be found for some standard shape surfaces. However, this application involves an odd shape and hard-to-analyze geometries that only experimental work could solve. The object of the pyrometer test is to determine the view factor between the interesting surfaces. This determination will not be done directly, i.e. the apparent variable that will be solved for is not the view factor. In fact, what is more important in this application is to read the exact value of the temperature. The pyrometer has a calibration factor that it is illusively called “emissivity”; it hasn’t to do at all with the actual emissivity of the billet material. First of all, the emissivity of the pyrometer denoted  $\varepsilon_p$  is larger than one; the emissivity however of any material is at most one. In the following, the physical meaning of this emissivity and the role it plays to determine the temperature will be presented. Consider a certain billet – sensor configuration as the one shown in Figure 4.15, the emissivity set on the pyrometer is  $\varepsilon_p$  and the radiation heat reaching the pyrometer is  $Q_p$ , the pyrometer will calculate the temperature of the surface according to a “corrected” radiation  $Q_c$  expressed as:

$$Q_c = \varepsilon_p \times Q_p \quad (4.13)$$

Obviously  $\varepsilon_p$  must be greater than 1 to make the above analysis valid otherwise the heat reaching the pyrometer will be greater than the heat emitted from the billet, which is physically impossible. Determining the exact value of  $\varepsilon_p$  is the core of the pyrometer test. This test is conducted on trial and error basis; the melting point (1083°C) is the reference to determine the exactness of  $\varepsilon_p$ . The pyrometer needs to be set in the measurement mode in order for the user to be able to insert the emissivity values and run the test. The chart in Figure 4.16 illustrates the methodology of this test.



**Figure 4.16: The process flowchart of the pyrometer test in the measurement mode.**

The data of Table 4.6 shows how the adjustments of the emissivity have affected the displayed temperature at melting.

**Table 4.6: The experimental results of the pyrometer test.**

Emissivity set on pyrometer	Displayed temperature at melting, °C
1.18	1034
1.15	1045
1.1	1058
1.05	1078
1.03	1096
1.04	1084

As noticed the convergence of the solution (displayed temperature = actual melting temperature of copper) occurred at the emissivity value of 1.04.

This trial-and-error process could be avoided if the pyrometer is set to a “smarter” mode of operation which is called the “engineering mode”. In this mode, the user does not have to enter any emissivity value; all what is required is to set the temperature at a certain reference point and the emissivity will be automatically calculated without being displayed. Experimentally, the melting temperature of copper must be inserted when melting occurs. This calibration is a one step process and easier to implement.

The engineering mode calibration was performed on the pyrometer after the measurement mode calibration had been done. One calibration is enough, however. It is only because the measurement mode is first explained and recommended by the manufacturer that it was first implemented. As expected, the billet material properties didn't play any role in the calibration process. The pyrometer had also another set of data that need to be included (response time, measurement accuracy...), but they all are of minor importance to the UDS process.

## **4.5 The Oxygenmeter Calibration**

The oxygenmeter senses the oxygen concentration in an environment by measuring an electric current generated in an oxidation-reduction reaction. The current-oxygen concentration relation which is linear must have at least two definite points in order to be

fully defined. The first point is obviously the null point (zero current at complete absence of oxygen). The process of defining the second point is the goal of this calibration test. The fuel cell inside the oxygenmeter depletes with time and thus its sensitivity (slope of current vs.  $O_2$  concentration curve) changes. Because of that, calibration tests are recommended after several uses (10 to 15) in order to redefine the scale and update the sensitivity. Although frequent calibrations may seem useful to the oxygenmeter because they set the sensitivity to its exact value, they actually speed up the depletion of the expensive fuel cell because they make it subject to air (oxygen rich gas) which is used in the calibration as will be noticed below.

The calibration requires feeding the oxygenmeter with a gas flow of known oxygen concentration; the value of the concentration is inserted to the oxygenmeter. Gas tanks that contain oxygen in a well-known concentration could be used as a source for this gas flow, but the easiest and more standard solution is to consider the surrounding atmosphere that contains 20.9% oxygen. Using standard atmosphere reduces calibration errors resulting from concentration uncertainties.

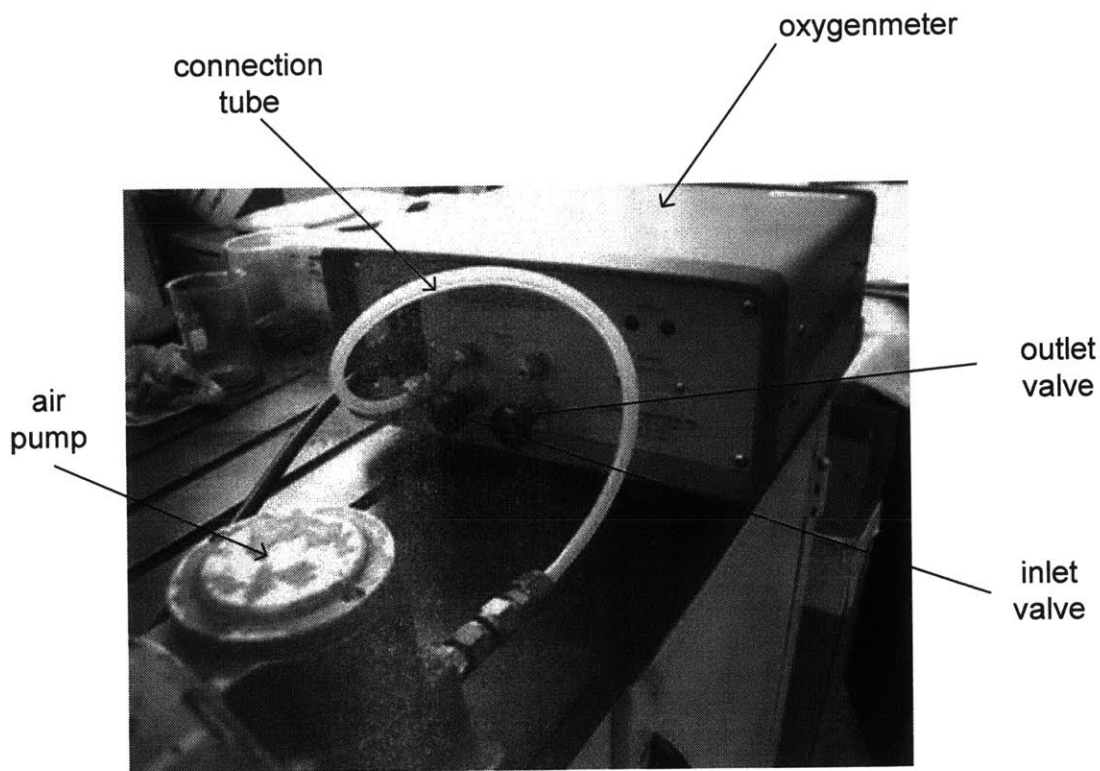


**Figure 4.17: The oxygenmeter test setup.**

The elements involved in this test are the oxygenmeter, an air pump and a connection tube, all shown in Figure 4.17. The steps taken in this test are described as follows:

- 1 – The pump inlet is left open to the atmosphere.
- 2 – The pump outlet is connected to the oxygenmeter inlet.
- 3 – The oxygenmeter outlet is also left open to the atmosphere.
- 4 – The outlet then the inlet valve of the oxygenmeter are opened.
- 5 – The pump is turned on, air flows inside the fuel cell, and the oxygenmeter outputs a concentration value scaled according to the previous calibration.
- 6 – Once the output value stabilizes, the calibration starts and one of the following actions is taken:
  - a – if the concentration value stabilizes at 20.9%, then the oxygenmeter calibration is still valid.
  - b – if the concentration stabilized value is different from 20.9%, the calibration key is then unlocked and turned until a 20.9% value appears on the screen as shown in Figure 4.18.
  - c – if case b applies with the calibration key turned throughout its entire range without being able to reach a 20.9% on the screen, the fuel cell is therefore depleted and needs to be replaced.
- 7 – The calibration key is locked.
- 8 – The pump is switched off.
- 9 – The oxygenmeter inlet then outlet valves are closed to save the fuel cell.



**Figure 4.18: The oxygenmeter calibration process.**

The fuel cell should never be pressurized with any gas. Therefore, under no circumstances should the outlet valve be closed while the inlet valve is open. It is a good practice to always shut the inlet valve before shutting the outlet one (see Figure 4.19).

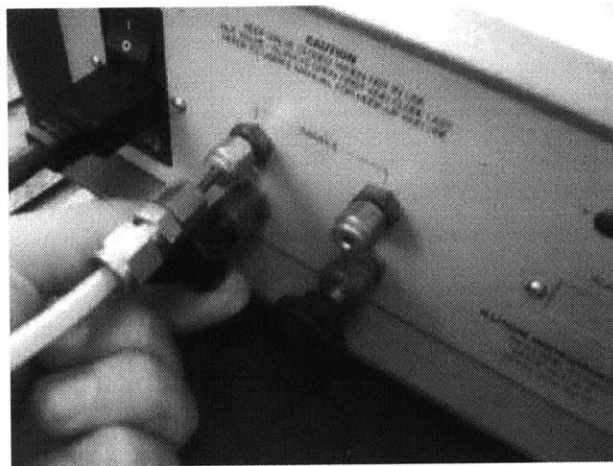


**Figure 4.19: The inlet valve closure.**

## **4.6 The Gas Management System General Test**

The gas management system is hard to be tested because it involves many parts. The control panel contains 10 elements (20 connections) and the vacuum parts contain another 20 feedthroughs and assembly connections. Not to mention about the tank and



oxygenmeter connections. Testing the entire system at once creates a big confusion ending up with no decisive conclusions. The system needs therefore to be separated before being tested. The test involves two parts: the evacuation, and the filling and controlling. The following sections will cover these two subtests.

#### **4.6.1 The evacuation test**

This test aims at determining the vacuum level that could be reached in the chambers. The vacuum chambers were disconnected from the control panel. The major points that needed to be recorded here are:

- 1 – The minimum pressure reached.
- 2 – The time it takes to reach this pressure.
- 3 – The detection of leakage if any.

The leakage problems faced here are of two types: large flow leakage and small flow leakage. Large flow leakage could be easily detected by either its sound or any soapy liquid detector's bubbles formation. If such leakage exists in the system, the vacuum pressure can't go below 2000millitorr, thus no pressure will be indicated on the vacuum gage which is upper-limited by that value. On the other hand, small flow leakage is hard to detect and even harder to solve. In such a case, the pressure would stabilize at a certain value within the range of 100 to 500millitorr but never drops below regardless of the evacuation time. There would be no sign to determine the source of leakage by the conventional detectors. The causes of this leakage could be either insufficient pressure on seals or impurities on the sealing surfaces. The minimum nominal vacuum pressure that can be achieved in this test is 35millitorr reached in 8 minutes.

#### **4.6.2 The filling and control test**

The second step of the gas management system test becomes to inspect both the control panel and the vacuum chambers in the so called filling test. Now that the chambers have made the vacuum test, they are connected to the control panel. The filling test involves a preliminary evacuation stage that tests the chambers and the control panel at once followed by the filling stage. It takes at most 25 seconds to fill the entire system

to a pressure of 55kPa. The repeated evacuation and filling test was performed and the results are shown in Table 4.7 and Figure 4.20.

**Table 4.7: The evacuation-filling test results.**

Run	Time, minutes	Pressure, <i>millitorr</i>
1	8	35
2	9	27
3	11	17

The evacuation process is easier for the drier gas N<sub>2</sub> (runs 2 and 3) than for the humid air (first run). The pressure in the last run is the most influencing factor of the environment inertness.



**Figure 4.20: The vacuum gage displaying the vacuum pressure with timer showing the time to reach that pressure.**

The third and last stage of this test is to check the controlling process. The chamber pressure control is never a problem as long as the chambers' sealing (tested in evacuation test) is achieved. The crucible pressurization requires the top plate-insulation block-crucible assembly to be sealed otherwise gas will leak to the chamber. The graphite gasket applied to the ceramic materials is not a powerful sealing tool. Problems were faced but they were solved with better tightening of the support ring. At the end, the relief valves were tested to ensure immediate drop of the chamber and especially the crucible pressure at relieving.

## 4.7 The Focus Range Test

The imaging system does not require an operation test. It only requires a special test that determines the system's focus range that will later become the allowable breakup range. This range depends on the optical viewports geometry and the camera field of view. During this test, the system elements (camera and stroboscope set at a random frequency) are normally located on their fixtures on the main frame. The heating chamber has the top plate sitting on top. A long stud (threaded rod) is inserted from the vibrator flange of the top plate via a special fitting and extends to the bottom of the heating chamber. Since the system is axisymmetric, the jet is supposed to flow on the symmetry axis of the chamber. This stud, in order to simulate the jet, needs to be placed straightly along this axis and clamped adequately as not to shake or deflect during the test and ruin the calibration. The test setup is shown in Figure 4.21.

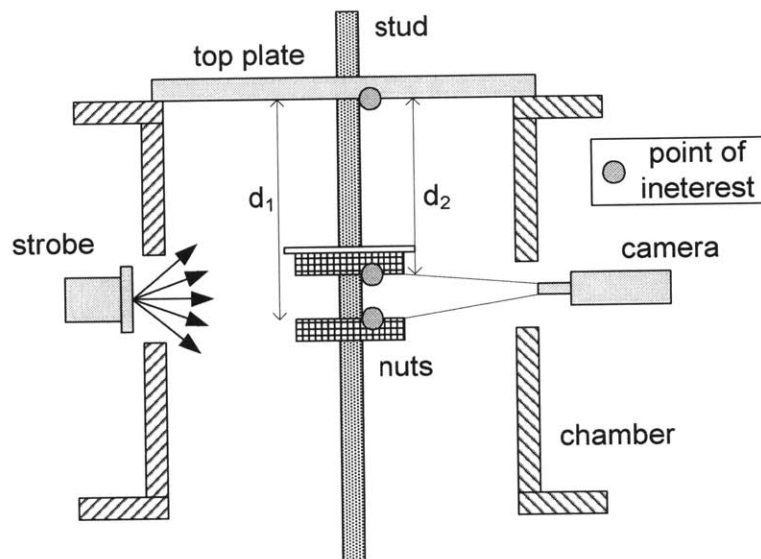


**Figure 4.21: The focus range test setup.**

The display monitor is turned on and the camera is adjusted with its fixture's gliders until the stud is observed in the middle of the screen. Two nuts and an alignment washer are threaded to the stud from its bottom, rotated upward until they start to show up on the screen. If the washer and nut are shown flipped upside down (nut on top of washer), the camera needs to be flipped over as to show them in the appropriate vertical direction. The upper nut is glided upward until it is about to disappear from the upper part of the display screen and the bottom one is glided as to become about to disappear from the lower part

of the screen. Three critical points are marked on the stud: the first (reference point) is where the stud coincides with the plate-chamber sealing surface, the second is at the bottom of the upper nut and the third is at the top of the lower nut. The stud is then disconnected and gently removed without disturbing the nuts position. The distance between the last indicated two points ( $d_1 - d_2$ ) is the focus range  $f_r$  of the imaging system, and the average distance between them and the reference point  $d_f$  is the average distance of breakup from the upper flange of the heating chamber.

Since  $d_1 = 23.5\text{cm}$  and  $d_2 = 22.23\text{cm}$ ,  $f_r$  and  $d_f$  became 1.27cm and 22.86cm respectively. The ideal charging plate should therefore have a height of  $f_r$  and located  $d_f$  from the upper flange of chamber. This aims to charge the droplets at all observed breakups.

## **Chapter 5**

# **CONCLUSION**

This chapter evaluates the outcomes of the high-temperature UDS apparatus. It also describes the problems faced during the spraying process and explains the possible reasons behind them. At the end, several recommendations on how to solve these problems are proposed. Some of the problems faced haven't been encountered before. The explained reasons for them are visualized from a simple process perspective with no regard to theoretical evidences. The proposed solutions may still be hard to be implemented in the current circumstances, but if applied, they could lead to a significant progress in the high-temperature UDS process. In conclusion, the operational status of the UDS apparatus needs to be slightly improved in order to overcome these obstacles. It will be the motivation of the future research to determine these unusual problems and solve them precisely without altering the apparatus general mode of operation.

### **5.1 Results**

The high-temperature UDS apparatus has passed all the tests that most of its systems were subject to. This however doesn't guarantee that the powder production problem is solved. There are still some details that are outside the scope of testing. They were not left as such accidentally. In fact, they were considered to be analyzed and tested when their problems showed up in the operation of the UDS. However, their role or their way of functioning will either make the test hard to be performed or even unreliable in case it was done. Several unveiled factors could be influencing these problems; few observations will not lead to any firm conclusion about them.

Practically, the UDS apparatus has not reached a stage of continuous stable jet breakup that last throughout the entire spraying period as it is the case with the current apparatus. There were some periods where the jet became unstable. Some solidified non uniform droplets (300-500 $\mu\text{m}$ ) were collected as shown in Figure 5.1. The uniformity of

the droplets is never attempted since the stability of the jet breakup is not realized. In the following, more UDS spraying problems will be mentioned and their possible causes will be explained.

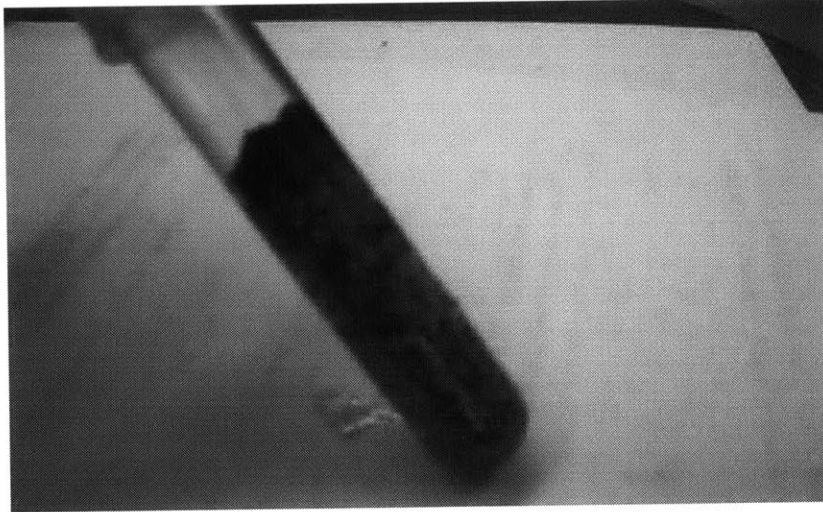


**Figure 5.1: Copper droplets collected from the UDS apparatus.**

## **5.2 The Spraying Problems**

In addition to the most relevant problem of jet unstable breakup, several other problems were faced during the spraying process. They are listed as follows:

- 1 – The orifice detachment from the crucible, resulting in molten copper draining to the bottom plate and chamber walls.
- 2 – The evaporation of silicone oil in the evacuation process and its recondensation on the bottom plate and chamber walls after pressurization.
- 3 – The evaporation of the silicone oil in the collection cup where the copper droplets were collected in it. The vapor silicone oil is smoky in nature, thus it blocks the view of the breakup and impairs the imaging system.
- 4 – One crucible was coated with graphite coverguard that severely outgases at high temperature and reacts with abundant nitrogen in the chamber.
- 5 – Occasional leakage from the top plate assembly (insulation block sealing) failing to pressurize the crucible.

6 – Inability to compress the crucible flange with the insulation block with sufficient force to reduce the leakage.

7 – Difficulty to clean the crucible bottom and orifice pocket conveniently to remove the residual oxides.

8 – The oxygenmeter overshoot and long settling time (10 to 15 minutes) when reading the  $O_2$  concentration. This requires the gas tanks to feed the apparatus for all that time in order to maintain the chamber pressurized (70kPa gage).

None of these problems is related to the systems testing of Chapter 4. They are also hard to be prevented because of their weak correlation to the determined factors of the UDS process. Nevertheless, some possible recommendations to cure these problems are proposed in Section 5.3.

### 5.3 Recommendations

The sources of the problems faced in the spraying process are hard to identify; this makes the problems themselves hard to solve. The repeatable problems are caused by either design defects or operational factors. As an example, the orifice detachment problem which took place in only 5% of the runs made is due to improper gluing or overpressurization of the crucible. There shouldn't be any problems with the adhesive properties as long as the process has worked in other runs. Nevertheless, the concept of having a V shape orifice inserted to a similar V hole in the bottom of the crucible where adhesive is glued from top as shown in Figure 5.2 is a better design than the current one. It prevents leakage without displacing the orifice regardless of the adhesive strength.

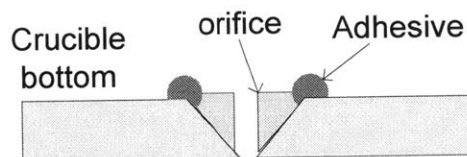


**Figure 5.2: Recommendation of implementing different orifice mounting setup.**

The problem caused by silicone oil in evacuation is due to its high vapor pressure ( $P_{vap} = 500$ millitorr), and that at collection is due to its low boiling point ( $T_{boil} = 200^{\circ}C$ ).

Nothing could be done to prevent the oil from evaporating. The solution would be to choose another quenching liquid of higher evaporating point and lower vapor pressure. The use of sand solves the problem completely; however, sand particles could be pumped out in the evacuation process because the collection cup is very close to the vacuum port which is axially focused toward the bottom plate. The suggestion becomes to place sand in the waste cup (far from the evacuation port) and give it the role of the collection cup. If copper powder is produced, it will be mixed with sand particles. Filtering the copper droplets from the relatively similar-size sand particles is a cumbersome process.

The problem of crucible outgasing or oxidation at high temperature is a graphite chemical property that can't be altered. Attempts to coat the crucible with a thin layer coverguard solution were later discarded after realizing that the problems were actually intensified. The insulation sleeve around the crucible is porous thus it transmits all gases generated from the crucible. This problem could be solved by using an auxiliary quartz crucible wrapped around the graphite one as shown in Figure 5.3. The advantages gained by the quartz crucible addition are:

- 1 – It is chemically inert at all temperatures, so no oxidation problems occur.
- 2 – It has zero porosity, thus nothing would be transmitted from the graphite crucible to the chamber.
- 3 – It has very low thermal conductivity and low emissivity, thus capable of replacing the insulation sleeve.



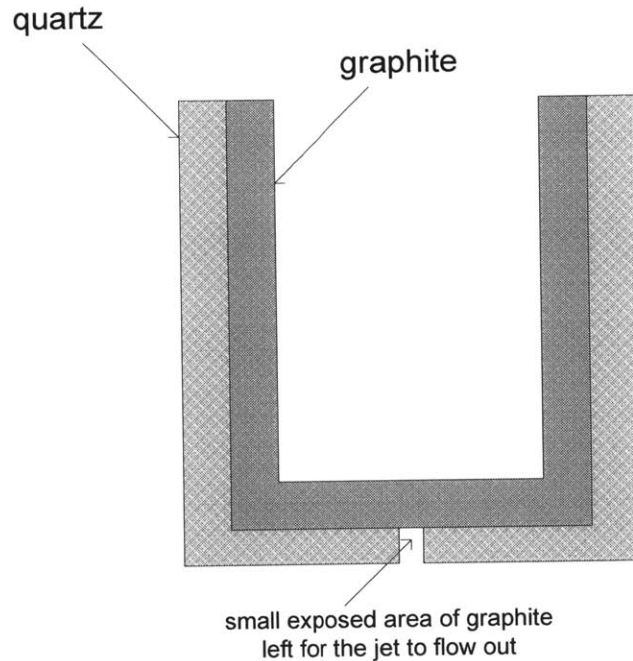


**Figure 5.3: The plan of crucible guarding.**

This suggestion was not implemented because the standard graphite crucible doesn't have a straight outer wall so that a quartz crucible could fit into it. Also the support of the quartz crucible is not easy with the current mounting mechanism implemented in the top plate assembly.

The occasional leakage that was faced in the top plate is mainly due to insufficient tightening of the support ring. The method of sealing is anyway substandard. Machining and later compressing a sharp knife edge of a brittle ceramic part is an uncommon practice.

The main problem of unstable jet breakup could be due to the following reasons:

- 1 – The formation of oxides around the orifice that is either caused by high oxygen content (45ppm) or improper cleaning of the crucible bottom and orifice pocket [9].
- 2 – Melt stirring caused by induction heating. Eddie currents shaking the melt particles to heat them up may have affected the imposed vibration transmitted by the vibration rod. The presence of copper particles solidified on the insulation block is a sign of melt splashing. Open crucible melting observation proved this postulate. The UDS, even if it were a frequency driven process, the amplitude of the imposed vibration must be greater

than that of the eddy currents vibration. No attempt was made to determine the amplitude of the eddy currents vibration to prove the above assumption because there is no explicit model to determine this value [7].

The attempt to switch the heater off during spraying so that the eddy currents would stop and breakup stabilizes was not fruitful, because the eddies vibration didn't die away instantaneously after switching the heater off, also the melt quickly solidifies and spraying stops. Open air melting observation shows that stirring stops and solidification begins at the same time. The jet deflection is due to either oxidation or impurities left on the orifice, but the relatively high oxygen content (45ppm) makes the first reason more valid.

# NOMENCLATURE

## A. Latin Symbols

$C$	general capacitance, <i>farad</i>
$C_o$	oscillator capacitance, <i>farad</i>
$C_1$	first Planck's constant = $3.74 \times 10^{-12} \text{ W.cm}^2$
$C_2$	second Planck's constant = $1.44 \text{ }^\circ\text{K.cm}$
$E$	modulus of elasticity, <i>GPa</i>
$E_s$	voltage supply, <i>V</i>
$H$	radiant power density, $\text{W/cm}^3$
$L$	spectral density $\text{W/cm}^3$ ; general inductance, <i>Henry</i>
$L_{cru}$	crucible inductance, <i>Henry</i>
$L_o$	oscillator inductance, <i>Henry</i>
$L_w$	billet inductance, <i>Henry</i>
$P_l$	load power, <i>Watt</i>
$P$	pressure, <i>kPa</i>
$Q$	heat flow, $\text{W/m}^2$
$R_{int}$	input resistance, <i>Ohm</i>
$R_l$	load resistance, <i>Ohm</i>
$R_{out}$	output resistance, <i>Ohm</i>
$R_s$	source and wiring resistance, <i>Ohm</i>
$R_r$	radiation ratio, <i>unitless</i>
$R_w$	billet resistance, <i>Ohm</i>
$R_{cru}$	crucible resistance, <i>Ohm</i>
$S_{ult}$	ultimate strength, <i>MPa</i>
$T$	temperature, $^\circ\text{K}$
$V_j$	exit jet velocity, <i>m/sec</i>
$d_d$	droplet diameter, <i>m</i>
$d_f$	average distance to breakup, <i>m</i>

$d_o$	orifice diameter, $m$
$f$	oscillator frequency, $Hz$
$f_r$	focus range, $m$
$f_s$	strobe frequency, $Hz$
$f_v$	frequency of the vibrating rod, $Hz$
$i$	electric current, $amp$
$k$	proportionality constant between strobe and vibrator frequency, <i>unitless</i>
$r$	radius, $m$
$r_i$	inner radius, $m$
$r_o$	outer radius, $m$ ; orifice diameter, $m$

## B. Greek Symbols

$\lambda_b$	breakup wavelength, $m$
$\lambda$	electromagnetic radiation wavelength, $m$
$\nu$	Poisson's ratio, <i>unitless</i>
$\alpha$	coefficient of linear thermal expansion, $^{\circ}K^{-1}$
$\sigma_r$	radial stress, $MPa$
$\sigma_t$	tangential stress, $MPa$
$\sigma_z$	axial stress, $MPa$
$\Delta T$	temperature difference, $^{\circ}K$
$\rho$	electrical resistivity, $Ohm.m$ ; density, $kg/m^3$
$\mu$	permeability, <i>unitless</i>
$\varepsilon$	emissivity, <i>unitless</i>
$\varepsilon_p$	pyrometer emissivity, <i>unitless</i>
$\eta$	efficiency, <i>unitless</i>
$\sigma$	Stefen-Boltzmann constant = $5.669 \times 10^{-12} W/cm^2.K^4$
$\delta$	skin depth, $m$
$\theta$	polar coordinate

## REFERENCES

- [1] Groover, Mikell P. "Fundamentals of Modern Manufacturing" Prentice Hall, Upper Saddle River, NJ, 1996.
- [2] Passow, Christian Henry "A study of Spray Forming Using Uniform Droplet Sprays" MIT, Cambridge, MA, 1992.
- [3] Alvarez, Juan Carlos "Development of a Process for the Production of Fluxless Solder Spheres for BGA Electronics Packaging" MIT, Cambridge, MA, 1999.
- [4] Johns, Lewis E. and Narayanan, R. "Interfacial Instabilities" Springer, New York, NY 2002.
- [5] Yim, Pyongwon "The Role of Surface Oxidation in the Break-Up of Laminar Liquid Metal Jets" MIT, Cambridge, MA, 1996.
- [6] Cherng, Jean-Pei Jeanie "The Effects of Deposit Thermal History on Microstructure Produced by UDS Forming" MIT, Cambridge, MA, 2002.
- [7] Davies, E.J. "Conduction and Induction Heating" Peter Peregrinus Ltd., London, UK, 1990.
- [8] Touloukian, Y.S. "Thermophysical Properties of High Temperature Solid Materials" vol 1, The Macmillan Company, New York, NY 1967.
- [9] Boley, Bruno A. and Weiner, Jerome H. "Theory of Thermal Stresses" John Wiley and Sons, New York NY, 1960.
- [10] Kim, Ho-Young "Spreading Behavior of Molten Metal Microdroplet" MIT, Cambridge, MA, 1999.
- [11] Davies, John and Simpson Peter "Induction Heating Handbook" McGraw Hill Book Company, London, UK, 1979.
- [12] Tudbury, Chester A. "Basics of Induction Heating" vol 1, John F. Rider Publisher, New Rochelle, NY, 1960.
- [13] Stansel, N.R. "Induction Heating", 1<sup>st</sup> edition, McGraw Hill Book Company, New York, NY, 1949.

[14] Kerlin, Thomas W. and Shepard, Robert L. "Industrial Temperature Measurement" The Instrument Society of America, Research Triangle Park, NC, 1982, pp213-226.

[15] Lawton, B. and Kilingerberg, G. "Transient Temperature in Engineering and Science" Oxford Science Publications and University Press, Oxford, UK, 1996

# **Appendix A**

## **Material Data Sheets**

This appendix contains the data sheet of the materials used in making the UDS parts mainly, the crucible set. The stress analysis of Section 4.1 is based on the data available from the manufacturers of ceramic parts. Plots of important copper properties as function of temperature are shown at the end.

## **A1 Combat Solid Boron Nitride Grade A**

### **A1.1 General Information**

Suggested for all but the most severe refractory and electrical applications, Combat Solid Boron Nitride Grade A is a high-performance material best used in a dry or inert environment to prevent hydration. Among its many advantages, Grade A's glassy  $B_2O_3$  binder creates a hard and dense yet fully machinable product, allowing for enormous customization and applicable use. It has a high performance and an economic price.

*CHEMICALLY:* Excellent resistance to most corrosive agents. Further, metals will not wet or adhere to it, permitting easy cleaning of deposited metals.

*THERMALLY:* Outstanding thermal shock resistance—the combination of thermal conductivity and low thermal expansion combine to provide long life service where severe thermal cycling is common. Grade A also provides excellent thermal conductivity—allowing the dissipation of localized hot spots, prolonging the life of components in the most severe areas.

*ELECTRICALLY:* Low dielectric constant material.

*MACHINABILITY:* Like other grades of Combat Boron Nitride, Grade A can be machined using standard high speed “tool steel” equipment. Machining by grinding may be used if preferred or stringent tolerances are required.

### **A1.2 Common Applications**

- 1 – High temperature electrical insulators and vacuum furnace supports which require electrical resistivity, high temperature strength, thermal shock resistance and low chemical reactivity.
- 2 – Crucibles and containers for high purity molten metals
- 3 – Insulators and source fixtures for ion implantation systems which require high temperature purity and electrical insulation.
- 4 – Radar components and antenna windows which require exacting electrical and thermal properties.
- 5 – Setterplates for the processing of other advanced materials which require stable, inert surfaces.
- 6 – Nozzles for powdered metal spraying.



### A1.3 Engineering Properties

Binder	Boric acid	
Binder Melting Point °C	550	
Density g/cc	2.0	
Open Porosity %	2.84	
Oxygen – max %	4	
Calcium – max %	0.1	
B <sub>2</sub> O <sub>3</sub> – max %	4.5	
Other Impurities – max %	0.2	
Maximum Use Temperature °C		
Oxidizing	850	
Inert:	1800	
Specific Heat @700°C J/g°C	1.61	
Hardness-Knoop (kg/mm <sup>2</sup> )	15.51-24.19	
Dielectric Strength volts/mil	2400	
Pressing Direction	Parallel	(Perpendicular)
Resistivity Ohm-cm RT	>10 <sup>14</sup>	(10 <sup>15</sup> )
Loss Tangent @ 8.8 GHz	0.0017	(0.0005)
Dielectric Constant @ RT	4.58	(4.15)
Thermal Conductivity @ RT W/m <sup>o</sup> K	30.13	(33.71)
Thermal Expansion Coefficient (RT-1500°C) m/m/°C ×10 <sup>-6</sup>	11.85	(3.12)
Flexural Strength MPa		
@ 25°C	75.6	(112.7)
@ 1500°C	6.2	(9.5)
Compressive strength @ RT Mpa	142.8	(186)

### A1.4 Availability

Custom machining of Combat Solid Boron Nitride Grade A for complex shapes based on customer specifications is provided. Solid bars, rods and plates are also available for customers who desire to fabricate their own custom shapes using conventional machine shop tools.

## **A2 Combat Solid Boron Nitride Grade AX05**

### **A2.1 General Information**

Grade AX05 boron nitride is one of the highest purity hexagonal boron nitride solids available. It is a diffusion bonded ceramic and does not depend on a B<sub>2</sub>O<sub>3</sub> binder for mechanical integrity. This high purity advantage allows for applications and uses not provided by other hot-pressed boron nitride solids. The end result is that Combat Boron Nitride Solid Grade AX05 is a unique advanced ceramic material that provides a host of exceptional properties. It is also known for its high corrosion resistance.

*CHEMICALLY:* Grade AX05 is extremely inert and non-wet by many molten materials such as metals, glasses, halide salts and other reagents. The chemical stability allows Grade AX05 to provide a stable, nonreactive material for nozzles, feedthroughs, crucibles and supports.

*THERMALLY:* Grade AX05 has minimal thermal expansion, high thermal conductivity and use temperature in certain inert atmospheres over 2000°C. Thermal shock stability is excellent over a wide range of use temperatures.

*MECHANICALLY:* Grade AX05 yields increasing relative strength vs. temperature. This important feature provides higher temperature performance to applications previously unattainable with B<sub>2</sub>O<sub>3</sub> bonded boron nitrides.

*ELECTRICALLY:* Grade AX05 is transparent to microwave energy. It also provides high resistivity and dielectric strength with a low loss tangent and dielectric constant. These characteristics make AX05 an excellent material for high power, low loss insulators, containers and fixtures.

*MACHINABILITY:* Grade AX05 can be machined to extremely close tolerances using standard high speed “tool steel” equipment. Machining by grinding may be used if preferred or stringent tolerances are required. Threads can be machined using taps and dies. Cutting oils and coolants should not be used for any reason.

### **A2.2 Common Applications**

- 1 – High temperature electrical insulators and vacuum furnace supports which require electrical resistivity, high temperature strength, thermal shock resistance and low chemical reactivity.
- 2 – Crucibles and containers for high purity molten metals
- 3 – Insulators and source fixtures for ion implantation systems which require high temperature purity and electrical insulation.
- 4 – Radar components and antenna windows which require exacting electrical and thermal properties.

5 – Setterplates for the processing of other advanced materials which require stable, inert surfaces.

6 – Nozzles for powdered metal spraying.

### A2.3 Engineering Properties

Binder	None	
Binder Melting Point	None	
Density g/cc	1.85	
Open Porosity %	12.57	
Oxygen – max %	1	
Carbon – max %	0.02	
Calcium – max %	0.04	
B <sub>2</sub> O <sub>3</sub> – max %	<0.2	
Other Impurities – max %	0.05	
Maximum Use Temperature °C		
Oxidizing	850	
Inert:	>2000	
Specific Heat J/g°C		
@RT	0.35	
@700°C	1.5	
Dielectric Strength volts/mil	2000	
Hardness-Knoop (kg/mm <sup>2</sup> )	3.42-4.91	
Pressing Direction	Parallel	(Perpendicular)
Resistivity Ohm-cm RT	>10 <sup>14</sup>	(10 <sup>15</sup> )
Loss Tangent @ 8.8 GHz	0.0012	(0.0003)
Dielectric Constant @ RT	4.0	(4.0)
Thermal Conductivity W/m/°K		
@ RT	78.0	(130.0)
@ 1500°C	19.4	(30.7)
Thermal Expansion Coefficient (RT-1500°C) m/m/°C ×10 <sup>-6</sup>	1.0	(0.3)
Flexural Strength MPa		
@ 25°C	17.9	(21.3)
@ 1500°C	42.6	(75.6)
Compressive strength @ RT MPa	17.9	(23.3)

### A2.4 Availability

Custom machining of Combat Solid Boron Nitride Grade AX05 for complex shapes based on customer specifications is provided. Solid bars, rods and plates are also available for customers who desire to fabricate their own custom shapes using conventional machine shop tools.

## A3 Alumina

### A3.1 General Information

It is a high purity ceramic of 99.5% (nominal) Al<sub>2</sub>O<sub>3</sub> content. Its purity, chemical resistance and high temperature capabilities prove invaluable for semiconductor processing applications. Its prime features are:

- 1 – Electrically and dimensionally stable at high temperatures.
- 2 – Low particle generation.
- 3 – Dense, non porous and vacuum tight.
- 4 – Excellent dielectric properties.
- 5 – Accepts moly-manganese metallising for high temperature brazing of vacuum tight assemblies.
- 6 – Excellent chemical and abrasion resistance.

### A3.2 Common Applications

- 1 – Wafer processing and handling devices.
- 2 – Components for semiconductor process chambers, spluttering targets, fixtures, etc.
- 3 – Laser devices for wide range of industrial, medical and defense duties.
- 4 – Power tubes for klystron and x-ray equipment.
- 5 – Flow meters and pressure sensors.

### A3. 3 Engineering Properties

Color		White		
Bulk density (fired)	Mg/m <sup>3</sup>	3.86		
Porosity (apparent),	%	0 (fully dense)		
Rockwell hardness	(R45N)	81		
Compressive strength,	MPa	>2070		
Young's modulus,	GPa	375		
Flexural strength,	MPa	310		
Thermal conductivity, @RT	W/m.K	29.3		
Specific heat, J/kg °K		880		
Thermal expansion coefficient,	10 <sup>-6</sup> /C			
25-200C		6.9		
200-400C		7.8		
400-600C		8.3		
600-800C		9.0		
800-1000C		9.4		
Maximum no-load temperature,	°C	1725		
Dielectric strength, @RT	dc kV/mm	31.5		
Dielectric constant, K <sup>l</sup> , @ 10MHz		25°C	300°C	500°C
@ 1000MHz		9.58	9.92	10.20
@ 8500MHz		9.30	—	—
		9.37	9.61	9.82

Dissipation factor, $\tan\delta$ , @ 10MHz	0.00003	0.00009	0.00040
@ 1000MHz	0.00014	—	—
@ 8500MHz	0.00009	0.00014	0.00025
Loss factor, $K^1 \cdot \tan\delta$ , @ 10MHz	0.00029	0.00089	0.00408
@ 1000MHz	0.00130	—	—
@ 8500MHz	0.00084	0.00135	0.00245
Volume resistivity, ohm.cm			
@ 25C	$>10^{14}$		
@ 300C	$2.0 \times 10^{11}$		
@ 600C	$6.0 \times 10^8$		
@ 900C	$2.5 \times 10^6$		
Te value, °C	$>975$		

Please note that all values quoted are based on test pieces and may vary according to component design. These values are not guaranteed in any way and should only be treated as indicative values. They should be used for guidance only and for no other purpose whatsoever.

## A4 Mullite

### A4.1 General Information

Mullite is a good, low cost refractory material with a nominal composition of  $3\text{Al}_2\text{O}_3 \cdot 2\text{SiO}_2$ . The raw materials are easily obtainable and are reasonably priced. It has excellent high temperature properties with improved thermal shock and thermal stress owing to the low thermal expansion, good strength and interlocking grain structure. Its key properties are:

- 1 – Good thermal shock and stress resistance.
- 2 – Low thermal conductivity.
- 3 – Good strength.
- 4 – Wear resistant.
- 5 – Usable to high temperatures.

### A4.2 Common Applications

- 1 – Protection tubes.
- 2 – Furnace liners.
- 3 – Electric insulators.

### A4.3 Engineering Properties

Density	gm/cc	2.8
Porosity	%	0
Color		off-white
Flexural Strength	MPa	180
Elastic Modulus	GPa	151
Shear Modulus	GPa	—
Bulk Modulus	GPa	—
Poisson's Ratio		0.25
Compressive Strength	MPa	1310
Hardness	Kg/mm <sup>2</sup>	1070
Fracture Toughness $K_{IC}$	MPa.m <sup>1/2</sup>	2
Maximum Use Temperature, no load	°C	1650
Thermal Conductivity W/m.°K		6
Coefficient of Thermal Expansion 1	$10^{-6}/°C$	5.4
Specific Heat J/Kg.°K		961.4
Dielectric Strength	ac-kv/mm	9.8
Dielectric Constant, @ 1 MHz		5.8
Dissipation Factor, @ 1 kHz		0.003
Volume Resistivity	ohm.cm	$>10^{13}$

## A5 Quartz

### A5.1 General Information

Fused silica is a non-crystalline (glass) form of silicon dioxide (quartz, sand). Typical of glasses, it lacks long range order in its atomic structure. Its highly cross linked three dimensional structure gives rise to its high use temperature and low thermal expansion coefficient. Its key properties are:

- 1 – Near zero thermal expansion.
- 2 – Exceptionally good thermal shock resistance.
- 3 – Very good chemical inertness.
- 4 – Can be lapped and polished to fine finishes.
- 5 – Low dielectric constant.
- 6 – Low dielectric loss.
- 7 – Good UV transparency.

### A5.2 Common Applications

- 1 – High temperature lamp envelopes.
- 2 – Temperature insensitive optical component supports.
- 3 – Lenses, mirrors in highly variable temperature regimes.
- 4 – Microwave and millimeter wave components.
- 5 – Aeronautical radar windows.

### A5.3 Engineering Properties

Density	gm/cc	2.2
Porosity	%	0
Color		clear
Flexural Strength	MPa	—
Elastic Modulus	GPa	73
Shear Modulus	GPa	31
Bulk Modulus	GPa	41
Poisson's Ratio		0.17
Compressive Strength	MPa	1108
Hardness	Kg/mm <sup>2</sup>	600
Fracture Toughness K <sub>IC</sub>	MPa.m <sup>1/2</sup>	—
Maximum Use Temperature (no load)	°C	1100
Thermal Conductivity	W/m•°K	1.38
Coefficient of Thermal Expansion	10 <sup>-6</sup> /°C	0.55
Specific Heat	J/Kg.°K	740
Dielectric Strength	ac-kv/mm	30
Dielectric Constant	@ 1 MHz	3.82
Dissipation Factor	@ 1 MHz	0.00002
Loss Tangent	@ 1 MHz	—

Volume Resistivity      ohm.cm       $>10^{10}$

#### **A5.4 Availability**

Quartz is available as some standard shapes (rods, plates, tubes and crucibles). However is machining is hard and expensive because it requires diamond tooling. Custom made items are therefore expensive. Quarts parts could be fused to each other, thus simplifying the machining and reducing the cost of complicated shapes.



## **A6 Graphite**

### **A6.1 General Information**

There are two types of graphite used in the industry: natural graphite and synthetic graphite. Natural graphite is a naturally occurring element and it is used mainly as a lubricant, carbon additive and pencil lead. Synthetic graphite is petroleum based composite material used in a variety of applications requiring superior to natural graphite properties. Synthetic graphite is also called artificial graphite, and is classified by a method of manufacturing and/or by production stage. There are four methods of manufacturing synthetic graphite: extrusion, vibration molding, compression molding and isostatic molding. There are also four production stages: baking, graphitization, purification and impregnation. The combination of methods of manufacturing and production stages determines the future properties of graphite. Manufacturing graphite is a lengthy and expensive process. However, the result of this process is a material offering a combination of some very unique properties:

- 1 – Excellent electrical conductivity
- 2 – Good thermal shock resistance
- 3 – High mechanical strength
- 4 – Low coefficient of thermal expansion
- 5 – Low coefficient of friction
- 6 – Superb chemical resistance

### **A6.2 Common Applications**

Graphite has many applications in several areas of manufacturing. The following list shows some of graphite's typical applications.

#### *1 – Electrical, Electrochemical, Electronic, EDM, Semiconductor:*

Brushes, Anodes, Cathodes, Current Collectors, Sliding Contacts, EDM Electrodes, Resistors, Brazing Tips, Heaters, Seed Holders

#### *2 – Metallurgical:*

Trays & Boats, Crucibles, Fluxing (Degassing) Tubes, Molds & Dies, Furnace Parts, Foundry Accessories, Canisters & Aluminum Extrusion Boards

#### *3 – Chemical:*

Vessels and Reactors, Bushings & Bearings, Packing Rings & Seals, Roller Guides, Valves, Rotors & Vanes

#### *4 – Aerospace:*

Rocket Nozzles

#### *5 – Nuclear:*

High Purity Structural Components, Reflectors, Moderators

### A6.3 Engineering Properties

Density g/cm <sup>3</sup>	2.25
Color	black
Crystal Structure	hexagonal
Water Absorption @ R.T. %	0.5 - 3.0
Hardness Mohs	1.0 - 1.5
Compressive Strength @ R.T. MPa	96
Tensile Strength @ R.T. MPa	4.8
Modulus of Elasticity GPa	4.8
Flexural Strength @ R.T. MPa	50
Max. Use Temperature (inert atm.) °C	3650
Thermal Shock Resistance ΔT (°C)	200 - 250
Thermal Conductivity W/m-K @ R.T.	24
Coefficient of Linear Thermal Expansion μm/m.°C (25°C - 1000°C)	8.39
Specific Heat cal/g-°C @ R.T.	0.16
Electrical Resistivity Ωcm @ R.T.	7 x 10 <sup>-3</sup>
Emissivity	0.9

### A6.4 Availability

Graphite is available as both standard finished items and basic geometrical shapes such as plates, rods, blocks and tubes. Graphite is machinable with HSS or carbide tools.

## **A7 Grafoil Flexible Graphite**

### **A7.1 General Information**

Grafoil flexible graphite is a distinctive sheet material that combines the high temperature and chemical resistance characteristics of graphite and the traditional characteristics of flexibility, compatibility, conformability, and resilience. These characteristics differentiate Grafoil flexible graphite from other forms of carbon and graphite and make it a superior and high-performance packing and gasketing material. Because of its unique properties and non-fibrous structure, grafoil gaskets and packings are particularly well suited for high performance and corrosive fluid sealing applications. Grafoil has long been considered as one of the safest materials for nearly all fluid sealing applications. Grafoil gaskets have been proven fire-safe in the presence of highly volatile fluids and extremely high temperatures. In addition it is widely used as replacement for asbestos based gasketing materials. In brief, Grafoil is:

- 1 – anisotropic.
- 2 – resilient and compressible.
- 3 – thermally stable.
- 4 – naturally lubricious.
- 5 – easily cut.
- 6 – made without binders, resins or other additives.

### **A7.2 Common Applications**

The most common applications of Grafoil is sealing in severe environments. It could be used for:

- 1 – Gasoline/diesel engine head gaskets.
- 2 – Exhaust manifold gaskets.
- 3 – Exhaust ring seals.
- 4 – Turbo charger gaskets.
- 5 – Intake manifold and crossover gaskets.
- 6 – Gas turbine seals and gaskets.
- 7 – Heat shields.
- 8 – Airbags.
- 9 – Noise and vibration harshness (NVH).
- 10 – Temperature and chemical resistant gasket and valve packing for chemical and petrochemical plants.

### **A7.3 Engineering Properties**

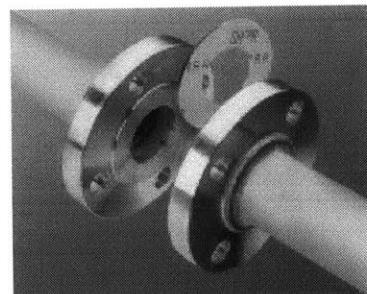
Density	g/cc	1.2
Leachable Chloride Content	ppm	<20
Sulfur Content	ppm	450
Carbon Content	%	99.9

Compressibility	%	43
Recovery	%	15
Creep Relaxation	%	<5
Sealability	mL/hr	0.5
Tensile Strength Along	MPa	6.9
Coefficient of Friction against Steel		
@ 0.03 MPa		0.018
@ 0.06 MPa		0.052
@ 0.08 MPa		0.157
Compressive Strength through Thickness	MPa	240
Modulus of Elasticity through Thickness		
Tension	MPa	1380
Compression	MPa	186
Functional/Temperature Range		
Neutral or Reducing Atmosphere	°C	-240 to 3000
Oxidizing Atmosphere	°C	-240 to 450
Thermal Conductivity		
Along Length & Width	W/m.°K	140
Through Thickness	W/m.°K	5
Thermal Expansion		
Parallel to Layers	µm/m.°C	-0.4
Through Thickness	µm/m.°C	27
Specific Heat (24°C)	J/kg·K	711
Surface Emissivity		0.5
Sublimation Point (Does not melt)	°C	3300
Thermal Shock Resistance		Excellent

#### A7.4 Availability

Grafoil flexible graphite can be combined with various interlayer materials to improve performance and handling. Carbon Steel Tanged Metal, Aluminum and PTFE are available.

Grafoil Flexible Graphite is available starting with ultra-thin 0.003" thick GT™ Y Grade, or standard materials from 0.005" up to 0.060" thick, in standard increments of 0.005". The standard production line widths are 24" and 39.4". Material can also be supplied in custom slit widths or cut sheets. Sheets could also be laminated to form virtually any thickness desired. A grafoil gasket sealing between two flanges is shown.



## **A8 Thermal Insulation Material: Alumina-Silica Fiber Paper**

### **A8.1 General Information**

Alumina Silica fiber refractory papers are non woven, non-asbestos, fiber-based products, engineered as thermal barrier materials for use in high temperature applications. They are a binderless product for applications where outgassing cannot be tolerated, and high purity compositions where the reducing of silica cannot be permitted.

Type ASPA-2 is premium grade, lightweight refractory material made from high purity alumina-silica fibers formed into a highly flexible sheets. It is produced with no organic volatiles and will not produce smoke or odor when heated. These alumina-silica fiber papers exhibit very low thermal conductivity and are designed for use in applications where purity, cracking resistance, high strength and resistance to heat are paramount. Due to their exceptional resistance to heat flow for their thickness, they provide maximum thermal resistance where space is at a premium. These materials are virtually shot free and are the cleanest refractory papers available. They are ideal for applications up to 1260°C.

### **A8.2 Common Applications**

Commonly used in the molten metal casting and heat treating industries, ASPA-2 is also used as specialty gasketing in the fuel cell, nuclear, glass and electronic industries, as well as many other applications which require high temperature stability and low thermal conductivity. It also offers excellent corrosion resistance and unique handling strength for easy die-cutting, wrapping and forming. It is found in:

- 1 – Annealing cover seals.
- 2 – Flexible high temperature pipe insulation.
- 3 – Furnace, kiln, reformer and boiler lining.
- 4 – Furnace door linings and seals.
- 5 – Investment casting mold wrap.
- 6 – Expansion joint seals.
- 7 – High temperature filtration.
- 8 – Glass furnace crown insulation.
- 9 – Useful when refractory ceramic fibers are not desired.
- 10 – Thermal reactor insulation.
- 11 – Soaking pit seals.
- 12 – Insulation for primary reformer header.
- 13 – High temperature gasketing.
- 14 – High temperature kiln and furnace insulation.

### **A8.3 Engineering Properties**

Composition %

Al<sub>2</sub>O<sub>3</sub> 51

SiO <sub>2</sub>	49
Other Oxides	trace
LOI, %	.5 max
Density, g/cc	0.128
Color,	White
Type of Binder,	None
Fiber Index, %	75
Maximum Use Temp, °C	1260
Melting Temp, °C	1760
Mullen Burst, kPa	138
Thermal Conductivity W/m K	
500°C	0.05
800°C	0.08
871°C	0.13
1100°C	0.16
Dielectric strength, V/mil	55

#### **A8.4 Availability**

The ASPA-2 composite refractory insulation is available in flexible sheets of widths 30cm, 45cm, 60cm, and 120cm. The sheet length ranges from 0.5m up to 30m. The sheet thickness is either 0.8mm, 1.6mm, 3.2mm or 6.4mm.

## **A9 Alumina Silicate**

### **A9.1 Engineering Properties**

Composition	Alumina Silicate
Porosity	2.5
Softening Temperature °C	1100
CTE $\times 10^6 / ^\circ\text{C}$	
@25-100 C	5.22
@100-600 C	6.48
Density	2.35
Color, unfired	Gray
Color, fired in air	pink
Maximum Temperature °C	1100
Flexural Strength MPa	68.9
Compressive Strength MPa	172.4
Tensile Strength MPa	17.2
Hardness (unfired) Mohs	1-2
Hardness (after firing) Mohs	6
Thermal Conductivity W/m.K	1.26

### **A9.2 Common Applications**

This material is suitable for making

- 1 – Thermal insulators
- 2 – Gas chromatographs
- 3 – Ceramic to metal sealing fixtures

## A10 Sapphire

### A10.1 General Information

Sapphire is by far the strongest, thermal shock and chemically resistant material available. It is known for the following properties:

- 1 – Chemical resistivity.
- 2 – Strength and stability.
- 3 – Scratch and abrasion resistance.
- 4 – High thermal conductivity.
- 5 – Moderate refractive index.
- 6 – Zero porosity.

### A10.2 Common Applications

In addition to the high temperature orifices, sapphire is used in the following applications:

- 1 – Lamp envelopes
- 2 – Solar cell coverplates
- 3 – Light pipes
- 4 – High pressure and vacuum windows
- 5 – Optical flats and prisms

### A10.3 Engineering Properties

crystal system	hexagonal
chemical formula	$\text{Al}_2\text{O}_3$
purity	99.99%
cleavage	conchoidal
specific gravity	3.99 - 3.98
dislocation density / $\text{cm}^2$	$10^5 - 10^4 / \text{cm}^2$
melting point °C	2050
softening point °C	1800
specific heat at 25°C cal/g	0.18
thermal conductivity at 25°C cal/sec.cm .°C	0.1
thermal expansion /°C	
face $\perp$ to c axis	$5.4 \times 10^{-6}$
face = to c axis	$6.2 \times 10^{-6}$
Hardness Mohs	9
Knoop scale face $\perp$ to c axis	1800
Knoop scale face = to c axis	2200
modulus of elasticity $\text{kg/cm}^2$	$4.4 \times 10^6$
modulus of rupture at 25°C $\text{kg/cm}^2$	4000
compressive strength at 25°C $\text{kg/cm}^2$	21000
ultimate tensile strength $\text{kg/cm}^2$	1900
chemical resistance	unattacked by common acids or NaOH



acids and alkalis attack at 300°C	0
porosity	0
dielectric constant (permittivity)	7.5 at 10.5
electrical resistance ohm/cm	
500°C	$10^{11}$
1000°C	$10^6$
2000°C	$10^3$

#### **A10.4 Availability**

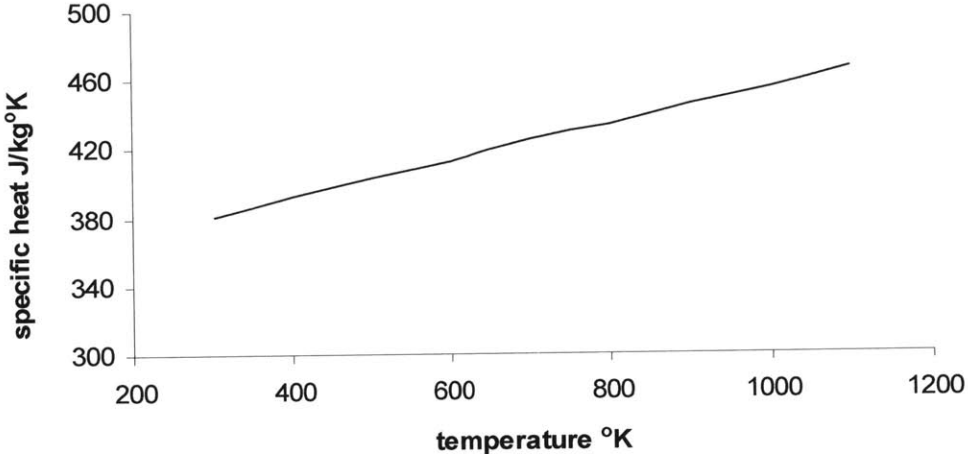
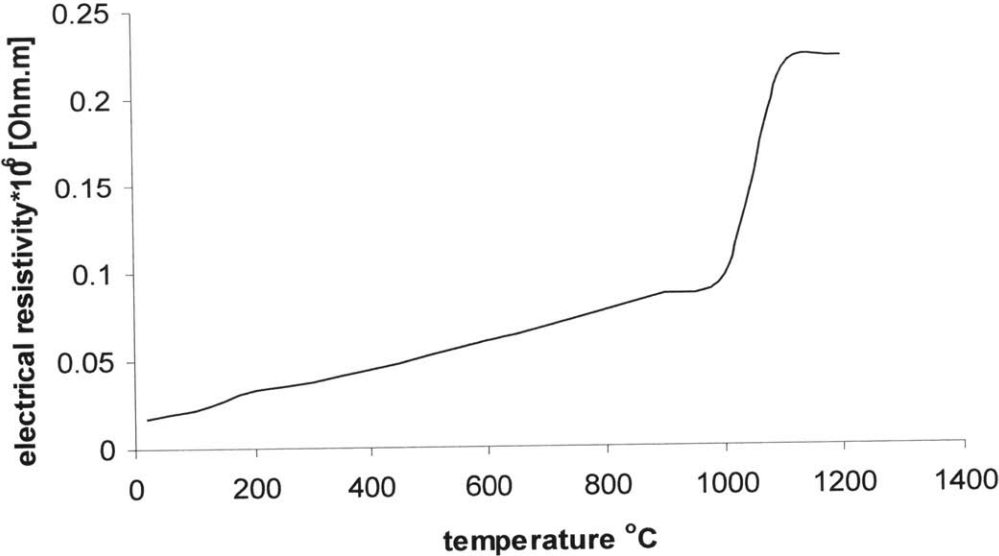
Sapphire substrates are available in round, rectangular, square or rod forms. Sizes are available from 0.254mm diameter rod up to 152.4 diameter windows. Thickness can be obtained in most common fractional sizes up to 76mm. Polishes are standard at 80-20. Special polishes down to 250 Angstroms are available. Sapphire machining is very hard and expensive, it is rarely done by tool, it laser machined instead.

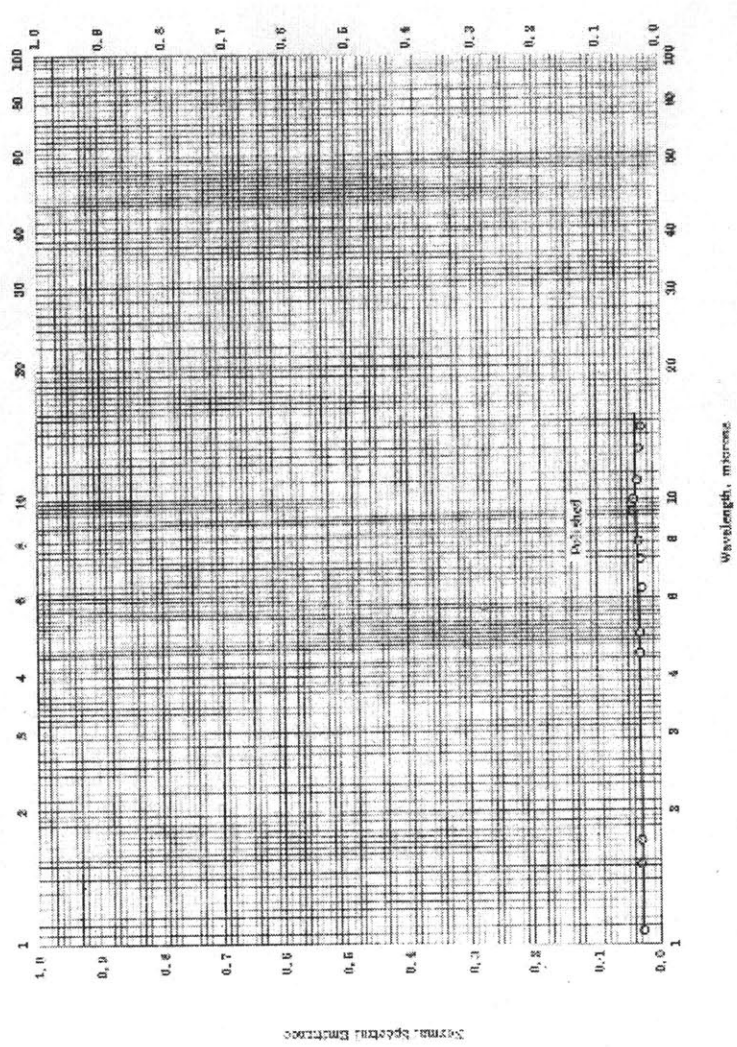
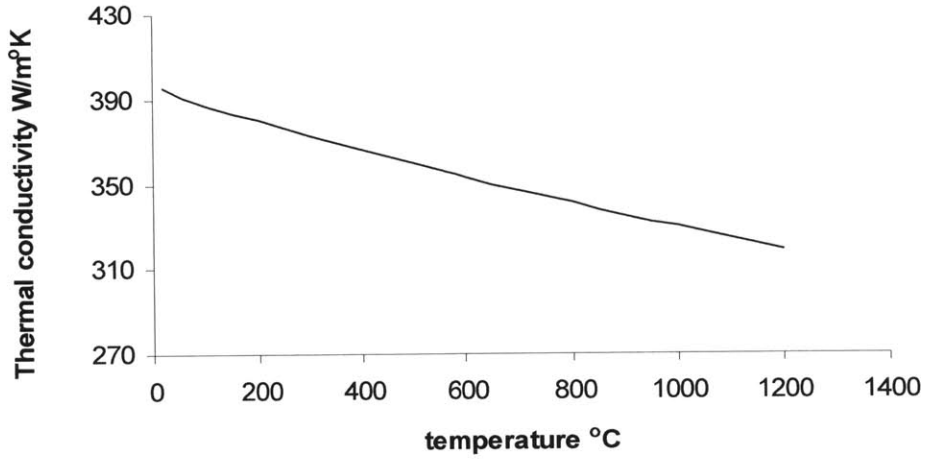
### A11 Copper

The properties of copper relevant to the thesis calculations are listed below:

- 1 – Electrical resistivity
- 2 – Specific heat
- 3 – Thermal conductivity
- 4 – Spectral emissivity

The first three properties vary with temperature; a plot of their variations is shown below.





# Appendix B

## Parts Drawings

This appendix contains the parts drawings of most of the UDS components designed and fabricated in the DBM. All drawings were generated using the CAD software tool *Solidworks*. The table below lists all the drawings by part name and corresponding drawing number.

Drawing number	Drawing name
B.1.1	Frame assembly
B.1.2	Main frame
B.1.3	Powder chamber frame
B.1.4	Heating chamber supporting plate
B.1.5	Powder chamber supporting plate
B.1.6	Eyehook assembly
B.1.7	Safety stopper
B.1.8	Powder chamber
B.1.9	Rail stopper
B.1.10	Waste cup fixture
B.2.1	Top plate assembly
B.2.2	Crucible
B.2.3	Crucible support ring
B.2.4	Insulation block
B.2.5	Vibration rod
B.2.6	Upper gasket
B.2.7	Lower gasket
B.2.8	Insulation sleeve
B.2.9	Insulation ring
B.2.10	Orifice
B.2.11	Pyrometer fixture
B.3.1	Coil assembly
B.3.2	Inductive coil
B.3.3	RF feedthrough
B.3.4	Insulator coil holder
B.3.5	Metal link
B.3.6	Cover cylinder
B.4.1	Bottom plate assembly
B.4.2	Flanged cylinder
B.4.3	Insulation disk
B.4.4	Collection cup
B.4.5	Bottom plate
B.5.1	Stroboscope assembly
B.5.2	Strobe_fixture_1
B.5.3	Strobe_fixture_2
B.5.4	Strobe_fixture_3
B.5.5	Camera fixture

B.6  
B.7

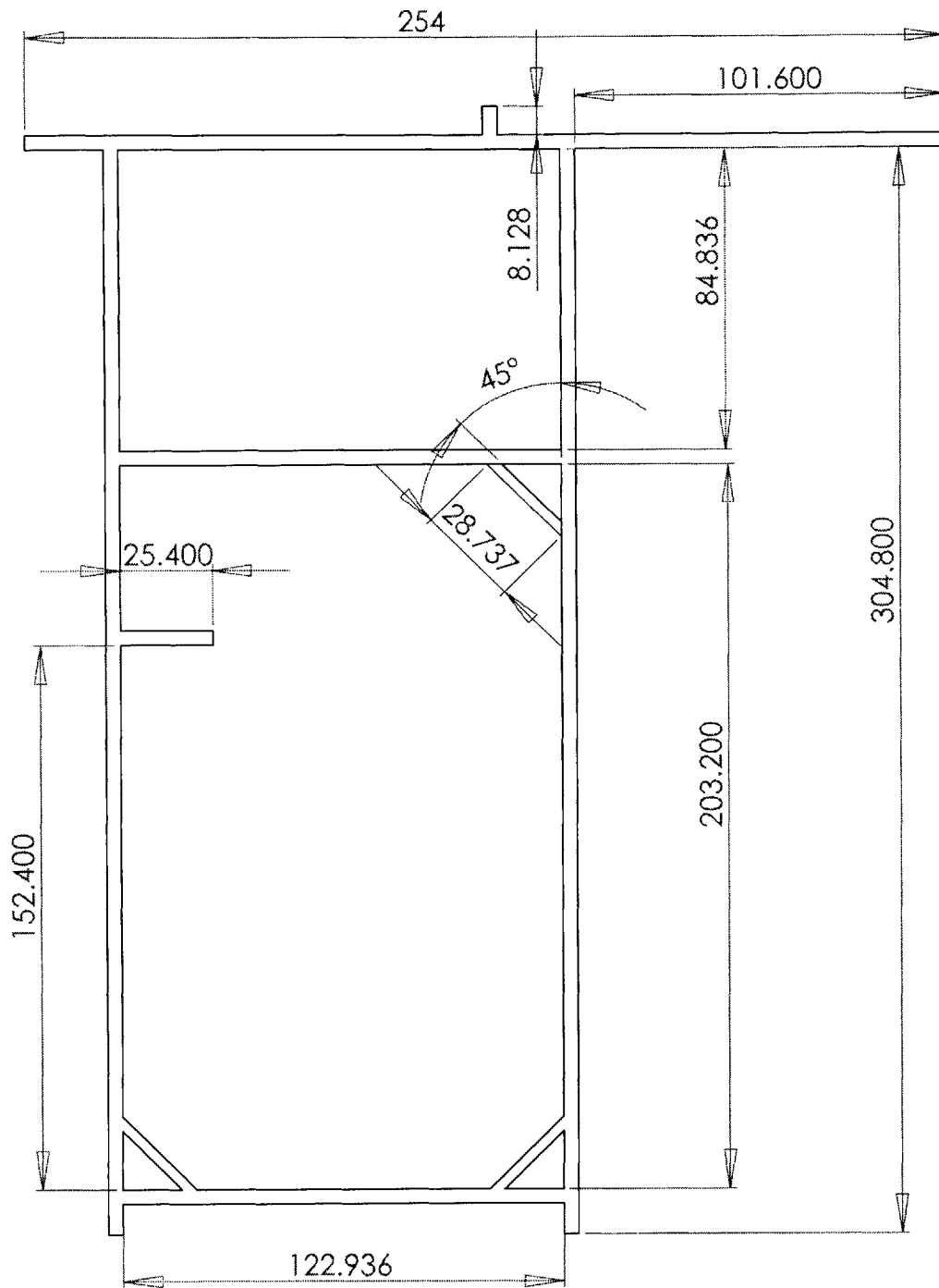
Gas management control panel  
Charging plate





**PROPRIETARY AND CONFIDENTIAL**  
 THE INFORMATION CONTAINED IN THIS DRAWING IS THE SOLE PROPERTY OF MIT DROPLET-BASED MANUFACTURING. ANY REPRODUCTION IN PART OR AS A WHOLE WITHOUT THE WRITTEN PERMISSION OF MIT DROPLET BASED MANUFACTURING IS PROHIBITED.

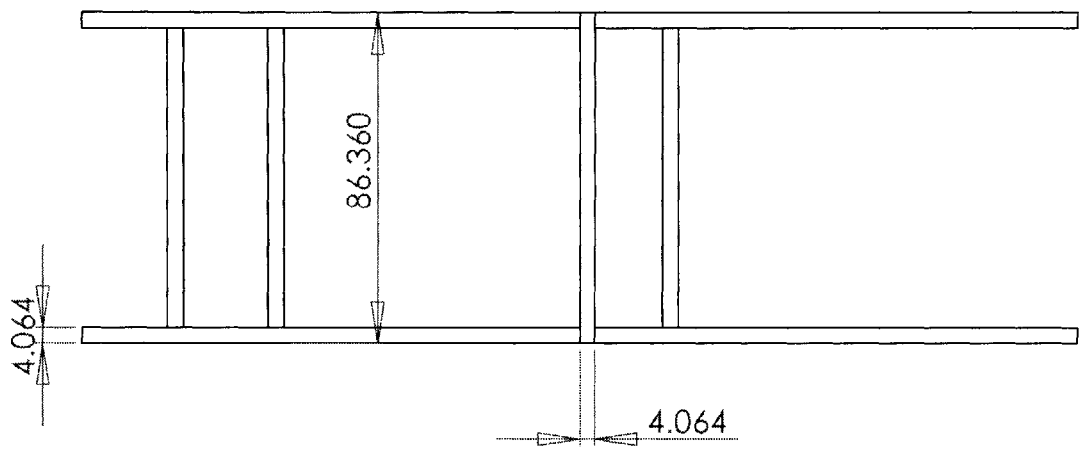
		DIMENSIONS IN CENTIMETERS TOLERANCES: TWO PLACE DECIMAL $\pm 0.005$ THREE PLACE DECIMAL $\pm 0.001$		NAME H. JOUMAA	DATE FALL 2003	MIT DROPLET-BASED MANUFACTURING	
		MATERIAL ALUMINUM		CHECKED		Main frame- isometric view	
		FINISH		ENG APPR.			
		APPLICATION DO NOT SCALE DRAWING		MFG APPR.			
NEXT ASSY	USED ON			Q.A.		REV.	
				COMMENTS: UDS APPARATUS PARTS		SIZE <b>A</b>	DWG. NO. B.1.2.1
						SCALE: 1:50	WEIGHT:
						SHEET 1 OF 3	



**PROPRIETARY AND CONFIDENTIAL**  
 THE INFORMATION CONTAINED IN THIS DRAWING IS THE SOLE PROPERTY OF MIT DROPLET-BASED MANUFACTURING. ANY REPRODUCTION IN PART OR AS A WHOLE WITHOUT THE WRITTEN PERMISSION OF MIT DROPLET BASED MANUFACTURING IS PROHIBITED.

		DIMENSIONS IN CENTIMETERS TOLERANCES: TWO PLACE DECIMAL ±0.005 THREE PLACE DECIMAL ±0.001		DRAWN H. JOUMAA	DATE FALL 2003	MIT DROPLET-BASED MANUFACTURING	
		MATERIAL ALUMINUM		CHECKED		Main frame-side view	
		FINISH		ENG APPR.		UDS APPARATUS PARTS	
NEXT ASSY	USED ON			MFG APPR.		SIZE <b>A</b>	DWG. NO. <b>B.1.2.2</b>
APPLICATION		DO NOT SCALE DRAWING		Q.A.		SCALE:1:50	WEIGHT:
				COMMENTS:			REV.
							SHEET 2 OF 3

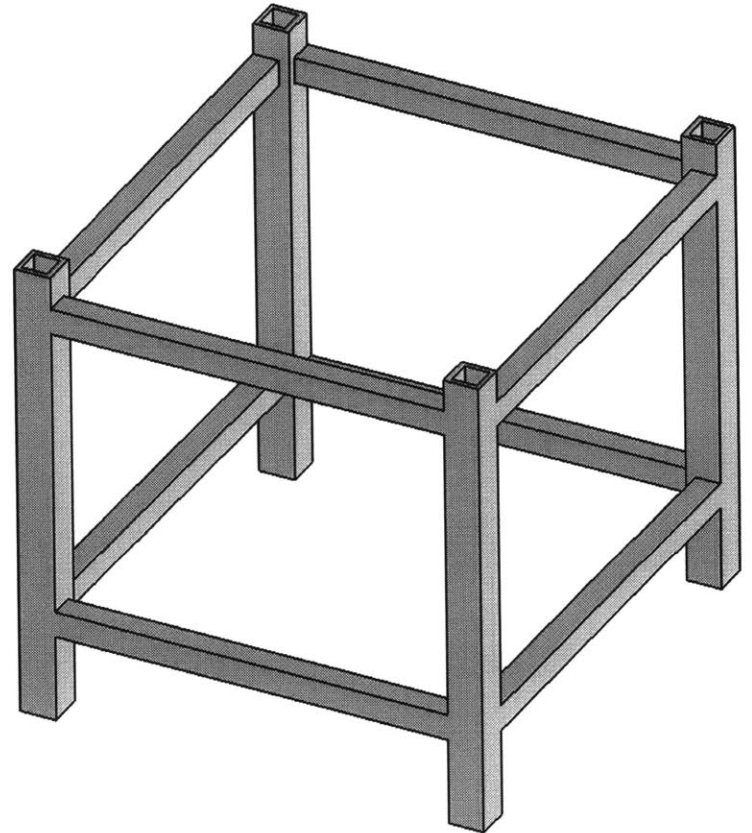
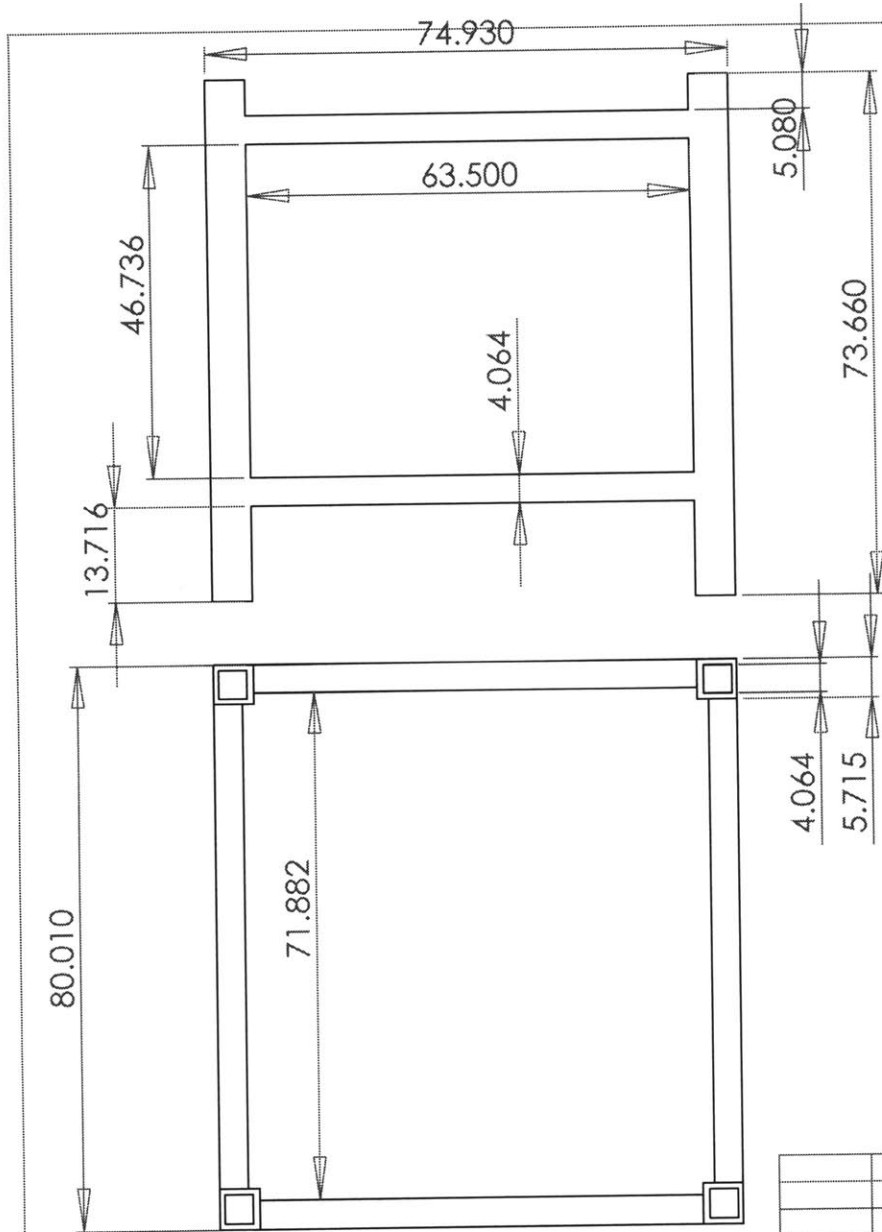




**PROPRIETARY AND CONFIDENTIAL**  
 THE INFORMATION CONTAINED IN THIS DRAWING IS THE SOLE PROPERTY OF MIT DROPLET-BASED MANUFACTURING. ANY REPRODUCTION IN PART OR AS A WHOLE WITHOUT THE WRITTEN PERMISSION OF MIT DROPLET BASED MANUFACTURING IS PROHIBITED.

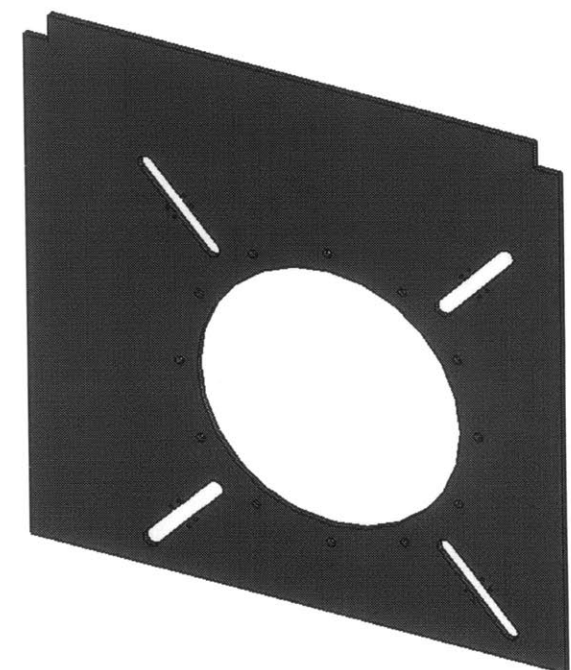
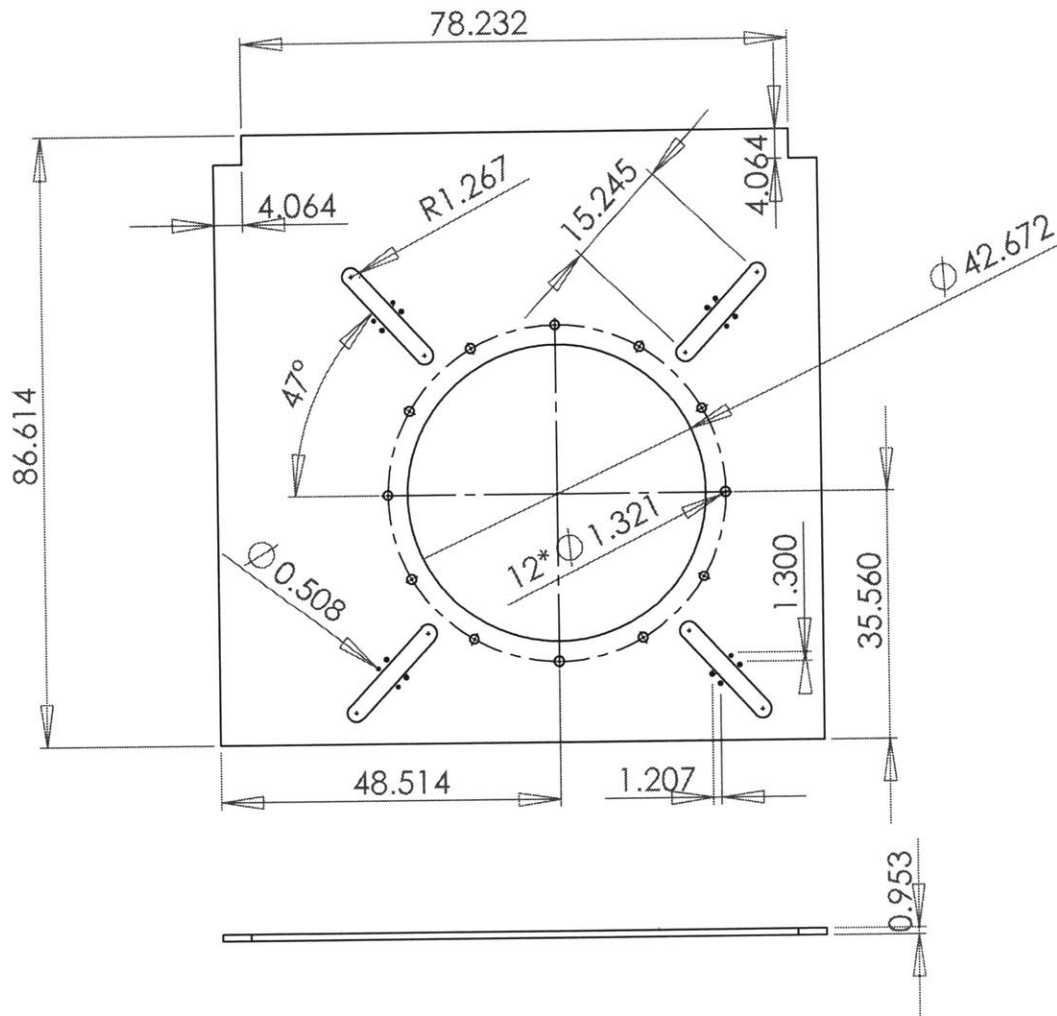
		DIMENSIONS IN CENTIMETERS TOLERANCES: TWO PLACE DECIMAL ±0.005 THREE PLACE DECIMAL ±0.001		DRAWN H. JOUMAA	NAME H. JOUMAA	DATE FALL 2003	MIT DROPLET-BASED MANUFACTURING	
		MATERIAL ALUMINUM		CHECKED			Main frame-Top view	
		FINISH		ENG APPR.				
NEXT ASSY	USED ON			MFG APPR.			UDS APPARATUS PARTS	
APPLICATION		DO NOT SCALE DRAWING		Q.A.				
				COMMENTS:			SIZE <b>A</b>	DWG. NO. B.1.2.3
							SCALE:1:50	WEIGHT:
							SHEET 3 OF 3	

REV.



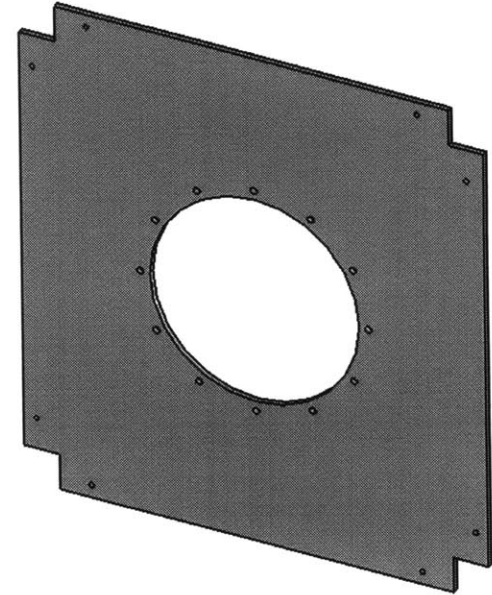
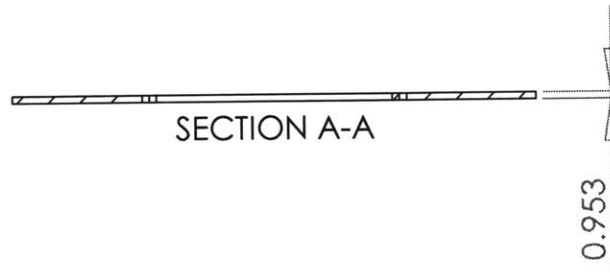
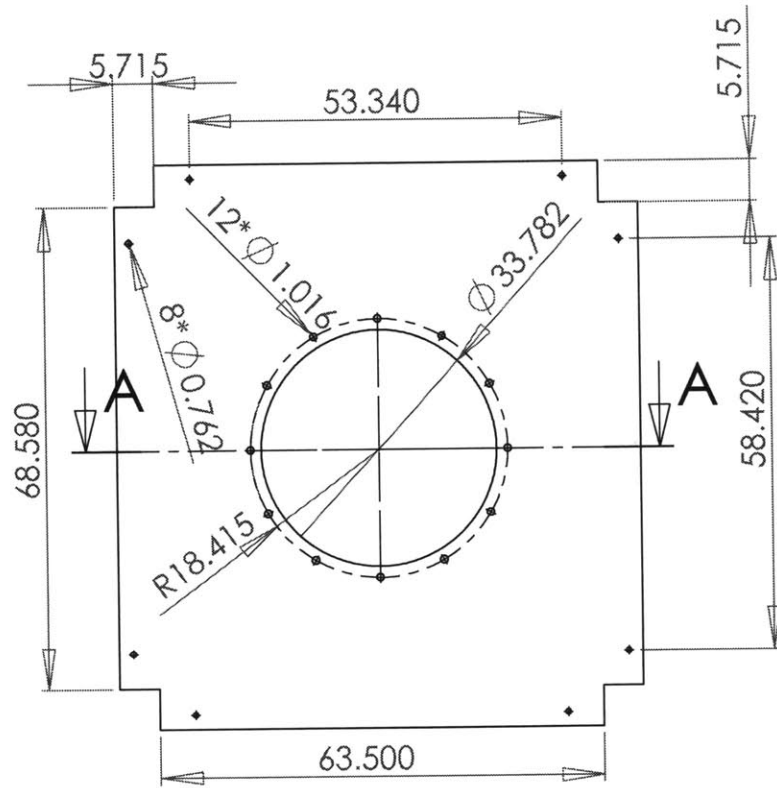
**PROPRIETARY AND CONFIDENTIAL**  
 THE INFORMATION CONTAINED IN THIS DRAWING IS THE SOLE PROPERTY OF MIT DROPLET-BASED MANUFACTURING. ANY REPRODUCTION IN PART OR AS A WHOLE WITHOUT THE WRITTEN PERMISSION OF MIT DROPLET BASED MANUFACTURING IS PROHIBITED.

		DIMENSIONS IN CENTIMETERS		NAME	DATE	MIT DROPLET-BASED MANUFACTURING	
		TOLERANCES:		DRAWN	H. JOUMAA	FALL 2003	Powder chamber frame
		TWO PLACE DECIMAL ±0.005		CHECKED			
		THREE PLACE DECIMAL ±0.001		ENG APPR.			
				MFG APPR.			
		MATERIAL		Q.A.			
		Aluminum		COMMENTS:			
		FINISH		UDS APPARATUS PARTS			
NEXT ASSY	USED ON					SIZE	DWG. NO.
APPLICATION		DO NOT SCALE DRAWING				A	B.1.3
						SCALE: 1:1	WEIGHT:
						SHEET 1 OF 1	



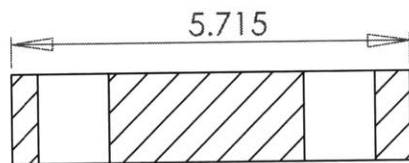
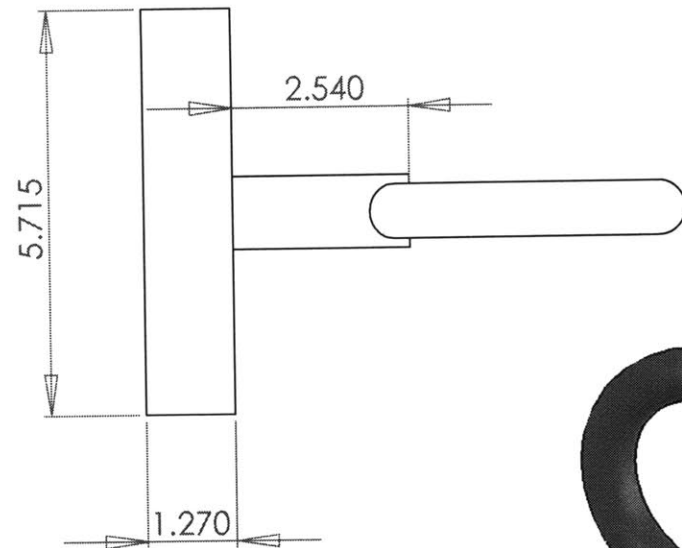
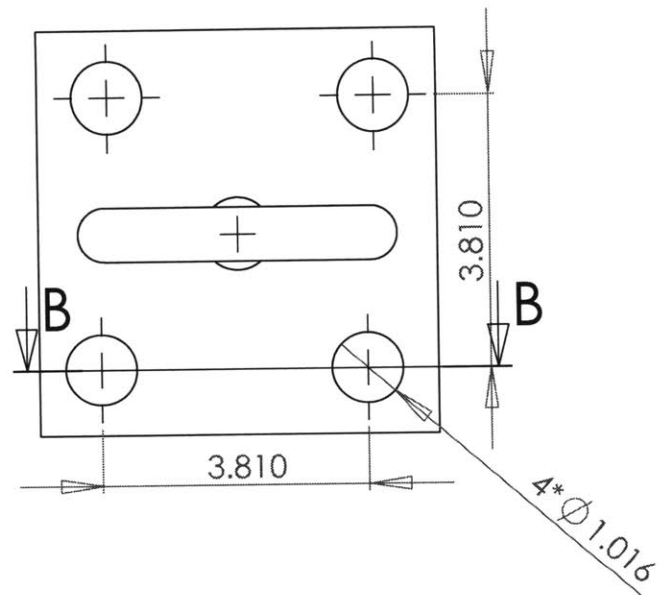
**PROPRIETARY AND CONFIDENTIAL**  
 THE INFORMATION CONTAINED IN THIS DRAWING IS THE SOLE PROPERTY OF MIT DROPLET-BASED MANUFACTURING. ANY REPRODUCTION IN PART OR AS A WHOLE WITHOUT THE WRITTEN PERMISSION OF MIT DROPLET BASED MANUFACTURING IS PROHIBITED.

		DIMENSIONS IN CENTIMETER TOLERANCES: TWO PLACE DECIMAL ± 0.005 THREE PLACE DECIMAL ± 0.001		NAME H. JOUMAA	DATE FALL 2003	MIT DROPLET-BASED MANUFACTURING	
		MATERIAL Aluminum		CHECKED		<h3>Heating chamber supporting plate</h3>	
		FINISH --		ENG APPR.			
NEXT ASSY		USED ON		MFG APPR.			
APPLICATION		DO NOT SCALE DRAWING		Q.A.			
				COMMENTS: UDS APPARATUS PARTS		SIZE A	DWG. NO. B.1.4
						SCALE: 1:1	WEIGHT:
						SHEET 1 OF 1	



**PROPRIETARY AND CONFIDENTIAL**  
 THE INFORMATION CONTAINED IN THIS DRAWING IS THE SOLE PROPERTY OF MIT DROPLET-BASED MANUFACTURING. ANY REPRODUCTION IN PART OR AS A WHOLE WITHOUT THE WRITTEN PERMISSION OF MIT DROPLET-BASED MANUFACTURING IS PROHIBITED.

		DIMENSIONS IN CENTIMETER TOLERANCES: TWO PLACE DECIMAL ± 0.005 THREE PLACE DECIMAL ± 0.001		NAME H. JOUMAA	DATE FALL 2003	MIT DROPLET-BASED MANUFACTURING		
				CHECKED		Powder chamber support plate		
				ENG APPR.				
				MFG APPR.				
				Q.A.				
				COMMENTS: UDS APPARATUS PARTS				
NEXT ASSY	USED ON	MATERIAL Aluminum	FINISH --			SIZE A	DWG. NO. B.1.5	REV.
APPLICATION		DO NOT SCALE DRAWING				SCALE: 1:1	WEIGHT:	SHEET 1 OF 1

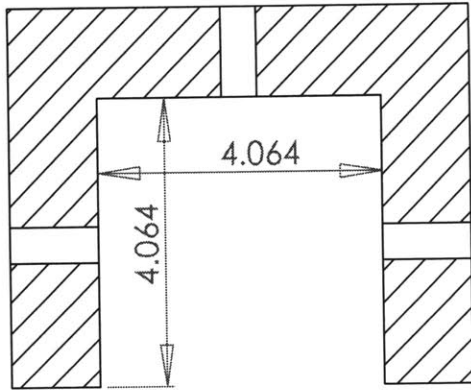


SECTION B-B

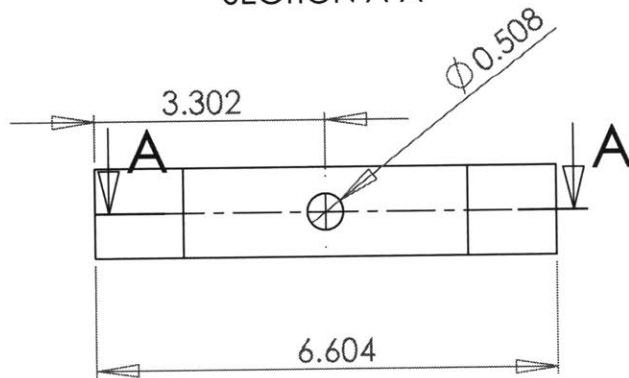
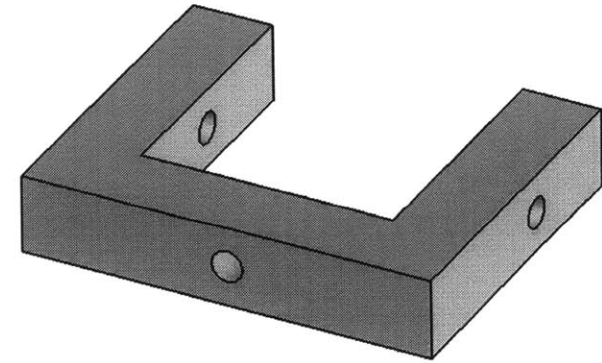
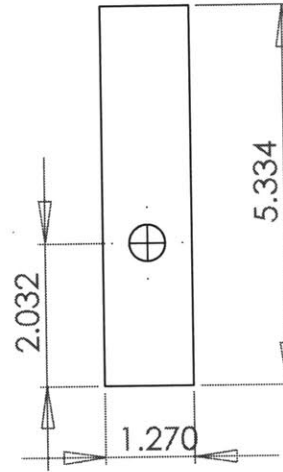


**PROPRIETARY AND CONFIDENTIAL**  
 THE INFORMATION CONTAINED IN THIS DRAWING IS THE SOLE PROPERTY OF MIT DROPLET-BASED MANUFACTURING. ANY REPRODUCTION IN PART OR AS A WHOLE WITHOUT THE WRITTEN PERMISSION OF MIT DROPLET-BASED MANUFACTURING IS PROHIBITED.

		DIMENSIONS IN CENTIMETERS		NAME	DATE	MIT DROPLET-BASED MANUFACTURING	
		TOLERANCES:		DPAWN	H. JOUMAA	FALL 2003	Eyehook assebmly
		TWO PLACE DECIMAL ± 0.005		CHECKED			
		THREE PLACE DECIMAL ± 0.001		ENG APPR.			
				MFG APPR.			
				Q.A.			
		MATERIAL		COMMENTS:			
		Aluminum		UDS APPARATUS PARTS			
NEXT ASSY	USED ON	FINISH				SIZE	DWG. NO.
		--				A	B.1.6
APPLICATION		DO NOT SCALE DRAWING				SCALE: 1:1	WEIGHT:
						SHEET 1 OF 1	

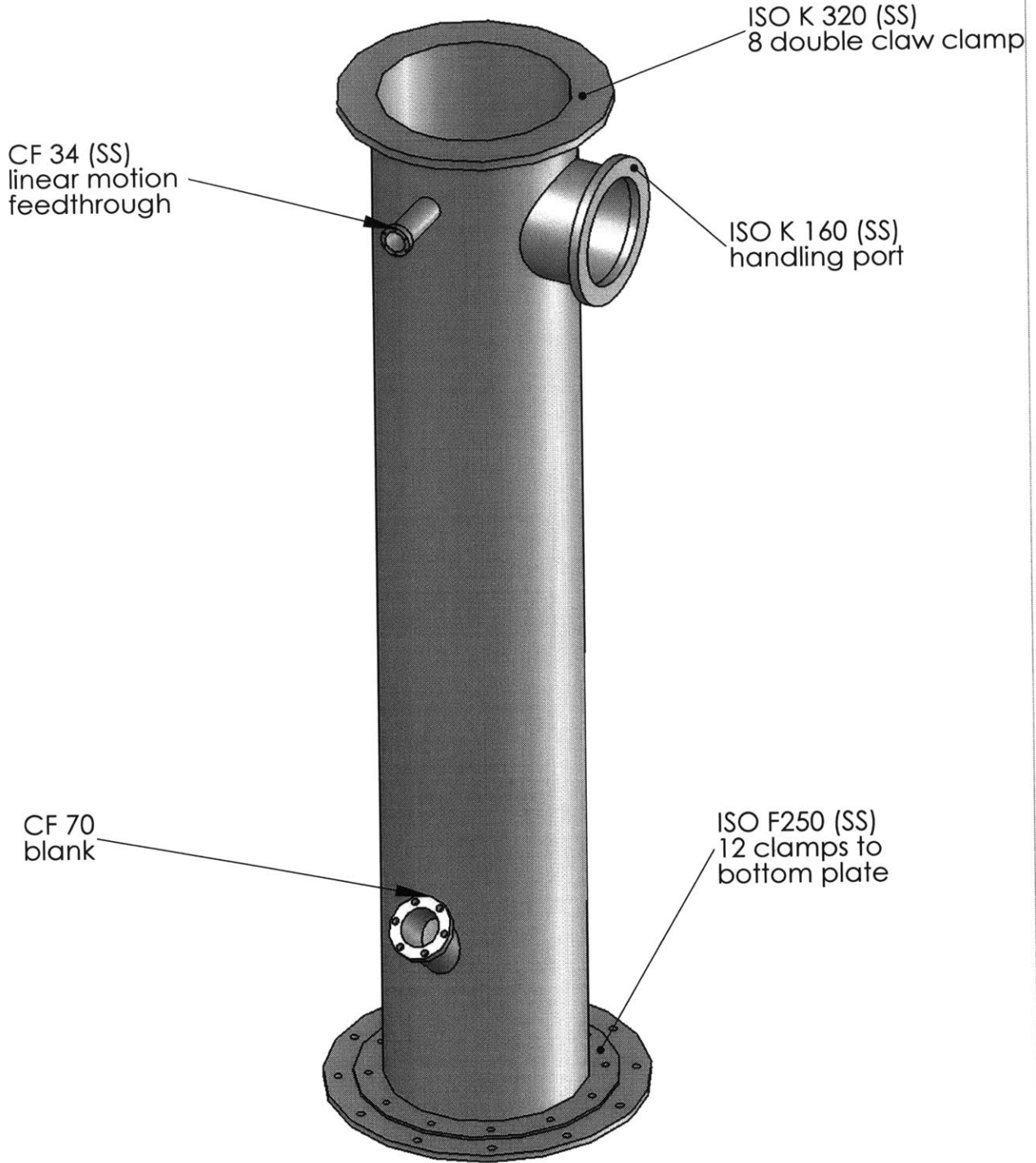


SECTION A-A



**PROPRIETARY AND CONFIDENTIAL**  
 THE INFORMATION CONTAINED IN THIS DRAWING IS THE SOLE PROPERTY OF MIT DROPLET-BASED MANUFACTURING. ANY REPRODUCTION IN PART OR AS A WHOLE WITHOUT THE WRITTEN PERMISSION OF MIT DROPLET BASED MANUFACTURING IS PROHIBITED.

		DIMENSIONS IN CENTIMETER TOLERANCES: TWO PLACE DECIMAL ± 0.005 THREE PLACE DECIMAL ± 0.001		NAME H. JOMAA	DATE FALL 2003	MIT DROPLET-BASED MANUFACTURING	
		MATERIAL Aluminum		CHECKED		Safety stopper	
		FINISH --		ENG APPR.			
NEXT ASSY	USED ON			MFG APPR.		Q.A.	
APPLICATION		DO NOT SCALE DRAWING		COMMENTS: UDS APPARATUS PARTS		SIZE A	DWG. NO. B.1.7
						SCALE: 1:1	WEIGHT:
						REV. SHEET 1 OF 1	

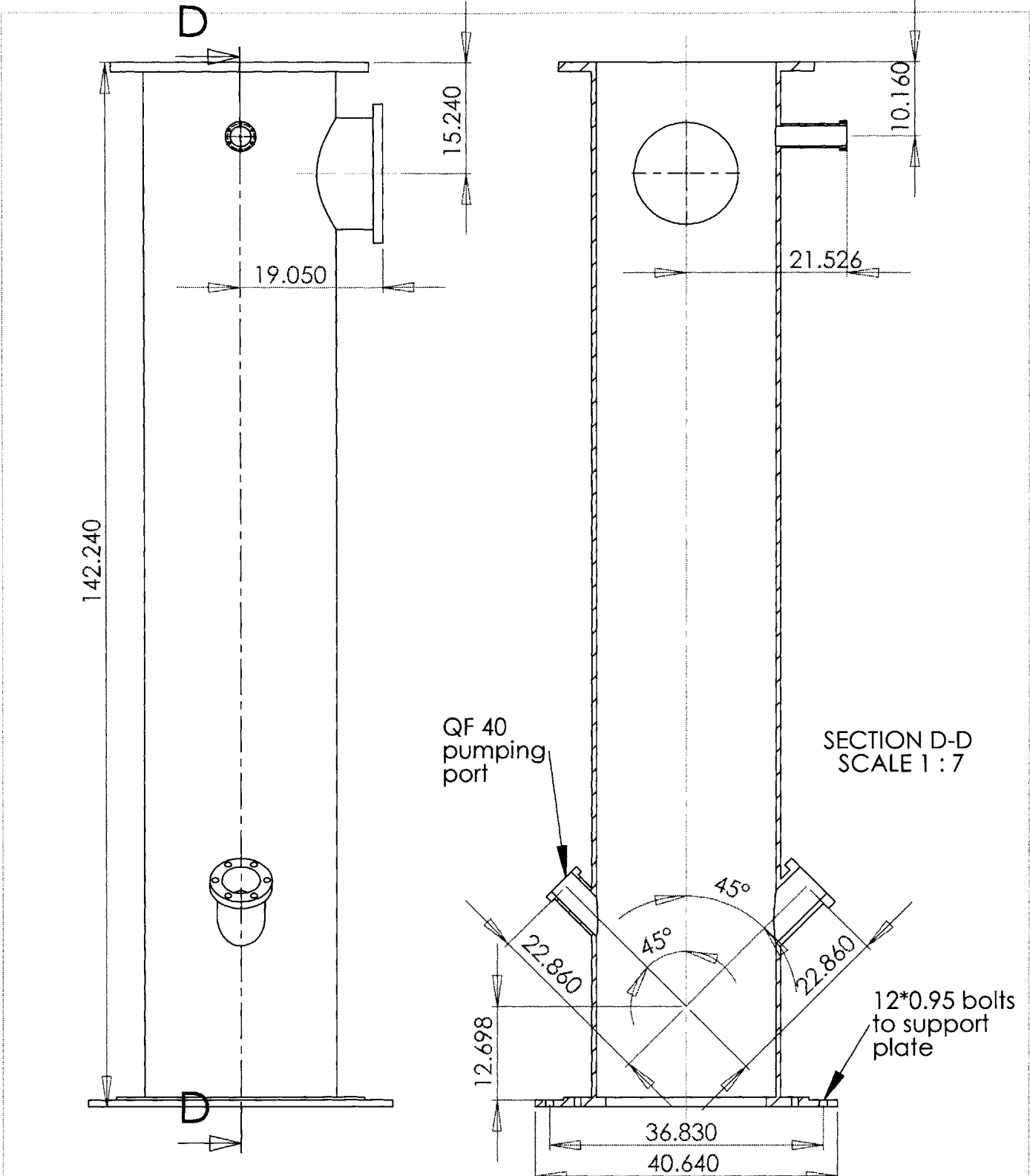


**PROPRIETARY AND CONFIDENTIAL**  
 THE INFORMATION CONTAINED IN THIS  
 DRAWING IS THE SOLE PROPERTY OF  
 MIT DROPLET-BASED MANUFACTURING.  
 ANY REPRODUCTION IN PART OR AS A  
 WHOLE WITHOUT THE WRITTEN  
 PERMISSION OF MIT DROPLET BASED  
 MANUFACTURING IS PROHIBITED.

		MATERIAL	Stainless Steel
		FINISH	
NEXT ASSY	USED ON	APPLICATION	
		DO NOT SCALE DRAWING	

	NAME	DATE
DRAWN	H. JOUMAA	FALL 2003
CHECKED		
ENG APPR.		
MFG APPR.		
Q.A.		
COMMENTS:		
UDS APPARATUS PARTS		

MIT DROPLET-BASED MANUFACTURING			
Powder chamber Isometric View			
SIZE	DWG. NO.	REV.	
A	B.1.8.1		
SCALE:1:1	WEIGHT:	SHEET 1 OF 2	



QF 40  
pumping  
port

SECTION D-D  
SCALE 1 : 7

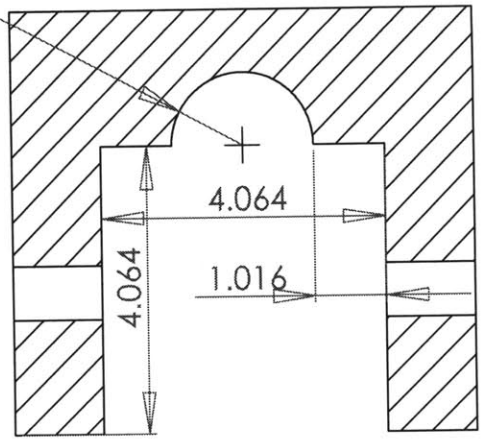
12\*0.95 bolts  
to support  
plate

		DIMENSIONS IN CENIMETERS TOLERANCES: TWO PLACE DECIMAL ±0.005 THREE PLACE DECIMAL ±0.001		NAME H. JOUMAA	DATE FALL 2003	MIT DROPLET-BASED MANUFACTURING	
		MATERIAL Stainless Steel		DRAWN		Powder chamber Side Views	
		FINISH		CHECKED			
NEXT ASSY		USED ON		ENG APPR.			
APPLICATION		DO NOT SCALE DRAWING		MFG APPR.			
				COMMENTS: UDS APPARATUS PARTS		SIZE A	DWG. NO. B.1.8.2
				SCALE:1:1		WEIGHT:	SHEET 2 OF 2

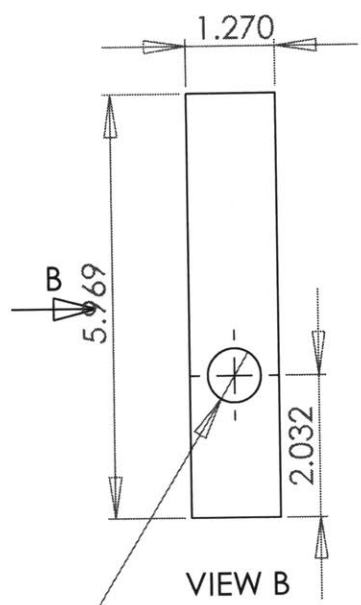
**PROPRIETARY AND CONFIDENTIAL**  
THE INFORMATION CONTAINED IN THIS  
DRAWING IS THE SOLE PROPERTY OF  
MIT DROPLET-BASED MANUFACTURING.  
ANY REPRODUCTION IN PART OR AS A  
WHOLE WITHOUT THE WRITTEN  
PERMISSION OF MIT DROPLET BASED  
MANUFACTURING IS PROHIBITED.



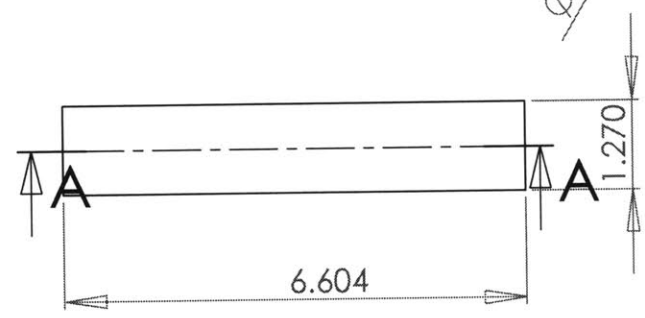
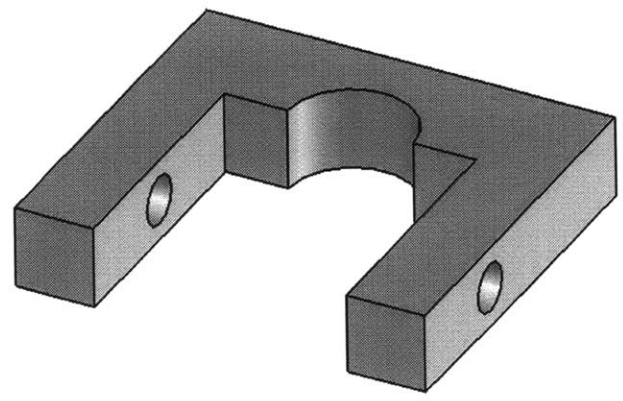
R1.016



SECTION A-A

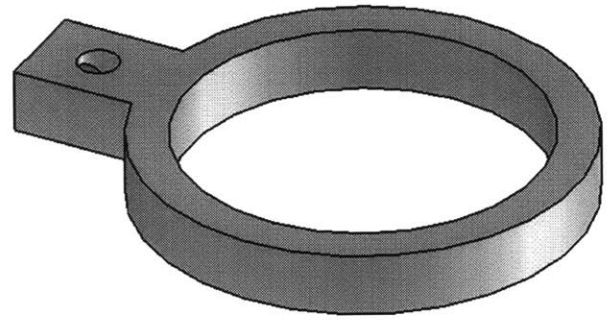
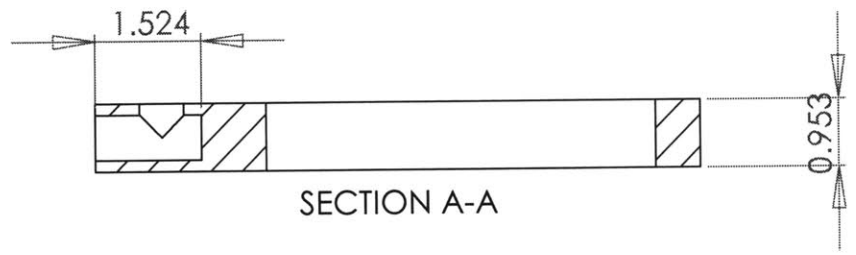
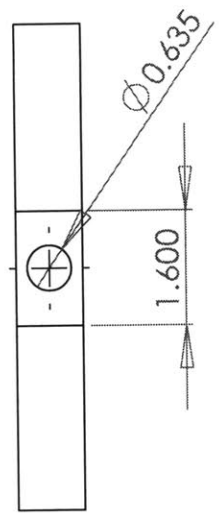
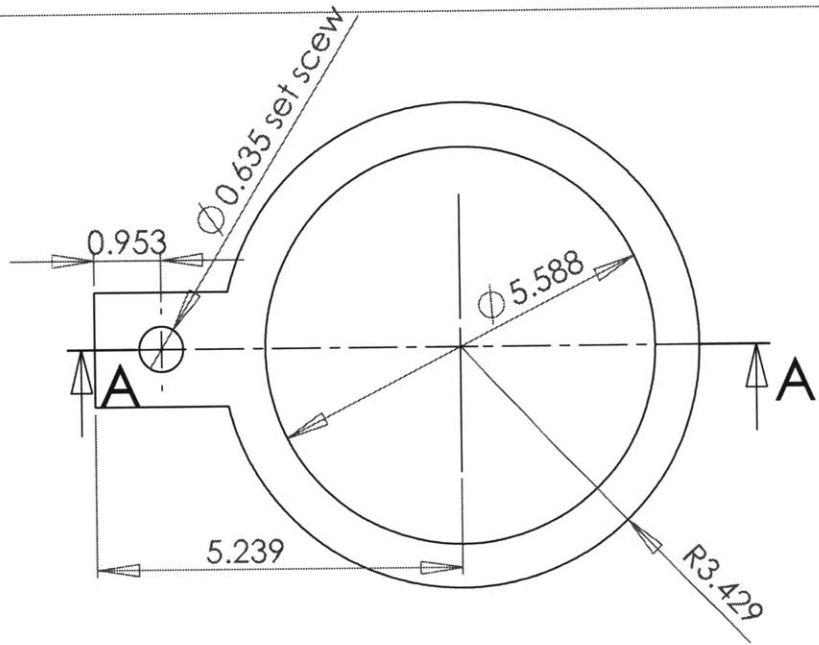


VIEW B



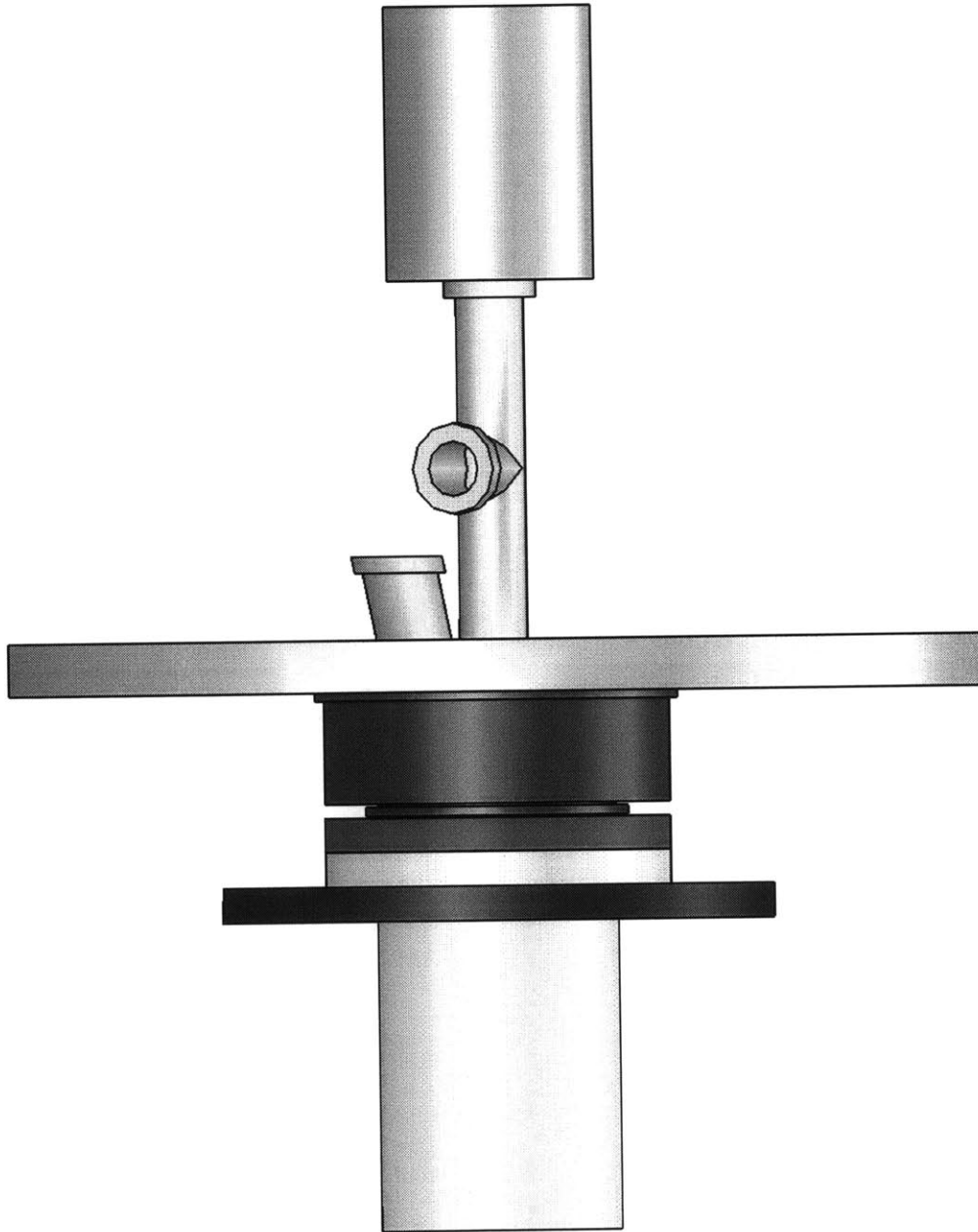
**PROPRIETARY AND CONFIDENTIAL**  
 THE INFORMATION CONTAINED IN THIS DRAWING IS THE SOLE PROPERTY OF MIT DROPLET-BASED MANUFACTURING. ANY REPRODUCTION IN PART OR AS A WHOLE WITHOUT THE WRITTEN PERMISSION OF MIT DROPLET BASED MANUFACTURING IS PROHIBITED.

		DIMENSIONS IN CENTIMETER TOLERANCES: TWO PLACE DECIMAL ± 0.005 THREE PLACE DECIMAL ± 0.001		NAME H. JOUMAA	DATE FALL 2003	MIT DROPLET-BASED MANUFACTURING		
				CHECKED		<b>Rail stopper</b>		
				ENG APPR.				
				MFG APPR.				
				Q.A.				
		MATERIAL Aluminum		COMMENTS: UDS APPARATUS PARTS		SIZE A	DWG. NO. B.1.9	REV.
NEXT ASSY	USED ON	FINISH --				SCALE: 1:1	WEIGHT:	SHEET 1 OF 1
APPLICATION		DO NOT SCALE DRAWING						



**PROPRIETARY AND CONFIDENTIAL**  
 THE INFORMATION CONTAINED IN THIS DRAWING IS THE SOLE PROPERTY OF MIT DROPLET-BASED MANUFACTURING. ANY REPRODUCTION IN PART OR AS A WHOLE WITHOUT THE WRITTEN PERMISSION OF MIT DROPLET BASED MANUFACTURING IS PROHIBITED.

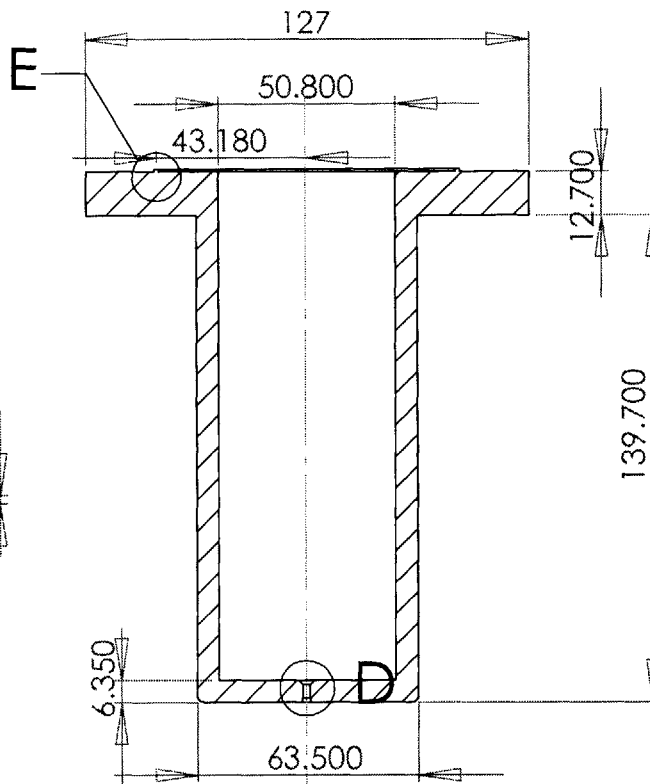
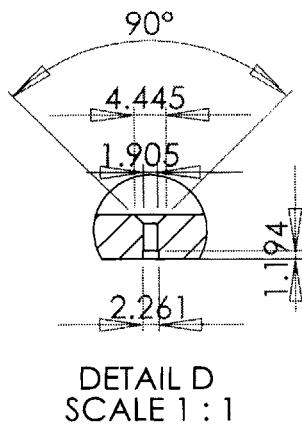
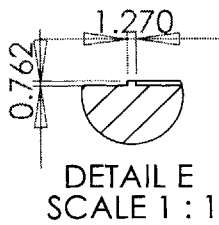
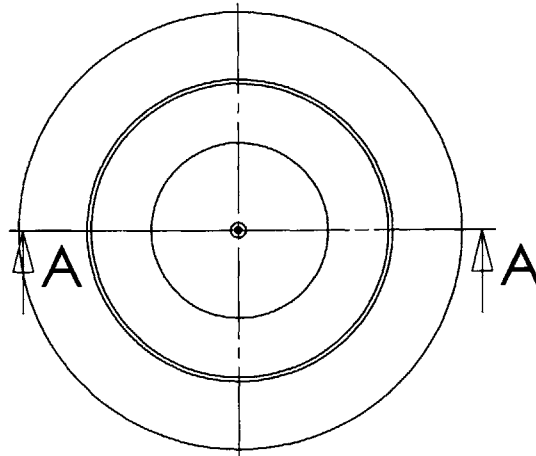
		DIMENSIONS IN CENTIMETER TOLERANCES: TWO PLACE DECIMAL $\pm 0.005$ THREE PLACE DECIMAL $\pm 0.001$		NAME H. JOUMAA	DATE FALL 2003	MIT DROPLET-BASED MANUFACTURING	
		MATERIAL Aluminum		CHECKED		Waste cup fixture	
		FINISH --		ENG APPR.			
NEXT ASSY	USED ON	COMMENTS: UDS APPARATUS PARTS		MFG APPR.			
APPLICATION DO NOT SCALE DRAWING		Q.A.					
		SIZE A	DWG. NO. B.1.10	SCALE: 1:1		WEIGHT:	REV. SHEET 1 OF 1



**PROPRIETARY AND CONFIDENTIAL**  
 THE INFORMATION CONTAINED IN THIS  
 DRAWING IS THE SOLE PROPERTY OF  
 MIT DROPLET-BASED MANUFACTURING.  
 ANY REPRODUCTION IN PART OR AS A  
 WHOLE WITHOUT THE WRITTEN  
 PERMISSION OF MIT DROPLET BASED  
 MANUFACTURING IS PROHIBITED.

				DRAWN	H. JOUMAA	DATE	FALL 2003
				CHECKED			
				ENG APPR.			
				MFG APPR.			
				Q.A.			
				COMMENTS:	UDS APPARATUS PARTS		
NEXT ASSY	USED ON	MATERIAL	FINISH				
APPLICATION		DO NOT SCALE DRAWING					

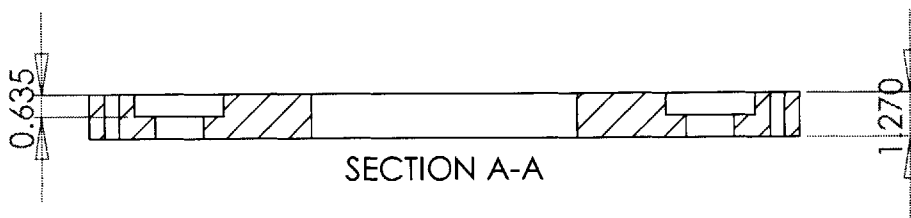
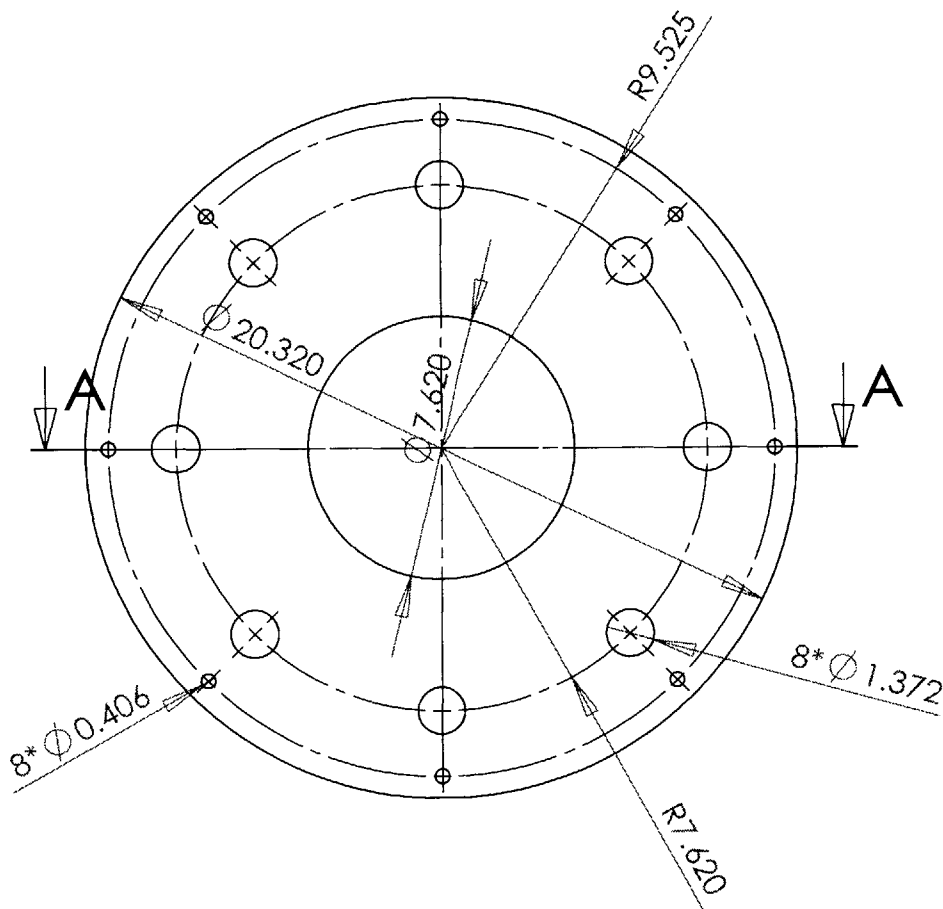
MIT DROPLET-BASED MANUFACTURING			
Top plate assembly			
SIZE	DWG. NO.	REV.	
<b>A</b>	<b>B.2.1</b>		
SCALE:1:1	WEIGHT:	SHEET 1 OF 1	



SECTION A-A

**PROPRIETARY AND CONFIDENTIAL**  
 THE INFORMATION CONTAINED IN THIS DRAWING IS THE SOLE PROPERTY OF MIT DROPLET-BASED MANUFACTURING. ANY REPRODUCTION IN PART OR AS A WHOLE WITHOUT THE WRITTEN PERMISSION OF MIT DROPLET BASED MANUFACTURING IS PROHIBITED.

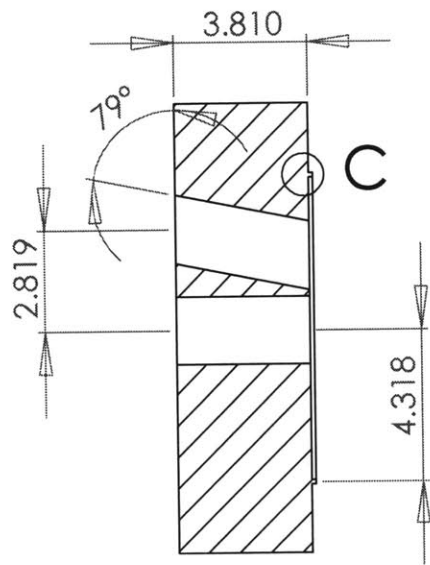
		DIMENSIONS IN MILLIMETERS TOLERANCES: TWO PLACE DECIMAL ±0.005 THREE PLACE DECIMAL ±0.001		NAME H. JOUMAA	DATE FALL 2003	MIT DROPLET-BASED MANUFACTURING	
		MATERIAL <b>Graphite</b>		DRAWN		Crucible	
		FINISH		CHECKED			
NEXT ASSY	USED ON			ENG APPR.		UDS APPARATUS PARTS	
APPLICATION	DO NOT SCALE DRAWING			MFG APPR.			
				Q.A.		SIZE <b>A</b>	DWG. NO. <b>B.2.2</b>
				COMMENTS:		SCALE:1:2	WEIGHT:
						SHEET 1 OF 1	



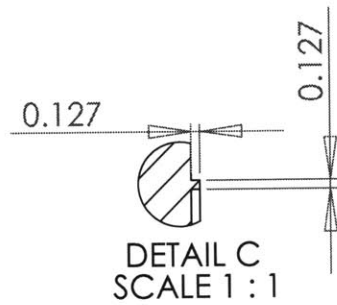
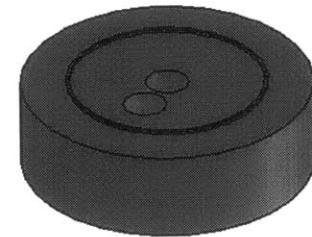
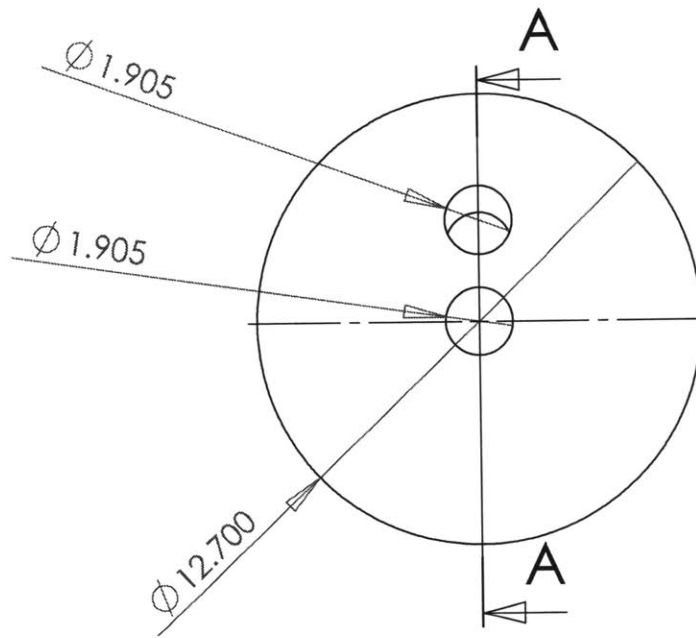
**PROPRIETARY AND CONFIDENTIAL**  
 THE INFORMATION CONTAINED IN THIS DRAWING IS THE SOLE PROPERTY OF MIT DROPLET-BASED MANUFACTURING. ANY REPRODUCTION IN PART OR AS A WHOLE WITHOUT THE WRITTEN PERMISSION OF MIT DROPLET BASED MANUFACTURING IS PROHIBITED.

		DIMENSIONS IN CENTIMETER TOLERANCES: TWO PLACE DECIMAL ±0.005 THREE PLACE DECIMAL ±0.001		NAME H. JOUMAA	DATE FALL 2003	MIT DROPLET-BASED MANUFACTURING	
		MATERIAL <b>Aluminum</b>		DRAWN		<b>Crucible support ring</b>	
		FINISH		CHECKED			
NEXT ASSY		USED ON		ENG APPR.			
APPLICATION		DO NOT SCALE DRAWING		MFG APPR.			
				Q.A.		UDS APPARATUS PARTS	
				COMMENTS:		SIZE <b>A</b>	DWG. NO. <b>B.2.3</b>
						SCALE:1:2	WEIGHT:
						SHEET 1 OF 1	

REV.

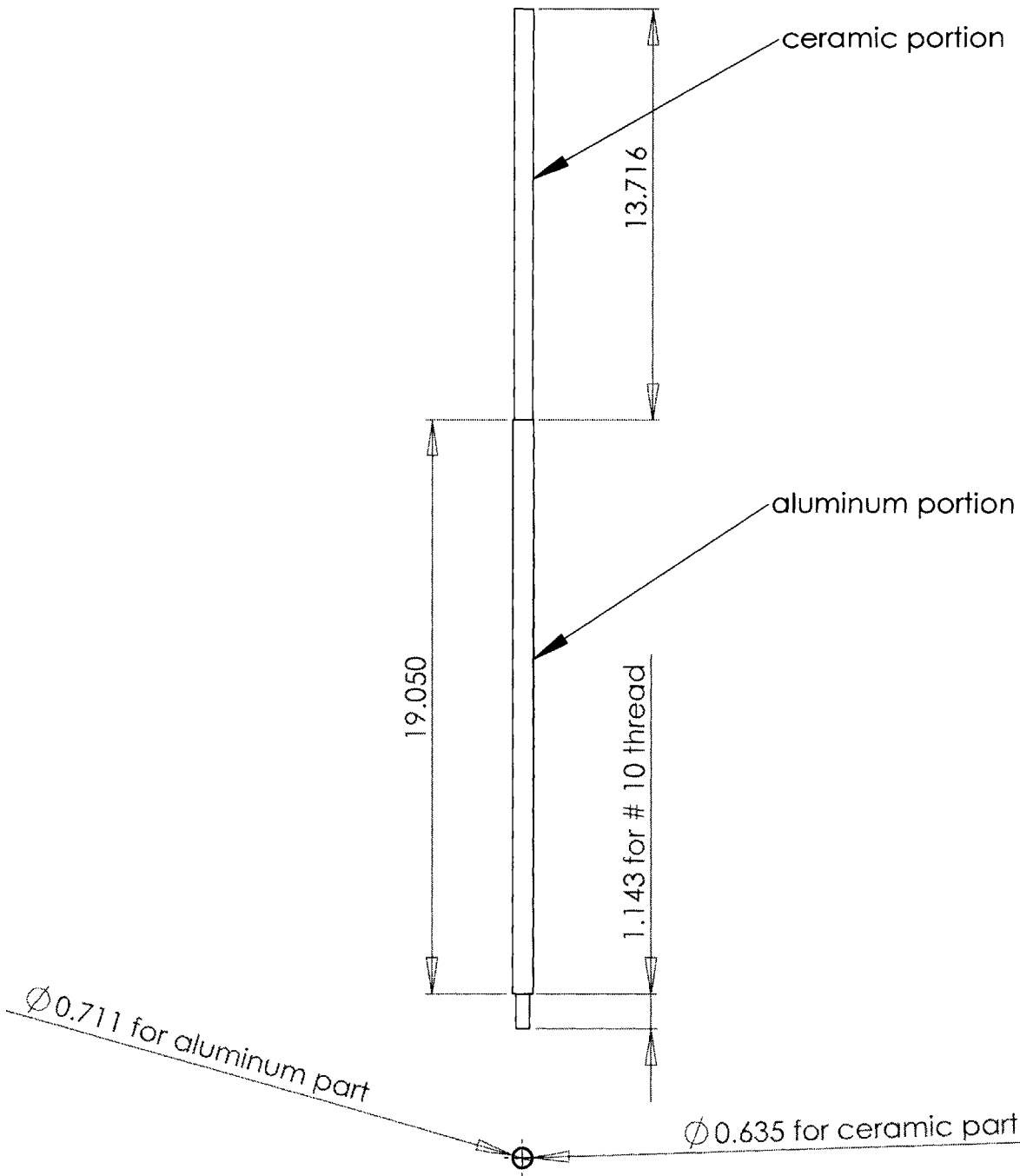


SECTION A-A



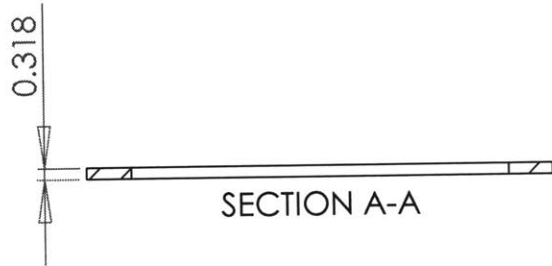
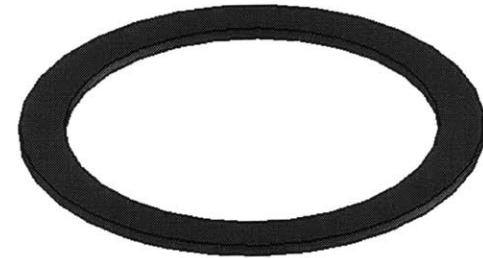
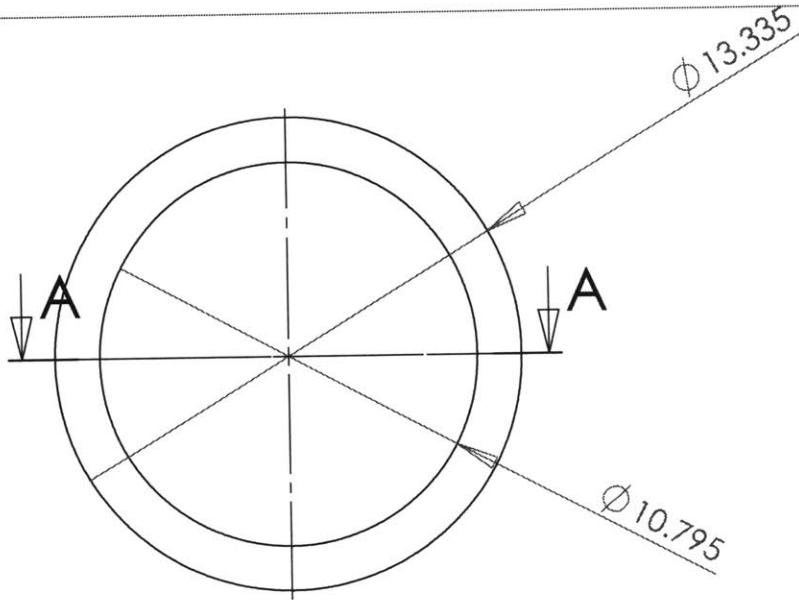
**PROPRIETARY AND CONFIDENTIAL**  
 THE INFORMATION CONTAINED IN THIS DRAWING IS THE SOLE PROPERTY OF MIT DROPLET-BASED MANUFACTURING. ANY REPRODUCTION IN PART OR AS A WHOLE WITHOUT THE WRITTEN PERMISSION OF MIT DROPLET BASED MANUFACTURING IS PROHIBITED.

		DIMENSIONS IN CENTIMETER		NAME	DATE	MIT DROPLET-BASED MANUFACTURING	
		TOLERANCES:		DRAWN	H. JOUMAA	FALL 2003	Insulation block
		TWO PLACE DECIMAL ± 0.005		CHECKED			
		THREE PLACE DECIMAL ± 0.001		ENG APPR.			
				MFG APPR			
				Q.A.			
		MATERIAL		COMMENTS:		SIZE	REV.
		Alumina Silicate		UDS APPARATUS PARTS		A	B.2.4
NEXT ASSY	USED ON	FINISH				SCALE: 1:1	WEIGHT:
APPLICATION		DO NOT SCALE DRAWING				SHEET 1 OF 1	



**PROPRIETARY AND CONFIDENTIAL**  
 THE INFORMATION CONTAINED IN THIS DRAWING IS THE SOLE PROPERTY OF MIT DROPLET-BASED MANUFACTURING. ANY REPRODUCTION IN PART OR AS A WHOLE WITHOUT THE WRITTEN PERMISSION OF MIT DROPLET BASED MANUFACTURING IS PROHIBITED.

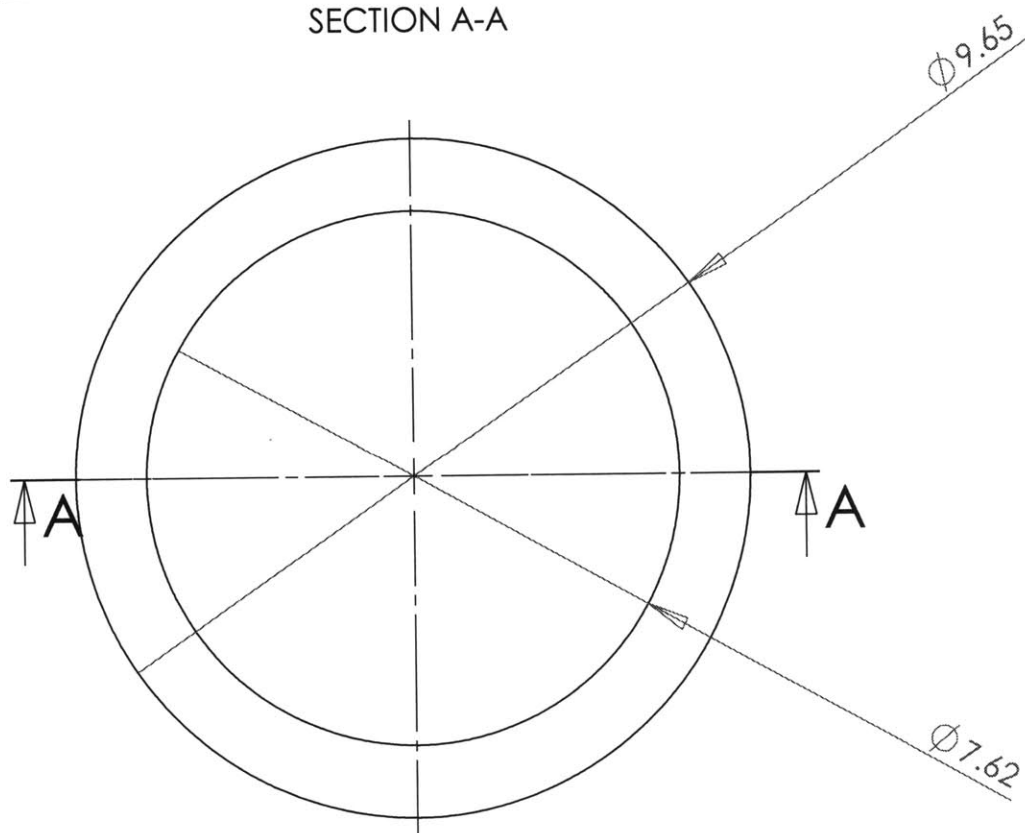
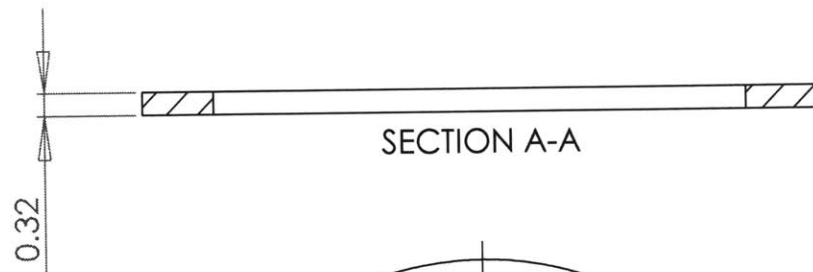
		DIMENSIONS IN CENTIMETER TOLERANCES: TWO PLACE DECIMAL ± 0.005 THREE PLACE DECIMAL ± 0.001		NAME H. JOUMAA	DATE FALL 2003	MIT DROPLET-BASED MANUFACTURING		
		MATERIAL Aluminum + Boron Nitride		CHECKED		vibration rod		
		FINISH		ENG APPR.				
		COMMENTS: UDS APPARATUS PARTS		MFG APPR.				
NEXT ASSY	USED ON			Q.A.		SIZE <b>A</b>	DWG. NO. <b>B.2.5</b>	REV.
APPLICATION		DO NOT SCALE DRAWING				SCALE:1:1	WEIGHT:	SHEET 1 OF 1



**PROPRIETARY AND CONFIDENTIAL**  
 THE INFORMATION CONTAINED IN THIS DRAWING IS THE SOLE PROPERTY OF MIT DROPLET-BASED MANUFACTURING. ANY REPRODUCTION IN PART OR AS A WHOLE WITHOUT THE WRITTEN PERMISSION OF MIT DROPLET-BASED MANUFACTURING IS PROHIBITED.

		DIMENSIONS IN CENTIMETERS		NAME	DATE	MIT DROPLET-BASED MANUFACTURING	
		TOLERANCES:		DRAWN	H. JOUMAA	FALL 2003	Upper gasket
		TWO PLACE DECIMAL $\pm 0.005$		CHECKED:			
		THREE PLACE DECIMAL $\pm 0.001$		ENG APPR.			
				MFG APPR			
				Q.A.			
NEXT ASSY	USED ON	MATERIAL	GRAFOIL-FLEXIBLE GRAPHITE	COMMENTS:		UDS APPARATUS PARTS	
		FINISH	--	SIZE	DWG. NO.	REV.	
APPLICATION	DO NOT SCALE DRAWING			A	B.2.6		
		SCALE: 1:1	WEIGHT:	SHEET 1 OF 1			

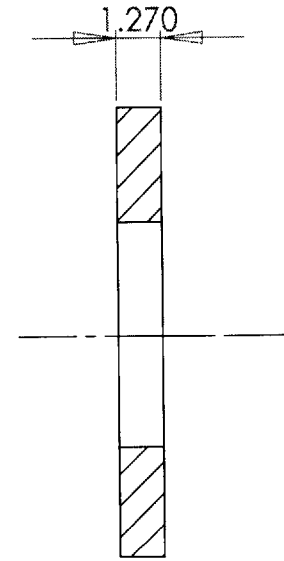
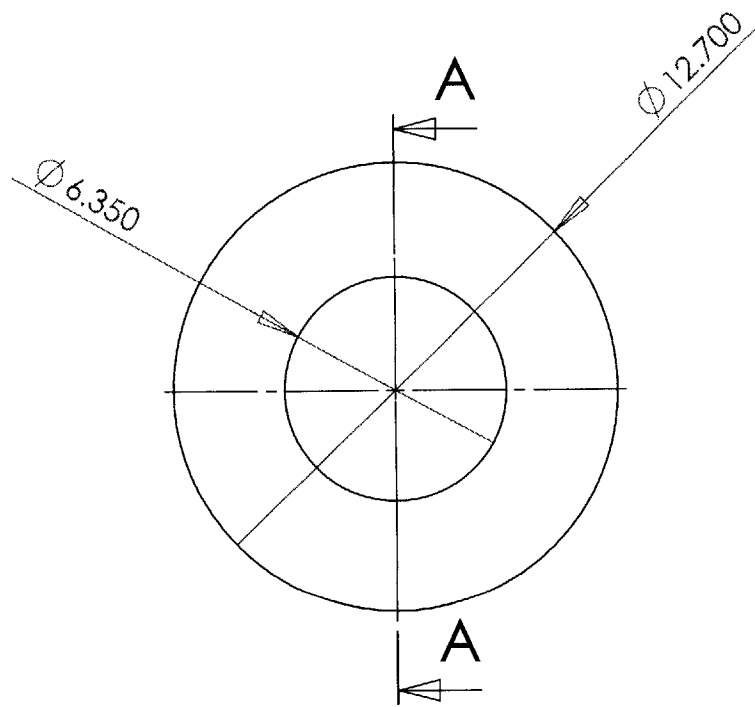




**PROPRIETARY AND CONFIDENTIAL**  
 THE INFORMATION CONTAINED IN THIS DRAWING IS THE SOLE PROPERTY OF MIT DROPLET-BASED MANUFACTURING. ANY REPRODUCTION IN PART OR AS A WHOLE WITHOUT THE WRITTEN PERMISSION OF MIT DROPLET BASED MANUFACTURING IS PROHIBITED.

		DIMENSIONS IN CENTIMETERS TOLERANCES: TWO PLACE DECIMAL ± 0.005 THREE PLACE DECIMAL ± 0.001	NAME H. JOUMAA	DATE FALL 2003	MIT DROPLET-BASED MANUFACTURING
			CHECKED		Lower gasket
			ENIG APPR.		
			MFG APPR.		
			Q.A.		
NEXT ASSY	USED ON	MATERIAL Grafoil-flexible graphite	COMMENTS: UDS APPARATUS PARTS		SIZE A
APPLICATION	DO NOT SCALE DRAWING	FINISH --			DWG. NO. B.2.7
			SCALE: 1:1	WEIGHT:	REV. SHEET 1 OF 1

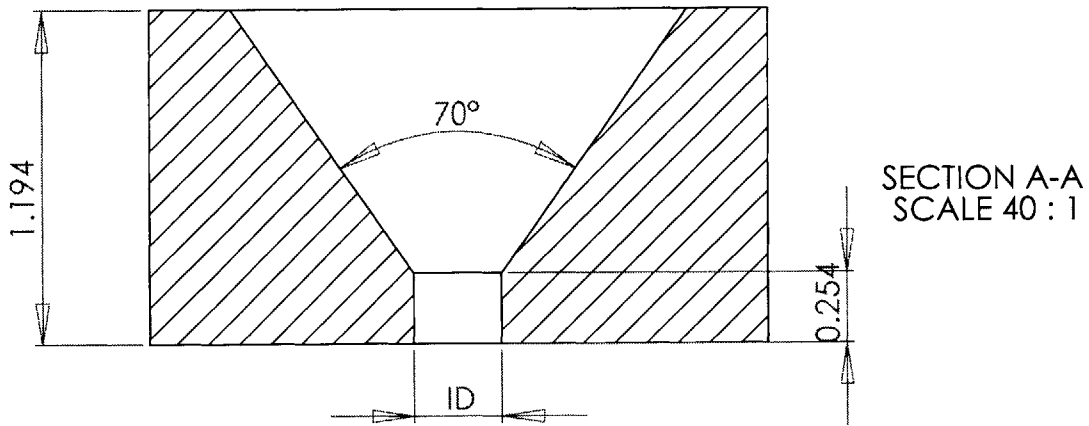
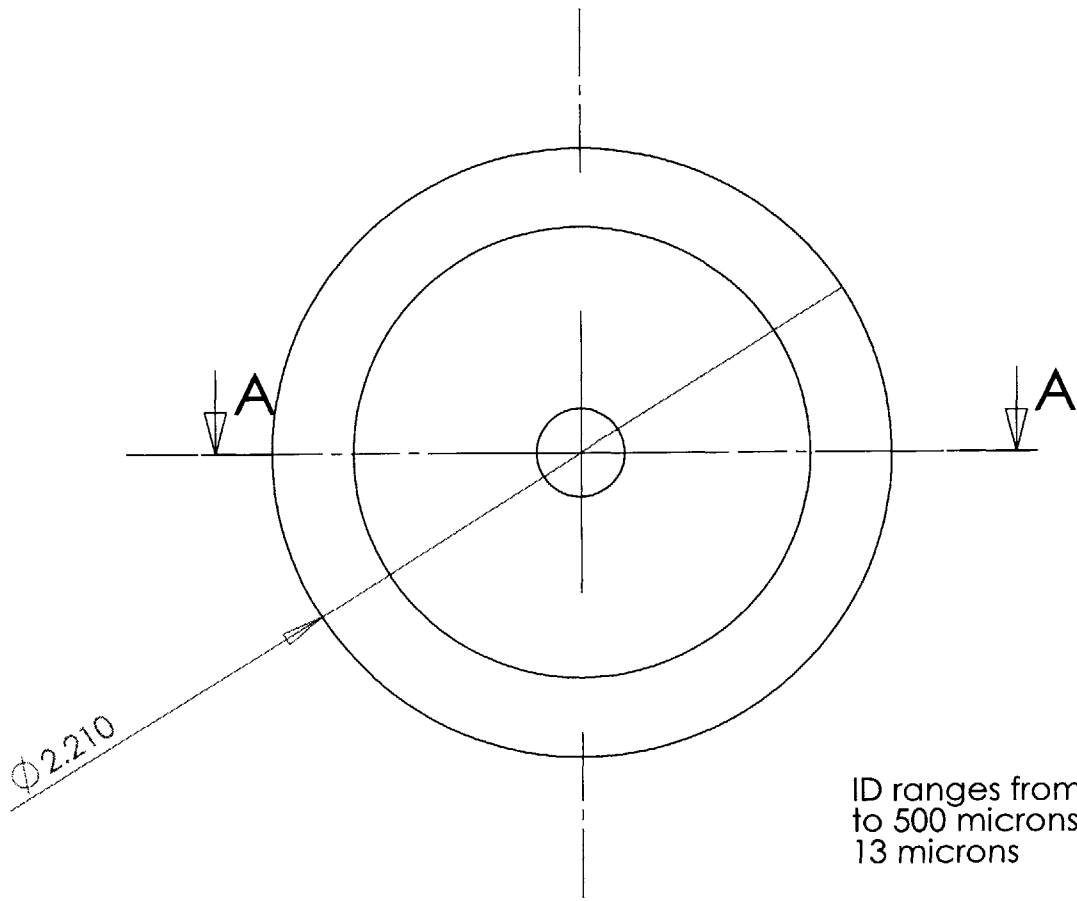




SECTION A-A

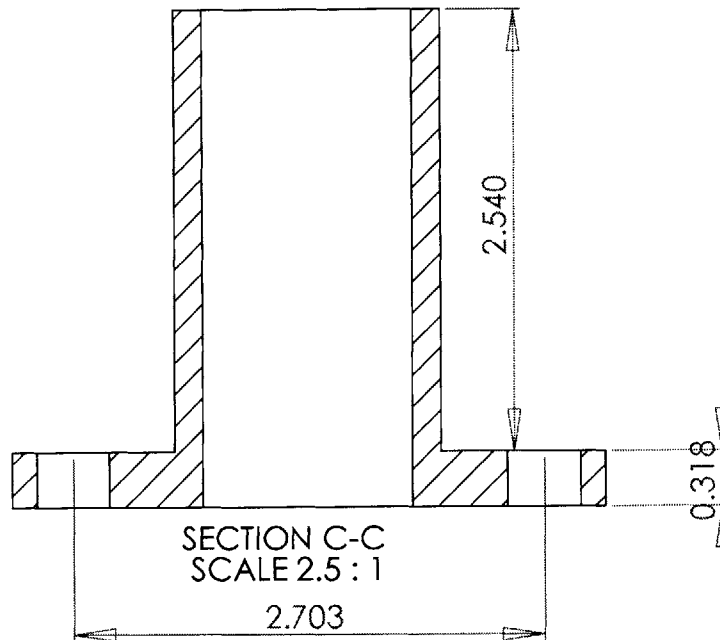
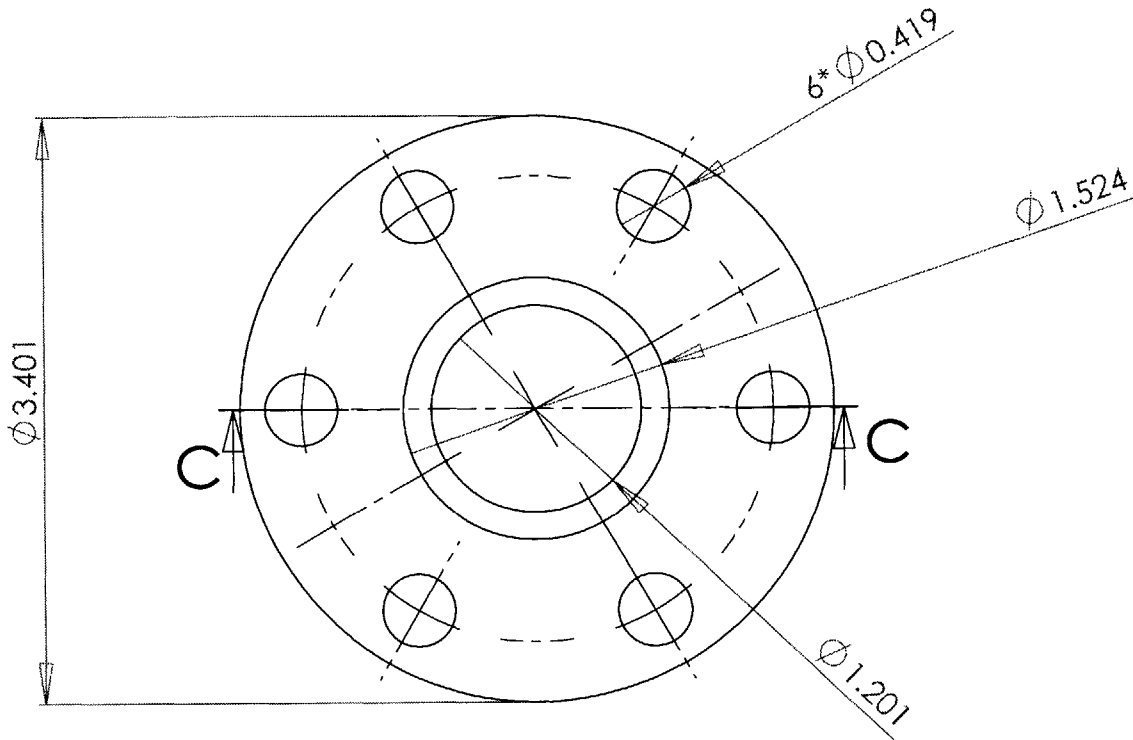
**PROPRIETARY AND CONFIDENTIAL**  
 THE INFORMATION CONTAINED IN THIS DRAWING IS THE SOLE PROPERTY OF MIT DROPLET-BASED MANUFACTURING. ANY REPRODUCTION IN PART OR AS A WHOLE WITHOUT THE WRITTEN PERMISSION OF MIT DROPLET BASED MANUFACTURING IS PROHIBITED.

		DIMENSIONS IN CENTIMETERS		NAME	DATE	MIT DROPLET-BASED MANUFACTURING	
		TOLERANCES:		DRAWN	H. JOUAAA	FALL 2003	Insulation ring
		TWO PLACE DECIMAL ±0.005		CHECKED:			
		THREE PLACE DECIMAL ±0.001		ENG APPR:			
				MFG APPR:			
		MATERIAL		Q.C.			
		ALUMINA-SILICA FIBERS		COMMENTS:			
NEXT ASSY	USED ON	FINISH --		UDS APPARATUS PARTS			
APPLICATION		DO NOT SCALE DRAWING		SIZE	DWG. NO.		REV.
				A	B.2.9		
				SCALE: IN	WEIGHT:		SHEET 1 OF 1



**PROPRIETARY AND CONFIDENTIAL**  
 THE INFORMATION CONTAINED IN THIS DRAWING IS THE SOLE PROPERTY OF MIT DROPLET-BASED MANUFACTURING. ANY REPRODUCTION IN PART OR AS A WHOLE WITHOUT THE WRITTEN PERMISSION OF MIT DROPLET BASED MANUFACTURING IS PROHIBITED.

		DIMENSIONS IN MILLIMETERS TOLERANCES: TWO PLACE DECIMAL $\pm 0.005$ THREE PLACE DECIMAL $\pm 0.001$		NAME H. JOUMAA	DATE FALL 2003	MIT DROPLET-BASED MANUFACTURING	
		MATERIAL SAPPHIRE	FINISH	COMMENTS: UDS APPARATUS PARTS		Orifice	
NEXT ASSY	USED ON	APPLICATION DO NOT SCALE DRAWING		SIZE <b>A</b>	DWG. NO. <b>B.2.10</b>	REV.	
				SCALE: 1:1	WEIGHT:	SHEET 1 OF 1	



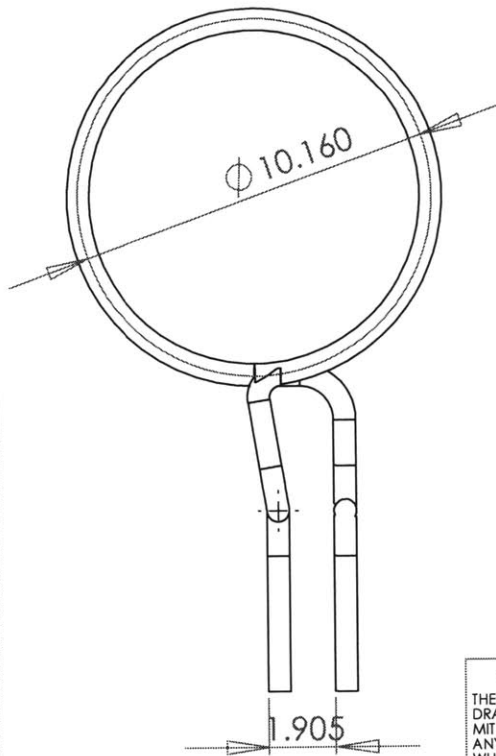
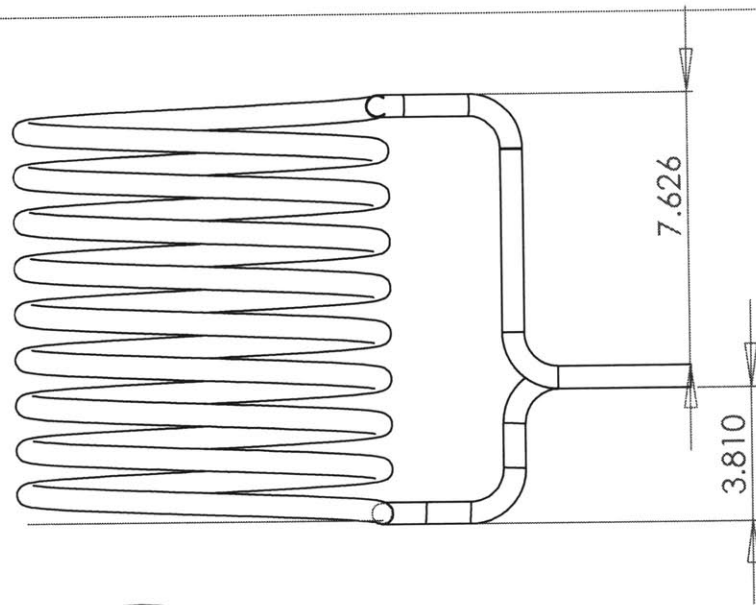
		DIMENSIONS IN CENTIMETERS TOLERANCES: TWO PLACE DECIMAL $\pm 0.005$ THREE PLACE DECIMAL $\pm 0.001$		NAME H. JOUMAA	DATE FALL 2003	MIT DROPLET-BASED MANUFACTURING	
		MATERIAL ALUMINUM		CHECKED		Pyrometer fixture	
		FINISH		ENG APPR.			
NEXT ASSY	USED ON			MFG APPR.			
APPLICATION		DO NOT SCALE DRAWING		Q.A.			
				COMMENTS: UDS APPARATUS PARTS		SIZE A	DWG. NO. B.2.11
						SCALE: 1:1	WEIGHT: SHEET 1 OF 1

**PROPRIETARY AND CONFIDENTIAL**  
THE INFORMATION CONTAINED IN THIS DRAWING IS THE SOLE PROPERTY OF MIT DROPLET-BASED MANUFACTURING. ANY REPRODUCTION IN PART OR AS A WHOLE WITHOUT THE WRITTEN PERMISSION OF MIT DROPLET BASED MANUFACTURING IS PROHIBITED.



**PROPRIETARY AND CONFIDENTIAL**  
 THE INFORMATION CONTAINED IN THIS DRAWING IS THE SOLE PROPERTY OF MIT DROPLET-BASED MANUFACTURING. ANY REPRODUCTION IN PART OR AS A WHOLE WITHOUT THE WRITTEN PERMISSION OF MIT DROPLET BASED MANUFACTURING IS PROHIBITED.

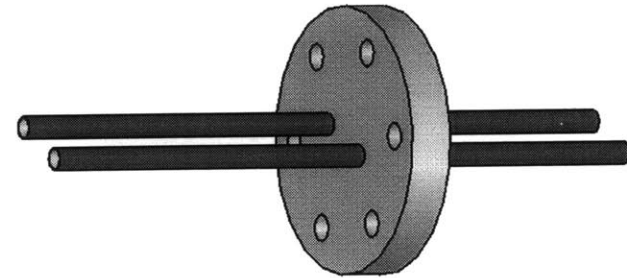
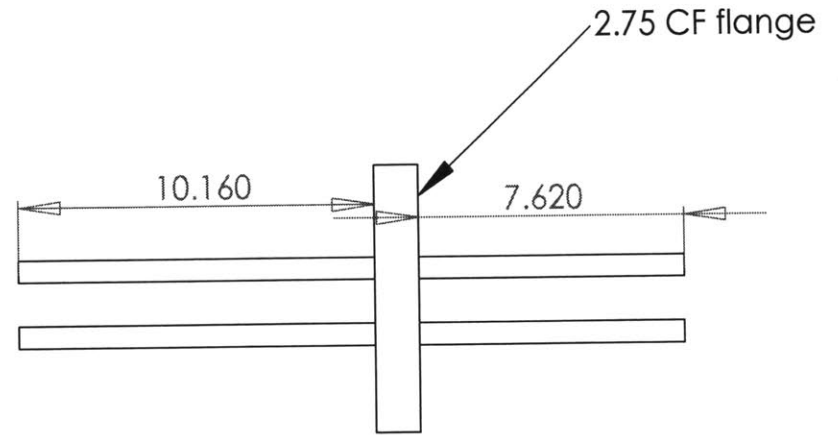
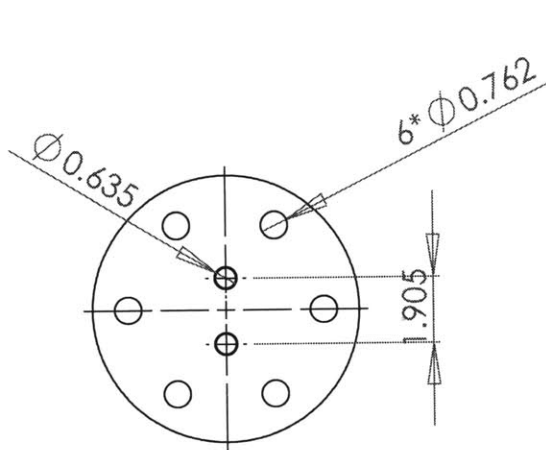
				NAME	DATE	MIT DROPLET-BASED MANUFACTURING			
				DRAWN	H. JOUMAA	FALL 2003	<h2 style="text-align: center;">Coil Assembly Isometric View</h2>		
				CHECKED					
				ENG APPR.					
				MFG APPR.					
				Q.A.			<b>UDS APPARATUS PARTS</b>		
				COMMENTS:					
NEXT ASSY	USED ON		MATERIAL				SIZE	DWG. NO.	REV.
			FINISH				<b>A</b>	<b>B.3.1</b>	
APPLICATION		DO NOT SCALE DRAWING					SCALE: 1:1	WEIGHT:	SHEET 1 OF 1



TRUE R0.318

**PROPRIETARY AND CONFIDENTIAL**  
 THE INFORMATION CONTAINED IN THIS DRAWING IS THE SOLE PROPERTY OF MIT DROPLET-BASED MANUFACTURING. ANY REPRODUCTION IN PART OR AS A WHOLE WITHOUT THE WRITTEN PERMISSION OF MIT DROPLET BASED MANUFACTURING IS PROHIBITED.

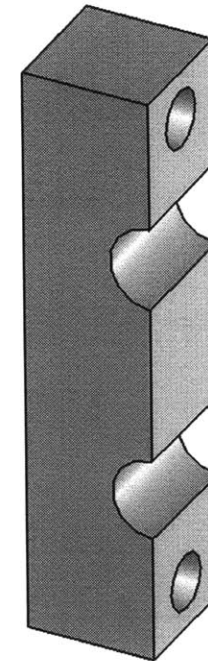
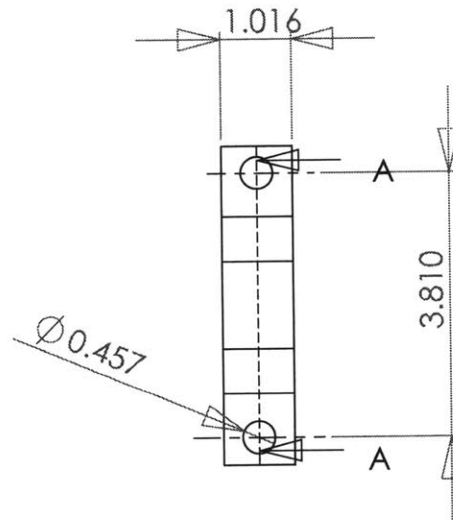
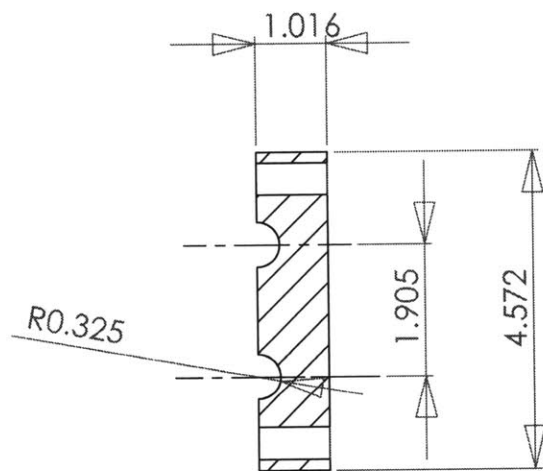
		DIMENSIONS IN CENTIMETERS TOLERANCES: TWO PLACE DECIMAL ±0.005 THREE PLACE DECIMAL ±0.001		NAME H. JOUMAA	DATE FALL 2003	MIT DROPLET-BASED MANUFACTURING	
		MATERIAL Copper		CHECKED		Inductive coil	
		FINISH --		ENG APPR.			
NEXT ASSY		USED ON		MFG APPR.			
APPLICATION		DO NOT SCALE DRAWING		Q.A.		COMMENTS: UDS APPARATUS PARTS	
				SIZE A	DWG. NO. B.3.2	REV.	
				SCALE: 1:1	WEIGHT:	SHEET 1 OF 1	



**PROPRIETARY AND CONFIDENTIAL**  
 THE INFORMATION CONTAINED IN THIS DRAWING IS THE SOLE PROPERTY OF MIT DROPLET-BASED MANUFACTURING. ANY REPRODUCTION IN PART OR AS A WHOLE WITHOUT THE WRITTEN PERMISSION OF MIT DROPLET BASED MANUFACTURING IS PROHIBITED.

		DIMENSIONS IN CENTIMETERS TOLERANCES: TWO PLACE DECIMAL $\pm 0.005$ THREE PLACE DECIMAL $\pm 0.001$	NAME H. JOUMAA	DATE FALL 2003	MIT DROPLET-BASED MANUFACTURING
		MATERIAL Stainless steel Copper tubes	CHECKED		RF Feedthrough
		FINISH ---	ENG APPR.		
NEXT ASSY	USED ON		MFG APPR.		
APPLICATION	DO NOT SCALE DRAWING		Q.A.		
			COMMENTS: UDS APPARATUS PARTS		
			SCALE: A	DWG. FIG. B.3.3	REV.
			SCALE: 1:1	WEIGHT:	SHEET 1 OF 1

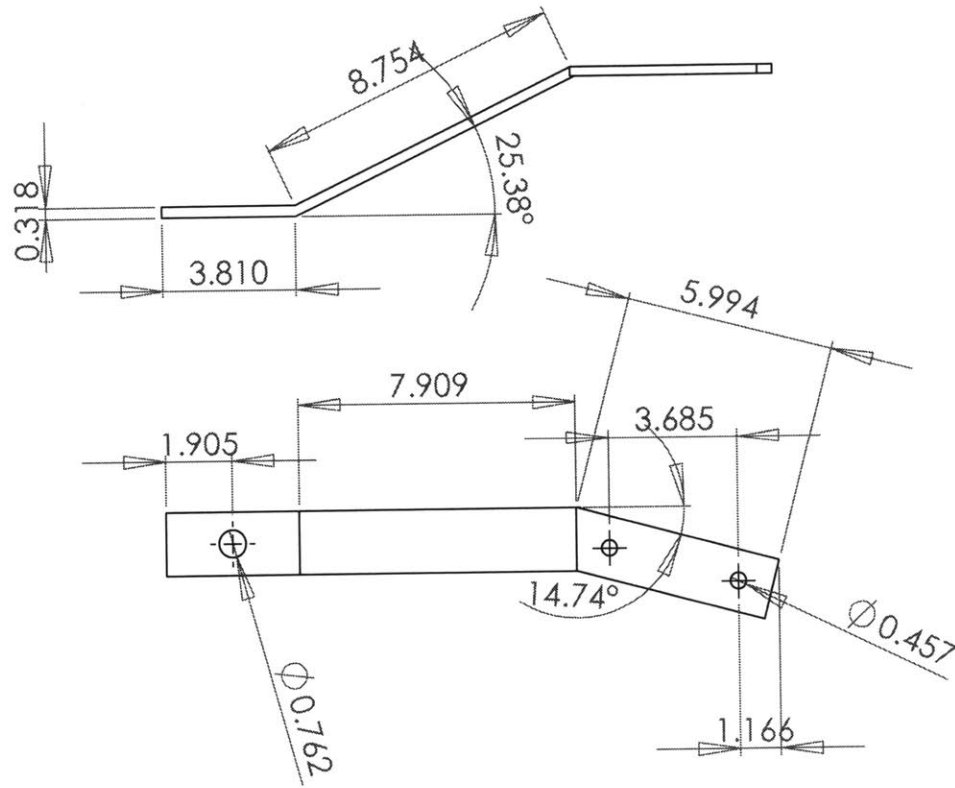




### SECTION A-A

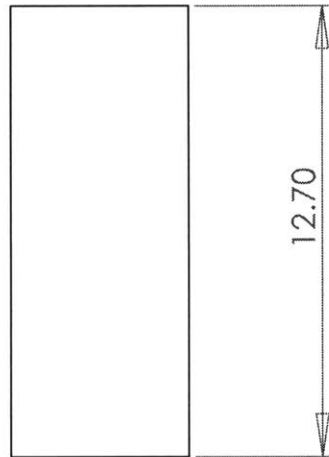
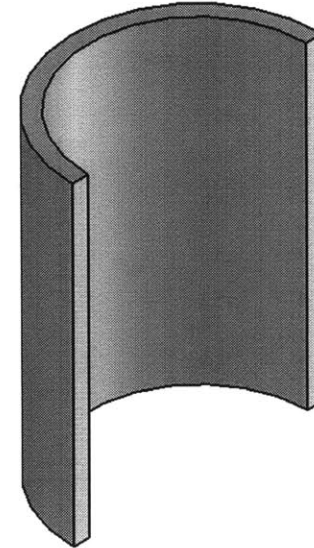
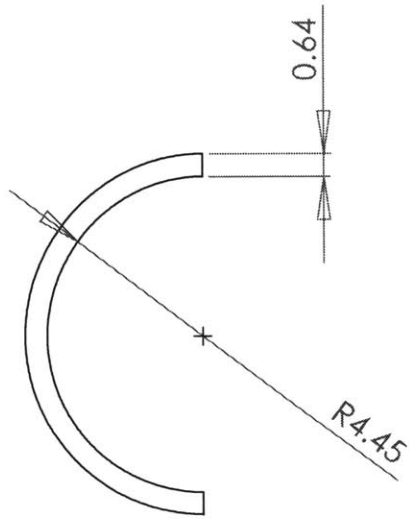
**PROPRIETARY AND CONFIDENTIAL**  
 THE INFORMATION CONTAINED IN THIS DRAWING IS THE SOLE PROPERTY OF MIT DROPLET-BASED MANUFACTURING. ANY REPRODUCTION IN PART OR AS A WHOLE WITHOUT THE WRITTEN PERMISSION OF MIT DROPLET BASED MANUFACTURING IS PROHIBITED.

		DIMENSIONS IN CENTIMETERS TOLERANCES: TWO PLACE DECIMAL ±0.005 THREE PLACE DECIMAL ±0.001		NAME	DATE	MIT DROPLET-BASED MANUFACTURING	
				DRAWN	H. JOUMAA	FALL 2003	Insulator coil holder
				CHECKED			
				ENG APPR.			
				MFG APPR.			
				Q.A.			SIZE: <b>A</b> DWG. NO.: <b>B.3.4</b> REV.: SCALE: 1:1    WEIGHT:    SHEET 1 OF 1
NEXT ASSY		USED ON		COMMENTS: UDS APPARATUS PARTS			
APPLICATION		DO NOT SCALE DRAWING					



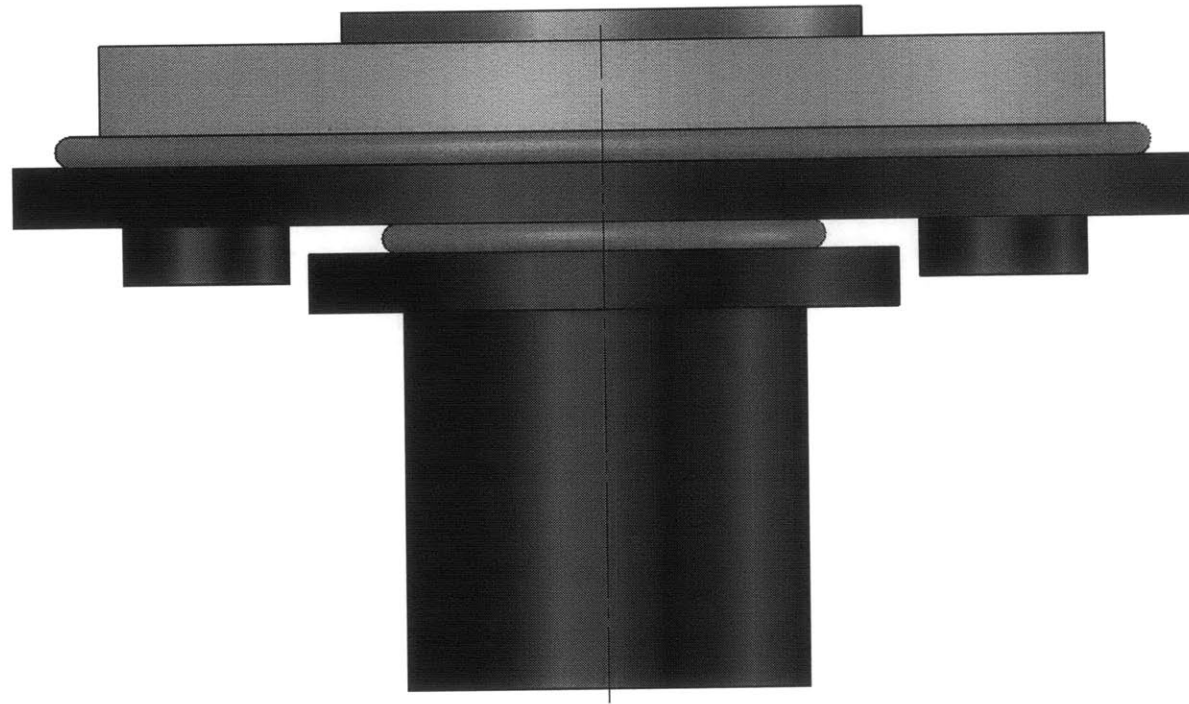
**PROPRIETARY AND CONFIDENTIAL**  
 THE INFORMATION CONTAINED IN THIS DRAWING IS THE SOLE PROPERTY OF MIT DROPLET-BASED MANUFACTURING. ANY REPRODUCTION IN PART OR AS A WHOLE WITHOUT THE WRITTEN PERMISSION OF MIT DROPLET BASED MANUFACTURING IS PROHIBITED.

		DIMENSIONS IN CENTIMETERS		NAME	DATE	MIT DROPLET-BASED MANUFACTURING	
		TOLERANCES:		DRAWN	H. JOUMAA	FALL 2003	Metal link
		TWO PLACE DECIMAL ±0.005		CHECKED			
		THREE PLACE DECIMAL ±0.001		ENG APPR.			
				MFG APPR.			
				Q.A.			
		MATERIAL		COMMENTS:			
		Stainless Steel		UDS APPARATUS PARTS			
NEXT ASSY	USED ON	FINISH				SIZE	DWG. FIG.
		---				A	B.3.5
APPLICATION		DO NOT SCALE DRAWING				SCALE: 1:1	WEIGHT:
						SHEET 1 OF 1	



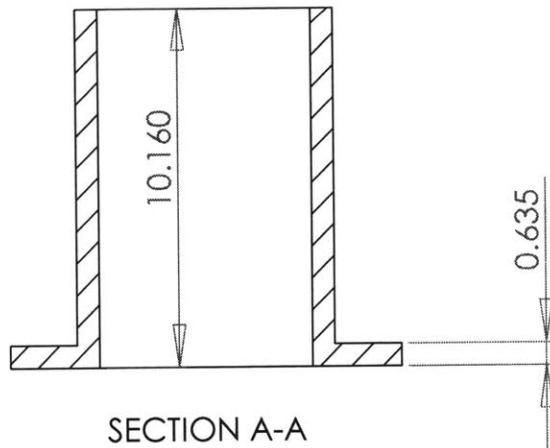
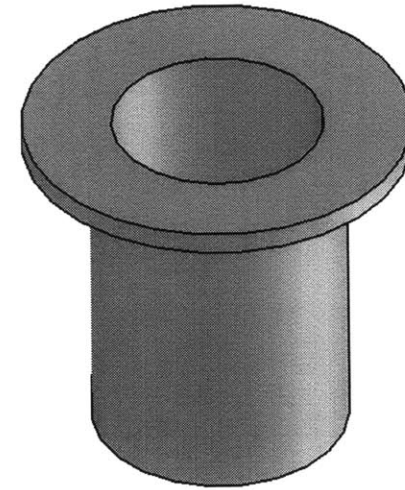
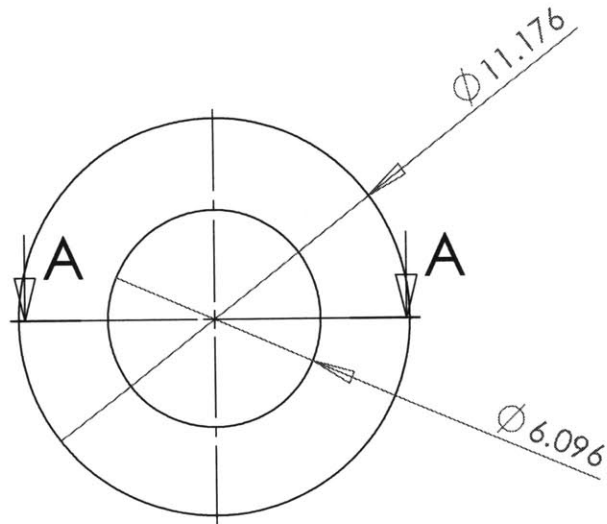
**PROPRIETARY AND CONFIDENTIAL**  
 THE INFORMATION CONTAINED IN THIS DRAWING IS THE SOLE PROPERTY OF MIT DROPLET-BASED MANUFACTURING. ANY REPRODUCTION IN PART OR AS A WHOLE WITHOUT THE WRITTEN PERMISSION OF MIT DROPLET BASED MANUFACTURING IS PROHIBITED.

		DIMENSIONS IN CENTIMETERS		NAME	DATE	MIT DROPLET-BASED MANUFACTURING	
		TOLERANCES:		DRAWN	H. JOUMAA	FALL 2003	Cover cylinder
		TWO PLACE DECIMAL ± 0.005		CHECKED			
		THREE PLACE DECIMAL ± 0.001		ENG APPR.			
				MFG APPR.			
				Q.A.			
		MATERIAL		COMMENTS:			
		Polymer, PMMA		UDS APPARATUS PARTS			
NEXT ASSY	USED ON	FINISH		SIZE		DWG. NO.	REV.
		--		A		B.3.6	
APPLICATION		DO NOT SCALE DRAWING		SCALE: 1:1		WEIGHT:	SHEET 1 OF 1



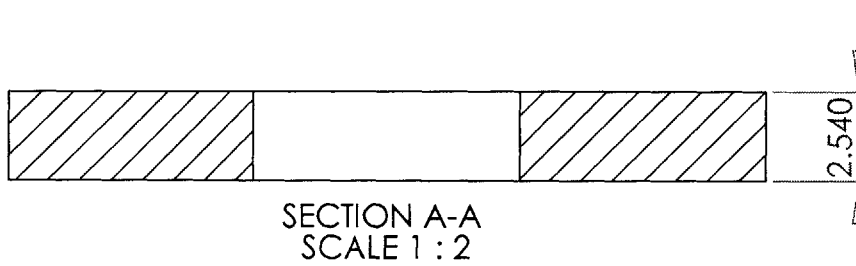
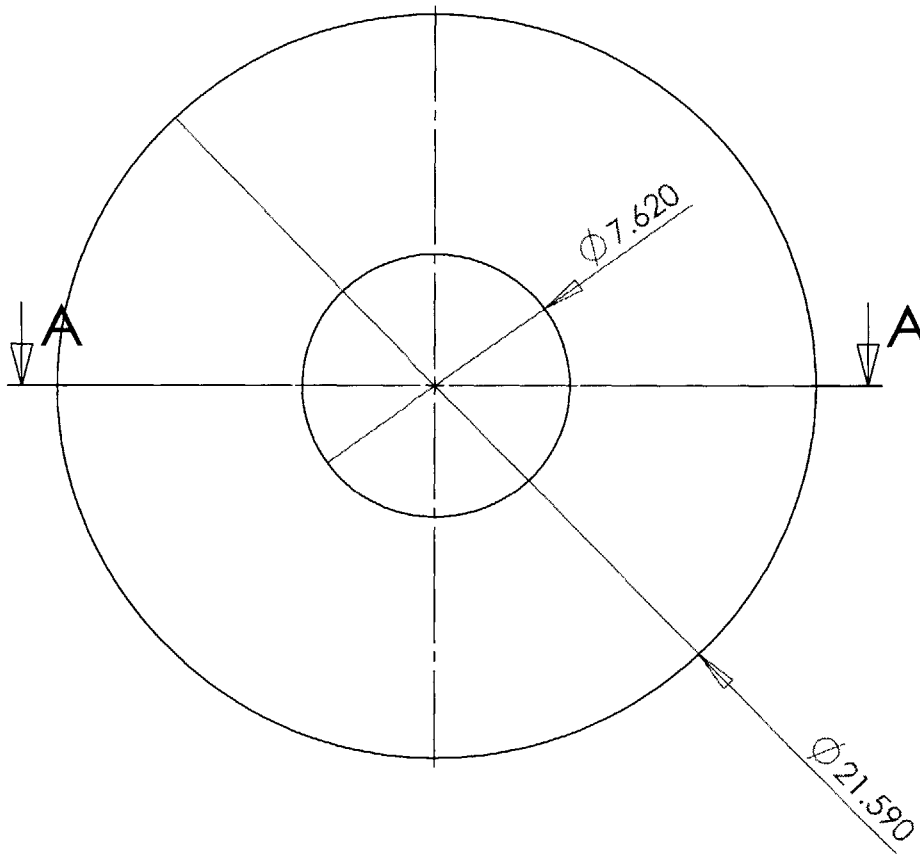
**PROPRIETARY AND CONFIDENTIAL**  
 THE INFORMATION CONTAINED IN THIS DRAWING IS THE SOLE PROPERTY OF MIT DROPLET-BASED MANUFACTURING. ANY REPRODUCTION IN PART OR AS A WHOLE WITHOUT THE WRITTEN PERMISSION OF MIT DROPLET BASED MANUFACTURING IS PROHIBITED.

				NAME	DATE	MIT DROPLET-BASED MANUFACTURING		
				DRAWN	H. JOUMAA	FALL 2003	Bottom plate Assembly	
				CHECKED				
				ENG APPR.				
				MFG APPR.				
				Q.A.			UDS APPARATUS PARTS	
				COMMENTS:				
NEXT ASSY	USED ON	MATERIAL	FINISH			SIZE	DWG. NO.	REV.
APPLICATION		DO NOT SCALE DRAWING				A	B.4.1	
						SCALE: 1:1	WEIGHT:	SHEET 1 OF 1



**PROPRIETARY AND CONFIDENTIAL**  
 THE INFORMATION CONTAINED IN THIS DRAWING IS THE SOLE PROPERTY OF MIT DROPLET-BASED MANUFACTURING. ANY REPRODUCTION IN PART OR AS A WHOLE WITHOUT THE WRITTEN PERMISSION OF MIT DROPLET BASED MANUFACTURING IS PROHIBITED.

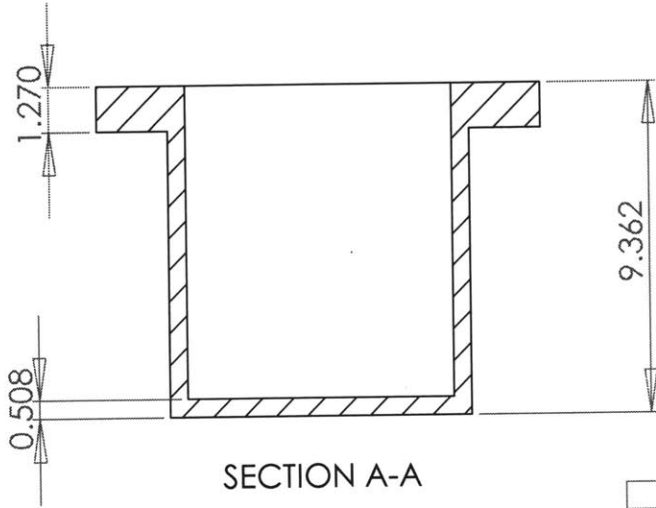
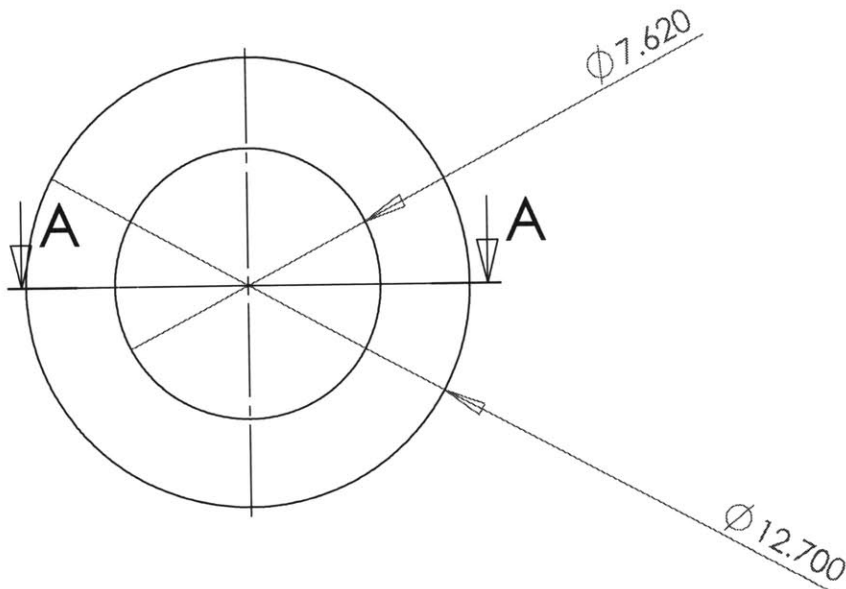
		DIMENSIONS IN CENTIMETERS TOLERANCES: TWO PLACE DECIMAL $\pm 0.005$ THREE PLACE DECIMAL $\pm 0.001$	NAME H. JOUMAA	DATE FALL 2003	MIT DROPLET-BASED MANUFACTURING
			CHECKED		<b>Flanged cylinder</b>
			ENG APPR.		
			MFG APPR.		
			Q.A.		
		MATERIAL <b>STEEL</b>	COMMENTS: <b>UDS APPARATUS PARTS</b>		
NEXT ASSY	USED ON	FINISH ---			SIZE <b>A</b>
APPLICATION	DO NOT SCALE DRAWING				DWG. NO. <b>B.4.2</b>
					SCALE: 1:1
					WEIGHT:
					SHEET 1 OF 1



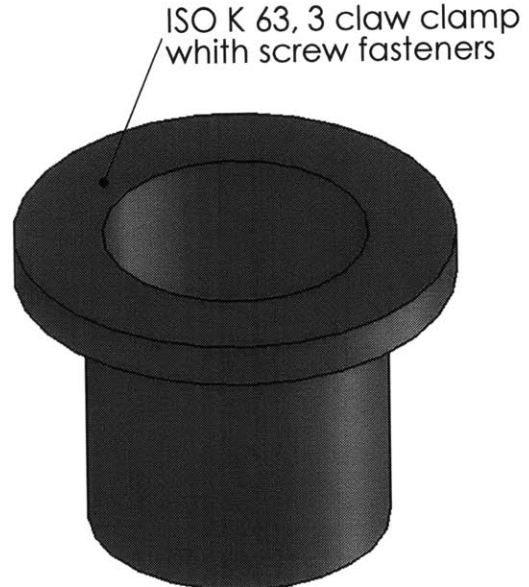
SECTION A-A  
SCALE 1 : 2

**PROPRIETARY AND CONFIDENTIAL**  
THE INFORMATION CONTAINED IN THIS DRAWING IS THE SOLE PROPERTY OF MIT DROPLET-BASED MANUFACTURING. ANY REPRODUCTION IN PART OR AS A WHOLE WITHOUT THE WRITTEN PERMISSION OF MIT DROPLET BASED MANUFACTURING IS PROHIBITED.

		DIMENSIONS IN CENTIMETERS TOLERANCES: TWO PLACE DECIMAL ± 0.005 THREE PLACE DECIMAL ± 0.001		DRAWN H. JOUMAA	NAME H. JOUMAA	DATE FALL 2003	MIT DROPLET-BASED MANUFACTURING	
		MATERIAL ALUMINA SILICA FIBERS		CHECKED	ENG APPR.	MFG APPR.	Insulation disk	
NEXT ASSY		USED ON		FINISH		COMMENTS: UDS APPARATUS PARTS		REV.
APPLICATION		DO NOT SCALE DRAWING		SIZE <b>A</b>		DWG. NO. <b>B.4.3</b>		SCALE: 1:1
				WEIGHT:		SHEET 1 OF 1		

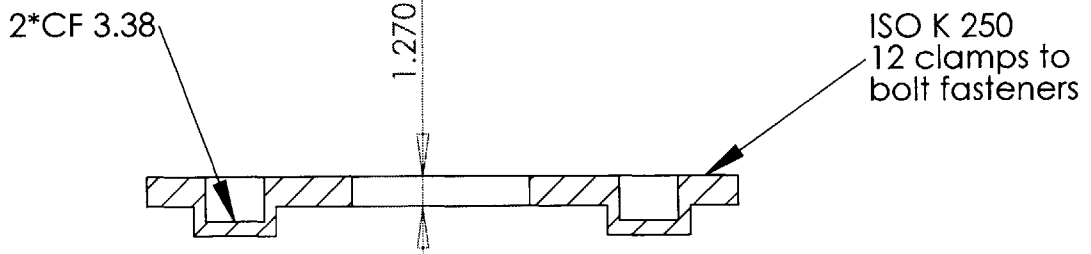
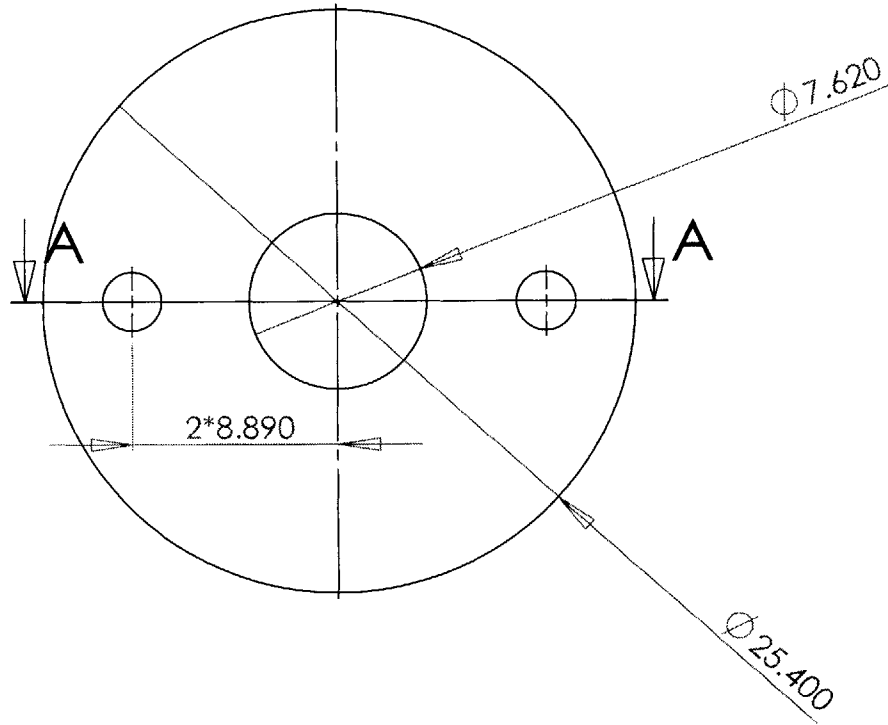


SECTION A-A



**PROPRIETARY AND CONFIDENTIAL**  
 THE INFORMATION CONTAINED IN THIS DRAWING IS THE SOLE PROPERTY OF MIT DROPLET-BASED MANUFACTURING. ANY REPRODUCTION IN PART OR AS A WHOLE WITHOUT THE WRITTEN PERMISSION OF MIT DROPLET BASED MANUFACTURING IS PROHIBITED.

		DIMENSIONS IN CENTIMETERS TOLERANCES: TWO PLACE DECIMAL ± 0.005 THREE PLACE DECIMAL ± 0.001		NAME H. JOUMAA	DATE FALL 2003	MIT DROPLET-BASED MANUFACTURING	
		MATERIAL Stainless Steel		CHECKED		Collection cup	
		FINISH ---		ENG APPR.			
		APPLICATION DO NOT SCALE DRAWING		MFG APPR.			
NEXT ASSY	USED ON			Q.A.		COMMENTS: UDS APPARATUS PARTS	
		SIZE A	DWG. NO. B.4.4			REV.	
		SCALE: 1:1	WEIGHT:			SHEET 1 OF 1	



SECTION A-A  
SCALE 1 : 3

		DIMENSIONS IN CENTIMETERS TOLERANCES: TWO PLACE DECIMAL $\pm 0.005$ THREE PLACE DECIMAL $\pm 0.001$		NAME H. JOUMAA	DATE FALL 2003	MIT DROPLET-BASED MANUFACTURING	
		MATERIAL STAINLESS STEEL		CHECKED		Bottom plate	
		FINISH		ENG APPR.			
NEXT ASSY	USED ON			MFG APPR.		SIZE <b>A</b>	
APPLICATION		DO NOT SCALE DRAWING		COMMENTS: UDS APPARATUS PARTS		DWG. NO. <b>B.4.5</b>	
						REV.	
				SCALE: 1:1		WEIGHT:	
						SHEET 1 OF 1	

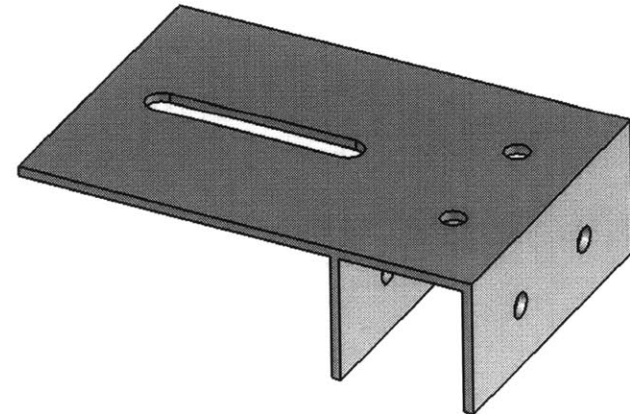
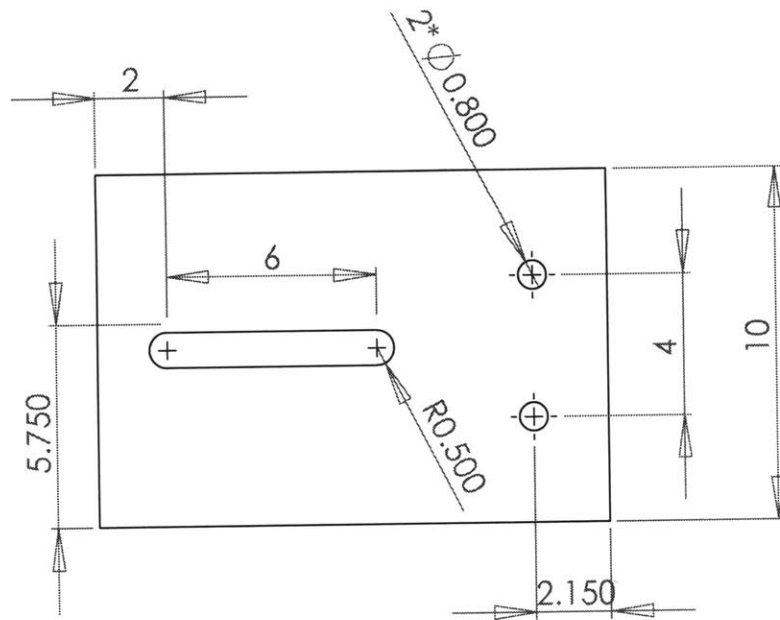
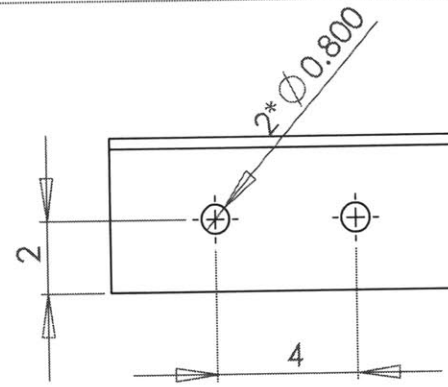
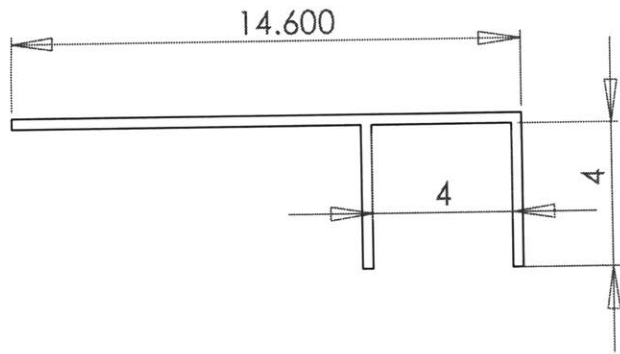
**PROPRIETARY AND CONFIDENTIAL**  
THE INFORMATION CONTAINED IN THIS DRAWING IS THE SOLE PROPERTY OF MIT DROPLET-BASED MANUFACTURING. ANY REPRODUCTION IN PART OR AS A WHOLE WITHOUT THE WRITTEN PERMISSION OF MIT DROPLET-BASED MANUFACTURING IS PROHIBITED.





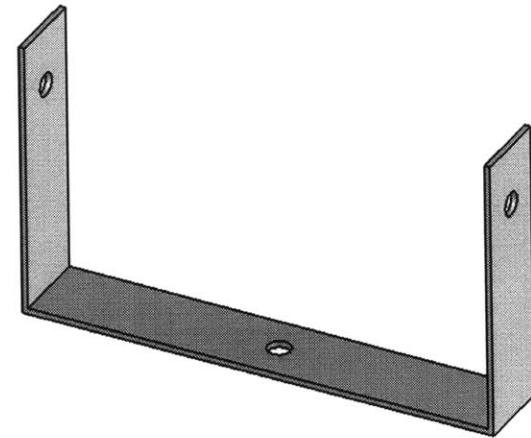
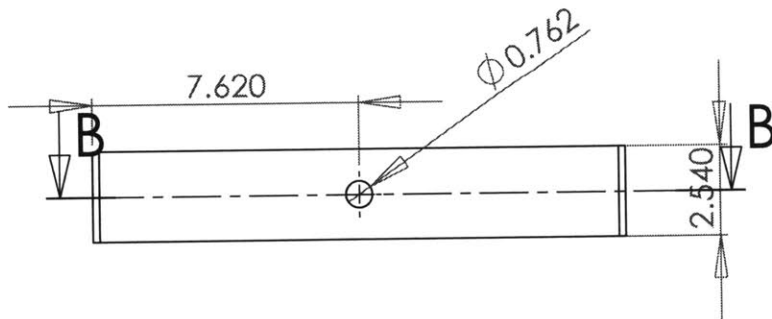
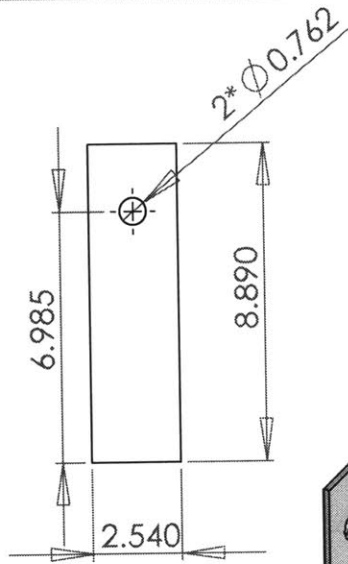
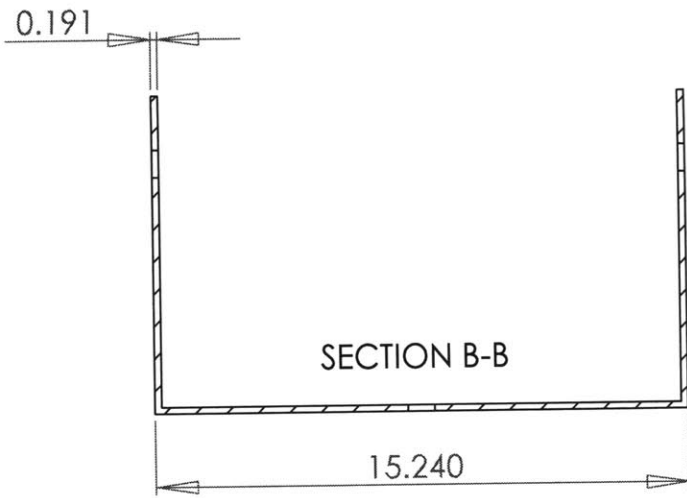
**PROPRIETARY AND CONFIDENTIAL**  
 THE INFORMATION CONTAINED IN THIS DRAWING IS THE SOLE PROPERTY OF MIT DROPLET-BASED MANUFACTURING. ANY REPRODUCTION IN PART OR AS A WHOLE WITHOUT THE WRITTEN PERMISSION OF MIT DROPLET BASED MANUFACTURING IS PROHIBITED.

				NAME	DATE	MIT DROPLET-BASED MANUFACTURING	
				DRAWN	H. JOUMAA	FALL 2003	
				CHECKED			
				ENG APPR.			
				MFG APPR.			
				Q.A.			
				COMMENTS:			
				UDS APPARATUS PARTS			
NEXT ASSY	USED ON	FINISH		SIZE	DWG. NO.	B.5.1	REV.
APPLICATION		DO NOT SCALE DRAWING		SCALE:1:1	WEIGHT:	SHEET 1 OF 1	



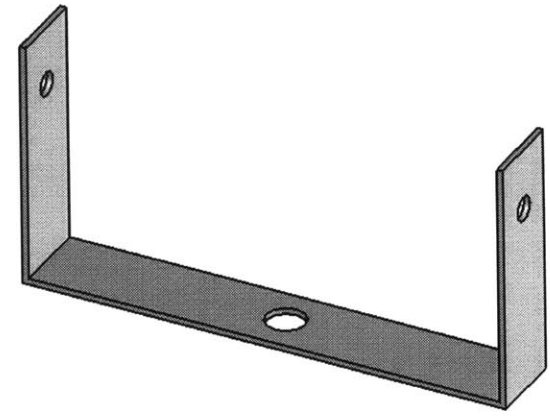
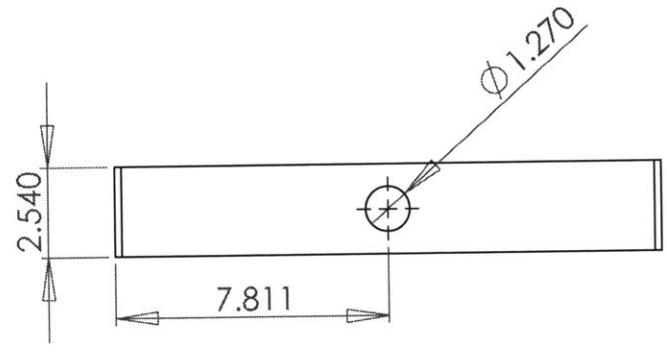
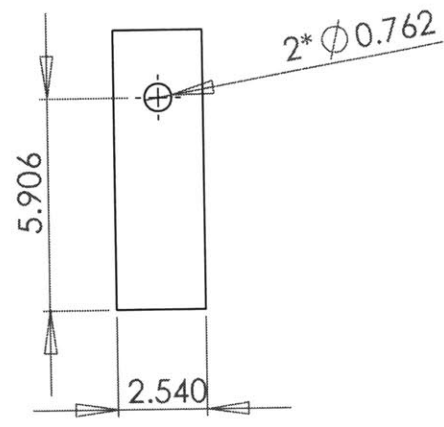
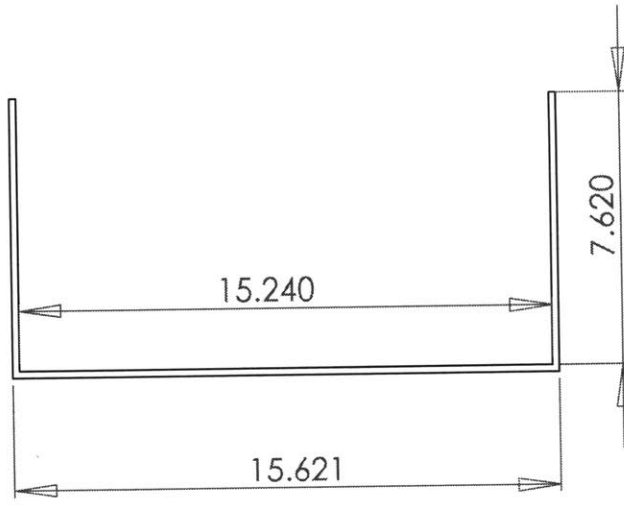
**PROPRIETARY AND CONFIDENTIAL**  
 THE INFORMATION CONTAINED IN THIS DRAWING IS THE SOLE PROPERTY OF MIT DROPLET-BASED MANUFACTURING. ANY REPRODUCTION IN PART OR AS A WHOLE WITHOUT THE WRITTEN PERMISSION OF MIT DROPLET BASED MANUFACTURING IS PROHIBITED.

		DIMENSIONS IN CENTIMETER TOLERANCES: TWO PLACE DECIMAL $\pm 0.005$ THREE PLACE DECIMAL $\pm 0.001$		NAME H. JOUMAA	DATE FALL 2003	MIT DROPLET-BASED MANUFACTURING	
		MATERIAL Aluminum		CHECKED		Strobe fixture_1	
		FINISH ---		ENG APPR.			
NEXT ASSY		USED ON		MFG APPR.			
APPLICATION		DO NOT SCALE DRAWING		COMMENTS: UDS APPARATUS PARTS		Q.A.	
				SIZE A	DWG. NO. B.5.2	REV.	
				SCALE: 1:1	WEIGHT:	SHEET 1 OF 1	



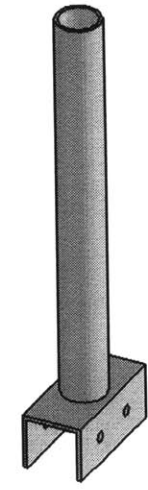
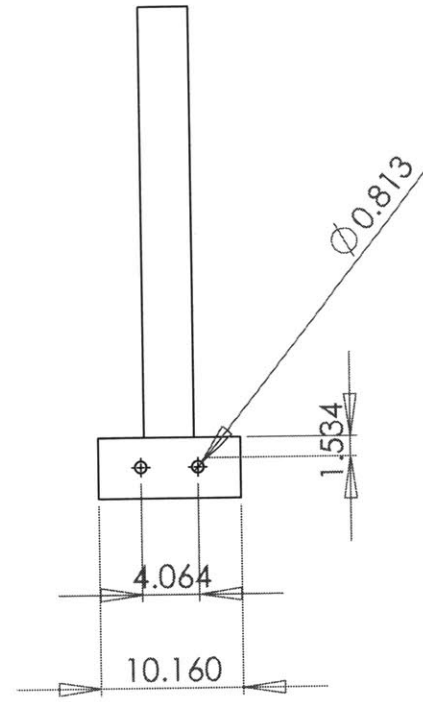
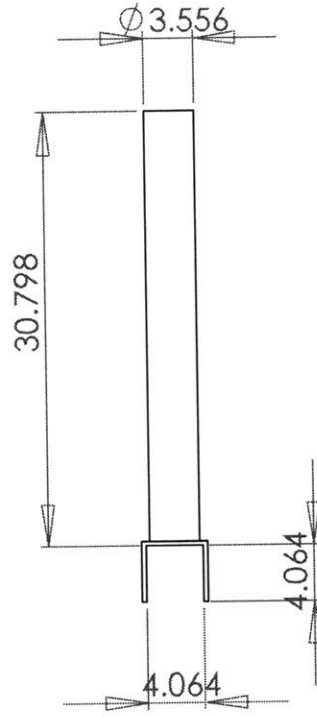
**PROPRIETARY AND CONFIDENTIAL**  
 THE INFORMATION CONTAINED IN THIS DRAWING IS THE SOLE PROPERTY OF MIT DROPLET-BASED MANUFACTURING. ANY REPRODUCTION IN PART OR AS A WHOLE WITHOUT THE WRITTEN PERMISSION OF MIT DROPLET BASED MANUFACTURING IS PROHIBITED.

		DIMENSIONS IN CENTIMETER		NAME	DATE	MIT DROPLET-BASED MANUFACTURING	
		TOLERANCES:		DPAWN	H. JOUMAA	FALL 2003	<b>Strobe fixture_2</b>
		TWO PLACE DECIMAL ± 0.005		CHECKED			
		THREE PLACE DECIMAL ± 0.001		ENG APPR.			
				MFG APPR.			
		MATERIAL		Q.A.			
		Aluminum		COMMENTS: UDS APPARATUS PARTS			
NEXT ASSY	USED ON	FINISH					
		--		SCALE: 1:1		WEIGHT:	REV.
APPLICATION		DO NOT SCALE DRAWING		DWG. NO.		B.5.3	
				SHEET 1 OF 1			



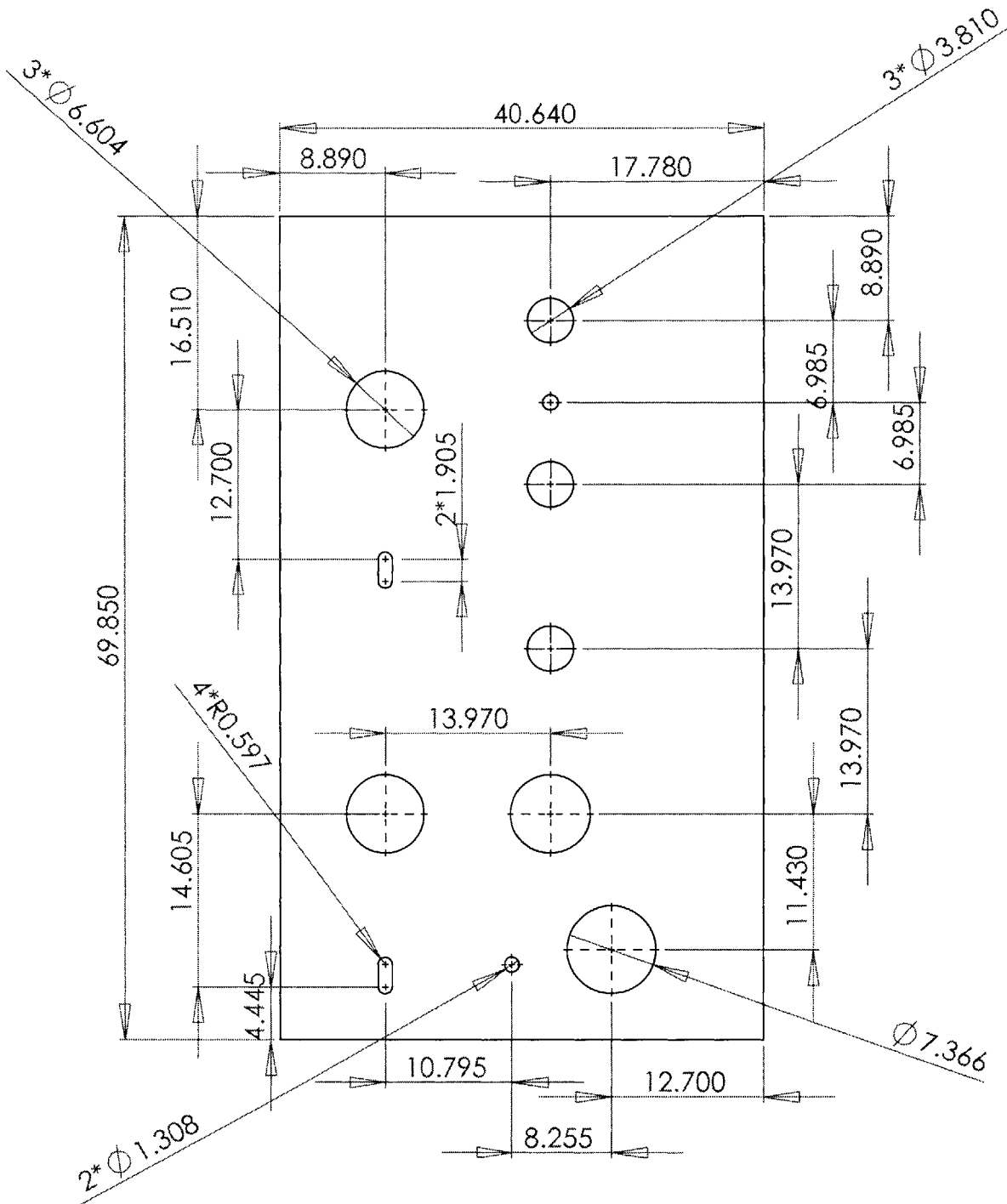
**PROPRIETARY AND CONFIDENTIAL**  
 THE INFORMATION CONTAINED IN THIS DRAWING IS THE SOLE PROPERTY OF MIT DROPLET-BASED MANUFACTURING. ANY REPRODUCTION IN PART OR AS A WHOLE WITHOUT THE WRITTEN PERMISSION OF MIT DROPLET BASED MANUFACTURING IS PROHIBITED.

		DIMENSIONS IN CENTIMETER TOLERANCES: TWO PLACE DECIMAL ± 0.005 THREE PLACE DECIMAL ± 0.001		NAME	DATE	MIT DROPLET-BASED MANUFACTURING	
				DRAWN	H. JOUMAA	FALL 2003	<b>Strobe fixture_3</b>
				CHECKED			
				ENG APPR.			
				MFG APPR.			
				Q.A.			
		MATERIAL	Aluminum	COMMENTS:			
NEXT ASSY	USED ON	FINISH	--	UDS APPARATUS PARTS			
APPLICATION			DO NOT SCALE DRAWING				
	SIZE	DWG. NO.					REV.
	A	B.5.4					
	SCALE: 1:1	WEIGHT:					SHEET 1 OF 1



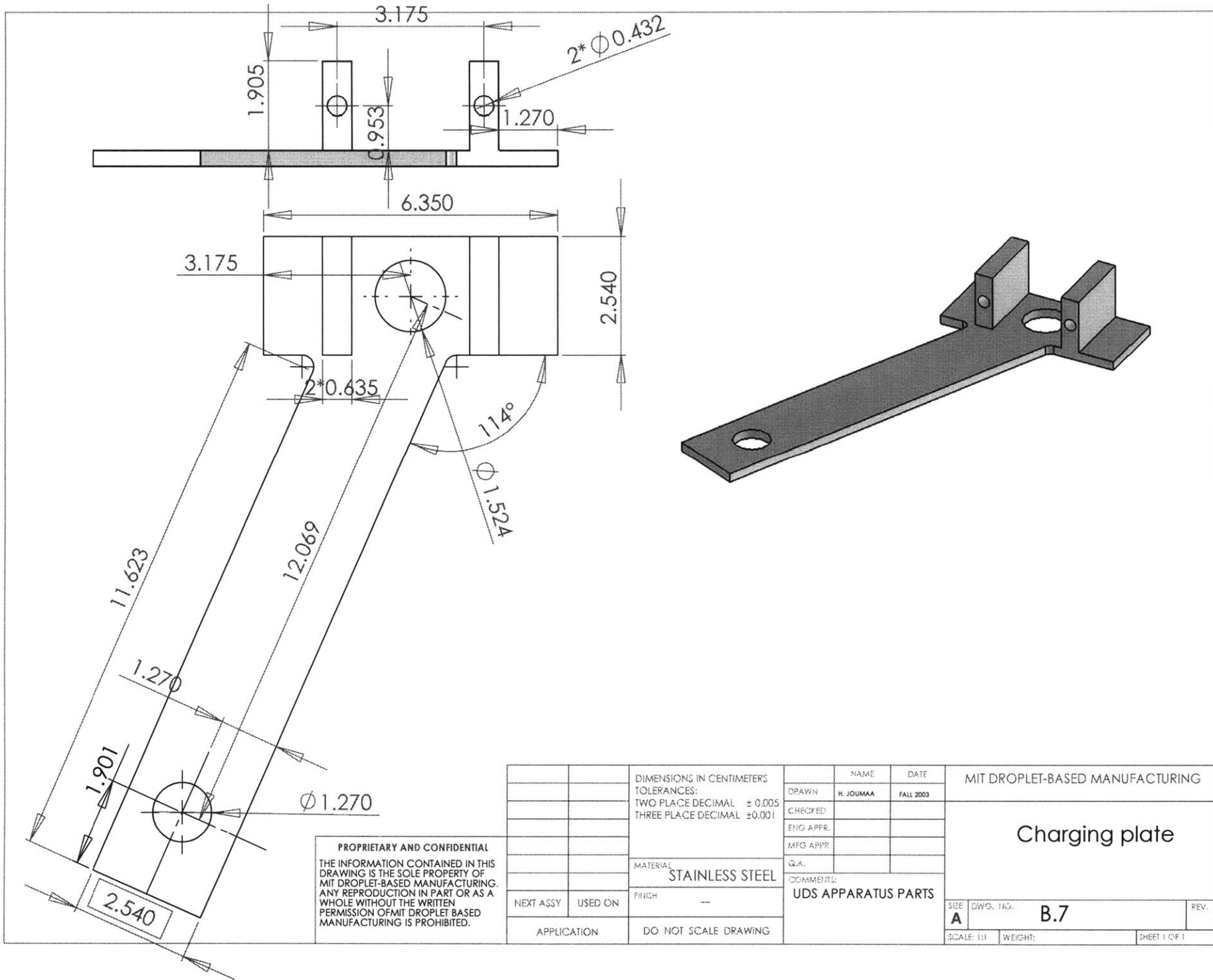
**PROPRIETARY AND CONFIDENTIAL**  
 THE INFORMATION CONTAINED IN THIS DRAWING IS THE SOLE PROPERTY OF MIT DROPLET-BASED MANUFACTURING. ANY REPRODUCTION IN PART OR AS A WHOLE WITHOUT THE WRITTEN PERMISSION OF MIT DROPLET BASED MANUFACTURING IS PROHIBITED.

		DIMENSIONS IN CENTIMETERS TOLERANCES: TWO PLACE DECIMAL ±0.005 THREE PLACE DECIMAL ±0.001		NAME	DATE	MIT DROPLET-BASED MANUFACTURING	
				DRAWN	H. JOUMAA	FALL 2003	<b>Camera fixture</b>
				CHECKED			
				ENG APPR.			
				MFG APPR			
				Q.A.			<b>UDS APPARATUS PARTS</b>
NEXT ASSY	USED ON	MATERIAL	Aluminum	COMMENTS:			
		FINISH	--				
APPLICATION		DO NOT SCALE DRAWING		SIZE	DWG. NO.	<b>B.5.5</b>	REV.
				SCALE: 1:1	WEIGHT:		SHEET 1 OF 1



**PROPRIETARY AND CONFIDENTIAL**  
 THE INFORMATION CONTAINED IN THIS DRAWING IS THE SOLE PROPERTY OF MIT DROPLET-BASED MANUFACTURING. ANY REPRODUCTION IN PART OR AS A WHOLE WITHOUT THE WRITTEN PERMISSION OF MIT DROPLET BASED MANUFACTURING IS PROHIBITED.

		DIMENSIONS IN CENTIMETERS TOLERANCES: TWO PLACE DECIMAL $\pm 0.005$ THREE PLACE DECIMAL $\pm 0.001$		NAME H. JOUMAA	DATE FALL 2003	MIT DROPLET-BASED MANUFACTURING	
		MATERIAL ALUMINUM		DRAWN	CHECKED	Gas management control panel	
		FINISH		ENG APPR.	MFG APPR.		
NEXT ASSY		USED ON		Q.A.	COMMENTS:		
APPLICATION		DO NOT SCALE DRAWING		UDS APPARATUS PARTS		SIZE <b>A</b>	DWG. NO. <b>B.6</b>
				SCALE:1:5		WEIGHT:	REV. SHEET 1 OF 1



**PROPRIETARY AND CONFIDENTIAL**  
 THE INFORMATION CONTAINED IN THIS DRAWING IS THE SOLE PROPERTY OF MIT DROPLET-BASED MANUFACTURING. ANY REPRODUCTION IN PART OR AS A WHOLE WITHOUT THE WRITTEN PERMISSION OF MIT DROPLET BASED MANUFACTURING IS PROHIBITED.

		DIMENSIONS IN CENTIMETERS		NAME	DATE	MIT DROPLET-BASED MANUFACTURING	
		TOLERANCES:		DRAWN	H. JOUMAA	FALL 2003	Charging plate
		TWO PLACE DECIMAL $\pm 0.005$		CHECKED:			
		THREE PLACE DECIMAL $\pm 0.001$		ENG APPR.			
				MFG APPR.			
		MATERIAL		Q.A.			UDS APPARATUS PARTS
		STAINLESS STEEL		COMMENTS:			
		FINISH					
NEXT ASSY	USED ON	APPLICATION		DO NOT SCALE DRAWING		SIZE	DWG. NO.
						<b>A</b>	<b>B.7</b>
				SCALE: 1:1	WEIGHT:	SHEET 1 OF 1	

## Appendix C

### Induction Heating Calculations

The induction heating calculations are done on a Matlab code that solves for the transfer efficiency of the heater as function of the frequency. The calculation involves an extensive use of the Bessel functions that are defined as follows.

Consider the time varying differential equations:

$$\frac{d^2 y}{dx^2} + \frac{1}{x} \frac{dy}{dx} - k^2 y = 0$$

where  $k$  is a constant.

The solution to this equation is:  $y = AI_o(kx) + BK_o(kx)$

$I_o$  and  $K_o$  are the Bessel and Kelvin functions defined as follows:

$$I_o(x) = 1 + \frac{(x/2)^2}{(1!)^2} + \frac{(x/2)^4}{(2!)^2} + \frac{(x/2)^6}{(3!)^2} + etc = \sum_{n=0}^{\infty} \frac{(x/2)^{2n}}{(n!)^2}$$

$$K_o(x) = I_o(x) \cdot (\ln 2 - \gamma - \ln x) + (x/2)^2 + \sum_{n=2}^{\infty} \sum_{p=1}^n \left(\frac{1}{p}\right) \frac{(x/2)^{2n}}{(n!)^2}$$

where  $\gamma$  is the Euler's constant, 0.5772157.

The four functions defined below are derived from the Bessel and Kelvin functions as follows:

$$\text{Bessel Real or } ber(x) = \text{Re}(I_o(x\sqrt{j}))$$

$$\text{Bessel Imaginary or } bei(x) = \text{Im}(I_o(x\sqrt{j}))$$

$$\text{Kelvin Real or } ker(x) = \text{Re}(K_o(x\sqrt{j}))$$

$$\text{Kelvin Imaginary or } kei(x) = \text{Im}(K_o(x\sqrt{j}))$$

The following codes generate all the previous four functions and their first derivatives.

```
function bei = bei(x);
bei = imag(besseli(0,x*sqrt(j)));
```

```
function beip = beip(x);
inc = 1e-5;
beip = (imag(besseli(0,(x + inc)*sqrt(j))) - imag(besseli(0,(x - inc)*sqrt(j))))/(2*inc);
```

```
function ber = ber(x);
ber = real(besseli(0,x*sqrt(j)));
```

```
function berp = berp(x);
```



```

inc = 1e-5;
berp = (real(besseli(0,(x + inc)*sqrt(j))) - real(besseli(0,(x - inc)*sqrt(j))))/(2*inc);

function kei = kei(x);
kei = imag(besselk(0,x*sqrt(j)));

function keip = keip(x);
inc = 1e-5;
keip = (imag(besselk(0,(x + inc)*sqrt(j))) - imag(besselk(0,(x - inc)*sqrt(j))))/(2*inc);

function ker = ker(x);
ker = real(besselk(0,x*sqrt(j)));

function kerp = kerp(x);
inc = 1e-5;
kerp = (real(besselk(0,(x + inc)*sqrt(j))) - real(besselk(0,(x - inc)*sqrt(j))))/(2*inc);

```

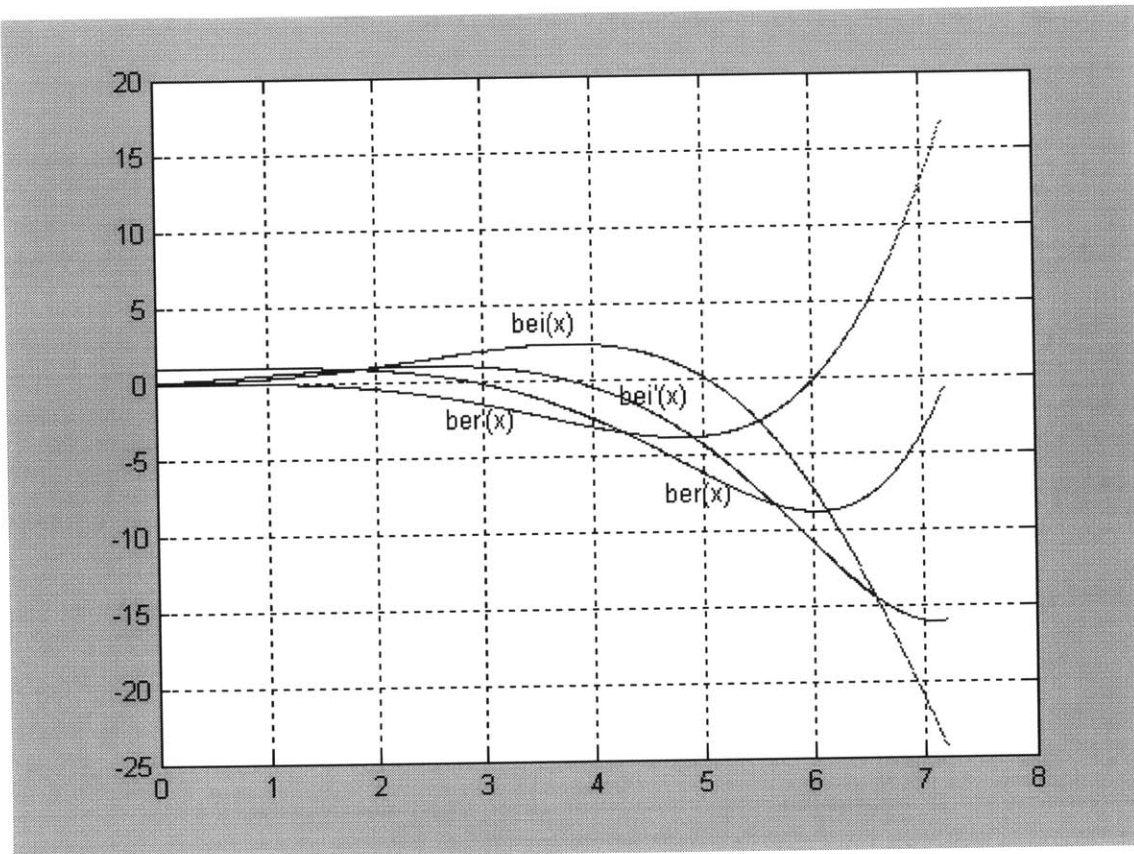


Figure C.1: Plot of Bessel functions and their first derivatives.

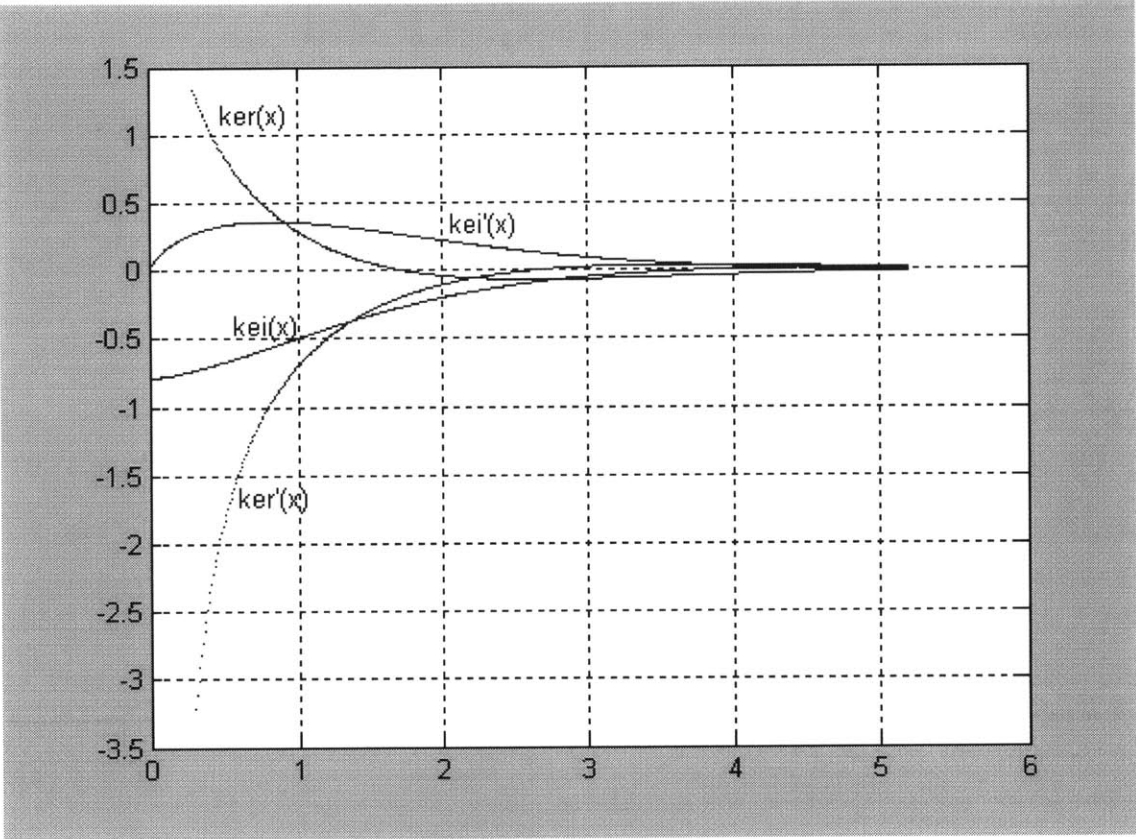


Figure C.2: Plot of Kelvin functions and their first derivatives.

The matching solver code is listed below:

```

%% Hady Joumma-Spring 2004
%% Droplet Based Manufacturing Laboratory

% program to solve for the matching equation of the
% induction heater
% Modeling: Copper billet and crucible as hollow cylinders

%% -----
%% -----frequency range-----
fmin = 100; %minimum frequency [Hertz]
fmax = 100000; %maximum frequency in Hz.
finc = 100; % increment frequency [Hz];

%% -----
%% -----properties of billet-----
ro = 5.2e-8; % electric resistivity of billet [ohm-m]
mu0 = 4*pi*1e-7; % absolute permeability.
mur = 1; %relative permeability of billet material
Ri = 0.2*(2.54/100); % inner radius in inches*(m/inch).

```

Ro = 0.8\*(2.54/100); %outer radius inches\*(m/inch).  
 Lb = 2.5\*(2.54/100); %length inches\*(m/inch).

%% -----  
 %% -----properties of crucible-----  
 ro\_cr = 70e-6; % electric resistivity of crucible [ohm-m]  
 mu0\_cr = 4\*pi\*1e-7; % absolute permeability.  
 mur\_cr = 1; %relative permeability of crucible material  
 Ri\_cr = 1\*(2.54/100); % inner radius in inches\*(m/inch).  
 Ro\_cr = 1.25\*(2.54/100); %outer radius inches\*(m/inch).  
 Lb\_cr = 2.5\*(2.54/100); %length inches\*(m/inch).

%% -----  
 %% -----properties of coil-----  
 roc = 2.2e-8; % conductivity of coil material [ohm-m]  
 Di = 9.32e-2; % inner diameter of coil [m]  
 Do = 10.86e-2; % outer diameter of coil [m]  
 d = (Do - Di)/2; % diameter of coil tube [m]  
 t = 1e-3; % thickness of coil tubing [m]  
 N = 10; % number of turns;  
 L = 9.3e-2; % length of coil and workpiece[m]  
 SF = (t\*N)/L; % Space factor of coil;  
 s = (N\*pi\*d)/(4\*L); % Shape factor;

%% -----  
 %% -----Solver-----

f = fmin; % loop frequency  
 while (f < fmax)

%% -----  
 %% -----billet equations-----  
 w = 2\*pi\*f; % angular speed [rad/sec]  
 delta = sqrt(2\*ro/(mur\*mu0\*w)); % skin depth  
 m = sqrt(2)/delta; % m- parameter [m^-1]

B = -2\*mur\*(berp(m\*Ri) + j\*beip(m\*Ri)) - j\*m\*Ri\*(ber(m\*Ri) + j\*bei(m\*Ri)); %  
 constant

A = 2\*mur\*(kerp(m\*Ri) + j\*keip(m\*Ri)) - j\*m\*Ri\*(ker(m\*Ri) + j\*kei(m\*Ri)); %  
 constant

R = B/A; % useful ratio for billet

%Hratio = (ber(m\*Ri) + j\*bei(m\*Ri))/(ber(m\*Ro) + j\*bei(m\*Ro)); % finding  
 H(Ri)/H(Ro)

%Hratio = Hratio\*(1 + R\*((ker(m\*Ri) + j\*kei(m\*Ri))/(ber(m\*Ri) + j\*bei(m\*Ri)))); %  
 finding H(Ri)/H(Ro)

```

%Hratio = Hratio/(1 + R*((ker(m*Ro) + j*kei(m*Ro))/(ber(m*Ro) + j*bei(m*Ro)))); %
finding H(Ri)/H(Ro)
%Hratio = abs(Hratio); % H(Ri)/H(Ro)

```

```

P1 = (2/(m*Ro))*((berp(m*Ro) + j*beip(m*Ro))/(ber(m*Ro) + j*bei(m*Ro)));
P2 = 1 + R*((kerp(m*Ro) + j*keip(m*Ro))/(berp(m*Ro) + j*beip(m*Ro)));
P3 = 1 + R*((ker(m*Ro) + j*kei(m*Ro))/(ber(m*Ro) + j*bei(m*Ro)));
P = real(P1*(P2/P3)); % power factor

```

```

%% -----
%% -----crucible equations-----
delta_cr = sqrt(2*ro_cr/(mur_cr*mu0_cr*w)); % skin depth
m_cr = sqrt(2)/delta_cr; % m- parameter [m^-1]

```

```

B_cr = -2*mur_cr*(berp(m_cr*Ri_cr) + j*beip(m_cr*Ri_cr)) -
j*m_cr*Ri_cr*(ber(m_cr*Ri_cr)...
+ j*bei(m_cr*Ri_cr)); % constant
A_cr = 2*mur_cr*(kerp(m_cr*Ri_cr) + j*keip(m_cr*Ri_cr)) -
j*m_cr*Ri_cr*(ker(m_cr*Ri_cr)...
+ j*kei(m_cr*Ri_cr)); % constant
R_cr = B_cr/A_cr; % useful ratio for crucible

```

```

P1_cr = (2/(m_cr*Ro_cr))*((berp(m_cr*Ro_cr) +
j*beip(m_cr*Ro_cr))/(ber(m_cr*Ro_cr) + j*bei(m_cr*Ro_cr)));
P2_cr = 1 + R_cr*((kerp(m_cr*Ro_cr) + j*keip(m_cr*Ro_cr))/(berp(m_cr*Ro_cr) +
j*beip(m_cr*Ro_cr)));
P3_cr = 1 + R_cr*((ker(m_cr*Ro_cr) + j*kei(m_cr*Ro_cr))/(ber(m_cr*Ro_cr) +
j*bei(m_cr*Ro_cr)));
P_cr = abs(real(P1_cr*(P2_cr/P3_cr))); % power factor

```

```

K = 2*pi*f*mu0*(N^2)/L; % useful parameter
% (See page 47 of Davies)

```

```

%% -----
%% -----Equivalent resistances-----
ResistanceW = K*pi*(Ro^2 - Ri^2)*mur*P; % billet equivalent resistance
ResistanceW_cr = K*pi*(Ro_cr^2 - Ri_cr^2)*mur_cr*P_cr; % crucible equivalent
resistance
deltac = sqrt(2*roc/(mur*mu0*w)); % skin depth for coil
Rcoil = K*pi*Di*deltac*s; % coil equivalent resistance

```

```

efficiency = (ResistanceW_cr)/(ResistanceW + Rcoil + ResistanceW_cr); % expression
for efficiency

```

```

plot(f,efficiency);
hold on;

```

```
f = f+finc;  
end  
  
grid on;  
xlabel('frequency [Hz]');  
ylabel('first transfer efficiency');  
return  
%% -----  
%% -----End of peogram-----
```

## Appendix D The recirculator internal water channels

